Development, testing, and validation of an energy-efficient dynamic positioning controller

by

© **Osama Alagili**

A thesis submitted to the School of Graduate Studies in partial fulfillment of the requirements for the degree of Doctor of Philosophy in Electrical Engineering.

Department of Electrical Engineering

Memorial University

June 2024

St. John's, Newfoundland and Labrador, Canada

Abstract

Exploration of the Arctic and Sub-Arctic regions is a daunting task due to the harsh environmental conditions, including low temperatures, ice floes, wind, and waves. Dynamic positioning (DP) is a crucial technology for ships operating in harsh weather conditions. The goal of this research is to develop energy efficient DP controllers that can withstand harsh environmental conditions. The scope of the thesis includes modelling and simulation of environmental disturbances on DP vessel; performance evaluation of a suite of DP controllers for moderate to harsh environmental conditions; development and simulation of an energy efficient DP system; and finally experimental implementation and evaluation of the proposed DP system.

Numerical modelling with real-time simulation capability helps design, test, and validate dynamically positioned and autonomous ships/platforms in harsh environments. However, advanced simulation technology is needed to predict the expected loads on these systems due to complex interactions with environmental disturbances. The first work presents wave, wind, current, and ice models that comply with real-time simulation requirements and capture the dynamic characteristics of relevant physical processes. A 3D dispersive numerical model was deployed to predict the wave parameters to compute the wave loads on a ship with known Response Amplitude Operators (RAO). A uniform current load was incorporated in a superposition manner by using a combined wave-current field dispersion relation capable of expressing the wave-number of an interactive wave-current field. The proposed models can be used to design, develop, and evaluate dynamic positioning and autonomous ship controllers' performance and train conventional, DP, and autonomous ship operators.

Next, the work evaluates the performance of several control schemes for DP application in moderate and extreme sea conditions. The controllers include nonlinear PID, sliding mode controller (SMC),multi-resolution PID controllers, model predictive controller (MPC) and nonlinear model predictive controller. Matlab/Simulink models of a full-scale ship and its scaled version are used to compare the efficacy of the controllers. An Unscented Kalman Filter is utilized to filter out wave-frequency motions. While all controllers were effective for moderate sea state, only nonlinear model predictive controller (NMPC) and multi-resolution proportional-integral derivative (MRPID) controllers could stabilize the ship under extreme sea states.The NMPC demonstrates the best ability to handle extreme disturbances.

Besides maintaining the position, one of the other goals of DP controller is to minimize the energy requirements and high frequency movements of the thrusters. An energy-efficient controller, called Green-NMPC was developed for the dynamic positioning of marine vessels. The Green-NMPC is motivated by the control goal of minimizing thruster demand. It is based upon the theoretical framework of the economic NMPC (ENMPC). Green-NMPC uses dynamic weights in the cost function depending on the vessel position in contrast to the constant weights in conventional NMPC. The proposed controller was tested for moderate to high sea wave conditions and reduced up to 50% thruster demand in sway direction compared to NMPC while maintaining the vessel positioning objectives. The Green-NMPC showed less thruster demand which was further verified quantitatively from the variance and the spectral strength of the thruster demand.

Finally, this research presents the experimental implementation of the proposed Green NMPC to a scaled version of a supply vessel named Magne Viking. Experiments were carried out at the National Research Council's wave basin. This is one of the very few experiments where the NMPCs were tested in a controlled environment with varying wave conditions, and the first experimental implementation of the Green NMPC. The experimental results on the station keeping tests validated that on average, the Green NMPC is the most energy efficient controller for the application. The Green NMPC minimizes the thruster movement by implementing a relaxed

control policy. The power spectrum of the thrusters further confirmed that Green NMPC has less high-frequency movements compared to the rest of the controllers. This implies that Green NMPC will cause less wear and tear on the thruster system.

Acknowledgements

Thanks to the Great Almighty "Allah SWT" who grant me the knowledge and determination to complete this work. Producing this project was a cumulative effort, hence, I wish to express deep gratitude to the many people who made it possible.

First, I would like to express my deepest appreciation to my academic advisors, Dr. Syed Imtiaz, Dr. Salim Ahmed, Dr. Hasanat Zaman, and Dr. Mohammed Islam for their guidance, support, encouragement, and patience during my graduate study. I appreciate my family's endless spiritual encouragement and trust, which was instrumental to accomplish this dissertation. I would like to thank my parents, brothers, sisters, and beloved wife for their continued sacrifice and moral support. They always aimed to motivate me with their inspirational words even though I was away from them thousands of miles.

During my study, I met many colleagues who assisted me immensely. Many thanks to all my colleagues at the Centre for Risk, Integrity and Safety Engineering (C-RISE), especially Dr. Hondanaidelage Fernando, and the National Research Council (NRC) team.

Finally, I would also like to gratefully acknowledge the financial support the Libyan government and the Ministry of Education provided.

Table of contents

List of tables

List of figures

List of symbols

η	Position vector; given relative to NED-frame
ν	Velocity vector; given relative to BODY-frame
x	Position along the xn-axis
y	Position along the yn-axis
ψ	Angle about the zn-axis
u	Speed in the xb-direction
v	Speed in the yb-direction
r	Angular speed about the zb-axis
τ	Force and moment vector
$\dot{\eta}_c$	Current speed; given relative to the NED frame
v_r	Vessel speed relative to fluid; given relative to the BODY frame
x_G	x coordinate of center of gravity

List of abbreviation

ADI	Alternative directional implicit
DGPS	differential global positioning system
DOF	Degrees of freedom
DP	dynamic positioning
IRW	Irregular wave
GRV	Gaussian Random Variable
EKF	extended Kalman filter
ENMPC	economic nonlinear model predictive controller
HST	DP head seas test
GPS	Global Positioning System
GNMPC	Green Nonlinear model predictive control
LF	low frequency motions
LP	Linear programming
LQR	Linear quadratic regulator
LPT	large position setpoint changes test
MIMO	multiple input multiple output
MIZ	marginal ice zone
MRPID	multi-resolution PID
MPC	Model predictive control
MPM	modified Pierson–Moskowitz
MSS	Marine Systems Simulator
NED	North-east-down

NMPC	Nonlinear model predictive control
NPID	non-linear proportional integral and derivative
NPO	non-linear passive observer
OAT	DP oblique angles test
OEB	Offshore Engineering Basin
OPC	Open Platform Communications
PID	proportional integral derivative control
PID-AFB	PID with acceleration feedback
RAO	Response amplitude operators
RMSE	Root Mean Square Error
RW	Regular wave
SMC	sliding mode control
UKF	Unscented Kalman filter
WF	wave frequency motions
WNW	White noise wave
WT	wavelet transforms

Chapter 1

Introduction

1.1 Background and Motivation

Dynamic positioning is a vital technology for modern marine vessels, particularly in offshore industries such as oil and gas exploration, subsea construction, and vessel-to-vessel transfers. These industries require vessels to remain in a fixed position for prolonged periods despite external forces such as wind, waves, and currents. Dynamic positioning enables a vessel to maintain a stable position without the need for anchors and mooring lines, which reduces the risk of damage to the seabed and decreases maneuverability. The process of dynamic positioning involves using sophisticated computer-controlled systems to monitor and analyze the vessel's movement, position, and external forces. The system then calculates and executes the appropriate thruster commands to maintain the vessel's position and heading. This is achieved through the use of sensors, including GPS, gyroscopes, and motion sensors, which continuously provide real-time data to the control system. Dynamic positioning is essential for marine safety and efficiency, as it reduces the risk of collisions and allows for safer and more efficient vessel-to-vessel transfers. The technology also enables offshore operations in harsh weather conditions, where traditional anchoring methods may not be feasible. Furthermore, dynamic positioning increases

operational flexibility, as vessels can be repositioned quickly and efficiently, which is particularly important in emergency situations. DP technology is essential for offshore operations, such as drilling, subsea construction, and support vessels for oil and gas platforms. DP systems must be able to operate in different sea states, which pose various challenges to the performance and stability of the vessel. Moreover, DP operations require significant amounts of energy, which can have a significant impact on the environment and increase the operational costs of the vessel.

This research aims to address these challenges by evaluating the performance of DP control systems for different sea states, modeling disturbances in harsh environments, and developing an energy-efficient DP controller for high sea conditions. However, one of the greatest threats to the Dynamic Positioning (DP) and Autonomous control systems of vessels and offshore installations is the multi-directionality of drifting sea ice with a wide variety of types and forms, ranging from isolated first-year floes to compacted multi-year ridges, [1]. In the sub-arctic, marginal ice zone (MIZ, the first ice-infested area encountered from the open ocean), wind, waves and sometimes current are present beside the broken ice field. This creates a very complex environment for offshore operations, particularly for DP operations. The already complicated icefield and vessel interaction get further complicated by waves as the ice-field characteristics change in the presence of waves in a complex manner and vice versa. The DP or autonomous control systems in the market today do not consider the forces and movements that exist in such a highly demanding environment. Numerical modelling and validation of these interaction phenomena in all possible environmental cases are essential and a key to understanding the problem and designing both the floating and control systems. Modelling and simulation of environmental disturbances for ocean surface vehicles have been used in ship simulators for naval training and ship hull designs [2]. Numerical simulations of the Arctic Ocean dynamics can be useful for designing, developing, testing, and validating DP and Autonomous ships/offshore platforms in harsh environment simulations [3]. Simulation technology needs to be developed to predict the expected loads on these systems due to the complex interactions with the disturbances. Modelling

complex environmental disturbances and their loads on the systems is an essential and critical component of such simulations. This work discusses the challenges faced by maritime operations in far offshore regions due to environmental factors such as larger waves, stronger winds, and turbulent surface currents. These disturbances can cause excessive wear and tear in thrusters and reduce energy efficiency. This work also discusses different types of filters and controllers that have been used to deal with these challenges, including nonlinear passive observers, Kalman filters, and model predictive controllers, and proposes a new controller called Green-NMPC that is based on an economic model predictive controller structure and uses a UKF-based observer module to filter out high-frequency noise. The proposed controller aims to minimize the operational cost of the DP operation, specifically the thruster demand, and thus wear and tear of the thruster without compromising the position constraints.

In summary the major challenges for DP systems are as follows:

1. Harsh Ocean Environments: DP systems operate in demanding ocean conditions, including large waves and high wind gusts.

2. Energy Consumption: These operations consume substantial energy to counteract environmental forces and maintain vessel position. Consequently, operational costs and emissions increase.

3. Energy Efficiency: There is a pressing need to enhance the energy efficiency of DP systems. Doing so not only reduces costs but also minimizes greenhouse gas emissions.

4. Thruster Strain: The constant strain on thrusters during DP operations results in accelerated wear and tear. As a consequence, supply vessels require more frequent maintenance and repairs, leading to additional costs.

1.2 Research objectives

This research focuses on developing a new energy-efficient DP controller capable of operating under harsh environmental conditions. The main tasks to attain the goal are given below:

1. Develop models of wave, current, wind, and ice that comply with the real-life simulation requirements and adequately capture the dynamic characteristics of the most relevant physical processes. The external disturbance models are then used in the development and evaluation of the most effective control scheme for different extreme sea conditions.

2. Evaluate the performances of a set of control schemes commonly used for DP system.Thus, linear and nonlinear model predictive control (MPC), the nonlinear proportional integral and derivative (PID) control, the sliding mode control (SMC) as well as the multi-resolution PID (MRPID) control schemes are evaluated for moderate and extreme sea states. The outcome of this study provides a clear picture of the current state of DP controller as well as the need for future research.

3. Theoretically develop an energy-efficient controller. The goal of the proposed controller is to reduce the energy demand of the vessel by minimizing unnecessary thruster demand. The controller is based upon the theoretical framework of the economic NMPC (ENMPC). ENMPC allows one directly incorporate the economic objectives in the NMPC optimization algorithm. The controller is extensively tested in simulation environment.

4. Upon satisfactory performance in the simulation environment, implement the NMPC and an energy efficient Green NMPC controller at National Research Council's wave basin. This is one of the very few experimental setup where controllers can be tested in a controlled environment with varying wave conditions.

1.3 Thesis Structure

This research is presented in a manuscript-style which includes two published journal articles, and two conference proceedings. This thesis consists of six chapters, Chapter 1 discusses the introduction and objective. Chapter 2 covers a brief literature review on DP control systems. Chapter 3 focuses on improved models of environmental disturbances including wave, wind, current, and ice. Chapter 4 covers performance evaluation of DP; various conventional DP systems including PID, NPID and MPC are cosidered for different sea states. It also proposes a new version of PID called multi Resolution PID (MRPID) for DP. Chapter 5 covers development of an energy efficient DP controller, the proposed controller called Green NMPC is based on the theory of Economic NMPC. The performance of the controller is compared with benchmark NMPC and PID controllers. Chapter 6 describes the experimental implementation and validation of the energy efficient DP controller. The controller was implemented on scaled model of Magne Viking supply vessel. Controller performances were compared with benchmark NMPC and PID controllers. Finally Chapter 7 presents the conclusions drawn from this research and outlines scopes for future works.

References

[1] Metrikin, I. Experimental and numerical investigations of dynamic positioning in discontinuous ice. *NTNU* (2015).

[2] Sandaruwan, D., Kodikara, N., Rosa, R., and Keppitiyagama, C. Modeling and simulation of environmental disturbances for six degrees of freedom ocean surface vehicle. *Institute of Physics: Colombo* (2009).

[3] Zaman, H., Islam, M., Alagili, O., Khan, M., Imtiaz, S., and Ahmed, S. Efficient modelling of harsh environment disturbances for dp and autonomous ships simulations. In *International Conference on Offshore Mechanics and Arctic Engineering* (2021), vol. 85161, American Society of Mechanical Engineers, p. V006T06A067.

Chapter 2

Literature Review

2.1 Dynamic Positioning Fundamentals

A dynamic positioning (DP) system, according to the International Marine Contractors Association, is "a system which automatically controls a vessel's position and heading exclusively by means of active thrust" [19]. The purpose of DP systems is station keeping, i.e. to maintain a vessel at a set position with a fixed heading. The first DP system, which consisted of an analogue control system getting position reference via a taut wire, was installed on the drilling ship Eureka in 1961. Station-keeping activities had previously been carried out using jack-up barges and anchor spreads. Compared to the pre-existing jack-up barge and anchoring approaches, station keeping is now achievable at higher depths and with a considerably reduced setup due to the introduction of DP-capable vessels. The vessel has good maneuverability and may be positioned in places where anchoring is neither possible or desirable, such as coral reefs, because it is not dependent on fixed mechanical equipment or anchors. All these methods have benefits and drawbacks, but the addition of DP systems considerably extended the range of feasible operations. The risks of system failures, high fuel costs are some drawbacks of DP systems. It can be argued that as the technology develops, some of the drawbacks of DP systems will be overcome.

A triplet of actions must be carried out for DP systems to be used for accurate low-speed trajectory following, assisted anchoring, weathervaning, and station keeping. An accurate estimate of the vessel's position and heading must be maintained, the forces and moments required to counteract environmental disturbances and position deviation must be calculated, and the vessel's propulsion unit must apply these forces. A typical DP system's functionality is frequently broken down into a set of different sub-systems, including:

- Operator system
- Position and heading reference systems
- Estimators, including signal processing
- Guidance, navigation, and control units
- Thrust allocators.
- Propulsion units including power generators.

Where it is stated that a system's strength is determined by its weakest link, the connections between these systems are depicted in Figure 2.1. Numerous commercial providers of full DP systems exist, although Kongsberg Maritime [23] is the biggest. These commercial systems include a variety of operational modes, including station maintenance, manual operator control, combined manual and automatic control, low-speed tracking, and target following. Commercial DP systems must adhere to several safety and dependability standards that are upheld by international certifying organizations including Det Norske Veritas, Lloyd's Register of Ships, and the American Bureau of Shipping.

2.2 Station Keeping of Marine Vessels

The floating vessels are maintained in position by position mooring (PM) either exclusively by thrusters known as dynamic positioning (DP) or exclusively by thruster assisted position mooring (PM) systems. Positioning control is used to refer to either

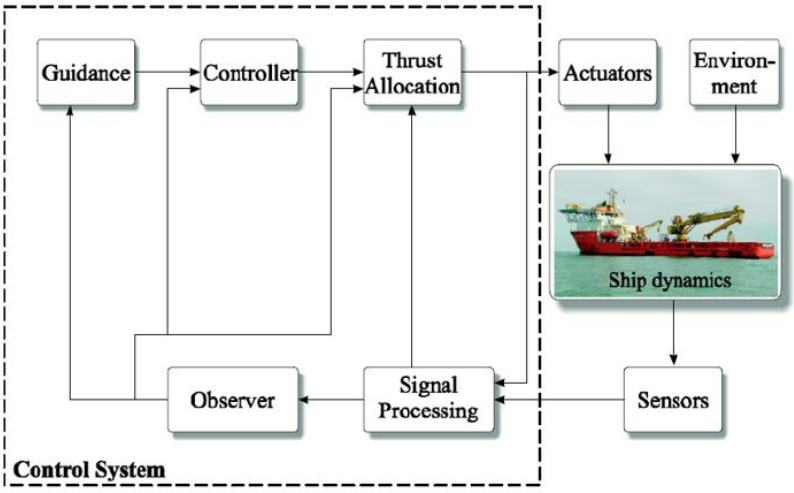

Figure 2.1: Figure depicting control part of DP system. Courtesy of [21].

PM or DP in this context [37]. The first DP systems for regulating yaw, surge, and sway motion were introduced in the 1960s. There were around 65 DP-equipped ships in 1980; by 1985, there were 150 such ships. About 200 ships with DP systems were built each year around the world between 2002 and 2003. Currently, more than 1000 ships have DP systems tailored for various purposes [34]. Most marine applications for DP systems include cable laying, pipe laying, anchor handling, platform supply, exploration drilling, production drilling, shuttle tanker off-take, and floating production. Other ship types, like cruise ships, naval ships, and fishing vessels, besides those utilized in the offshore industry, are increasingly using DP systems. It's interesting to note that cruise ships operating in the Caribbean are prohibited from anchoring to prevent potential damage to the coral reefs, necessitating the use of DP system. For military weapons to be able to aim at the proper targets, navy ships need to be in an exact position. As a result, the market for DP systems offers promising futures.

2.2.1 Low Speed Maneuvering and Transit

A marine vessel must maintain its assigned speed along a path while in low-speed maneuvering control. Traditionally, the two goals have been accomplished separately

in low-speed maneuvering [28]. While the operator assigns the speed, the ship's control system automatically sails it along the predetermined path. In 2005, [32] and [30] proposed adaptive maneuvering control, which combines the two control objectives into a single task. This work was an expansion of [31]'s proposal for robust output maneuvering for the class of nonlinear systems. The ship must transit on a fixed or altered heading due to the autopilot system. [25] proposed the PID controller for the heading and the model for the vessel's heading angle. The nonlinear damping was added to the control plant model by [26]. The nonlinear state space equation was created by [7] for station keeping and low-speed maneuvering [27].

2.2.2 Development of Estimation and Control Systems for DP

The requirement for a position reference system and the requirement that the vessel be able to apply individual forces and moments in the various degrees of freedom (DOF) were two crucial factors in the lengthy development period. Fully actuated vessels can apply separate forces and moments in all DOFs. Figure 2.2 depicts the thruster arrangement of a fully actuated vessel that can apply independent forces and moments in all DOFs. The initial DP systems used low-pass and notch-filtered position measurements with linear decoupled PID controllers in cascade for each DOF. Early DP systems utilized single input, single output PID controllers along with traditional low-pass and/or notch filters. Introducing phase lag and subpar wave filtering properties are disadvantages of low-pass and/or notch filter observer. Also unavailable are non-measurable states like velocity. Additionally, the controller has no model prediction or dead reckoning options in the event of measurement loss. The surge, sway, and yaw motions are connected from a hydrodynamic perspective, but the single-input, single-output PID controller views each motion as independent, which negatively impacts the performance of maritime boats equipped with such systems. [3]-[4] and [29] introduced more sophisticated techniques, including the model-based observer employing Kalman filter theory to avoid the time delay in

estimating and the multi-variable output feedback PID controller for superior performances. [10] demonstrated the connection between notch filter and Kalman filter observers. The expanded Kalman filtering techniques and stochastic optimum control theory, which are discussed in ([6],[9],[11],[12],[13], and [14]), were made possible by the Kalman filter and the multioutput PID controller. A summary of important studies on DP that have used different control techniques is shown in Table 2.1.

Table 2.1: List of the DP controllers that have been documented in the literature.

Reference	**Type of Controller(s)**	**Proposed work and conditions**
[33]	Identification system	For the purpose of automatic control design, 1. The numerical values of the model's parameters are determined through towing tests. 2. Adaptive maneuvering experiments for a scaled-down ship in a marine control laboratory.
[38]	Multivariable control law	The research proposed a DP control law with roll and pitch dampening for small-waterplane-area marine vessels.
[24]	PID	Case(1): single-output PID Case(2):hybrid controller using multi-output PID with position measurement. Case(3):hybrid controller using multi-output PID with position measurement and acceleration measurements.

Reference	**Type of Controller(s)**	**Proposed work and conditions**
[40]	Fuzzy controller	This paper's nonlinear fuzzy controller was developed as a gain scheduled PID approach with "soft" transitions between controller regimes.
[18]	SMC	1. This study suggests a control strategy based on the uncertainty and disturbance estimator (UDE) and sliding mode control (SMC). 2. While the SMC allows the vessel to follow its trajectory, the UDE determines the overall disturbance in the DP vessel.
[44]	MPC	A novel dynamic optimization method adopting the model predictive control (MPC) strategy is proposed.
[16],[45],[39]	NMPC	These works propose an MPC-based control algorithm for the DP problem. This algorithm consists of two stages: 1. The linear stage, which is activated when it approaches the required position. 2. The nonlinear stage, which employs a nonlinear predictive model.

Reference	Type of Controller(s)	Proposed work and conditions
[20],[1]	NMPC, LMPC, PID	In these studies, the following two features relating NMPC scheme are presented: 1. Sideslip angle compensation. 2. Environmental disturbance counteraction for the position and velocity tracking of underactuated surface vessels as well as collision avoidance of static and dynamic objects.
[5]	NDO-NMPC, DO-LMPC	1. The nonlinear disturbance observer NDO is used to assess disturbances, which were unknown in the past. 2. The disturbance estimations are then added to the receding optimization problem to create the NMPC.
[17]	Lag-NMPC, Lag-LMPC, NMPC	The article presents a robust nonlinear model predictive control strategy for ship dynamic positioning using the Laguerre function.
[15]	ENMPC	Economic nonlinear model predictive control (NMPC) techniques where the stage cost does not penalise the distance to a predefined equilibrium.

Reference	Type of Controller(s)	Proposed work and conditions
[2]	Green-NMPC, NMPC, and PID	This paper aims to minimize thruster demand while maintaining position constraints by using Green-NMPC control. The simulation conditions involved varying sea states.

The integral controller is used to counteract the mean environmental loads brought on by wind, wave, and current, while feedback proportional and derivative control actions are employed to adjust for dynamical environmental pressures. The PID controller gain matrices' tuning has a big impact on how well a vessel performs. For instance, if the integrated controller is not properly tuned, the vessel may drift away, a condition known as drift-off. [36] suggested a design for controller gain matrices based on the LQG algorithm to address drift-off concerns. The nonlinear back-stepping controller was proposed by[21]. The observer and controller are the main implementaion blocks in the DP system studies listed above. Model predictive controllers (MPC) are being considered for use in DP applications due to the use of model-based filters. Since the controller is model-based, model-based filters like the KF and EKF perfectly match it. Furthermore, MPC minimizes the offset over a prediction horizon to determine the control action. As a result, the controller has a long-term perspective and does not act overly controlling immediately. The literature has reported on using nonlinear model predictive controllers (NMPC) and linear MPC in high- and low-speed reference tracking and station-keeping [46]. [45] used a linear MPC for DP application on a semi-submersible platform. A relaxed dynamic positioning control technique utilizing NMPC was introduced by [22].[20] estimated states and unknown disturbances using an NMPC method and two tightly connected UKFs. Real-time performance evaluation of the controller was conducted on a high-fidelity simulator. In summary, first- and second-order wave frequencies were filtered out by the controllers described in the literature using a variety of model-based filters. Utilization of the controller configuration to handle the wave frequencies and noise has not received as much attention. Additionally, maintaining

the position tightly has been the main goal of the control objectives. As a result, these controllers frequently impose high and unpredictable control demands. This may significantly shorten the thrusters' usable lives. These control needs are sometimes artificially reduced by imposing a ramp rate, introducing move accumulation, and applying a filter. Meanwhile, all these techniques are ad hoc; therefore, they don't provide the best control performance. While PID control is a widely used and effective method for dynamic positioning in various applications, including supply ships, it does have limitations, particularly when operating under harsh environmental conditions. Some of the key limitations include:

A. Inability to Handle Nonlinearities: PID controllers assume that the system is linear. Hence, they could find it difficult to deal with nonlinearities in the dynamics of the ship or external environmental factors like inconsistent currents or extremely high waves.

B. Restricted flexibility: PID controllers may encounter difficulties in adjusting to swiftly changing environmental conditions. Unexpected and extreme events, like powerful wind gusts or choppy waves, might cause delayed reactions and make it harder to maintain an exact posture.

C. Sensitivity tuning: PID control requires precise tuning of the derivative, integral, and proportional gains in order to achieve optimal performance. However, the ideal tuning parameters could change depending on the surroundings, making the controller sensitive to variations, and perhaps producing less-than-ideal results.

D. Limited Predictive Capability: PID controllers are unable to predict effect of potential environmental disturbances. The controller could find it difficult to counteract environmental forces in extreme sea conditions, which could cause it to stray away the intended position.

E. Need for Manual Tuning: Manual tuning might be time-consuming and may not ensure robust operation in all environmental conditions, yet manual tuning

is frequently necessary to achieve optimal PID controller performance.

F. Traditional controllers are susceptible to the high frequency disturbances which can cause excessive thruster movements leading to wear and tear and higher energy consumption.

In order to enhance the functionality of dynamic positioning systems, reliable control that can satisfy all the needs of DP operations in harsh environmental circumstances must be identified. Nonlinear model predictive control (NMPC) can be considered in more extreme environments. NMPC is a sophisticated control strategy that accounts for nonlinearities in system dynamics and can handle complex processes. However, like any control method, NMPC also has limitations, especially when applied to dynamic positioning operations in harsh environmental conditions.

A. Computational Complexity: NMPC involves solving optimization problems at each time step, which can be computationally demanding. In harsh conditions where rapid adjustments are required, the computational burden may become a limitation, potentially leading to delays in control action.

B. Sensitivity to Model Accuracy: NMPC relies on an accurate dynamic model of the ship. In harsh environmental conditions, where the dynamics may be challenging to model accurately, inaccuracies in the model can lead to suboptimal control performance.

C. Tuning Requirements: NMPC often involves tuning several parameters, including the prediction horizon and control weighting factors. Achieving optimal tuning may take a lot of effort and time, and the performance of the controller can be sensitive to these parameters.

D. Measurement Noise: NMPC relies on accurate measurements for feedback. In real-world scenarios, sensor measurements may be subject to noise, and the controller may need to incorporate additional strategies, such as filtering or advanced sensor fusion techniques, to mitigate the impact of noisy measurements.

Despite these limitations, NMPC remains a powerful tool for dynamic positioning, especially in scenarios where accurate modelling and real-time optimization are crucial. Ongoing research and algorithm advancements may address some of these limitations and further enhance the applicability of NMPC in challenging, extreme sea environments. To raise NMPC's level of performance, from the economic NMPC, the Green NMPC was conceptualized to decrease gas emissions, lower energy consumption in thrusters, and lower maintenance costs by lessening the strain on the thrusters, hence extending their lifespan.

2.2.3 State, Parameter and Disturbance Estimation for DP

The DP system requires measurements of heading and position. Gyrocompasses and the Global Positioning System are the easiest ways to get these, although any precise position reference system will work. Inertial navigation systems may measure the motion and acceleration of the vessel; however, they are frequently not available due to financial constraints. It is necessary to estimate the vessel's velocity using the available observations and a model of the dynamics of the vessel. The model should also try to account for the effects of outside disturbances. The vessel velocity and disturbances estimations will undoubtedly be improved by more precise modelling and optimal model usage. Finding a model that sufficiently approximates the complex vessel mechanics and the much more complicated systems characterizing the environmental disturbances constitutes the modelling challenge. In a real implementation, the estimator may additionally handle errors, perform defect detection, and sensor integration, which is the task of merging measurements from several sensors. The model-based state estimator is also accountable for maintaining an estimate using only the mathematical model, or dead reckoning if measurements are lost. Additionally, estimates of the disturbance forces affecting the vessel due to the disruptive impacts of the sea, wind, and current are desired by the estimator. The wind speed and direction are frequently just measured, and the forces caused by wind disturbance are approximated using a look-up table. The forces caused by waves and currents are more challenging to quantify because there are no measurement tools

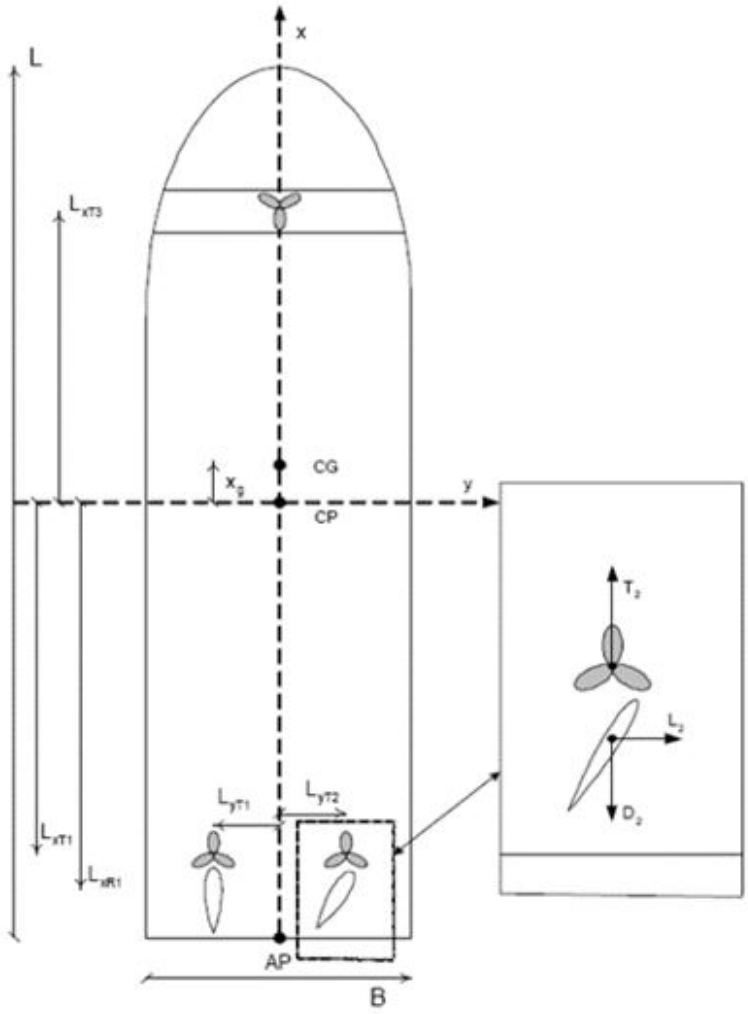

Figure 2.2: Illustration depicting the actuator configuration of Cybership II. Courtesy of [32].

for them, and they are not easily distinguishable from other effects. As a result, they are frequently combined rather than divided into low-frequency (LF) and high-frequency (HF) components. The HF component, also known as wave-frequency (WF), is primarily caused by oscillating wave-induced forces, whereas the LF components manifest as drift forces. The motion from the LF component and the WF

component are presumed to be super-positioned, as shown in Figure 2.3. The vessel

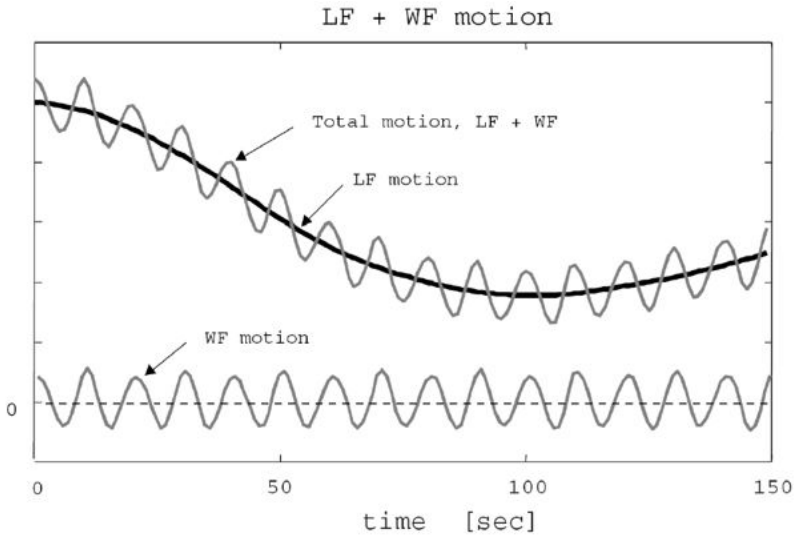

Figure 2.3: Illustration depicting LF and WF motion. Courtesy of [8].

usually cannot counterbalance the motion caused by the WF components because it moves at a rate far quicker than its bandwidth. Since no greater performance can be attained, attempting to counteract them will result in unnecessary strain on the actuator system and energy waste. To eliminate the WF components, wave-filtering is used for motion estimations.

The Kalman filter, an optimum filtering technique, was suggested for implementation in [4]. The initial applications used heading-dependent Kalman gains with gain-scheduled linear approximations about the yaw axes. Due to the many tuning options, these methods were challenging. Later implementations greatly reduced the number of tuning parameters by using an expanded Kalman filter and included a framework for parameter estimation; for example, see [9]. Nonlinear passive observers used in recent methods by Strand and Fossen are easier to tune [41]. The tendency has been to create global observers, which has reduced the number of tuning parameters. Adaptive estimators are also offered [43] that estimate vessel parameters and gains for changing sea states.

The nonlinear passive observer was created as a result ([9]; and [43]). [9] introduced the passive nonlinear observer and suggested the design of observer gains based on passivity. They also provided formal stability proof for the observer. [30] expanded the passive nonlinear observer by including recursive adaptive wave filtering in order to have more effective filtering for the wave frequency (WF) motions. The difficulty in tuning is a drawback of the nonlinear passive observer with recursively adaptive WF filtering [43].

Recently, efforts have been made to increase the DP vessels' performance under challenging conditions. Instead of combating the wave frequency (WF) motions frequently brought on by first-order wave loads, the DP system typically counteracts the low frequency (LF) motions brought on by wind, current, and slowly altering drift wave loads. In order to isolate the LF motions for feedback control from the overall motions, the traditional observers with wave filtering can estimate the WF motions. This approach is successful in areas with moderate seas. Separating WF and LF motions becomes unclear in extreme sea conditions, especially, when the WF motions are low frequency and inside the LF domain. In addition to wind-generated waves, swell waves, which are frequently enormous and have lengthy periods, may be present [42]. As a result, both WF and LF motions must be corrected for by the DP control system. [35] suggested an observer for the output PID controller without WF filtering to solve this issue. As opposed to simply LF motions under typical environmental conditions, the projected states include all motions.

References

[1] Abdelaal, M., Fränzle, M., and Hahn, A. Nonlinear model predictive control for trajectory tracking and collision avoidance of underactuated vessels with disturbances. *Ocean Engineering 160* (2018), 168–180.

[2] Alagili, O., Khan, M. A. I., Ahmed, S., Imtiaz, S., Zaman, H., and Islam, M. An energy-efficient dynamic positioning controller for high sea conditions. *Applied Ocean Research 129* (2022), 103331.

[3] Balchen, J. G., Jenssen, N. A., Mathisen, E., and Sælid, S. A dynamic positioning system based on kalman filtering and optimal control. *IEEE* (1980).

[4] Balchen, J. G., Jenssen, N. A., and Sælid, S. Dynamic positioning using kalman filtering and optimal control theory. In *IFAC/IFIP symposium on automation in offshore oil field operation* (1976), vol. 183, Amsterdam, Holland, p. 186.

[5] Deng, F., Yang, H.-L., Wang, L.-J., and Yang, W.-M. Ukf based nonlinear offset-free model predictive control for ship dynamic positioning under stochastic disturbances. *International Journal of Control, Automation and Systems 17*, 12 (2019), 3079–3090.

[6] Fossen, T. Guidance and control of ocean vehicles. john willey & sons. *Inc., New York* (1994).

[7] Fossen, T. I. A nonlinear unified state-space model for ship maneuvering and control in a seaway. *International Journal of Bifurcation and Chaos 15*, 09 (2005), 2717–2746.

[8] Fossen, T. I., and Strand, J. P. Passive nonlinear observer design for ships using lyapunov methods: full-scale experiments with a supply vessel. *Automatica 35*, 1 (1999), 3–16.

[9] Fung, P., and Grimble, M. Dynamic ship positioning using a self-tuning kalman filter. *IEEE Transactions on Automatic Control 28*, 3 (1983), 339–350.

[10] Grimble, M. Relationship between kalman and notch filters used in dynamic ship positioning systems. *Electronics Letters 13*, 14 (1978), 399–400.

[11] Grimble, M., Patton, R., and Wise, D. The design of dynamic ship positioning control systems using extended kalman filtering techniques. In *OCEANS'79* (1979), IEEE, pp. 488–497.

[12] Grimble, M. J., and Johnson, M. A. *Optimal control and stochastic estimation: theory and applications*. John Wiley & Sons, Inc., 1986.

[13] Grimble, M. J., Patton, R., and Wise, D. Use of kalman filtering techniques in dynamic ship-positioning systems. In *IEE Proceedings D (Control Theory and Applications)* (1980), vol. 127, IET, pp. 93–102.

[14] Grimble, M. J., Patton, R. J., and Wise, D. The design of dynamic ship positioning control systems using stochastic optimal control theory. *Optimal Control Applications and Methods 1*, 2 (1980), 167–202.

[15] Grüne, L., Pannek, J., Grüne, L., and Pannek, J. Economic nmpc. *Nonlinear Model Predictive Control: Theory and Algorithms* (2017), 221–258.

[16] Guerreiro, B. J., Silvestre, C., Cunha, R., and Pascoal, A. Trajectory tracking nonlinear model predictive control for autonomous surface craft. *IEEE Transactions on Control Systems Technology 22*, 6 (2014), 2160–2175.

[17] Hou, X., Deng, F., Yang, H., Yu, D., Zhang, H., and Li, B. Robust nonlinear model predictive control for ship dynamic positioning using laguerre function. *IEEE Access 10* (2022), 127563–127574.

[18] Hu, C., Wu, D., Liao, Y., and Hu, X. Sliding mode control unified with the uncertainty and disturbance estimator for dynamically positioned vessels subjected to uncertainties and unknown disturbances. *Applied Ocean Research 109* (2021), 102564.

[19] IMCA, A. Guide to dp electrical power control systems. *International Marine Contractors Association(IMCA) http://www. imcaint. com/documents/publications. html* (2016).

[20] Jayasiri, A., Nandan, A., Imtiaz, S., Spencer, D., Islam, S., and Ahmed, S. Dynamic positioning of vessels using a ukf-based observer and an nmpc-based controller. *IEEE Transactions on Automation Science and Engineering 14*, 4 (2017), 1778–1785.

[21] Lindegaard, K.-P. Acceleration feedback in dynamic positioning.

[22] Liu, Z. Sensor fusion and observer design for dynamic positioning. *Ph. D. dissertation* (2015).

[23] Maritime, K., and Benelux, B. Kongsberg maritime. *Internett]. Available: http://www. km. kongsberg. com/ks/web/nokbg0237. nsf/AllWeb/AFA3D0473C700E69C1256C4F003DB3C0* (2018).

[24] Nguyen, T. D., Sørensen, A. J., and Quek, S. T. Design of hybrid controller for dynamic positioning from calm to extreme sea conditions. *Automatica 43*, 5 (2007), 768–785.

[25] Nomoto, K., Taguchi, T., Honda, K., and Hirano, S. On the steering qualities of ships. *International Shipbuilding Progress 4*, 35 (1957), 354–370.

[26] Norrbin, N. H. Theory and observation on the use of a mathematical model for ship maneuvering in deep and confined water. In *Proc. 8th Symposium on naval Hydrodynamics* (1977).

[27] PA, B. A unified mathematical model describing the maneuvering of a ship travelling in a seaway. *Trans RINA 140* (1997), 131–149.

[28] Pettersen, K. Y., and Lefeber, E. Way-point tracking control of ships. In *Proceedings of the 40th IEEE conference on decision and control (Cat. No. 01CH37228)* (2001), vol. 1, IEEE, pp. 940–945.

[29] Saelid, S., Jenssen, N., and Balchen, J. Design and analysis of a dynamic positioning system based on kalman filtering and optimal control. *IEEE Transactions on Automatic Control 28*, 3 (1983), 331–339.

[30] Skjetne, R. The maneuvering problem. *NTNU, PhD-thesis 1* (2005), 95–98.

[31] Skjetne, R., Fossen, T. I., and Kokotović, P. V. Robust output maneuvering for a class of nonlinear systems. *Automatica 40*, 3 (2004), 373–383.

[32] Skjetne, R., Fossen, T. I., and Kokotović, P. V. Adaptive maneuvering, with experiments, for a model ship in a marine control laboratory. *Automatica 41*, 2 (2005), 289–298.

[33] Skjetne, R., Smogeli, Ø., and Fossen, T. I. Modeling, identification, and adaptive maneuvering of cybership ii: A complete design with experiments. *IFAC Proceedings Volumes 37*, 10 (2004), 203–208.

[34] Sørensen, A. Short course on marine control systems. *National University of Singapore, 3rd-5th May* (2004).

[35] Sorensen, A., Lindegaard, K.-P., and Hansen, E. D. D. Locally multiobjective h/sub 2/and h/sub/spl infin//control of large-scale interconnected marine structures. In *Proceedings of the 41st IEEE Conference on Decision and Control, 2002.* (2002), vol. 2, IEEE, pp. 1705–1710.

[36] Sorensen, A., Strand, J. P., and Nyberg, H. Dynamic positioning of ships and floaters in extreme seas. In *OCEANS'02 MTS/IEEE* (2002), vol. 3, IEEE, pp. 1849–1854.

[37] Sørensen, A. J. Structural issues in the design and operation of marine control systems. *Annual Reviews in Control 29*, 1 (2005), 125–149.

[38] Sørensen, A. J., and Strand, J. P. Positioning of small-waterplane-area marine constructions with roll and pitch damping. *Control Engineering Practice 8*, 2 (2000), 205–213.

[39] Sotnikova, M. V., and Veremey, E. I. Dynamic positioning based on nonlinear mpc. *IFAC Proceedings Volumes 46*, 33 (2013), 37–42.

[40] Stephens, R. I., Burnham, K. J., and Reeve, P. J. A practical approach to the design of fuzzy controllers with application to dynamic ship positioning. *IFAC Proceedings Volumes 28*, 2 (1995), 370–377.

[41] Strand, J. P., and Fossen, T. I. Nonlinear passive observer design for ships with adaptive wave filtering. In *New Directions in nonlinear observer design*. Springer, 2007, pp. 113–134.

[42] Torsethaugen, K. Model for a doubly peaked wave spectrum. *SINTEF report STF22 A 96204* (1996).

[43] Torsetnes, G. Nonlinear control and observer design for dynamic positioning using contraction theory. *Director Thor. I. Fossen. Universidad Noruega de Ciencia y Tecnología NTNU, Trondheim* (2004).

[44] Wang, K., Yan, X., Yuan, Y., Jiang, X., Lin, X., and Negenborn, R. R. Dynamic optimization of ship energy efficiency considering time-varying environmental factors. *Transportation Research Part D: Transport and Environment 62* (2018), 685–698.

[45] Wang, Y., Sui, Y., Wu, J., and Jiao, J. Research on nonlinear model predictive control technology for ship dynamic positioning system. In *2012 IEEE International Conference on Automation and Logistics* (2012), IEEE, pp. 348–351.

[46] Yu, S., Li, X., Chen, H., and Allgöwer, F. Nonlinear model predictive control for path following problems. *International Journal of Robust and Nonlinear Control 25*, 8 (2015), 1168–1182.

Chapter 3

Performance Assessment of DP Control Systems for Different Sea States

This chapter was published.

https://ieeexplore.ieee.org/document/9267928

Abstract

Performances of a set of control schemes for dynamic positioning (DP) are studied in this work; DP performance is essential for future developments of autonomous shipping technology. The linear and nonlinear model predictive control (MPC), the nonlinear proportional integral and derivative (PID) control, the sliding mode control (SMC) as well as the multi-resolution PID (MRPID) control schemes are evaluated under two different sea conditions, namely, moderate and extreme seas. Matlab/Simulink models of a full-scale ship and its corresponding scaled model are used to benchmark the efficacy of the controllers. An Unscented Kalman Filter (UKF) is used to estimate vessel motions and to control low frequency (LF) motions while filtering out wave frequency (WF) motions. The tuning of the controllers is also taken into consideration. Of the five controller schemes, the NMPC shows the best ability to efficiently deal with extreme disturbances. Although all of the controllers were able to maintain the ship position under moderate conditions, only the NMPC and the MRPID controllers were able to stabilize the ship under extreme sea states. Findings from this research are expected to help operators of DP systems in choosing the most effective control scheme for different sea conditions. Also, the results are supportive of further control system development for dynamic positioning and autonomous shipping systems.

keywords: Smart sensing, Autonomous ships,dynamic positioning, offshore drilling/production, control algorithms, decision support system, alarm monitoring

3.1 Introduction

As maritime operations move into deeper waters far from the shores, new challenges are emerging. The main concerns are environmental disturbances such as wind gusts, surface currents, and large waves. This type of dynamic and ever-changing environment requires the use of dynamic positioning (DP). Turbulent waters are not only common but can become extreme within a short time period as one travels farther from shore. In response, vessels need to have a robust controller that can manage motion couplings for six degrees of freedom (DOF). Extreme seas are typical in the North Atlantic, occurring around a third of the time (hence, the commonality of the nautical term "on the high seas"). Under conditions of extreme seas, the waves are not only higher than the norm but endure longer. In this case, wave-frequency (WF) motions occur at similar or the same frequency regimes as the vessel's low-frequency (LF) motions. Using a wave filter to separate the WF from the LF under these conditions can be challenging, as critical LF motions that need to be compensated for by the controller get removed by the filter. To resolve this dilemma, [18] suggested not applying the wave filter for extreme sea conditions as a means to keep stability and performance at optimal levels. The suggestion was then tested in [15] and [1]. In both of these studies, the hybrid controller featured a nonlinear passive observer (NPO) without wave filtering and a proportional integral derivative control with acceleration feedback (PID-AFB). Comparisons between simulations of a PID controller with wave filtering and a hybrid controller showed that for varied sea conditions (calm to extreme), the hybrid controller performed better. In [12], a PID-AFB controller was introduced; virtual inertia was included with the physical inertia, and both were increased according to feedback for the system's measured acceleration [12]. In other studies, examining the performance of controllers, sliding mode control (SMC) has been employed to design controllers for use in complex high-order nonlinear dynamic scenarios. Both [7] and [17] utilize the SMC algorithm for multiple input multiple output (MIMO) nonlinear systems, intending to develop a controller that can take into account parameter inaccuracies such as external loads, inertia, mass, damping, and actuators [7], [17]. In [16], wavelet transforms (WT) were employed in a position

control system. The error signal was first divided into components, then multiplied by the respective gains, and finally summed together to determine the final control command. A self-tuning technique that used wavelet networks was proposed for a wavelet PID controller [3]. The Green DP system, which employs MPC, was introduced by [21]. Two studies subsequently applied MPC to a DP system, finding the outcome satisfactory [9], [22]. Constraints posed by DP were then explored in [4]. The non-linear MPC may be employed in both high-speed and low-speed reference tracking and station-keeping [14]. NMPC frames the control problem as seeking a solution for objective functions, such as non-linear system dynamics [5], [25]. NMPC tends to give better outcomes because state and input constraints can be satisfied by computing control commands. A few NMPC-related methods that can be applied to DP problems have been published in the literature. For instance, the study in [14] proposed the use of an NMPC controller in DP coupled with a UKF-based state estimation. However, this proved unsuccessful due to the very poor solutions given for online optimization problems [14]. Researchers in [2] proposed a linear MPC adaptable to semi-submersible platform DP, while those in [23] used an NMPC controller in a simplified non-linear model according to the controller's design requirements. A relaxed dynamic positioning control approach that employed NMPC was introduced in [24]. The research in [13] involved sensor fusion as well as observer design techniques that utilized UKF in DP operations.MPC formulations [11], [20] to solve the DP problem that takes into consideration state and input constraints along with the thruster allocation algorithm (TAA) were also considered in the literature. Note that including TAA in the formulation will result in near-optimal solutions because of crucial restrictions (e.g., rate of rotation and thruster saturation), but it will still make the optimal control problem more complex. Because of this, real-time control computation is likely not a practical approach to this problem [8].

The present paper implements five DP controllers (NMPC, MPC, MRPID, SMC, and NPID-AFB) into full-scale as well as scaled model ships using a non-linear passive observer (NPO) for both moderate and extreme seas to evaluate each controller's performance. The main performance metrics applied in this work are position and

heading (pose) accuracy.

3.2 DP Control Systems

3.2.1 Nonlinear PID with Acceleration Feedback (NPID-AFB)

The proportional integral derivative controller with acceleration feedback (PID-AFB) [12] differs from traditional PID controllers in that it includes an extra inertia term K_m, which feeds back along with the measured acceleration and is included in the system's inertia matrix M. The inclusion of K_m makes the system more robust by reducing its sensitivity to disturbances. The control law depicted in Eqs. 3.1 and 3.2 generate the control input (τ).

$$\tau = \tau_{PID-AFB} = R^T(\psi)\tau_{PID} - K_m\dot{\nu} \tag{3.1}$$

$$\tau_{PID} = -K_p\tilde{\eta} - R(\psi)K_d\nu - K_i\int_0^t \tilde{\eta}(\tau)d\tau \tag{3.2}$$

The control objective is to force $\tilde{\eta} \to 0$ when $t \to \infty$, where $\tilde{\eta} = \eta - \eta_d$ is the error between the actual and desired position. As the aim is station keeping, the desired position is constant and $\dot{\eta_d} \approx 0$. The positive definite gain matrices $K_p \in R^{3\times3}$, $K_d \in R^{3\times3}$ and $K_i \in R^{3\times3}$ belong to the PID-part of the controller. The AFB gain matrix $K_m \in R^{3\times3}$ is chosen as proposed by [1] with $K_m = M^* + \Delta K$, where M^* is a modified inertia matrix $\Big(M^* = [X_{\dot{u}} \quad 0 \quad 0,0 \quad Y_{\dot{v}} \quad 0,0 \quad (N_{\dot{v}} - Y_{\dot{r}}) \quad 0]\Big)$. $\Delta K = \Delta K^T$. The AFB gain matrix is written as:

$$K_m = \begin{bmatrix} K_{11} & K_{12} & 0 \\ K_{21} & K_{22} & 0 \\ K_{31} & K_{32} & 0 \end{bmatrix} = \begin{bmatrix} X_{\dot{u}} + \Delta K_{11} & 0 & 0 \\ 0 & Y_{\dot{v}} + \Delta K_{22} & 0 \\ 0 & N_{\dot{v}} - Y_{\dot{r}} & 0 \end{bmatrix} \tag{3.3}$$

where $X_{\dot{u}}, Y_{\dot{v}}, N_{\dot{v}}, Y_{\dot{r}}$ represent hydrodynamic added-mass terms.

3.2.2 Sliding Mode Control (SMC)

The purpose for using the SMC algorithm [6],[7][17], is to deal with parameter uncertainties for damping and mass as well as for neglected time delays, unmodeled dynamics, and so on [17]. In Eq.(3.4), a tracking measure is described.

$$s := \dot{\tilde{\eta}} + 2\Lambda\tilde{\eta} + \Lambda^T\Lambda \int_0^t \tilde{\eta}(\tau)d\tau \tag{3.4}$$

where s denotes a sliding surface that is dependent on both position error $\tilde{\eta}$ and the NED velocity error $\dot{\tilde{\eta}} = \dot{\eta}$; the tuning parameter, $\Lambda \in R^{3\times3}$ and $\Lambda > 0$, indicate the controller's bandwidth. By describing the virtual reference vector $\dot{\eta_r}$ we can reformulate Eq. (3.4) as:

$$s = \dot{\eta} - \dot{\eta_r} \tag{3.5}$$

$$\dot{\eta_r} = \dot{\eta_d} - 2\Lambda\tilde{\eta} + \Lambda^T\Lambda \int_0^t \tilde{\eta}(\tau)d\tau \tag{3.6}$$

So that

$$\dot{s} = \ddot{\eta} - \ddot{\eta_r} \tag{3.7}$$

In cases where s=0, Eq. (3.7) indicates a sliding surface with $\tilde{\eta}$ converging to zero exponentially. Equations of motion are defined within a NED frame, given the importance of controlling the position. For the implementation, integral part within Eq. (3.7) has been included independent of the control input. In [6], equations of motion have been formulated as:

$$M^*(\eta)\ddot{\eta} + D^*(\eta)\dot{\eta} = b + \tau^* \tag{3.8}$$

where , $M^*(\eta) = R(\psi)MR^T(\psi), D^*(\eta) = R(\psi)DR^T(\psi), \tau^* = R(\psi)\tau_{SMC}$, and

τ_{SMC} as shown in (3.9)

$$\tau_{SMC} = M\dot{\nu_r} + D\nu_r - R^T(\psi)K_d s - K_s \times tanh(\phi^{-1}R^T(\psi)s)) \tag{3.9}$$

where , $M\dot{\nu_r} + D\nu_r$ is the feedforward term, $R^T(\psi)K_d s$ s is the PD controller term and $K_s \times tanh(\phi^{-1}R^T(\psi)s)$ is the robustifying term. Choosing K_s as,

$$K_s \geq \left\| R^T(\psi)b + \tilde{M}\dot{\nu_r} + \tilde{D}\nu_r \right\| + \delta, \delta > 0 \tag{3.10}$$

with K_s dominating any bias or error of the actual or estimated inertias as well as damping uncertainties, and positive constant δ maintaining $K_s > 0$.

3.2.3 Multiresolution PID Control (MRPID)

In MRPID [16], frequency-dependent error components can be multiplied according to the respective gain of each and then summed together. In the present paper, sub-PIDs of every low- and medium-frequency error component are provided, though high-frequency terms are neglected. The technique formulates control commands that denote force and torque inputs for a vessel ($u_A = F_X, F_Y, T$) :

$$u_A = PID_{A,H}e_H + PID_{A,M_1}e_{M_1} + ... + PID_{A,M_{N-1}}e_{M_{N-1}} + PID_L e_L \tag{3.11}$$

The MRPID controller has a large number of tuning parameters, thereby ensuring a better resolution. Error vectors are generated through mirroring and then appending previous error data [16]. Wavelet-based decomposition can then be implemented using the generated error vector, giving error signals in x,y, and ψ. Based on the literature, we choose wavelets, deciding on "Daubechies" of order 4. Then, L = 8 and F = 4 gave N = 2, or two-level decomposition.

3.2.4 Model Predictive Control (MPC)

The model predictive control (MPC) has been widely adopted throughout different industries, as MPC can easily handle constraints. Furthermore, using a model as a means to anticipate future conditions and responses enables both a prediction and subsequent correction aspect. MPC represents a model-based control algorithm whose essential features include feedback correction, receding optimization, and predictive modeling (internal modeling). In this process, the latest measurement readings are obtained during sampling time which are then applied for solving open-loop optimization problems that have been defined as a prediction horizon. The solution provides control sequences whose initial components are applied to the system, and the process begins anew by again finding the latest measurement readings. Fig 3.1 shows a simplified version of MPC structure. In using MPC in a ship dynamic positioning system, low-frequency motion measurements first need to be removed from the vessel's overall position information. Then, the DP vessel's linear low-frequency state-space model needs to be changed to a discrete state equation:

$$x_{k+1} = Ax_k + Bu_k + G\omega_k \tag{3.12}$$

$$y_k = Cx_k + \nu k \tag{3.13}$$

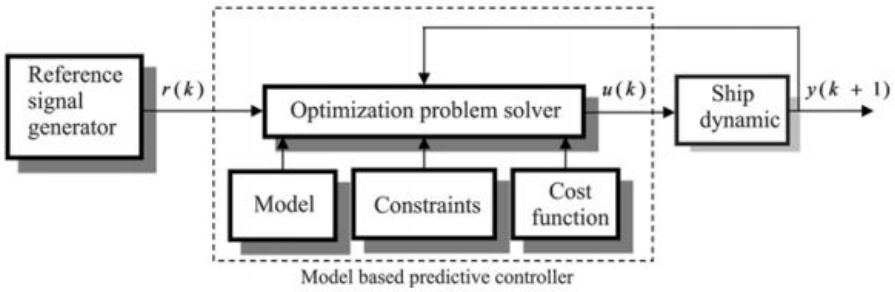

Figure 3.1: The basic structure of model predictive control

Here, the initial state $x_0 = x, x_k$ denotes the state variable vector regarding

velocities and positions, such as sway, yaw and surge, at time k. u_k represent control input vector, ω_k the 3D unmodeled disturbance vector, y_k the output position vector, v_k the Gaussian white noise, and A, B, C, are G indicate the constant matrix.

3.2.5 Nonlinear Model Predictive Control (NMPC)

The latest computing and algorithmic advances have made NMPC the standard technique for designing controllers in non-linear systems that feature state and input constraints. NMPC solves for constrained open-loop optimal control problems in every iteration. Because predictive control relies on full state knowledge, state estimators generally have to be activated, unless a reduced model is used. Usually, the initial control action alone is applied while the remainder are discarded, though they can also be utilized for 'warm-starting' the NMPC for subsequent time instants [9], [22]. NMPC schemes penalize any deviations from their references made by states and inputs. NMPC weights are then chosen in relation to the importance of the deviations. Each iteration of the optimal control problem expressed in Eq. (3.14) is solved by the NMPC, giving an optimal motion command $\{u_k\}_{k=t_0}^{t_0+T_H}$ and state series $\{x_k\}_{k=t_0}^{t_0+T_H}$. The initial control commands of force and torque demands ($[F_{x1}, F_{y1}, T_{\psi 1}]$) are then applied in the system.

$$J_{t_0} = \arg\min_{x,u} \sum_{k=t_0}^{t_0+T_H} \|u_k - u_r\|^2 L + \sum_{k=t_0}^{t_0+T_H} \|x_k - x_r\|^2 M \tag{3.14}$$

$$s.t. x_{k+1} = f(x_k, u_k),$$

$$\mu(u_k, x_k) \leq 0$$

where, L and M, denote the constant positive definite weighting matrices, u_r and x_r represent reference inputs and states, respectively, f indicates the numerical integration for system dynamics over selected time grid, μ expresses constraint function for system inputs and states, and t_0 represents start time of control computations. Note that while system dynamics constraints cover all six of the states $[\eta \quad v]$, only

position and orientation vector η has been penalized, along with control inputs. A pseudo-code for the NMPC algorithm is presented in [10].

3.3 System Modeling and State Estimation

3.3.1 Ship Model

A mathematical control plant model (CPM) describes the most crucial physical characteristics for dynamical processes. CPMs are widely applied in model-based observer or controller design [19]. Equation (3.15,3.16,3.17, and 3.18) expresses a CPM written for DP of extreme seas [18]:

$$\dot{\eta} = R(\psi)\nu \tag{3.15}$$

$$M\dot{\nu} = -D\nu + R^T(\psi)b + \tau \tag{3.16}$$

$$\dot{b} = -T_b^{-1}b + E_b w_b \tag{3.17}$$

$$y = \eta + \nu \tag{3.18}$$

with $\eta \in R^3$ being the position and heading vector, and the velocity vector being $\nu \in R^{3\times3}$. In this formulation, the rotation matrix $R(\psi) \in R^{3\times3}$ changes velocity from a body fixed to a north-east-down (NED) reference frame. The bias model built as state $b \in R^3$ indicates slowly varying environmental forces. This model employs the zero-mean Gaussian white noise vector $\omega_b \in R^{3\times3}$ and disturbance scaling matrix $E_b \in R^{3\times3}$, while $T_b \in R^{3\times3}$ denotes the user-specified diagonal matrix for positive bias time constants. Specifically, here, the matrix $M \in R^{3\times3}$ comprises the inertia matrix for the rigid-body as well as the added-mass terms, whereas linear damping comprises the matrix $D \in R^{3\times3}$. Meanwhile, the controller generates the commanded forces along with the moment vector $\tau \in R^3$. $\tau = (\tau_c + \tau_\omega + \tau_i)$ indicates applied force that has τ_c for the control input, τ_ω designates the wind force and τ_i is the ice load , $y \in R^3$ denotes the sensor output measurement, and $\nu \in R^3$ indicates the measurement noise vector.

3.3.2 Ocean Waves

For the purpose of this study, 'extreme' seas refer to a sea state that is characterized by large wave height ($H_s \geq 9m$) along with peak wave frequency ($\omega_p \leq 0.46rad/s$). 'Moderate' seas here refer to a sea states characterized by moderate wave height ($H \leq 2.5m$) with peak wave frequency ($\omega_p \leq 0.79rad/s$). These sea states are further illustrated in [6]. In this study, we use a MATLAB/Simulink simulator to simulate wave action for extreme seas. The simulator features an environment module that simulates wind, wave, and current specs. We formulated wave amplitude as shown in Eq. (3.19):

$$A = \sqrt{2S(\omega)\Delta\omega} \tag{3.19}$$

with $\Delta\omega$ designating constant difference between frequencies. Amplitude can be utilized for developing time-domain realizations for wave spectra, as in Eq. (3.20):

$$\xi(t) = \sum_{k=1}^{N}\sum_{i=1}^{M}\sqrt{2S(\omega_k,\beta_i)\Delta\omega_k\Delta\beta_i}sin(\omega_k t + \varepsilon_{ki}) \tag{3.20}$$

Where β describes the angle at which waves impact the vessel, ϵ describes phase, and A expresses wave amplitude for the current sea state. Along with wave height H_s and wave period T_s , we can specify sea state according to frequency spectrum, mean wave direction, directional spectrum, as well as how many frequencies and directions appear on the designated spectral grid. We can decrease the amount of harmonic wave components by discarding those that feature negligible energy content. Fig 3.2, below illustrates the wave spectrum with harmonic components, calm sea condition with wave height $H_s = 0.1m$, and harsh sea condition with wave height $H_s = 10m$ and wave number = 400.

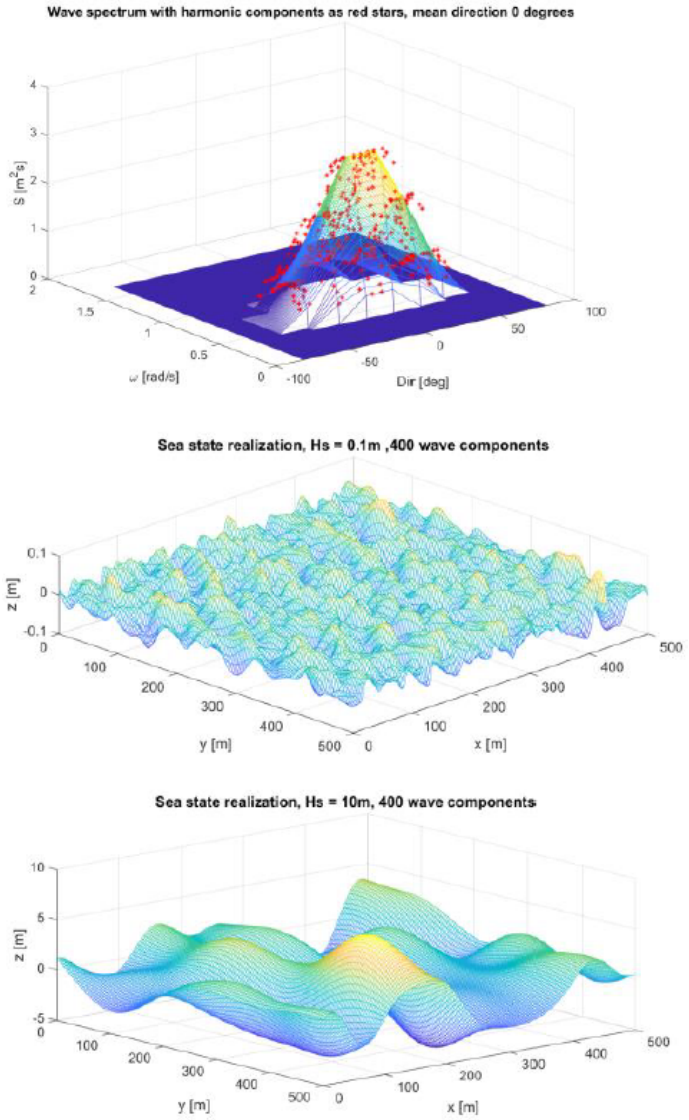

Figure 3.2: Wave spectrum with harmonic components, calm sea condition, and harsh sea condition with wave number = 400.

3.3.3 Wind

Wind can be considered as having two components, namely, a mean component and a fluctuating component (gust). The mean component is reduced in relation to

distance-to- ground, while the fluctuating component remains more or less the same in relation to distance-to-ground [6]. Although comprised of two components, wind is actually a 3D phenomenon that includes velocities of the horizontal plane that are parameterized by velocity (U) and direction (ψ) . Mean velocity $\bar{U}$ for elevation (z) can be expressed as:

$$\frac{\bar{U}(z)}{\bar{U}_{10}} = \frac{5}{2}\sqrt{k}ln\frac{z}{z_0}, z_0 = 10exp(-\frac{2}{5\sqrt{k}}) \tag{3.21}$$

$\bar{U}_{10}$ denotes 1-hour mean wind speed at an elevation of 10 m, while (k) indicates the sea surface drag coefficient. Variations to mean wind velocity can be implemented using a first-order Gauss-Markov process, as expressed in Eq. (3.22)

$$\dot{\bar{U}} + \mu\bar{U} = \omega \tag{3.22}$$

where, ω denotes Gaussian white noise and $\mu \geq 0$ is a constant. Wind direction variations can be implemented using a similar approach, as formulated in Eq. (3.23):

$$\psi + \mu_2\psi = \omega_2, \psi_{min} \leq \psi \leq \psi_{max} \tag{3.23}$$

where ω_2 and μ_2 indicate, respectively, white noise and a positive constant. Like waves, wind gusts are typically described using a spectrum. However, this spectrum uses measurements that have been made over land. More up-to-date measurements provide alternative representations, as shown in Eq. (3.24).

$$S(f) = \frac{4kL\bar{U}_{10}}{(2+\tilde{f}^2)^{\frac{5}{6}}}, \tilde{f} = \frac{Lf}{\bar{U}_{10}} \tag{3.24}$$

With, (L) denoting scaling length, (k) sea surface drag coefficient, and (f) frequency in Hz. The wind gusts are modelled based on a NORSOK wind spectrum that features 100 individual frequency components.

3.3.4 Water Current Model

In surface vessels, a 2D current model suffices. For current measurements obtained from magnitude V_c and direction of NED frame ψ_c , a current velocity vector ν_c can be expressed as in Eq. (3.25):

$$\nu_c = [V_c cos(\psi_c), V_c sin(\psi_c), 0]^T \tag{3.25}$$

Any variations found in current velocity can be implemented using the first-order Gauss-Markov Process, as follow:

$$\dot{V_c} + \mu V_c = \omega \tag{3.26}$$

Where (ω) denotes Gaussian white noise, and $(\mu \geq 0)$ indicates a constant. If $\mu = 0$, this would denote a process of random walk, with magnitude of velocity being constrained by saturation elements, as expressed in Eq. (3.27):

$$V_{c,min} \leq V_c \leq V_{c,max} \tag{3.27}$$

Current direction variations can be implemented in the same way, as shown in Eq. (3.24).Like wind, current can also be divided into two components, namely wind-generated and tidal-generated currents. However, unless clear measurement data are available, the two components are better considered as one [6].

Occasionally, the variations in current according to depth are required. In these cases, should no actual field measurements be accessible, DNV advises using the current profile $(V_c(Z))$, with (z) as depth (positive downwards):

$$V_c(Z) = V_{c,tide}(Z) + V_{c,wind}(Z) \tag{3.28}$$

$$V_{c,tide}(Z) = V_{c,tide}(\frac{h - Z}{h})^{1/7}, for \quad Z \geq 0 \tag{3.29}$$

$$V_{c,wind}(Z) = V_{c,wind}(\frac{h_0 - Z}{h_0})^{1/7}, for \quad 0 \leq Z \leq h_0 \tag{3.30}$$

$$V_{wind}(Z) = 0, for \quad Z \geq h_0 \tag{3.31}$$

where $(V_{c,tide})$ indicates surface level tidal current velocity, $(V_{c,wind})$ denotes surface level wind-generated current velocity, (h) represent water depth, and (h_0) serves as the reference depth of wind-generated currents $(e.g., h_0 = 50m)$. Furthermore, wind-generated current could be expressed as, $((V_{c,wind}) = 0.015\bar{U}10,)$.

3.3.5 Nonlinear Passive Observer (NPO)

The observer is a critical component in the DP system due to its roles (among others) of filtering and state estimation. In instances where sensors fail or are too costly, an observer is able to provide state estimations for non-measured states. Furthermore, if a vessel undergoes signal loss due to a failed sensor, the process of dead reckoning may be employed in the observer's prediction model. In [1], the researchers introduced a

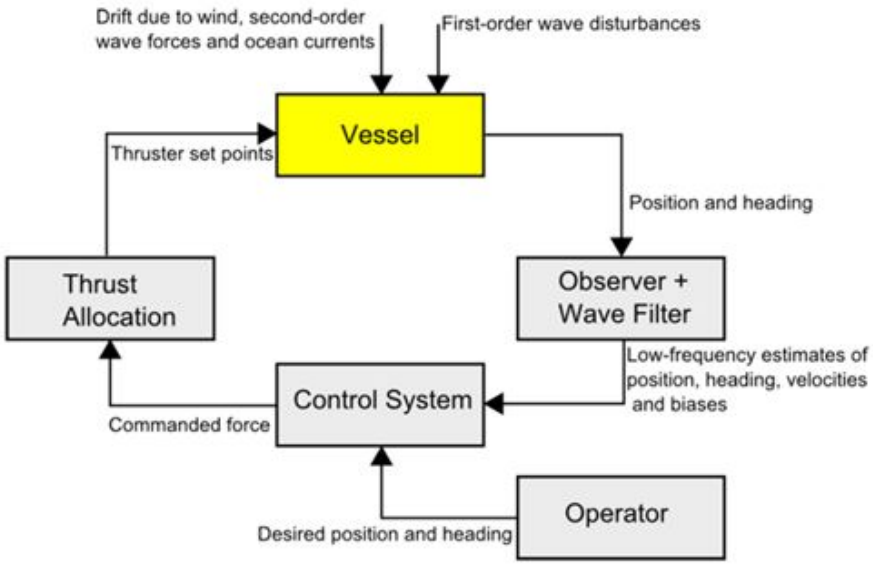

Figure 3.3: Illustration of conventional DP system.

wave-filter less observer for use in extreme seas:

$$\dot{\hat{\eta}} = R(y)\hat{\nu} + K_1\tilde{y} \tag{3.32}$$

$$\dot{\hat{b}} = -T_b^{-1}\hat{b} + K_2\tilde{y} \tag{3.33}$$

$$M\dot{\hat{\nu}} = -D\hat{\nu} + R^T(y)\hat{b} + \tau + R^T(y)K_3\tilde{y} \tag{3.34}$$

$$\hat{y} = \hat{\eta} \tag{3.35}$$

where $\hat{\eta}$ and $\hat{\nu}$ represent estimated pose and velocity vectors, respectively, $\hat{b}$ denotes estimated bias state, and $\hat{y}$ indicates estimated output (the values for matrices M and D appear above).Hence, the rotation matrix can be expressed as $R(y) = R(\psi)$,while $K_1 \in R^{3\times3}$, $K_2 \in R^{3\times3}$ and $K_3 \in R^{3\times3}$ comprise positive definite observer gain matrices.

3.4 Simulation Results

3.4.1 Simulation Setup

The simulations used 3-DOF nonlinear vessel with parameters shown in Table 3.I. Simulation sample time was set as 0.01s, and set-points were given as (0, 0, 0), for X,Y and ψ values. To create the five different controllers, we use a MATLAB/Simulink simulator and toolbox add-ons. The sea state conditions are shown in Table 3.II.

Table 3.1: Specifications of the ship model

Parameters	Units	Full Scale	Down-scale
Length, L	m	88.7	2.275
Breadth, B	m	17.04	0.437
Draught, T	m	5.967	0.153
Displacement	m^3	4508	0.076

Table 3.2: Simulated sea states

Parameters	Units	Moderate	Extreme
Wind Speed	m/s	8.1-10.7	24.6-28.2
Surface Currents	m/s	0.543-0.705	0.85-1.05
Waves, Significant Height, H_s	m	1.25-2.5	9.0-12.5
Peak Wave Frequency ω_p	rad/s	0.79-0.68	0.46-0.39

3.4.2 Down-scale Model with Moderate Sea Conditions

In this study, moderate disturbances acting in X, Y, and Yaw, in the down-scale model were considered. The disturbance loads cannot be used directly to adjust the environmental model in MATLAB Simulink without scaling, and we used the Froude Scaling (1:30) to adjust disturbance loads to the down-scale model. Equality in the Froude number gives similar wave forces acting on the down-scaled model and full-scale model. Fig 3.4 shows the performances of the five controllers considered for this

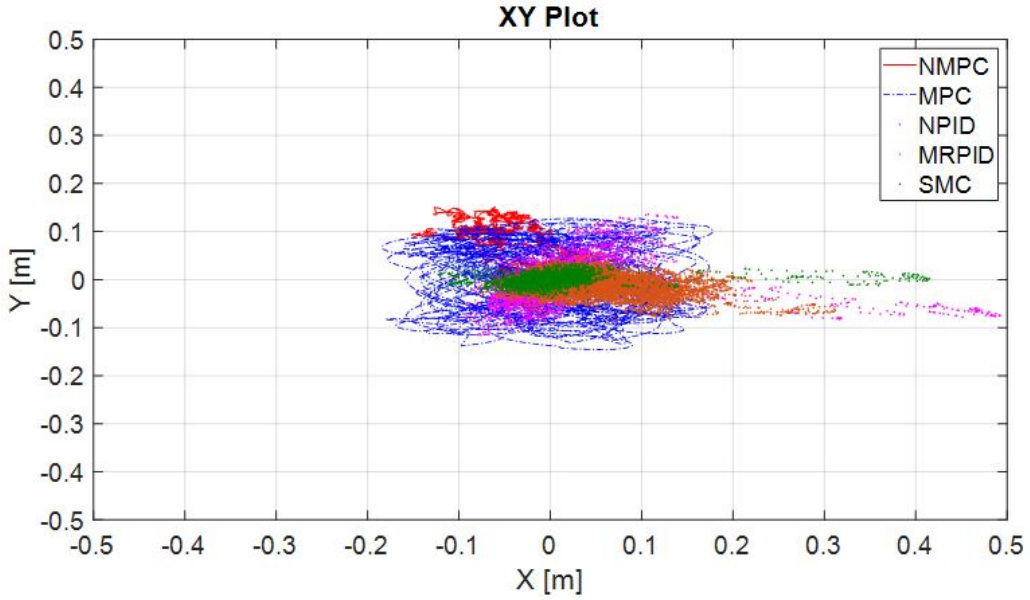

Figure 3.4: X, Y plots of DP with NMPC, MPC, MRPID, SMC, and NPID controllers under low disturbance for the down-scale model.

study. It can be seen that, although there are variations in performance, all of the five controllers are able to stabilize the vessel and maintain its position. A closer look reveals that the NMPC, the MRPID as well as the SMC perform better compared to the MPC and NPID-AFB. Although results are not presented here, for the full scale model with moderate sea conditions, all of the five controllers satisfactorily maintained the position of the vessel.

3.4.3 Full-scale Model with Extreme Sea Conditions

Fig 3.5 shows results for ship position under extreme sea conditions with the full scale model. The results for the NMPC and the MRPID controllers are plotted as the NPID-AFB, MPC and SMC controllers were found to be not able to stabilize the vessel under extreme conditions. The performance of the NMPC controller was comparatively better than that of the MRPID controller for extreme sea conditions. In general, performance of the NMPC was consistently better than other algorithms for both moderate and extreme sea conditions.

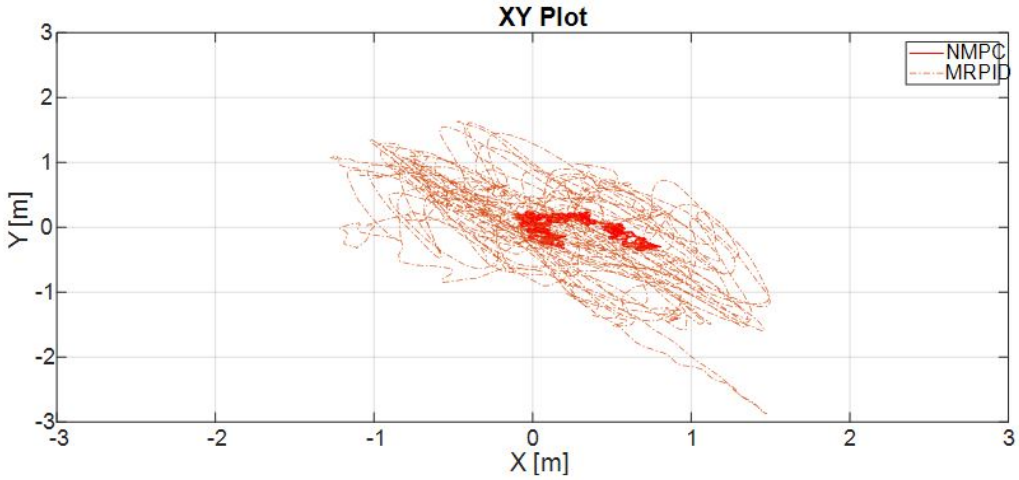

Figure 3.5: X, Y plots of DP with NMPC and MRPID controllers under high disturbance for the full-scale model.

3.5 Concluding Remarks

Based on the simulation study it can be concluded that many of the available control algorithm for dynamic positioning can effectively control the vessel under moderate sea conditions. However, under extreme conditions, the performance may deteriorate to the extent that the controller may fail to stabilize the process. For the extreme sea conditions considered for this study, only the NMPC and the MRPID controllers were able to stabilize the vessel while each of the five controllers effectively maintained the vessels position under moderate sea conditions. It is recommended that the performance of a controller is tested under different conditions before its implementation in cases where sea conditions may become extreme.

References

[1] Brodtkorb, A. H., Sørensen, A. J., and Teel, A. R. Increasing the operation window for dynamic positioned vessels using the concept of hybrid control. In *International Conference on Offshore Mechanics and Arctic Engineering* (2014), vol. 45370, American Society of Mechanical Engineers, p. V01AT01A046.

[2] Chen, H., Wan, L., Wang, F., and Zhang, G. Model predictive controller design for the dynamic positioning system of a semi-submersible platform. *Journal of Marine Science and Application 11* (2012), 361–367.

[3] Cruz-Tolentino, J. A., Ramos-Velasco, L., and Espejel-Rivera, M. A self-tuning of a wavelet pid controller. In *2010 20th International Conference on Electronics Communications and Computers (CONIELECOMP)* (2010), IEEE, pp. 73–78.

[4] Fannemel, Å. V. Dynamic positioning by nonlinear model predictive control. Master's thesis, Institutt for teknisk kybernetikk, 2008.

[5] Findeisen, R., Imsland, L., Allgower, F., and Foss, B. A. State and output feedback nonlinear model predictive control: An overview. *European journal of control 9*, 2-3 (2003), 190–206.

[6] Fossen, T. I. *Handbook of marine craft hydrodynamics and motion control*. John Wiley & Sons, 2011.

[7] Fossen, T. I., and Foss, B. A. Sliding control of mimo nonlinear systems. *mic-journal* (1991).

[8] Fossen, T. I., Lindegaard, K.-P., and Skjetne, R. Inertia shaping techniques for marine vessels using acceleration feedback. *IFAC Proceedings Volumes 35*, 1 (2002), 343–348.

[9] Guerreiro, B. J., Silvestre, C., Cunha, R., and Pascoal, A. Trajectory tracking nonlinear model predictive control for autonomous surface craft. *IEEE Transactions on Control Systems Technology 22*, 6 (2014), 2160–2175.

[10] Jayasiri, A., Nandan, A., Imtiaz, S., Spencer, D., Islam, S., and Ahmed, S. Dynamic positioning of vessels using a ukf-based observer and an nmpc-based controller. *IEEE Transactions on Automation Science and Engineering 14*, 4 (2017), 1778–1785.

[11] Johansen, T. A., and Fossen, T. I. Control allocation—a survey. *Automatica 49*, 5 (2013), 1087–1103.

[12] Lindegaard, K.-P. Acceleration feedback in dynamic positioning. *NTNU* (2003).

[13] Liu, Z. Sensor fusion and observer design for dynamic positioning. *Ph. D. dissertation* (2015).

[14] Mayne, D. Q., Rawlings, J. B., Rao, C. V., and Scokaert, P. O. Constrained model predictive control: Stability and optimality. *Automatica 36*, 6 (2000), 789–814.

[15] Nguyen, T. D., Sørensen, A. J., and Quek, S. T. Design of hybrid controller for dynamic positioning from calm to extreme sea conditions. *Automatica 43*, 5 (2007), 768–785.

[16] Parvez, S., and Gao, Z. A wavelet-based multiresolution pid controller. *IEEE Transactions on Industry Applications 41*, 2 (2005), 537–543.

[17] Slotine, J.-J. E., Li, W., et al. *Applied nonlinear control*, vol. 199. Prentice hall Englewood Cliffs, NJ, 1991.

[18] Sorensen, A., Strand, J. P., and Nyberg, H. Dynamic positioning of ships and floaters in extreme seas. In *OCEANS'02 MTS/IEEE* (2002), vol. 3, IEEE, pp. 1849–1854.

[19] Sørensen, A. J. Marine control systems. *Propulsion and Motion Control of Ships and Ocean Structures 3* (2012).

[20] Veksler, A., Johansen, T. A., Borrelli, F., and Realfsen, B. Dynamic positioning with model predictive control. *IEEE Transactions on Control Systems Technology 24*, 4 (2016), 1340–1353.

[21] Wang, Y. Application of model predictive control to dynamic positioning system. *Master thesis* (2006).

[22] Wang, Y., Shi, X., and Bian, X. Restriction control of marine dynamic positioning system based on model predictive control. *Ship Eng 3* (2007), 22–25.

[23] Wang, Y., Sui, Y., Wu, J., and Jiao, J. Research on nonlinear model predictive control technology for ship dynamic positioning system. In *2012 IEEE International Conference on Automation and Logistics* (2012), IEEE, pp. 348–351.

[24] Xia, G., Liu, J., Chen, X., Wang, D., and Yang, R. Ekf based model identification for a relaxed dynamic positioning ship using nmpc method. In *2015 IEEE International Conference on Mechatronics and Automation (ICMA)* (2015), IEEE, pp. 1313–1318.

[25] Yu, S., Li, X., Chen, H., and Allgöwer, F. Nonlinear model predictive control for path following problems. *International Journal of Robust and Nonlinear Control 25*, 8 (2015), 1168–1182.

Chapter 4

Efficient Modelling of Harsh Environment Disturbances for DP and Autonomous Ships Simulations

This chapter was published.

https://publications-cnrc.canada.ca/fra/voir/objet/?id=2189f127-e8a7-4bdd-b2a6-eec78fc89168

Abstract

Numerical modelling of the Arctic ocean dynamics with real-time simulation capability is useful for designing, developing, testing, and validating Dynamically Positioned (DP) and Autonomous ships/offshore platforms. However, advanced simulation technology needs to be developed to predict the expected loads on these systems due to the complex interactions with environmental disturbances. This paper presents models of waves, currents, wind, and ice that comply with the real-time simulation requirements and adequately capture the dynamic characteristics of the most relevant physical processes. A 3D dispersive numerical model is deployed to predict the wave parameters to be utilized to compute the wave loads on a ship with known Response Amplitude Operators (RAO). A uniform current load is then incorporated in a superposition manner by using a combined wave-current field dispersion relation capable of expressing the wavenumber of an interactive wave-current field. The mean and the gust wind components are added to the resultant force components. A multiple regression-based ice model is used to predict the loads caused by an ice field characterized by varied ice thickness, concentration, floe size, drift speed and directions. The interaction between the ice field and waves is assumed negligible. The stationkeeping performance of a generic DP-controlled ship subjected to the environmental disturbances defined by the time traces of the combined forces and moments obtained by the above methods for a range of environmental conditions. The proposed models can be beneficial for designing, developing, and evaluating dynamic positioning and autonomous ship controllers' performance. Another application may be developing a realistic simulation environment to train conventional,

DP-controlled and autonomous ship operators.

keywords: Dynamic positioning, wind force, wave force, current force, ice force, 3D wave models, 3D wave-current interaction models.

4.1 Introduction

The offshore industry has raised its research and development endeavour to explore and extract oil and gas from Arctic and Sub-Arctic offshore regions. The physical environment in these regions presents several challenges: cold, temperatures, darkness, precipitation, fog, extreme winds, currents and waves, icing, etc. [20]. One of the greatest threats to the Dynamic Positioning (DP) and Autonomous control systems of vessels and offshore installations operating in these regions is the multi-directionality of drifting sea ice with a wide variety of types and forms, ranging from isolated first-year floes to compacted multi-year ridges [21]. In the sub-arctic, marginal ice zone (MIZ, the first ice infested area encountered from the open Ocean), wind, waves and sometimes current is present besides the broken ice-field. This creates a very complex environment for offshore operations, particularly for DP operations. The DP or autonomous control systems in the market today do not take account of the forces and movements that exist in such a highly demanding environment. Numerical modelling and validation of each interaction phenomenon in all possible environmental cases are essential and key to understanding the problem and designing both the floating and control systems. Modelling and simulation of environmental disturbances for ocean surface vehicles have been used in ship simulators for naval training, ship hull designs, military science and entertainment activities such as computer games [29]. Numerical simulations of the Arctic ocean dynamics can help design, develop, test, and validate DP and Autonomous ships/offshore platforms in harsh environment simulations. Simulation technology needs to be developed to predict the expected loads on these systems due to the complex interactions with the disturbances. Modelling complex environmental disturbances and their loads on the systems is an essential and critical component of such simulations. This paper presents models of waves,

currents, wind, and ice that comply with the real-time simulation requirements and adequately capture the most relevant physical processes. Section 2 presents a brief review of existing models for various environmental disturbances modelling. For the wave model, the authors proposed a 3D dispersive numerical model to predict the wave parameters to be utilized to compute the wave loads on a ship with known Response Amplitude Operators (RAO). A uniform current load is then incorporated in a superposition manner by using a combined wave-current field dispersion relation capable of expressing the wavenumber of an interactive wave-current field. The mean and the gust wind components are added to the resultant force components. Multiple regression based ice models are then used to predict the forces and moment caused by an ice field characterized by varied ice thickness, concentration, floe size, drift speed, and directions. The combined loads are assumed to be the summation of the wind loads, wave and current interaction loads, and ice loads. The interaction between the ice field and waves is assumed negligible. In Section 3, the authors present the time traces of the individual and combined loads exerted by these disturbances on a Generic DP ship for a range of environmental conditions. Section 4 presents the implementation of the environmental disturbances model to the DP vessel in a simulated environment to evaluate the DP performance. A few concluding remarks and recommendations for future work follow in Section 5.

4.2 Environmental Disturbances

A brief discussion of various existing environmental disturbance models is presented in this Section. Focus is given to the wave and current interactions and ice force models. Several wave, wind and current models are proposed in the literature, ranging from very simple empirical/analytical to complex high-fidelity numerical models; however, literature to capture their interactions is limited. Also, modelling of ice dynamics in the presence of waves is scarce in the literature.

4.2.1 Wind Models

The wind load at any instance is the summation of the mean and the gust load components at a given point, both of which are functions of time and space and vary on elements of a given structure. For a single-point loading method, it is assumed that mean and gusty velocities are constant at all locations on the structure. On the other hand, when the structure is quite large, distributed multiple points of wind force method might be utilized where the surface of the structure would be divided into multiple sections, and the mean and gusting wind forces are computed separately on each Section. The gusting wind load component for each small Section is evaluated separately using a correlation strategy [10], and then a superposition is made for the total wind gusting force on the structure. The instantaneous wind force (F_w) on any structure that has r number of elements can be given by the following superposition equation [11]:

$$F_{wind}(t) = \frac{1}{2}\rho_a \sum_{j=1}^{r} C_{Daj} A_j (\bar{U}_{aj} + u_{gj}(t) - \dot{x}(t))^2 \tag{4.1}$$

where ρ_a is the air density, C_{Da} is the drag coefficient in air, A is the projected area and $\bar{U}_a$ is the mean wind velocity on any element, and u_g is the wind gust; $\dot{x}$ is the structural velocity, which can be considered negligible for our cases. The gust wind force on the structure can be predicted by the following empirical equation presented in [31]:

$$\frac{S_w(n)n}{4kN} = \frac{\bar{U}_{a10}^2}{(2+N^2)^{\frac{5}{6}}} \tag{4.2}$$

where, n is the frequency, $S_w(n)$ the spectrum, k (= 0.003 to 0.005) the drag coefficient,$\bar{U}_{a10}$ the velocity at a height of $10m$ averaged over one hour and $N = 1200n/\bar{U}_{a10}$. See also, [8] and [6] for more information. The mean force, F_{windM}, and fluctuating force, F_{windG}, on any structure can be expressed as follows:

$$F_{windM}(t) = \frac{1}{2}\rho_a C_{Da} A \bar{U}_a^2 \tag{4.3}$$

$$F_{windG}(t) = \frac{1}{2}\rho_a C_{Da} A \bar{U}_a u_g(t) \tag{4.4}$$

For modelling DP operation in a testing facility, particularly in the presence of ice, the wind forces are sometimes modelled as a certain percentage of total thruster capacity [12]. The total thruster capacity of the DP vessel is reduced to compensate for the virtual presence of wind load.

4.2.2 Current Models

The magnitudes of currents vary with the location in the Ocean and also their generation mechanism. For example, a strong wind could generate a strong current over a certain water depth, but a tidal current usually moves the whole ocean water body. Wave breaking and river discharge can generate localized strong current. Current is typically modelled as uniform over depth or linearly or non-linearly varying sheared current. The current force is modelled based on the empirical formulation to account for the global and local current drag coefficients, current magnitude and direction, and projected area, as discussed below. The computation of the current force is often done in a very straightforward manner. In general, currents impart non1linear forces on the structure and could be characterized as a drift force due to the current only case. The velocity of currents could be depth-dependent, but the current velocity is considered vertically uniform for simplicity. The force due to currents (F_c) only can be evaluated using the following equation:

$$F_c = \frac{1}{2}\rho_w C_{Dc} A U_c^2 \tag{4.5}$$

where U_c is the wave-particle velocity, A the projected area and C_Dc is the drag coefficient for current. The above current model can be further improved if the two-dimensional current model introduced by [7] and [4] is used. The same formulation can be used for predicting the wind and current loads; we use notations for current to illustrate the method. In this method, the resultant wind or current force acting

on a surface vessel is defined in terms of relative current speeds $u_{current}$ and $v_{current}$ illustrated in Fig 4.1.

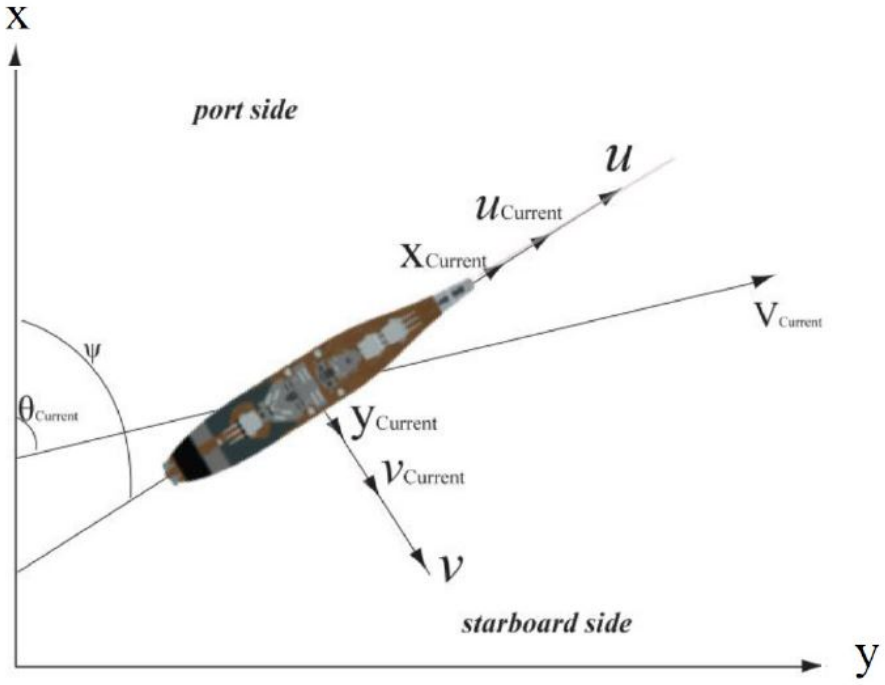

Figure 4.1: Notations for two dimensional current or wind model [4]

$\theta_{current}$ is the angle between X-axis and the direction of the current. Then $u_{current}$ and $v_{current}$ determined as follows:

$$u_{current} = V_{current} cos(\theta_{current} - \psi) - u \tag{4.6}$$

$$\nu_{current} = V_{current} sin(\theta_{current} - \psi) - \nu \tag{4.7}$$

The resultant current forces acting on a surface vessel with respect to the ship's fixed reference frame:

$$X_{current} = \frac{1}{2} R_{wx} \rho_w A_T u_{current}^2 \tag{4.8}$$

$$Y_{current} = \frac{1}{2} R_{wy} \rho_w A_L u_{current}^2 \tag{4.9}$$

where, R_{wx} and R_{wy} - Current drag coefficients, A_T - transverse current projected area of the vessel (underwater for current and above water for wind), A_L - lateral current projected area of the vessel. A similar yet more accurate model was proposed by [26]. We recommend the model presented in [26] as it accounts for the instantaneous vessel yawing the corresponding changes in the speed and directions of current as well as the project surface areas.

4.2.3 Waves Models

Of the three main environmental forces (wave, wind, and current), the horizontal wave drift force is quite important. For the cases of regular waves and current, a 3D numerical model with the assumption of inviscid and incompressible fluid flow is developed and utilized in this work to evaluate wave kinematics. An explicit type numerical scheme is used for the simulation of the numerical model. A detailed description of this wave model can be obtained in [37], [38],[40]. On the other hand, for the irregular waves, a Boussinesq type numerical model with modified dispersion relation is developed and adopted in this study. The description of this numerical model is available in [38],[40]. The same model is upgraded for the interacted wavecurrent coexisting field. An ADI (Alternative Directional Implicit) method is employed for the solution of the non-linear equations.

The wave force on a unit length of a structure can be calculated when the wave kinematics are known using Morisons's equation as follows:

$$F_w(t) = \frac{1}{2} \rho_w C_D A u \left| u \right| + C_M \rho_w V \dot{u} \tag{4.10}$$

where u is the wave particle velocity, $\dot{u}$ the wave acceleration, C_D and $C_M (= 1 + C_m)$ are the drag and mass coefficients, C_M the added mass coefficient, V the volume, D the diameter and $A (= D * 1)$ is the area per unit length.

The mean drift force due to viscosity effects can be obtained by utilizing the instantaneous velocity of the water particle in the above equation and integrating the obtained expression over one wavelength [5]:

$$F_{wdrift} = \frac{2}{3\pi}\rho_w \omega^2 C_{Dv} D a^3 \tag{4.11}$$

The viscous drift coefficient $C_D v$ can be obtained from the empirical formula by [5] and varies roughly from 1.27 to 1.62. The prediction of wave loads due to regular and irregular waves and waves and current interactions can also be obtained using the RAO (Response Amplitude Operator) approach, as long as the instantaneous surface elevation and the RAO of the vessel for the wave environment are known. In this approach, the wave force RAOs for specific vessels for various operating conditions are calculated using commercial potential flow solvers such as ANSYS-AQWA or WAMIT or a similar solver. The RAO curves are then utilized to derive the wave force and moment spectrums in the irregular sea for the specified theoretical spectrum. The corresponding wave force/moment values were extracted directly from the force/moment RAO for the single frequency regular sinusoidal wave.

To obtain the forces and moments due to an irregular sea, the traditional linear superposition principle is used. This principle allows summing the responses of a system due to components of the irregular sea in a linear fashion to predict motions in an irregular sea state. The wave forces and moments in the mathematical model adopted in [18] also follow the same superposition principle assuming a linear system.

4.2.4 Ice Force Models

One of the challenging tasks in developing a real-time simulator for environmental disturbances involving ice is to develop, validate and implement a statistically reliable numerical model that can predict the ice loads in real-time and at the same time accounts for most of the relevant physical processes of the complex and dynamic ice-ice, ice-environment and ice-vessel interactions.

Several published numerical works have been used to understand and model the ice forces acting on stationary or DPcontrolled or moored floating platforms or slowly manoeuvring ships in managed or broken sea ice. The authors of [16] presented an extensive literature review of various existing techniques and approaches for modelling broken ice-structure interactions. In [16], the authors categorized the existing methods into Analytical Methods, Empirical-Statistical Methods, Numerical Methods and Hybrid Methods. Popular analytical techniques known as a "Micro" model and a "Macro" model were used for modelling and simulations of ice interaction with moored structures by [2],[3], and [41]. [30] extended the approach to simulate 6 degrees-of-freedom motion of vessels transiting through the ice. Amongst the empirical methods, [19] developed a pioneering empirical method for predicting ice-structure interaction forces due to broken ice using the "equivalent level ice thickness" approach. [24] developed an empirical-statistical modelling technique for predicting the ice forces on a DP vessel. The method offers a balanced combination of physical ice model tests and numerical techniques to justifiably predict statistically valid ice forces on a DP-controlled vessel due to actions of a broken ice field. The major shortcoming of the approach is its lack of details of the floe dynamics that would decrease the fidelity in visualization in the simulation. To improve the fidelity of this approach, the techniques, as outlined in Fig 4.2, have been implemented

In this technique, the time-average ice forces are expressed as functions of nominal managed ice variables, e.g. ice thickness and strength, floe size, floe concentration, and floe velocity and direction, using advanced multivariable statistical analysis of existing database acquired during an ice basin testing campaign. The next step is to relate the time-average to the discrete ice impact forces on the DP/Autonomous vessel using statistical distribution and Monte Carlo methods [24]. The procedure used to develop this model is outlined below.

The details of the model is provided in[24].

- Developed multiple-regression based models for mean and average of peaks of thruster forces, for mean loading span and frequencies.

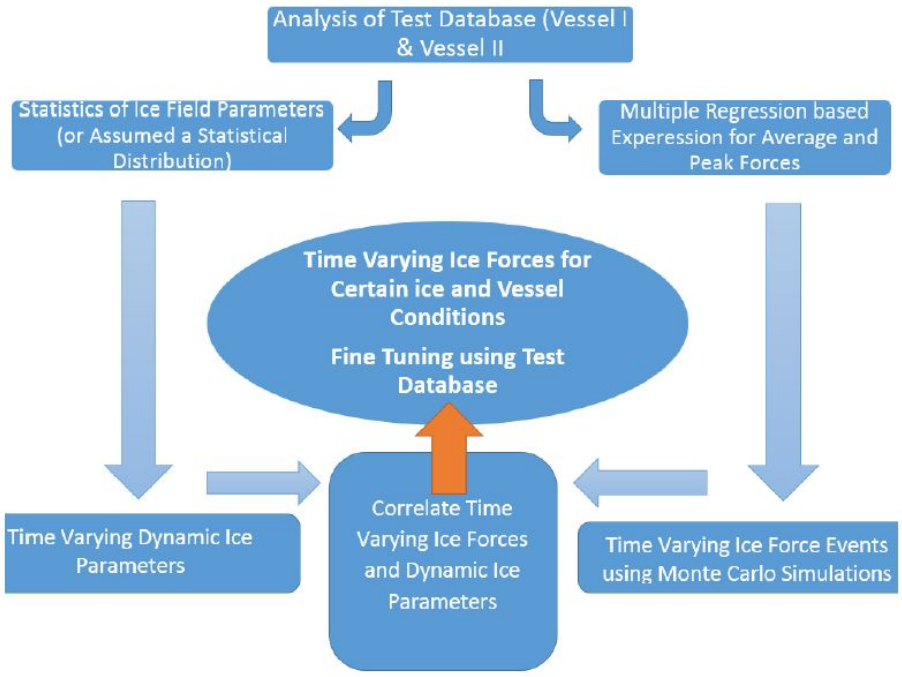

Figure 4.2: Flow chart of the empirical statistical technique [28].

- Developed models for predicting force peaks and peak time for one or multiple events using Monte Carlo Simulations.
- Generated time series for thruster forces and yawing moment using idealized loading profiles.
- Applied correction factors to account for idealization and regression errors.
- Converted thruster forces to ice forces using specialized random noise.

Fig 3.3 compares the model testing measurements and corresponding statistical model predictions for a test case. The predicted forces/moments are statistically comparable with the corresponding measurements.

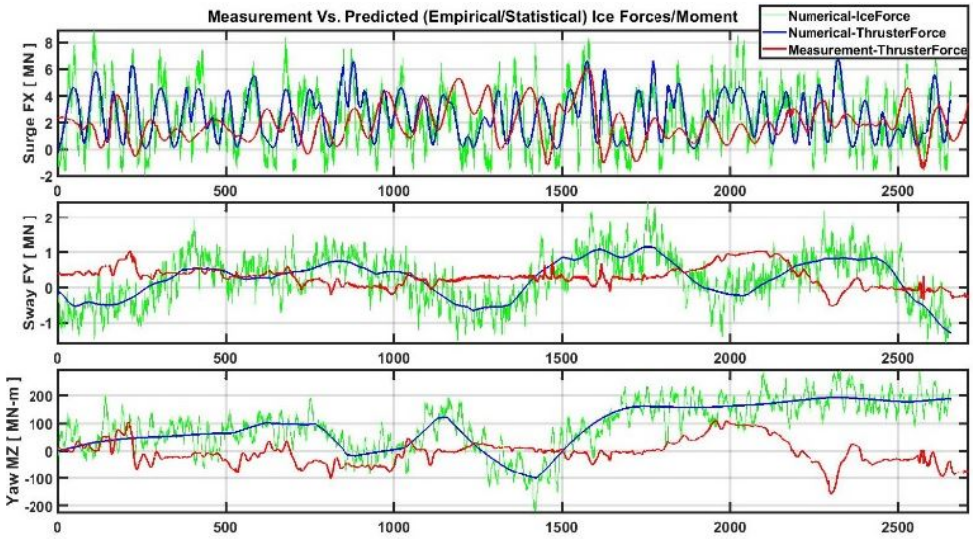

Figure 4.3: Comparison of measured and predicted global forces (thruster and ice) on a Drillship, ice thickness 2M, 90% concentration, floe size 50M, drift speed 0.5 knot and $\pm 2^{\circ}$ heading.

4.2.5 Waves and Currents Interaction Models

The presence of a wave over a current field remained as an interesting research topic among ocean engineers and researchers. When a wave and a current are in the same direction, the wavelength increases, and the height decreases to accommodate extra energy. On the other hand, when the wave and current are opposite, the wavelength decreases, and as compensation, the wave height increases.

The above-mentioned wave models use a dispersion relation that contains the current parameter will account for the modified wavenumbers following equation [13],[34],[39] below:

$$\omega - \vec{U_c}.\vec{k} = \sqrt{gktanhkd} \tag{4.12}$$

Where $\vec{k}(k_x, k_y)$ is the wavenumber, d the mean water depth, $\vec{U}(U_{cx}, U_{cy})$ the current velocity, and g is the acceleration due to gravity. The descriptions of the wave-current interaction models can be found in many literatures, See also [36] for details.

The total force for the combined wave-current field F_wc can be obtained from the

following relation:

$$F_{wc}(t) = \frac{1}{2}\rho C_D A u_{wc} |u_{wc}| + C_M \rho V \dot{u}_{wc} \tag{4.13}$$

where u_{wc} is the velocity and $\dot{u}_{wc}$ is the acceleration of the combined wave-current field that be obtained from [37] depending on the requirements of the modelling and C_M is the mass coefficient. See [37] for details.

In this paper for the regular wave and regular wave-current interaction, simulation is done following [35]. The above force expression, Eq. (4.13) is based on Morison's formulation. Alternatively, the total force for the combined wave-current field can be obtained by using the RAO technique using modified surface elevation and then superimpose the current load as per Section 4.2.1.

4.2.6 Waves and Ice Interaction Models

The ice and wave interaction is important in the marginal ice zone (MIZ) for two primary reasons: firstly, ocean waves influence the sea ice cover, which then affects large scale wind patterns and ocean currents; secondly, ice floes scatter and dampen waves, which has to be taken into account in forecasts of wave heights [23]. The grease ice and broken ice floes present in the MIZ, play an important role in damping the high frequency waves that would otherwise lead to fast-breaking of the inner, continuous sea ice [25]. [25] presented a brief survey of the existing sea ice and wave interaction modelling, both physical and numerical and field measurements.

[14] treated the wave attenuation by interaction with sea ice with a percent transmission of wave energy through the ice as a simple linear function of ice concentration. Rogers and [15] modified a third-generation model for wind-generated surface gravity waves WAVEWATCH III® to represent the effect of ice on waves as a dissipative source function with three alternative formulations of varying complexity.

[32] reported a wave-ice interaction model for the MIZ that calculates the attenuation of ocean surface waves by sea ice and the concomitant breaking of the ice into smaller floes by the waves. The rate of attenuation is calculated using a thin elastic

plate (representing ice floes) scattering model, and a probabilistic approach is used to derive a breaking criterion in terms of the significant strain. This determines if the local wave field is sufficient to break the ice cover. An estimate of the maximum allowable floe size when ice breakage occurs is used as a parameter in a floe size distribution model, and the MIZ is defined in the model as the area of broken ice cover. [27] investigated various models of ocean wave propagation in ice-infested seas. [33] explored these models as well, however, obtained unrealistic attenuation coefficients for continuous ice sheet/high concentration ice-field. The "Transport equation models" hold a special status because they can incorporate models from the other categories as source terms in the transport equation.

Successful modelling of wave-ice interaction is challenging. In particular, both field and laboratory data are still too scarce. Several competing models exist where each model can be approximately fitted to the available observations. [23] proposed a new set of methodology and instruments to perform sea ice and wave interactions measurements and compared several datasets.

4.3 Model Implementation

A generic Drillship vessel is used for the present simulation cases. The full-scale vessel has an overall length of 206 m, has a 45 m beam and displaces around 100,000 MT at 12 m draught [17]. The forces and moments (environmental load on the horizontal plane) were predicted on the vessel due to the environmental disturbance cases as identified in Table 4.1. The time traces of the forces and moments exerted by these disturbances (individual cases as well as combined cases) on the Drillship for a range of environmental conditions are presented in this Section.

To obtain the wave loads due to wave only or wave and current field, the wave kinematics are first predicted using a vertically integrated 3D numerical model [35]. This model can efficiently compute the dynamics of ocean waves in the presence or in the absence of the ocean current. The Vessel forces and moments were then predicted using the surface elevation and RAO-based methods described above. The wave force

Table 4.1: Simulation matrix for environmental models

Case	Environment Condition	Wave			Current		Ice		
No.	Conditions	$\frac{H}{H_s}(m)$	$\frac{T}{T_p}(m)$	Angle	$U(\frac{m}{s})$	Angle	ConC; Floe(m); Thick(m)	Drift (Kts)	Angle
1	Regular wave only	8	8	0	NA	NA	NA	NA	NA
2	Regular wave only	8	12	0	NA	NA	NA	NA	NA
3	Regular wave only	8	12	45	NA	NA	NA	NA	NA
4	Irregular waves (JON-SWAP)	15	14.6	0	NA	NA	NA	NA	NA
5	Irregular waves, [16]	15	14.6	0	0	NA	NA	NA	NA
6	Regular wave with collinear current	8	12	0	-2.5	180	NA	NA	NA
7	Irregular waves [16] with collinear current	15	14.6	0	1	NA	NA	NA	NA
8	Managed Ice Field	NA	NA	NA	1.2	0	90%, 50m, 2m	1.2	0
9	Managed Ice Field	NA	NA	NA	0.25	10	80%, 50m, 2m	0.5	10
10	Waves and Current, Managed Ice Field	1.5	14.6	0	1	0	90%, 50m, 2m	1.2	0
11	Waves and Current, Managed Ice Field	1.5	14.6	0	1	0	80%, 50m, 2m	0.5	10

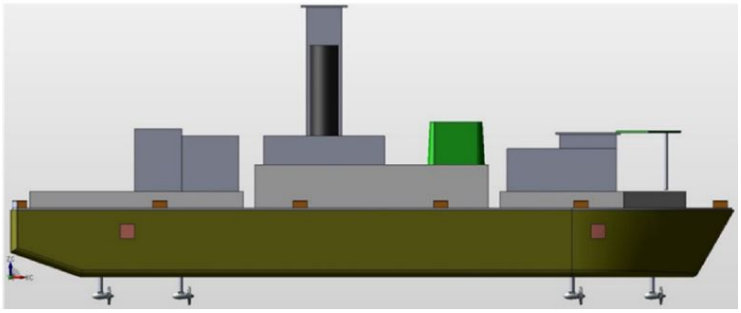

Figure 4.4: The generic Drillship hull utilized in the present research.

RAOs from ANSYS-AQWA for the drillship vessel and for different practical wave conditions were obtained for 0° to 180° wave heading in an interval of 15°. The values required in between those headings were obtained by interpolation. The first-order wave loads on the vessel were then estimated using the transfer function for a given wave. The forces and moments due to the broken ice field is obtained using the regression-based model [24]. For the sake of the present simulations, the wave and ice interaction is assumed negligible.

Computations are carried out using Case 1, Case2 and Case 3. The obtained results are quite reasonable (not shown in this paper for space limitations). The validations of the 2D version of these models are reported in [39],[38].

The results of irregular waves and forces for Case 4, shown in Fig 4.5, are simulated using JONSWAP spectrum is used for the simulation of the wave-only case. But for the case of interaction of irregular waves [22] with a current, [9] spectrum is utilized shown by Eq. 4.12. Fig 4.6 shows results for surface elevations and forces due to a regular wave interaction with an opposite current. The computational condition is described in Case 6. In Fig 4.7, the predicted surface elevation is compared with the RAO-based reconstructed surface elevation for Case 6. Fig 4.8 describes the results for instantaneous surface elevations and force components when an irregular wave field interacts with a vertically uniform current for Case 7. Fig 4.9 compares the power spectrums for irregular waves without (Case 5) and with (Case 7) current.

Fig 4.10 and 4.11 present the ice forces and moment in the horizontal plane on the

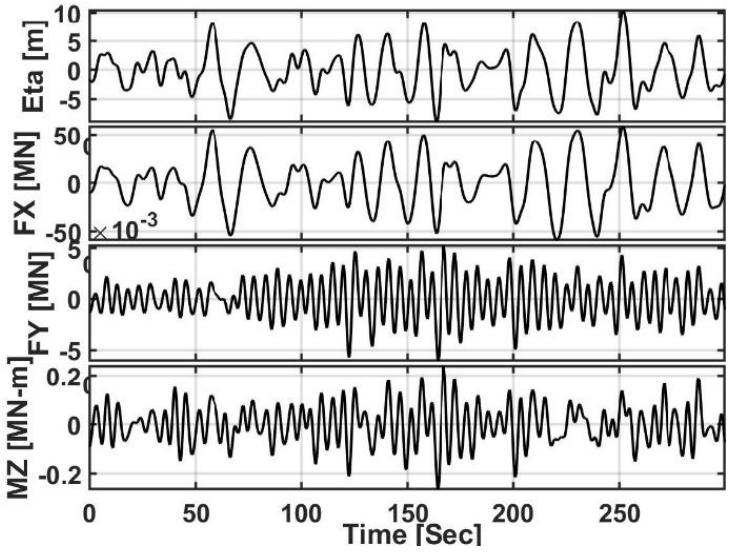

Figure 4.5: Wave elevations and forces for case-4 with JONSWAP SPECTRUM (H_s = 15 m, T_p = 14.6 s)

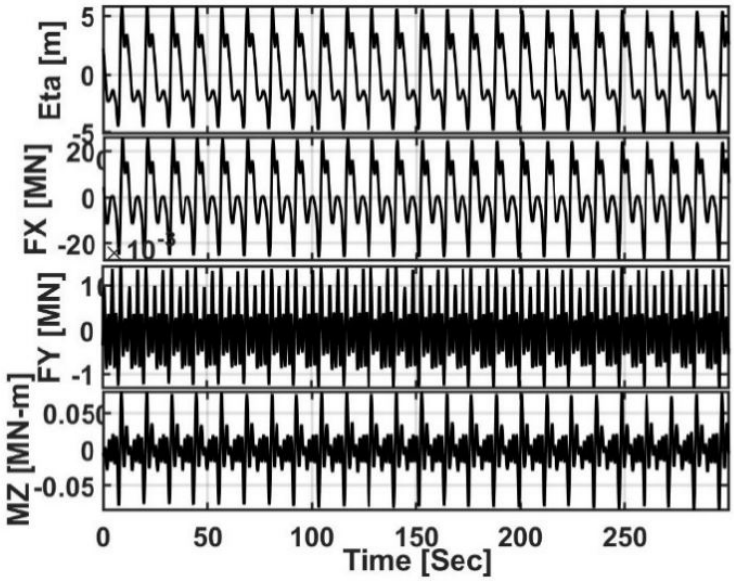

Figure 4.6: Surface elevations and wave forces for case-6, regular wave with non-collinear current (H = 8 m, T = 12 s, U = -2.5 m/s, wave angle = 0^o and current angle = 180^o)

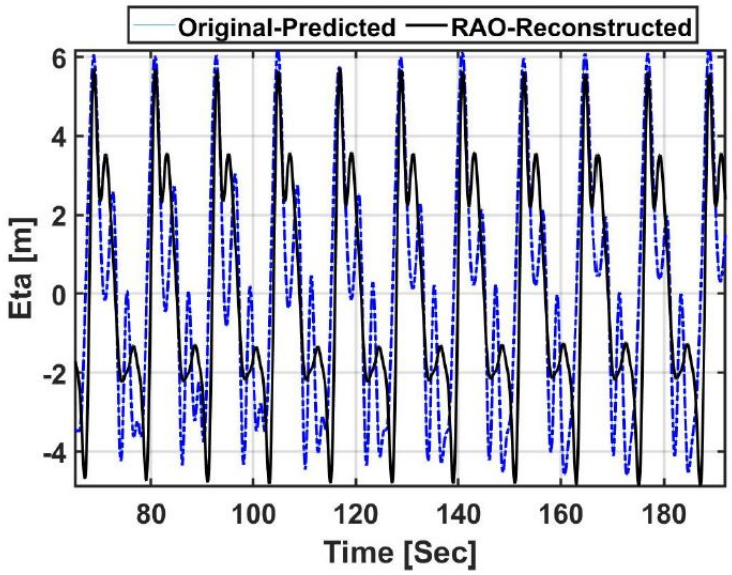

Figure 4.7: Comparisons of the surface elevations between the predicted and RAO-based reconstruction.

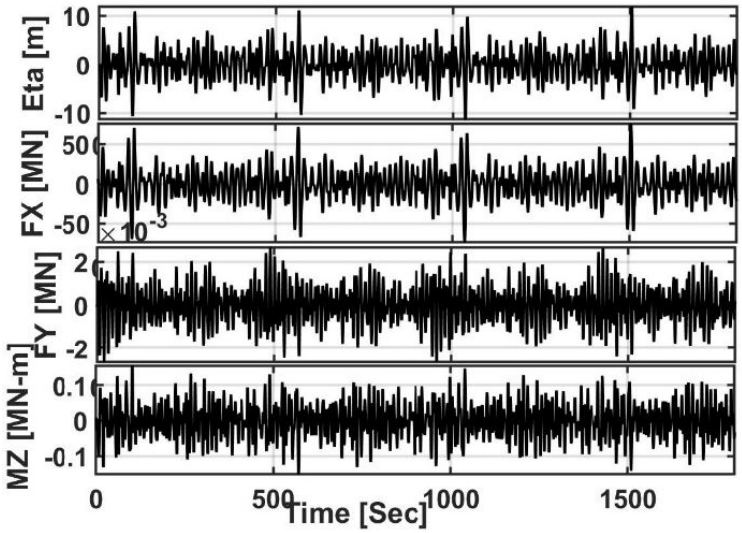

Figure 4.8: Wave elevations and forces for case-7 with GODA [16] SPECTRUM (H_s = 15 m, T_p = 14.6 s and U = 1.0 m/s)

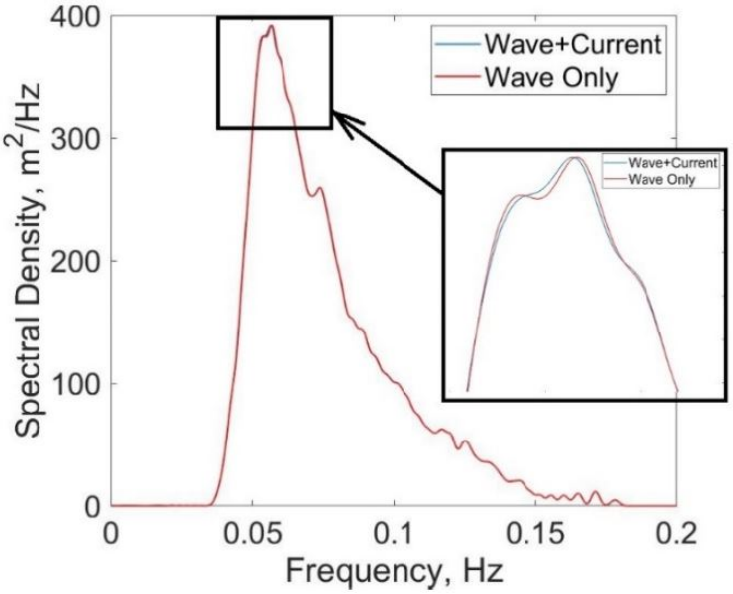

Figure 4.9: Comparison of the power spectrums for irregular waves with and without uniform current for case 7 using [16] SPECTRUM (H_s = 15 m, T_p = 14.6 s and U = 1.0 m/s)

Drillship due to cases 8 and 9, respectively, as described in Table 4.1. Both conditions are considered extremely harsh, whereas the first case is for a headon condition, and the next case is in an oblique condition. Fig 4.12, through Fig 4.14, presented the simulated disturbances that include ice, waves, and current. In these predictions, the interactions between the wave and current were included. However, wave and ice-field interactions were neglected. Fig 4.12 shows the linear superimposition of the forces in the surge direction. A further discussion on the ice load characteristics is beyond the scope of this paper.

4.4 Real-time Simulations

The dynamic positioning (DP) performance of the Drillship vessel under the influence of two cases (Case 10 and Case 11 in Table 4.1) of environmental disturbances comprising ice, wave and current is investigated in this Section. The vessel equipped

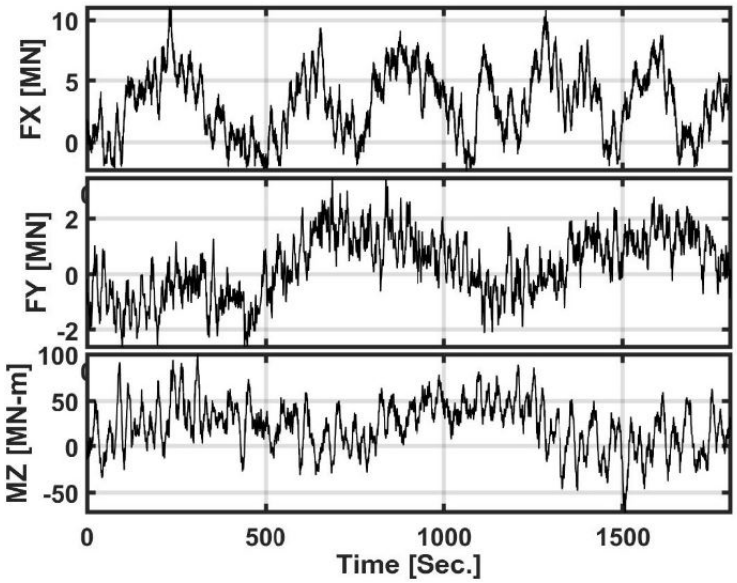

Figure 4.10: Ice loads in a managed ice field, ice thickness 2M, 90% concentration, floe size 50M, drift speed 1.2 knots and head-on conditions.

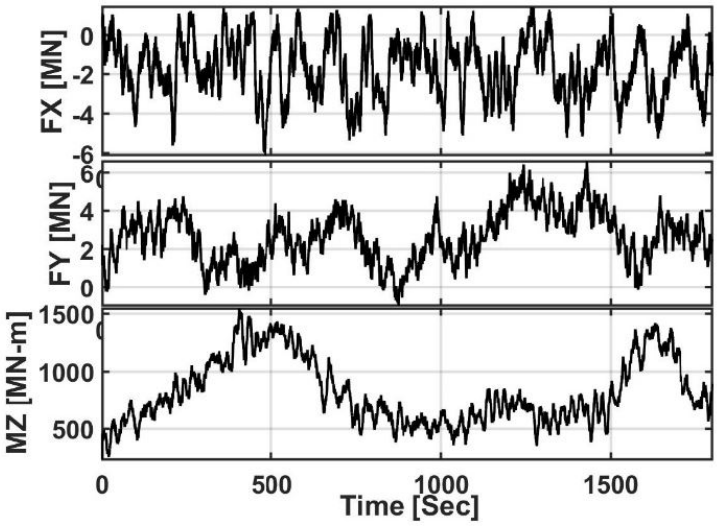

Figure 4.11: Ice loads in a managed ice field, ice thickness 2M, 90% concentration, floe size 50M, drift speed 0.5 knots and 100 oblique condition.

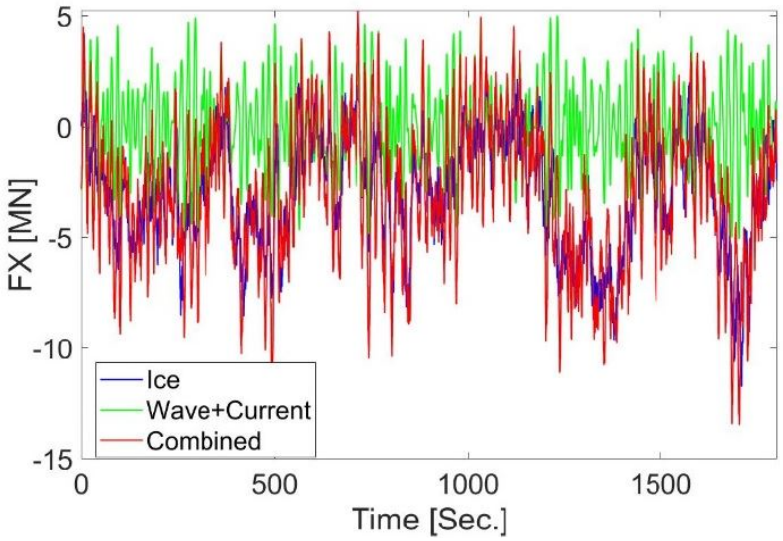

Figure 4.12: Combined wave, current and ice loads in surge, ice thickness 2M, 90% concentration, floe size 50M, drift speed 1.0 knot, waves with $H_s = 1.5$ m, $T_p = 14.6$ s and current with $U = 1.0$ m/s

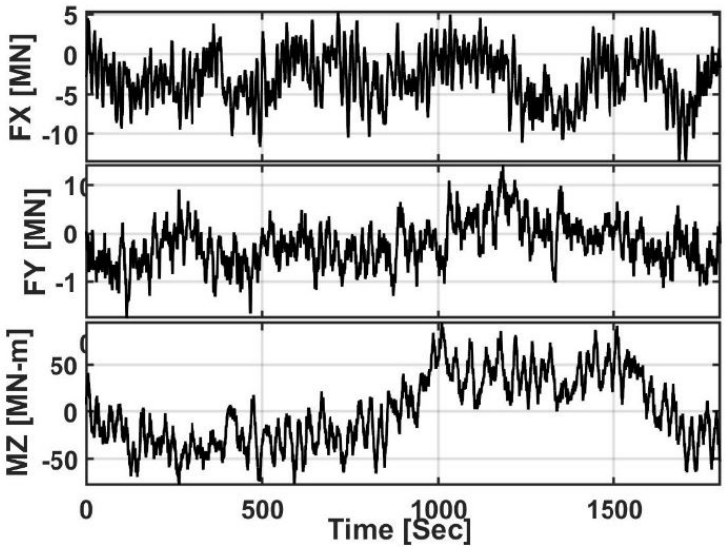

Figure 4.13: Combined wave, current and ice loads in surge, sway and yaw for case-10, ice thickness 2 M, 90% concentration, floe size 50 M, drift speed 1.2 knot, waves with $H_s = 1.5$ m, $T_p = 14.6$ s and current with $U = 1.0$ m/s

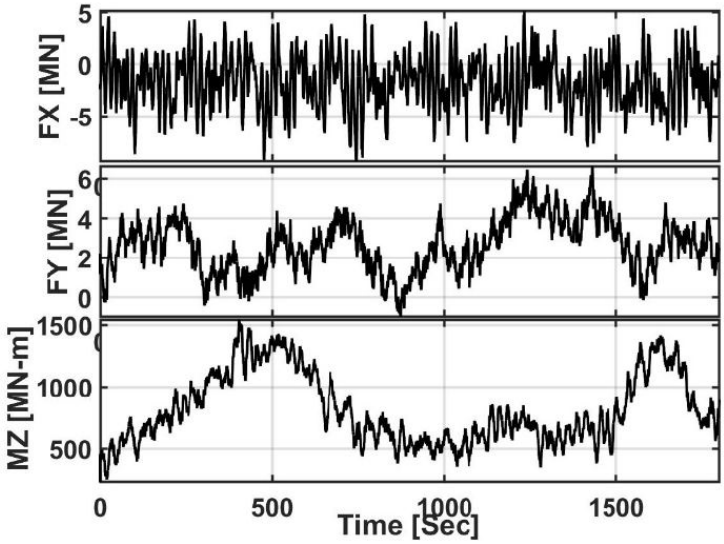

Figure 4.14: Combined wave, current and ice loads in surge, sway and yaw for case-11, ice thickness 2 M, 80% concentration, floe size 50 M, drift speed 0.5 knot, waves with $H_s = 1.5$ m, $T_p = 14.6$ s and current with $U = 1.0$ m/s

with a non-linear proportional integral and derivative (NPID) control system with acceleration feedback type control system [1] were simulated and evaluated under the two different extreme sea conditions. Matlab/Simulink models of the fullscale ship are used, which were developed under the scope of a multi-year R & D project [1]. In the model, an unscented Kalman filter (UKF) is used to estimate vessel motions and to control low frequency (LF) motions while filtering out wave frequency (WF) motions.

Fig 4.15 and Fig 4.17 show the thruster responses during the stationkeeping of the drillship with a target (0,0,0) deg and (0,0,10) deg, respectively, for the two corresponding disturbance cases. Fig 4.16 and Fig 4.18 show the corresponding offsets. Both cases show that the vessel could not maintain its station in the target location and orientation. This is attributed to the extreme ice, wave and current conditions. These simulations were carried out to demonstrate the processes of environmental disturbances modelling for real-time simulation applications and not to investigate DP systems capability, no further discussion on the DP system's capability is offered.

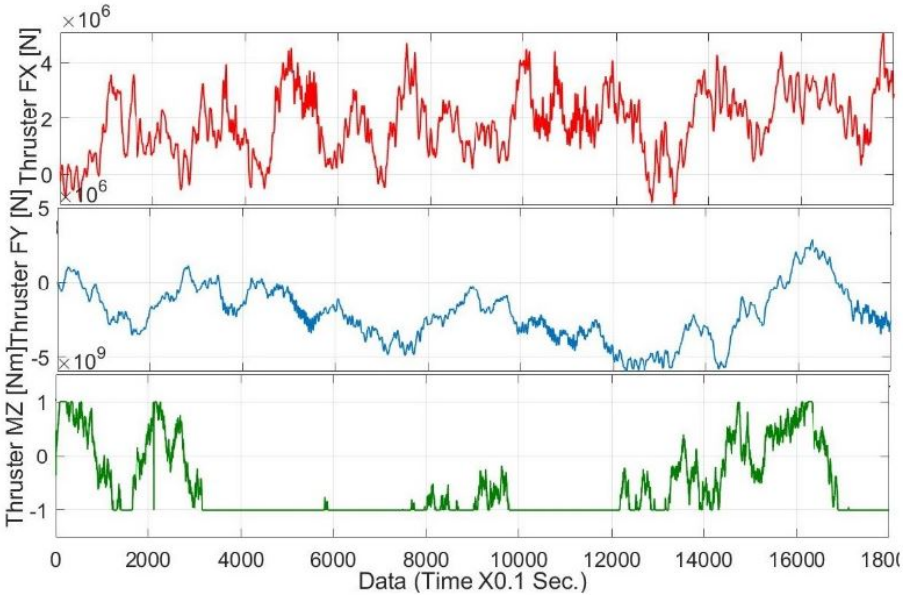

Figure 4.15: The thruster loads during the DP operations of the Drillship with NPID controller subjected to case-10 disturbances loads.

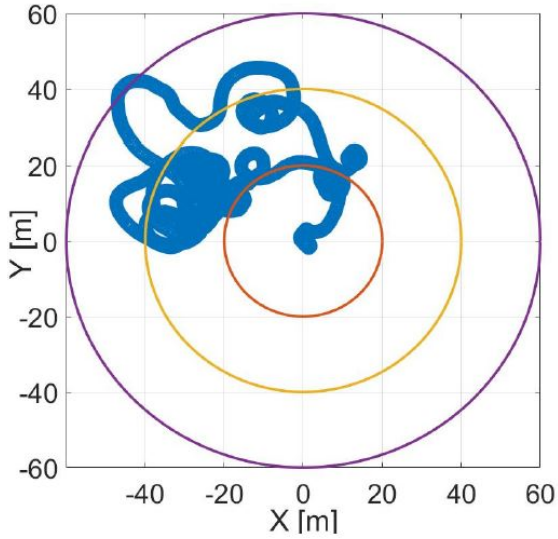

Figure 4.16: The X, Y offsets of the DP vessel with the target position of 0 M, 0 M, 0 DEG for case-10.

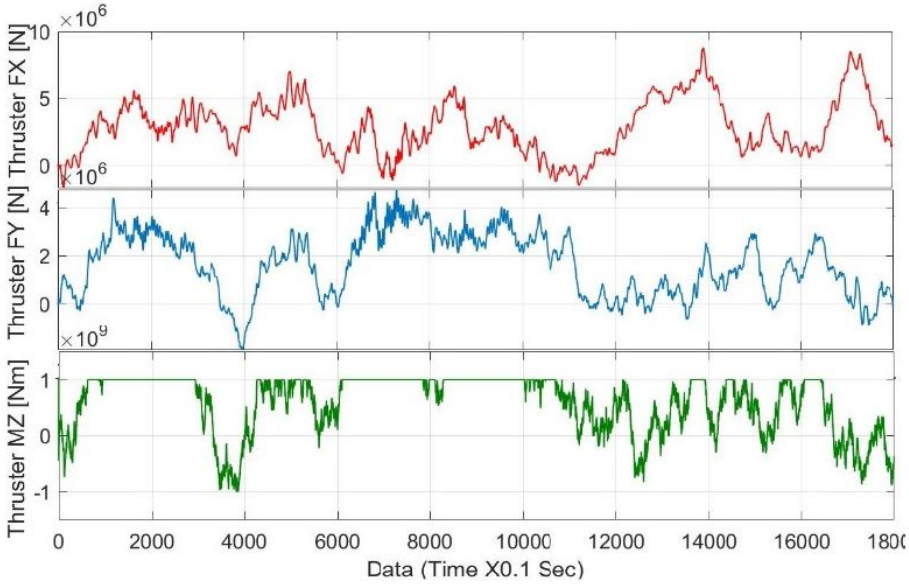

Figure 4.17: The thruster loads during the DP operations of the Drillship with NPID controller subjected to case-11 disturbances loads.

In a previous comparative study to investigate five state-of-the-art control schemes, the authors found that the NMPC (non-linear model predictive control) showed the best ability to deal with extreme disturbances efficiently [67]. Although all five controllers were able to maintain the ship position under moderate conditions, only the NMPC and the MRPID (multi-resolution PID) controllers were able to stabilize the ship under extreme sea states. The authors plan to investigate further the performance of NMPC and MRPID to improve its performance to deal with several realistic external disturbances that include wind, waves, currents, and ice, including the two scenarios presented above.

Regardless of the modelling approach taken, the availability (and quality) of measured data is paramount to the success of the environmental disturbance model development. For the range of environmental conditions and scenarios of interest (dictating wave characteristic and interactions with current, the presence of ice, type and characteristics), and for each vessel of interest (e.g. Drillship, supply vessel, ice breaker, etc.), the current modelling technique require the availability of a dataset

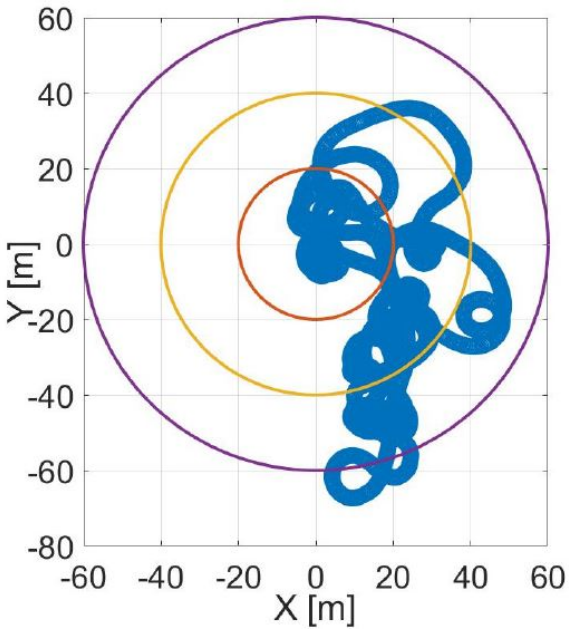

Figure 4.18: The X, Y offsets of the DP vessel with the target position of 0 M, 0 M, 10 DEG for case-11

that extends the range of conditions and operations expected from the models. The authors plan to carry out an extensive test program to evaluate a ship's performance with different controllers for DP and Autonomous operations in an environment consisting of wave, current and/or ice.

4.5 Conclusion and Future Work

In the numerical simulation, the combined environmental loads due to wind, wave, current, and ice are utilized to perceive the response of the NPID controller in keeping the DP vessel at the target (0, 0, 0) position. Each of the wave, current, ice and interaction models presented can be used for real-time and faster than real-time simulations.

The wave-current models used here for various simulations are all validated for

limited cases and are published in different conferences and journals. The ice force models are developed and validated using an extensive dataset of DP vessel's interactions with managed ice-field. The wave and ice interaction models are still in the development phase, and besides some rudimentary empirical techniques, the complex interactions are not well understood.

Regardless of the modelling approach taken, the availability (and quality) of measured data is paramount to the success of the environment disturbance model development. The present modelling techniques and performance of the DP-controller require further validations using basin test data.

The external disturbance models developed or recommended in this research are expected to help to develop and evaluate the most effective control scheme for different extreme sea conditions. The results also support control system development for dynamic positioning and autonomous operations of ships and offshore platforms. These models should be rigorously tested and validated for DP and autonomous operations in realistic environmental conditions.

Acknowledgements

The collaboration between NRC-OCRE and Memorial University (MUN), Canada is appreciated.

References

[1] Alagili, O., Khan, M. A. I., Ahmed, S., Imtiaz, S., Zaman, H., and Islam, M. Performance assessment of dp control systems for different sea states. In *2020 IEEE/OES Autonomous Underwater Vehicles Symposium (AUV)* (2020), IEEE, pp. 1–6.

[2] Bonnemaire, B., Serré, N., Lundamo, T., Fredriksen, A., Jensen, A., Gürtner, A., and Teigen, S. Ice breaking and accumulation around a moored structure: ice basin tests and numerical simulations. In *OTC Arctic Technology Conference* (2014), OTC, pp. OTC–24579.

[3] Bonnemaire, B., Tan, X., Serré, N., Fredriksen, A., Metrikin, I., and Gürtner, A. Post-simulations of ice basin tests of a moored structure in broken ice-challenges and solutions. In *OTC Arctic Technology Conference* (2015), OTC, pp. OTC–25531.

[4] Bortnowska, M. Prediction of power demand for ship motion control system of sea mining ship fitted with tubular winning system. *Polish Maritime Research 14*, 4 (2007), 24–30.

[5] Dev, A. K. Environmental forces for dynamic positioning: Ships vs. semi-submersibles. In *4th International Conference on Technology and Operation of Offshore Support Vessels, Singapore. Pages* (2011), pp. 64–78.

[6] Faltinsen, O. *Sea loads on ships and offshore structures*, vol. 1. Cambridge university press, 1999.

[7] Fossen, T. I. Marine control systems–guidance. navigation, and control of ships, rigs and underwater vehicles. *Marine Cybernetics, Trondheim, Norway, Org. Number NO 985 195 005 MVA, www. marinecybernetics. com, ISBN: 82 92356 00 2* (2002).

[8] Gade, R. H., and Scanlan, R. H. Aspects of hurricane winds as recorded at an instrumented suspension bridge, resolution of eighth joint meeting. *Center for Building Technology Institute for Applied Technology National Bureau of Standards* (1976).

[9] Goda, Y. Statistical variability of sea state parameters as a function of wave spectrum. *Coastal Engineering in Japan 31*, 1 (1988), 39–52.

[10] Gurley, K., and Kareem, A. Gust loading factors for tension leg platforms. *Applied ocean research 15*, 3 (1993), 137–154.

[11] Gurley, K. R., Tognarelli, M. A., and Kareem, A. Analysis and simulation tools for wind engineering. *Probabilistic Engineering Mechanics 12*, 1 (1997), 9–31.

[12] Hals, T., and Efraimsson, F. Dp ice model test of arctic drillship. In *Proc. of the Dynamic Positioning Conference* (2011).

[13] HASANAT ZAMAN, M., and TOGASHI, H. Modeling horizontally two dimensional wave-current coexistence field over uneven topography. In *The Proceedings of the... International Offshore and Polar Engineering Conference* (1997), vol. 3, International Society of Offshore and Polar Engineers, pp. 838–845.

[14] Hopkins, M. A., and Shen, H. H. Simulation of pancake-ice dynamics in a wave field. *Annals of Glaciology 33* (2001), 355–360.

[15] Hopkins, M. A., and Tuhkuri, J. Compression of floating ice fields. *Journal of Geophysical Research: Oceans 104*, C7 (1999), 15815–15825.

[16] Islam, M., Mills, J., Gash, R., and Pearson, W. A literature survey of broken ice-structure interaction modelling methods for ships and offshore platforms. *Ocean Engineering 221* (2021), 108527.

[17] Islam, M., Wang, J., Gash, R., Pearson, W., and Mills, J. Physical model testing i for investigating the effects of managed ice-field characteristics on a dynamic positioning vessel. *Cold Regions Science and Technology 192* (2021), 103376.

[18] Journee, J., and Pinkster, J. Introduction in ship hydromechanics. *Delft University of Technology 8* (2002).

[19] Keinonen, A., and Robbins, I. Icebreaker performance models, seakeeping, icebreaker escort, vol. 3–icebreaker escort model user's guide. Tech. rep., Technical Report, Transport Canada, Calgary, 1998.

[20] Løset, S., Shkhinek, K. N., Gudmestad, O. T., and Høyland, K. V. *Actions from ice on Arctic offshore and coastal structures*. Lan St. Petersburg, 2006.

[21] Metrikin, I. Experimental and numerical investigations of dynamic positioning in discontinuous ice. *NTNU* (2015).

[22] Mills, J., Islam, M., Pearson, W., and Gash, B. Dp in ice environments—development of a dynamic positioning in ice validation platform (dpivp). *Simulation 99*, 6 (2023), 621–641.

[23] Mosig, J. E. M. *Contemporary wave–ice interaction models*. PhD thesis, University of Otago, 2018.

[24] Pearson, W., Gash, R., Islam, S., and Mills, J. Dp in ice environments—ice force modelling using physics engine based dem techniques for dp vessels in managed ice. Tech. rep., Technical report, no. NRC-OCRE-2019-TR-010, 2019. St. John's, NL, Canada ..., 2019.

[25] Rabault, J. An investigation into the interaction between waves and ice. *arXiv preprint arXiv:1810.07022* (2018).

[26] Raman-Nair, W., Gash, R., and Sullivan, M. Effect of wind and current on course control of a maneuvering vessel. In *2014 Oceans-St. John's* (2014), IEEE, pp. 1–5.

[27] Rogers, W., and Zieger, S. New wave-ice interaction physics in wavewatch iii®. In *Proc. 22nd IAHR Intl. Symp. on Ice* (2014).

[28] S, I., M, L., B, G., W, P., and J, M. Dp in ice environments-ice force modelling using empirical-statistical methods for dp vessel in managed ice. *NRC Technical Report No* (2019).

[29] Sandaruwan, D., Kodikara, N., Rosa, R., and Keppitiyagama, C. Modeling and simulation of environmental disturbances for six degrees of freedom ocean surface vehicle. *Colombo* (2009).

[30] Tan, X., Su, B., Riska, K., and Moan, T. A six-degrees-of-freedom numerical model for level ice–ship interaction. *Cold Regions Science and Technology 92* (2013), 1–16.

[31] Taylor, A., Anthony, K., Harris, R., Berrman, P., Wootton, L., Scruton, C., WYATT, T., and Shears, M. The modern design of wind-sensitive structures. *Transport and Road Research Laboratory (TRRL)* (1971).

[32] Tolman, H. L. Treatment of unresolved islands and ice in wind wave models. *Ocean modelling 5*, 3 (2003), 219–231.

[33] Williams, T. D., Bennetts, L. G., Squire, V. A., Dumont, D., and Bertino, L. Wave–ice interactions in the marginal ice zone. part 1: Theoretical foundations. *Ocean Modelling 71* (2013), 81–91.

[34] Zaman, M., and Baddour, R. Loading on a fixed vertical slender cylinder in an oblique wave-current field. In *International Conference on Offshore Mechanics and Arctic Engineering* (2004), vol. 37432, pp. 83–91.

[35] Zaman, M. H. Suppression of ocean waves by uniform forced currents. In *International Conference on Offshore Mechanics and Arctic Engineering* (2008), vol. 48210, pp. 235–244.

[36] Zaman, M. H., and Baddour, E. Interaction of waves with non-colinear currents. *Ocean engineering 38*, 4 (2011), 541–549.

[37] Zaman, M. H., and Baddour, E. Loading due to interaction of waves with colinear and oblique currents. *Ocean Engineering 81* (2014), 1–11.

[38] Zaman, M. H., Togashi, H., and Baddour, R. E. Propagation of monochromatic water wave trains. *Ocean engineering 34*, 13 (2007), 1850–1862.

[39] Zaman, M. H., Togashi, H., and Baddour, R. E. Deformation of monochromatic water wave trains propagating over a submerged obstacle in the presence of uniform currents. *Ocean Engineering 35*, 8-9 (2008), 823–833.

[40] Zaman, M. H., and Winsor, F. A 3d wave model to simulate the interaction of wave field in the presence of multi-structures. In *2014 Oceans-St. John's* (2014), IEEE, pp. 1–10.

[41] Zhou, L., Riska, K., Moan, T., and Su, B. Numerical modeling of ice loads on an icebreaking tanker: Comparing simulations with model tests. *Cold regions science and technology 87* (2013), 33–46.

Chapter 5

An Energy-Efficient Dynamic Positioning Controller for High Sea Conditions

This chapter was published.

https://www.sciencedirect.com/science/article/abs/pii/S0141118722002632

Abstract

In constantly changing high sea environments characterized by large waves, turbulent surface currents, and high wind gusts, a dynamic positioning (DP) system with enhanced positioning capabilities is becoming essential. The controller in a DP system calculates the force needed by the propellers and thrusters to counteract environmental forces and keep the vessel at its desired position. In addition to maintaining the position, minimizing the thruster demand is another control objective pursued by a type of controllers, termed as energy-efficient DP or the so-called "Green DP". In line with this objectives, the present work proposes a controller that minimizes thruster demand while maintaining position constraints. This novel energy-efficient controller (i.e., like Green-DP) exploits the structure of the economic nonlinear model predictive controller (ENMPC) and adopts "green" objectives and performance metrics, including thruster energy efficiency. The MATLAB/Simulink simulator and toolbox add-ons were used in a simulation environment to demonstrate the performance of the proposed energy efficient DP, called Green-NMPC. The controller was tested for moderate to high sea wave conditions. The controller reduced up to 50% thruster demand in sway direction compared to NMPC while maintaining the vessel positioning objectives.

5.1 Introduction

Maritime operations in far offshore regions face additional environmental challenges. For instance, waves tend to be larger, winds stronger, and surface currents more turbulent. Unless these disturbances are filtered or adequately dealt with by the controller, they can cause excessive thruster movements leading to wear and tear in the thruster, poor controller performance, and reduced energy efficiency [17]. The noise effect in a dynamic positioning (DP) controller is commonly dealt with using different types of filters and observers. For example, [3] and [14]applied a nonlinear passive observer (NPO) along with a nonlinear proportional–integral–derivative controller with acceleration feedback (NPID-AFB). Model based filters such as, Kalman filter (KF) ([2]; [7];[8];[16]), nonlinear extensions of KF including extended Kalman filter (EKF) [20], unscented Kalman filter (UKF) [18] showed more success in filtering noise, and first and second order wave frequencies. Application of model based filter has also lead to interest in the use of model predictive controller (MPC) in the DP applications. As the controller is modelbased it is a natural fit for model based filters such as the KF and the EKF. Additionally, MPC calculates the control action by minimizing the offset over a prediction horizon. Therefore, the controller has a long term view and does not exert excessive control action immediately. Applications of Linear MPC and nonlinear model predictive controller (NMPC) have been reported in literature for station-keeping as well as high- and low-speed reference tracking [22]. In [19], researchers implemented a linear MPC for DP use in a semi-submersible platform. [11] presented a relaxed dynamic positioning control method using NMPC. [10] used two tightly coupled UKF to estimate states and unknown disturbances, together with an NMPC algorithm. The controller performance was evaluated in real-time on a high-fidelity simulator. To summarize, the controllers reported in the literature used various model based filters to filter out first order and second order wave frequencies. There has been less work on using the controller configuration to deal with the wave frequencies and noise. Also, the control objectives have been mostly to maintain the position tightly. As a result these controllers often impart large and erratic control demand. This can be severely diminishing to

the useful life of the thrusters. In some cases, such control demands are artificially minimized by applying a filter, imposing a ramp rate, and introducing move accumulation. However, all these are ad hoc methods and thus do not deliver optimal control performance.

Kongsberg Inc. has been marketing a more environmentally friendly control system under the name "Green DP", which is claimed to minimize excessive thruster movements. The idea is to minimize the thruster movement, especially during moderate environmental conditions to minimize energy consumption and provide a greener option. The controller has three major components: environmental compensator, model predictive controller, and position predictor. In order to minimize thruster demand a low gain PD controller was used. In addition to the PD controller an NMPC was used with constraints set at the outer boundary of the operational region to prevent the vessel from drifting outside the operational region [9]. However, no further details about the controller structure are available in the published literature. In contrast to Green-DP the proposed method used NMPC solely for the entire operational region.

Motivated by the goals of Green DP, in this paper, we propose a controller that is formulated on the structure of economic NMPC (ENMPC). The goal of the controller is to minimize the operational cost of the DP operation, specifically the thruster demand and thus wear and tear of the thruster without compromising the position constraints. In a typical NMPC, the cost minimized at each step is not necessarily directly related to the economic cost of the plant operation. Usually, a linear programming (LP) layer will provide the optimal setpoint by minimizing the costs associated with a steady-state operation. In ENMPC, the cost information is directly included in the optimization layer. The setpoint tracking stage cost of an NMPC is changed to economic cost in an ENMPC [1].

This work presents a controller that is based on the ENMPC structure with significant modifications to achieve the "green" objective. We call the controller "Green-NMPC". The proposed Green-NMPC also uses a UKF-based observed module to

filter out high-frequency noise from the sensor measurements. The controller performance is compared with two benchmark controllers, NMPC and NPID. The present work's further contribution is to evaluate each controller's performance in high sea conditions, while most results in the literature are reported for mild to moderate sea conditions. For this study, the term "high" indicates wave height greater than 6 m as well as wave peak periods of more than 10 s ($T_p > 10s$). Such conditions are generally the norm in the North Atlantic and prevail for nearly half the time the vessels are at sea.

The remainder of the paper is organized as follows: Section 2 provides the system description of the 3-DOF (degrees of freedom) dynamic model ship, Section 3 describes the disturbances and their simulation, Section 4 presents the proposed Green-NMPC structure, Section 5 presents the results and discussions, and Section 6 concludes the paper.

5.2 Mathematical Modeling of Vessel

For a ship depicted in Fig. 5.1, a simplified mathematical model of vessel dynamics and kinematics with 3 DOF [10] is presented in Eq. (5.1).

$$M_{RB}\dot{v} + M_A\dot{v}_r + C_{RB}(v)v + C_A(v_r)v_r + D(v_r)v_r = \tau \tag{5.1}$$

$$\dot{\eta} = J(\psi)v \tag{5.2}$$

where , $M_{RB} \in R^{3\times3}$ and $M_A \in R^{3\times3}$ are the rigid body mass matrix representing the inertia of the vessel and the hydrodynamic added-mass matrix, and, $C_{RB} \in R^{3\times3}$ and $C_A \in R^{3\times3}$ are the rigid body Coriolis and centrifugal components as well as added-mass derivatives corresponding to the velocity coupling, the matrix, $D \in R^{3\times3}$ includes energy dissipative terms due to relative motion between vessel and surrounding fluid, $\tau = \tau_c + \tau_{c.s} + \tau_\omega$ is the applied force with τ_c is the control input,

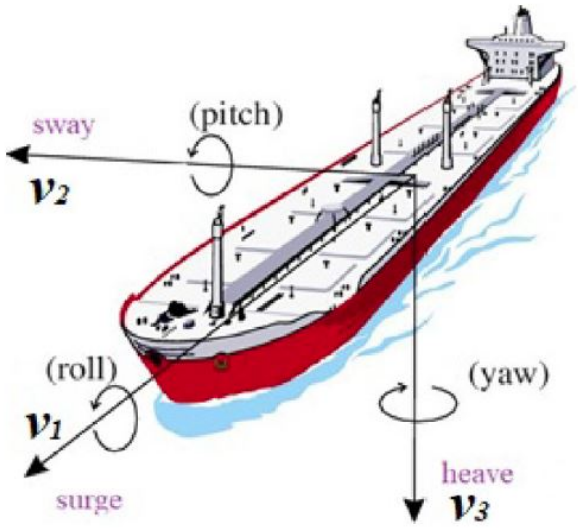

Figure 5.1: Schematic diagram of a vessel with its motion directions [5].

$\tau_{c.s}$ is the surface current force, and τ_ω is the wave force. Furthermore, $\eta = [x,\ y,\ \psi]^T$ where (x, y) is the horizontal position vector relative to the inertial frame and ψ is the vessel heading in an inertial frame $J(\psi) \in R^{3\times3}$ is the rotational matrix between the inertial frame and the body frame. Also, $\nu = [\nu_1,\ \nu_2,\ \nu_3]^T$ with ν_1, ν_2, and, ν_3 are the body-fixed surge velocity, sway velocity, and yaw rate, respectively. The term ν_r represents velocity relative to the current. Fig. 5.1 shows the sign conventions.

The rotational matrix $J(\psi)$ is computed as follows:

$$J(\psi) = \begin{bmatrix} cos(\psi) & -sin(\psi) & 0 \\ sin(\psi) & cos(\psi) & 0 \\ 0 & 0 & 0 \end{bmatrix} \tag{5.3}$$

The vessel is considered to have a typical set of sensors including accelerometer, gyroscope, attitude sensor, and differential global positioning system (DGPS) sensor.

Table 5.1: Definition of sea states (Price, 1974).

Number	Description of sea state	Significant wave height,H_s[m]	Peak Wave Frequency ω_p[rad/s]	Probability in North Atlantic
1	Moderate	1.25–2.5	0.79–0.68	40.99
2	Rough	2.5–4.0	0.68–0.60	21.33
3	Very rough	4.0–6.0	0.60–0.53	7.01
4	Very rough	6.0–9.0	0.53–0.46	2.69
5	Extreme	9.0–14.0	0.46–0.39	0.43

5.3 Disturbance Modeling

The setpoint stabilization under various environmental disturbances is of prime importance in ship DP operations. This study simulates wave action for various sea states. The simulator features an environment module that simulates wave, and surface current. Wave characteristics of different sea conditions are provided in Table.5.1.

5.3.1 Ocean Waves

The wave disturbance was simulated using the wave module of the MSS toolbox. Fig. 5.2 shows the overall methodology for calculation of the wave force. The input parameters to the module are significant wave height, H_s and average zero crossing wave period, T_z. The modified Pierson–Moskowitz (MPM) expressions were used to calculate the wave given by

$$S(\omega) = A_{MPM}\omega^{-5}exp(-B_{MPM}\omega^{-4}) \tag{5.4}$$

where, $S(\omega)$ describes a wave spectrum, with $\Delta\omega$ designating constant difference between frequencies; are given by,

$$A_{MPM} = \frac{4\pi^3 H_s^2}{T_z^4} \tag{5.5}$$

$$B_{MPM} = \frac{16\pi^3}{T_z^4} \tag{5.6}$$

The time-domain realizations for wave spectra is given by Eq. (5.7),

$$\xi(t) = \sum_{k=1}^{N} \sum_{i=1}^{M} \sqrt{2S(\omega_k, \beta_i)\Delta\omega_k \Delta\beta_i} sin(\omega_k t + \varepsilon_{ki}) \tag{5.7}$$

where for each wave, the phase angle ε_{ki} is uniformly distributed over the interval $(0, 2\pi)$ or equivalently, $(-\pi, \pi)$, β_i describes the angle at which waves impact the vessel, ε_k describes phase, ω_k is the randomly selected wave frequencies, N frequencies and M directions are selected from the range $\Delta\omega$ and $\Delta\beta$ [5]. The wave accelerations are calculated as follows:

$$a_1(t) = \sum_{k=1}^{N} \sum_{i=1}^{M} \omega_k^2 \sqrt{2S(\omega_k, \beta_i)\Delta\omega_k \Delta\beta_i} cos(\omega_k t + \varepsilon_{ki}) \tag{5.8}$$

$$a_3(t) = \sum_{k=1}^{N} \sum_{i=1}^{M} -\omega_k^2 \sqrt{2S(\omega_k, \beta_i)\Delta\omega_k \Delta\beta_i} cos(\omega_k t + \varepsilon_{ki}) \tag{5.9}$$

Assuming that the forces are distributed evenly along the vessel's main dimension, the first order and second order wave-induced forces are calculated using Eqs. (5.10) and (5.11) respectively.

$$\tau_{\omega 1} = \begin{bmatrix} \rho_\omega V a_1 cos(\beta_0) \\ \rho_\omega V a_1 sin(\beta_0) \\ \rho_\omega V D a_3 \end{bmatrix} \tag{5.10}$$

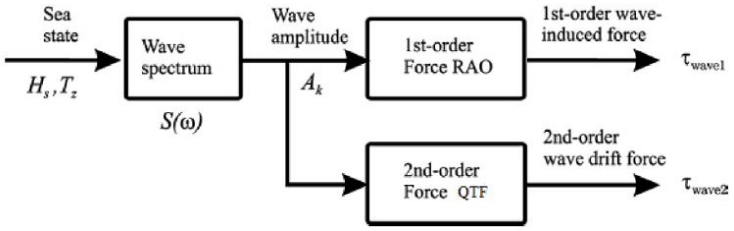

Figure 5.2: Overall structure of the proposed dynamic positioning system

$$\tau_{\omega 2} = \begin{bmatrix} \frac{1}{8}\rho_\omega g(R_x(\omega)\xi)^2 Bcos(\beta_0) \\ \frac{1}{8}\rho_\omega g(R_y(\omega)\xi)^2 Lcos(\beta_0) \\ \frac{1}{8}\rho_\omega g(R_\psi(\omega)\xi)^2 BLDcos(\beta_0) \end{bmatrix} \tag{5.11}$$

where R_x, R_y, and R_ψ are reflection coefficients, ρ_ω is the density of water, V is the velocity of the ship, and β_0 is the main wave direction. L is the length, B is the width and D is the draught of the ship. Finally, Eq. (5.12) gives the total wave force acting on the ship [5]; [6].

$$\tau_\omega = \tau_{\omega 1} + \tau_{\omega 2} \tag{5.12}$$

5.3.2 Water current model

The 2D non-rotational current velocity is:

$$\dot{\eta}_c = \begin{bmatrix} V_c cos\beta_c \\ V_c sin\beta_c \\ 0 \end{bmatrix}^T \tag{5.13}$$

where current velocity is V_c and the angle between x-axis and the direction of current is β_c . Both V_c and β_c are slowly-varying 1st-order Gauss–Markov processes given as:

$$\dot{V}_c + \mu_1(V_c - V_{c0}) = \omega_1 \tag{5.14}$$

$$\dot{\beta}_c + \mu_2(\beta_c - \beta_{c0}) = \omega_2 \tag{5.15}$$

with V_{c0} and β_{c0} are mean values, $\mu_1 > 0$, $\mu_2 > 0$ and ω_1, ω_2 are Gaussian variables. In this study we used $\mu_1 = 0.1$, $\mu_2 = 0.2$, $\omega_1 \sim N(0, 0.02)$, $\omega_2 \sim N(0, 0.01)$. If $\mu_1 = 0$ and $\mu_2 = 0$, this would denote a random walk process, with a magnitude of velocity being constrained by saturation elements, as expressed in Eq. (5.16) [5]; [6],

$$V_{c,min} \leq V_c \leq V_{c,max} \tag{5.16}$$

The relative current velocities with respect to ship's fixed reference frame are:

$$V_{c,x} = V_c cos(\beta_c - \Psi) - \nu_1 \tag{5.17}$$

$$V_{c,y} = V_c sin(\beta_c - \Psi) - \nu_2 \tag{5.18}$$

Accordingly the resultant current forces acting on a surface vessel are given by,

$$\tau_{c,x} = \frac{1}{2} R_{wx} \rho_w A_T V_{c,x}^2 \tag{5.19}$$

$$\tau_{c,y} = \frac{1}{2} R_{wy} \rho_w A_L V_{c,y}^2 \tag{5.20}$$

where R_{wx} and R_{wy} are current drag coefficients, A_T is underwater transverse current projected area of the vessel, and A_L is underwater lateral current projected area of the vessel [5]; [23].

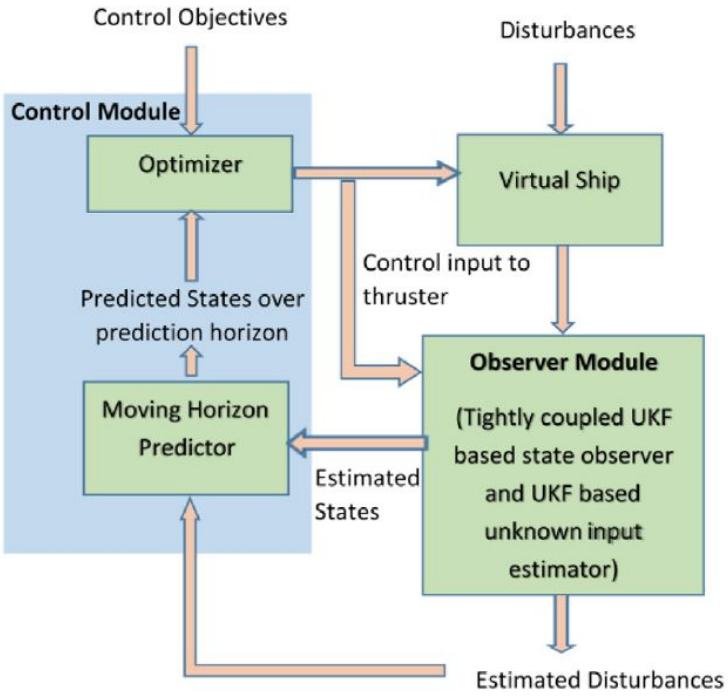

Figure 5.3: Overall structure of the proposed dynamic positioning system

5.4 Proposed Energy Efficient Controller

The overall structure of the proposed dynamic positioning system is shown in Fig. 5.3. A virtual ship is considered as the system, further we considered wave, and current are the two unmeasured disturbances acting on the system. These disturbances move the ship away from the desired position. It is required to estimate the unknown disturbances as well to generate control actions to negate the disturbance effect. The objectives were satisfied in two stages. In the first stage, two tightly coupled UKFs were used to estimate the states and unknown disturbances. Estimated states were used as the initial state of an NMPC based controller, and an optimal real-time solution was proposed. In [10], a similar formulation for NMPC was used. However, the objective of the NMPC was to maintain the position of the vessel precisely, which demanded aggressive thruster action. In the proposed Green-NMPC,

the objective function is defined such that it allows the vessel to float inside the safety limit with reduced thruster movements. The weights in the objective function are functions of the deviation from the target position rather than constant values as in typical NMPC operations. Thus, both safety targets and energy efficiency are achieved through the improvement of the controller. Different components of the dynamic positioning system are described in the following subsections.

5.4.1 Observer Module

For estimating potential sensor biases, unknown disturbances and overall vessel states, an observer module is used that employs two parallel UKF sub-modules. UKF 1 is used to estimate potential sensor bias and overall vessel states. UKF 2 estimates disturbance inputs by applying the vessel's dynamic model Eq. (5.1) in conjunction with the UKF 1 state estimation results. The two UKF modules iteratively estimate the noise and bias free states and unknown inputs. The details of the algorithm can be found in [10].

5.4.2 Control Module

Consider a discrete time-constrained dynamic system

$$\eta_{k+1} = f(\eta_k, u_k); \quad g(\eta_k, u_k) \leq 0 \tag{5.21}$$

where f is the nonlinear system dynamics and g is the linear or nonlinear constraint function. For the DP system, the economic stage cost function, $\varphi^{ec}(\eta_k, u_k)$, is defined as follows:

$$\varphi^{ec} = L_x \left\| F_{x,k} - F_{x,k-1} \right\|^2 + L_y \left\| F_{y,k} - F_{y,k-1} \right\|^2 + L_\psi \left\| T_{\psi,k} - T_{\psi,k-1} \right\|^2 \tag{5.22}$$

where $L_{l\in x,y,\psi}$ is a function defined in Eq. (5.26), F_x and F_y are the thruster forces in surge and sway direction, and T_ψ is the torque for yaw rotation.

When the cost function is not strongly convex a quadratic regularization term is added to the cost function [13]. The cost function with the regularization term has the following form:

$$\varphi(\eta_k, u_k) = \varphi^{ec}(\eta_k, u_k) + \|\eta_k - \eta_s\|^2 \pi \tag{5.23}$$

The ENMPC tries to find a feasible set of control actions that can keep the system within the constraints by minimizing the cost function

$$\begin{aligned} \min_{\eta_k, u_k} O(\eta_k, u_k) &= \sum_{k=0}^{N_p-1} \varphi(\eta_k, u_k) \\ \text{s.t.} \quad \eta_{k+1} &= f(\eta_k, u_k); \\ g(\eta_k, u_k) &\leq 0 \end{aligned} \tag{5.24}$$

The final stage cost function in expanded form is:

$$\begin{aligned} \varphi^{ec} = L_x \|F_{x,k} - F_{x,k-1}\|^2 + L_y \|F_{y,k} - F_{y,k-1}\|^2 + L_\psi \|T_{\psi,k} - T_{\psi,k-1}\|^2 \\ + \|x_k - x_r\|^2 \pi_1 + \|y_k - y_r\|^2 \pi_2 + \|\psi_k - \psi_r\|^2 \pi_3 \end{aligned} \tag{5.25}$$

A conventional NMPC uses constant weight matrices $L = [L_x + L_y + L_\psi]$ and $\pi = [\pi_1 + \pi_2 + \pi_3]$ for penalizing inputs and states, respectively. These parameters are chosen to minimize corresponding deviations based on operational requirements. In our proposed Green-NMPC, the components of matrix L are set as a function of the position of the vessel along the x and y directions. The weight components are defined to meet the following performance criteria.

1. If the position of the vessel is well inside the safety limits, there is less concern about the position of the vessel. The controller's objective shifts to minimizing the thruster energy. In order to mimic this behavior, the weight corresponding to the

thruster force needs to be set to a high value when the vessel is well inside the safety limits. It allows the controller to penalize thruster demands more compared to the state deviations. As a result, thruster demand is minimized significantly. Having a relaxed weight on state deviation, the controller allows the vessel to float around inside the safe operation region instead of tracking the reference tightly.

2. When the vessel nears the safety limits, the controller's priority changes to maintaining the position and keeping the vessel within the safety limits. Accordingly, as the vessel nears a safety limit, weights on the thruster force should be low so that the controller does not penalize the objective function for thruster usage. This will allow the controller to utilize all available thruster power to keep the vessel within safety limits.

To fulfill these two criteria, the weight functions (L_x, L_y) were set as continuously varying nonlinear function of the respective axis distance. For example, L_x that penalizes the thruster force F_x is defined as a function of x fulfilling the above requirements. After several trial and error, we selected the nonlinear function defined in Eq. (5.26).

$$L_x = 100 - \frac{x^4(log(|T_{th}|) - |x|)}{|T_{th}|} \tag{5.26}$$

where, T_{th} is the position threshold, and x is the current x-axis position of the vessel. L_y is also defined similarly.

Fig. 5.4 (solid blue line) shows the shape of the weight function. Clearly, the weight function is convex. However, the convexity of the stage cost function Eq. (5.25) is still uncertain. The economic stage cost may not be strictly increasing, therefore, it does not satisfy the Lyapunov based criteria for stability analysis [21]. Significant work has been done to develop cost functions for the ENMPC that adhere to the Lyapunov function to provide a stable solution. According to [4], the cost function Eq. (5.25) can be admitted as Lyapunov function if,

Condition 1: the system is weakly controllable, i.e.,

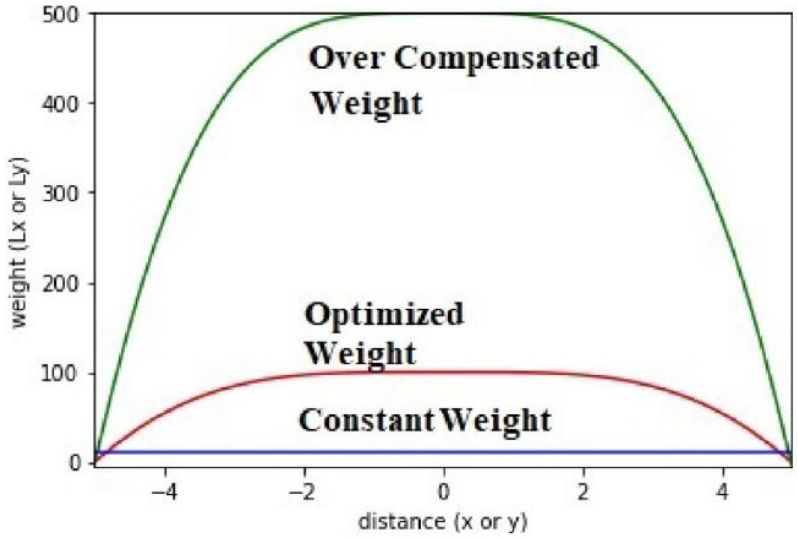

Figure 5.4: Shapes of weighting function L used in Green NMPC.

$$\sum_{kk=1}^{N-1} |u_k - u_s| \leq \gamma(|\eta - \eta_s|)$$

Where γ is a positive constant, and subscript s denotes steady-state point.

Condition 2: the rotated stage cost function follows strong duality. The rotated stage cost is given by adding the constraints to the cost function (Eq. 5.25), changing the optimization problem to the following form:

$$\begin{aligned}\varphi_{rotated}(\eta_k, u_k) = L_x \left\|F_{x,k} - F_{x,k-1}\right\|^2 + L_y \left\|F_{y,k} - F_{y,k-1}\right\|^2 \\ + L_\psi \left\|T_{\psi,k} - T_{\psi,k-1}\right\|^2 + \left\|x_k - x_r\right\|^2 \pi_1 \\ + \left\|y_k - y_r\right\|^2 \pi_2 + \left\|\psi_k - \psi_r\right\|^2 \pi_3 + {\lambda_s}^T(\eta_k - f(\eta_{k-1}, u_{k-1}))\end{aligned} \quad (5.27)$$

$$\min_{u_k, \eta_k} \sum_{k=0}^{N_p-1} \varphi_{rotated}(\eta_k, u_k) \quad (5.28)$$

$$\text{s.t.} g(\eta_k, u_k) \leq 0$$

where λ_s is the multiplier from the equality constraints. Note that the inequality constraints are not added to the rotated cost. To prove duality, it has to be shown that the solutions of Eqs. (5.25) and (5.28) will give the same outcome. We performed extensive simulation, reported in Section 5.2, to investigate the convergence of the algorithm. The proposed Green-NMPC for dynamic positioning calculates the required thruster force (i.e., the forces for the X and Y directions, along with the torque) to regulate the ship's position. This approach solves a constrained objective function to evaluate the optimum control action at each time step. Estimated states from the observer module are used as the initial states for the controller. The predicted state trajectories are evaluated using the vessel model and estimated disturbance over a fixed prediction horizon T_H from the initial state. The NMPC approach uses moving horizon predictions over the fixed windows to solve at each iteration ([12];[22]). After penalizing the deviation of the states and control inputs from the references, the following objective function is solved at any time step t_0:

$$\begin{aligned} J_{t_0} = \arg\min_{\eta,u} \quad & \sum_{k=t_0}^{t_0+T_H} L_x \left\|F_{x,k} - F_{x,k-1}\right\|^2 + L_y \left\|F_{y,k} - F_{y,k-1}\right\|^2 \\ & + L_\psi \left\|T_{\psi,k} - T_{\psi,k-1}\right\|^2 + \left\|x_k - x_r\right\|^2 \pi_1 \\ & + \left\|y_k - y_r\right\|^2 \pi_2 + \left\|\psi_k - \psi_r\right\|^2 \pi_3 \end{aligned} \tag{5.29}$$

Or more compactly,

$$J_{t_0} = \arg\min_{\eta,u} \sum_{k=t_0}^{t_0+T_H} \left\|u_k - u_{k-1}\right\|^2 L + \sum_{k=t_0}^{t_0+T_H} \left\|\eta_k - \eta_r\right\|^2 \pi \tag{5.30}$$

$$\text{s.t.} \eta_{k+1} = f(\eta_k, u_k)$$

$$\mu(u_k, \eta_k) \leq 0$$

where π is constant weighting matrix and L is continuously varying nonlinear function as defined in Eq. (5.26), x_r denote reference states, and t_0 indicates the control

computation's start time, η_k and u_k are system states and thruster input at time step 'k'. System dynamics' constraints cover each state (six in total), ($[\eta \quad v]$), but only the control inputs u_k, position, and orientation vector η_k are penalized. The reference state vector serves as the setpoint; for the DP problem, setpoint remain at zero. The Green-NMPC solves the objective function at every time step. The output is a series of control actions $u_k = [F_{xk}, F_{yk}, T_{\psi k}]_{k=t_0}^{t_0+T_H}$ and predicted states $\eta_k = [x_k, y_k, \psi_k]_{k=t_0}^{t_0+T_H}$. From the set of control actions, the first set of forces and torque ($[F_{x1}, F_{y1}, T_{\psi 1}]$) is applied to the thruster and the entire optimization step is repeated in the next time step.

5.5 Results and Discussion

To demonstrate the performance of the proposed algorithm, specifically energy efficiency and maintaining ship position, several simulations were carried out using the Cybership II ship model described in Appendix A. We considered two models of Cybership II: (i) a low frequency model of Cybership II without any thruster dynamics, and (ii) a low frequency model of Cybership II with detailed thruster dynamics. The parameters for the normalized model are calculated by dividing each parameter by the mass of the vessel. For simulation, the sampling time is set at 0.1 s, and a prediction horizon of 7 samples were selected. The x and y axis limits were set to $-5m < x < 5m$ and $-5m < y < 5m$. The thruster limits, torque (T_ψ) and applied force (F_x, F_y), were set to -250N-m$< T_\psi <$ 250N-m and $-25N < F_x, F_y < 25N$ respectively. The MATLAB function "fmincon" is utilized for optimization. The results of the Green-NMPC are compared with an NMPC [10] and a Nonlinear PID (NPID) [6] controller for identical environmental conditions. In this study, the controller's performance was evaluated for two sea conditions: 'moderate' and 'high'. 'Moderate' condition refers to a sea state characterized by wave height (H = 2.5 m) with peak wave frequency ($\omega_p = 0.79\ rad/s$). The 'high' condition refers to a sea state that is characterized by large wave height (H = 6 m) along with peak wave frequency ($\omega_p = 0.53\ rad/s$). Parameters for these and other sea states are provided

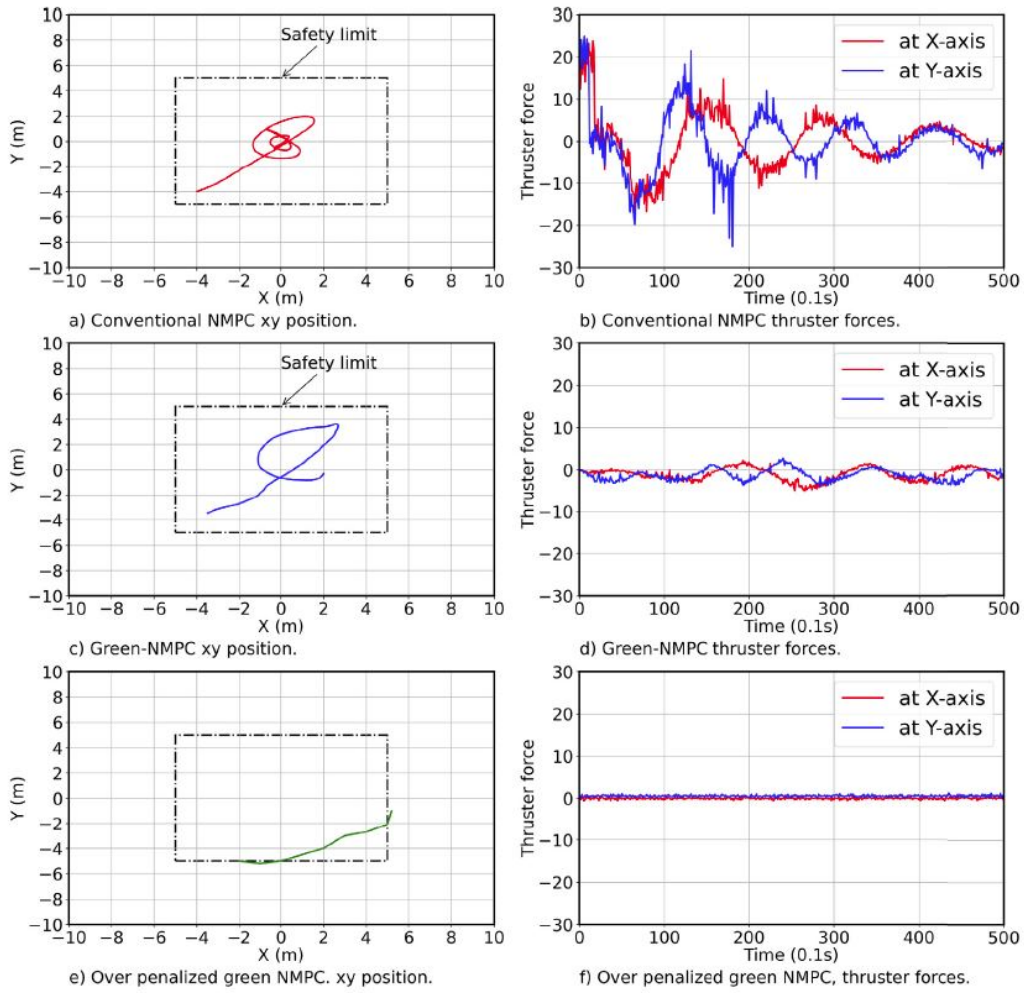

Figure 5.5: Effect of weight function on ship position and thruster demand for conventional NMPC (constant weight), Green-NMPC (with optimized weight function), and the Green- NMPC (with over-penalized weight function).

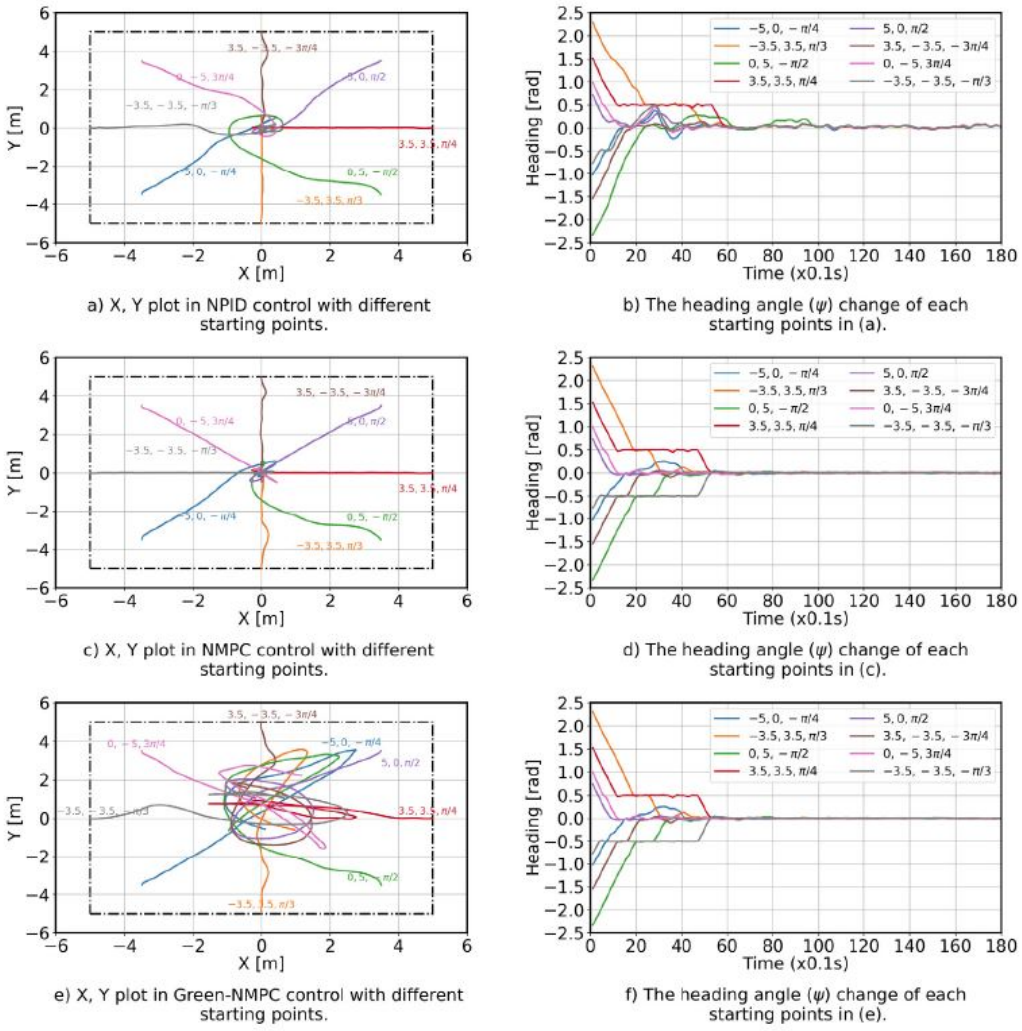

Figure 5.6: Convergence comparison of NPID, NMPC, and Green-NMPC controllers: ship X, Y position and heading angle ψ changing with time for ship starting from different initial points.

in Table 5.1 [15].

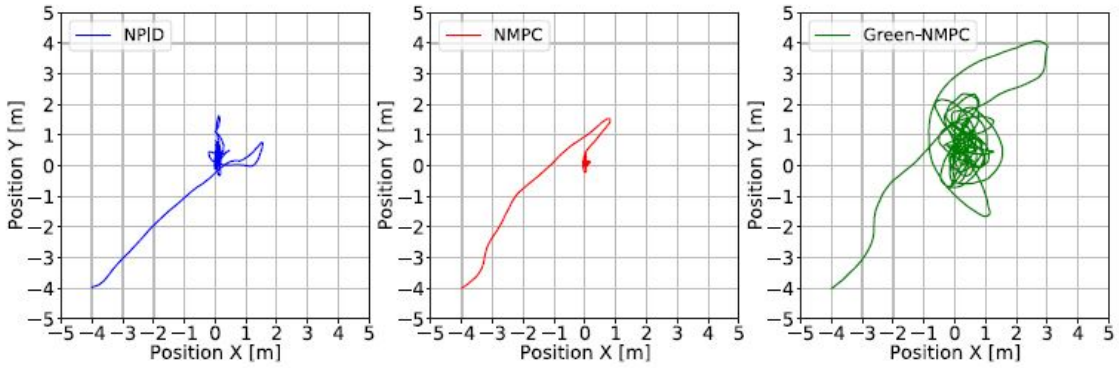

Figure 5.7: Position of the vessel in xy-plane starting from [-4, -4, 0] for high sea state (wave parameters: $H_s = 6$ m, $\omega_p = 0.53\ rad/s$, $\beta_0 = 0$; current parameters: $V_{c0} = 1.5\ m/s$, $\beta_{c0} = 0$).

5.5.1 Selection of Weight Function Parameters

The nonlinear weighting function (L_x, L_y) is plotted in Fig. 5.4. The proposed function was developed considering that safety limits are at -5 m and 5 m in both X and Y directions, (T_{th}) was set to 10 m equal to the range of motion along x and y direction. Setting the maximum weight to 100 signifies that priority of minimizing the thruster demand increases by two order of magnitude compared to maintaining the position when the vessel is close to the setpoint. The x^4 term makes the curve flat near origin, while the "log" term forces the weights to 0 at the boundaries. To illustrate the impact of changing the weight function, three different weight functions were selected, and the performance of dynamic positioning and thruster demands were observed qualitatively. For the first case (blue in Fig. 5.4), weight is kept constant similar to a conventional NMPC. For the second case (red in Fig. 5.4), the weight function is as described in Eq.(5.30) with optimized parameters that were subsequently used for the proposed Green-NMPC. Finally, the green line in Fig. 5.4 is for an overcompensated weight function after multiplying Eq. (5.26) by a factor of 5.

The responses of the DP system for these three weight functions are shown in Fig. 5.5(a to f). For all three cases, the starting point is set at (-4, -4, 0), and the safe operation region is defined as -5 m to 5 m coordinates for both X and Y directions. The vessel position and thruster force, and torque (Fig. 5.5(b, d, f)) are presented to demonstrate the impact of the weight functions. Results show that conventional NMPC tightly controls the position of the vessel with a significant.

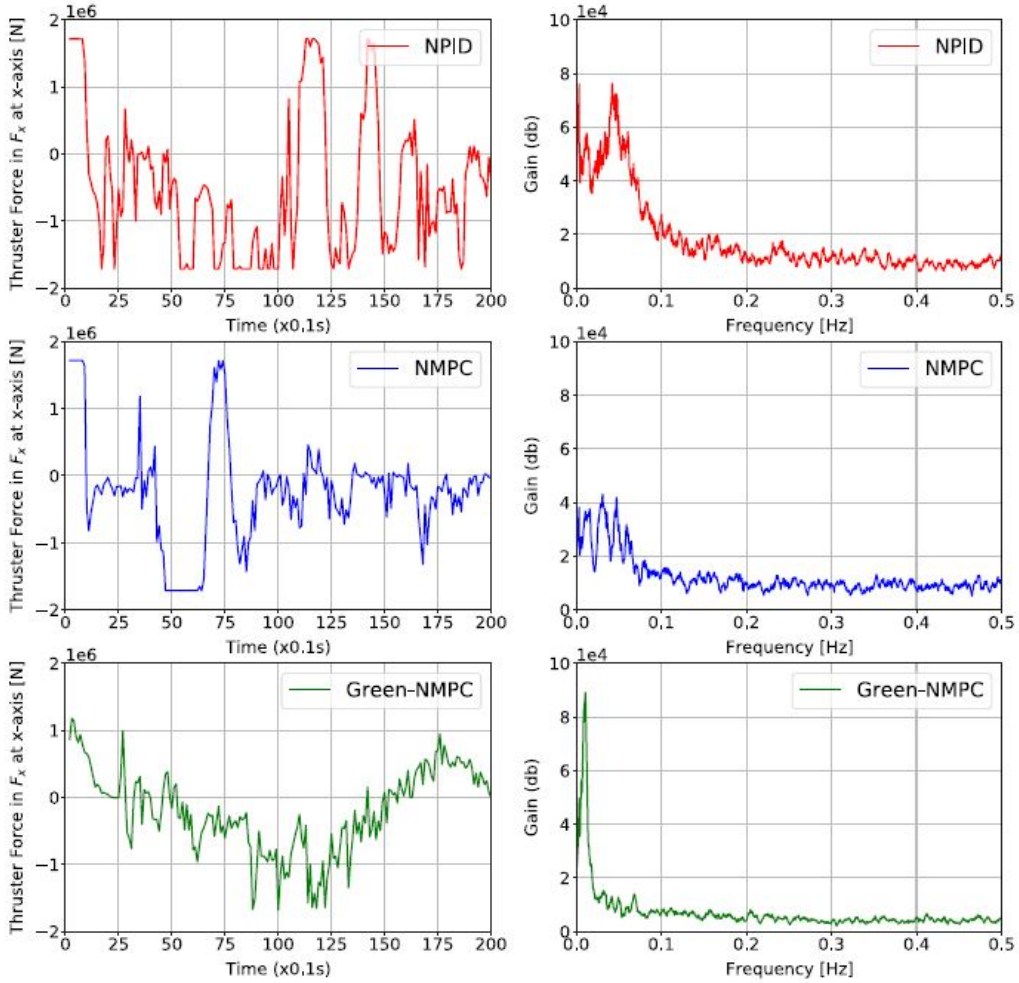

Figure 5.8: Thruster force and spectral density along x direction for different controllers for high sea state (wave parameters: $H_s = 6$ m, $\omega_p = 0.68\ rad/s$, $\beta_0 = 0$; current parameters: $V_{c0} = 1.5\ m/s$, $\beta_{c0} = 0$).

Thruster demand in both X and Y directions. For a similar scenario, the Green-NMPC reduces the thruster demand significantly using the penalty function. Finally, for the over penalized Green-NMPC, the weight function is significantly larger than the previous case. Due to its high weight, it has very little thruster fluctuations, and energy is reduced significantly. However, the safety objective is violated for this case, and the controller failed to keep the vessel inside the safety limits for a short duration. From this study, it is concluded that the weight function needs to be carefully chosen, maintaining a balance between safety criteria and energy consumption. For the Green-NMPC, the weight function described by Eq. (5.26) (second case of the current study) was used.

5.5.2 Convergence and Stability of the Controllers

In order to demonstrate the convergence and stability of the controller, eight different starting points were considered for the vessel.The controllers were used to drive the vessel to its origin. Current, and 'moderate' wave condition as given in Table 5.1 were the main disturbances. Fig. 5.6(a-f) show NPID, NMPC, and Green-NMPC's setpoint.

Table 5.2: Power and variance of control signals from different controllers for high sea state (wave parameters: $H_s = 6$ m, $\omega_p = 0.68\ rad/s$, $\beta_0 = 0$; current parameters: $V_{c0} = 1.5\ m/s$, $\beta_{c0} = 0$).

Direction	Property	NPID	NMPC	Green-NMPC
X	Power comparison	100%	93.7%	67.5%
	Variance $[N^2]$	11.04×10^6	10.61×10^6	6.86×10^6
Y	Power comparison	100%	111.8%	54.0%
	Variance $[N^2]$	15.07×10^6	18.19×10^6	9×10^6
ψ	Power comparison	100%	109.8%	116.6%
	Variance $[(N-m)^2]$	9.93×10^6	12.12×10^6	11.69×10^6

Stabilization. The XY position of the vessel for NPID, NMPC, and Green-NMPC controllers are shown in Fig. 5.6(a, c, e) when the reference was set at the origin [0, 0, 0]. Results show that for all cases, vessel positions were well within the safety limits.

Table 5.3: Power and variance of control signals from different controllers for high sea state (wave parameters: $H_s = 6$ m, $\omega_p = 0.68\ rad/s$, $\beta_0 = 0$; current parameters: $V_{c0} = 1.5\ m/s$, $\beta_{c0} = 0$).

Direction	Property	NMPC	Green-NMPC
X	Power comparison	100%	89.29%
	Variance $[N^2]$	1.07×10^7	6.86×10^6
Y	Power comparison	100%	81.74%
	Variance $[N^2]$	1.595×10^7	9.227×10^6
ψ	Power comparison	100%	90.2%
	Variance $[(N-m)^2]$	9.77×10^6	8.167×10^6

However, as Green-NMPC relaxes the point reference tracking to area tracking inside the safety limits there is more vessel movement for Green NMPC. Fig. 5.6(e) and (f) show that Green-NMPC maintains the vessel movement within the safety limits. At each time step, the target was attained and maintained. The vessel heading eventually converged to 0 rad setpoint (see Fig. 5.6(b, d, f)).

5.5.3 Performance Comparison of the Controllers at Different Sea Conditions

The performance of the controllers were evaluated for 'high' sea conditions. The simulation conditions for 'high' sea conditions are provided in Table 5.1. Safety limits are set at $-5m$ and $+5m$ in both X and Y directions. Hence, a safe operating area is essentially a $10m \times 10m$ square on the XY plane. The position of the vessel on the XY plane is plotted to observe whether the controller can keep the vessel inside the safe operation square. Controllers' performances were also assessed based on the control demands of the thrusters. The variance and power of the control signals are evaluated for each case. A controller that can maintain vessel position within the safe operating region with the least variance in control signal and power demand is considered to be the best. Simulations were performed first on the low frequency Cybership II model without any thruster dynamics, followed by simulations on the

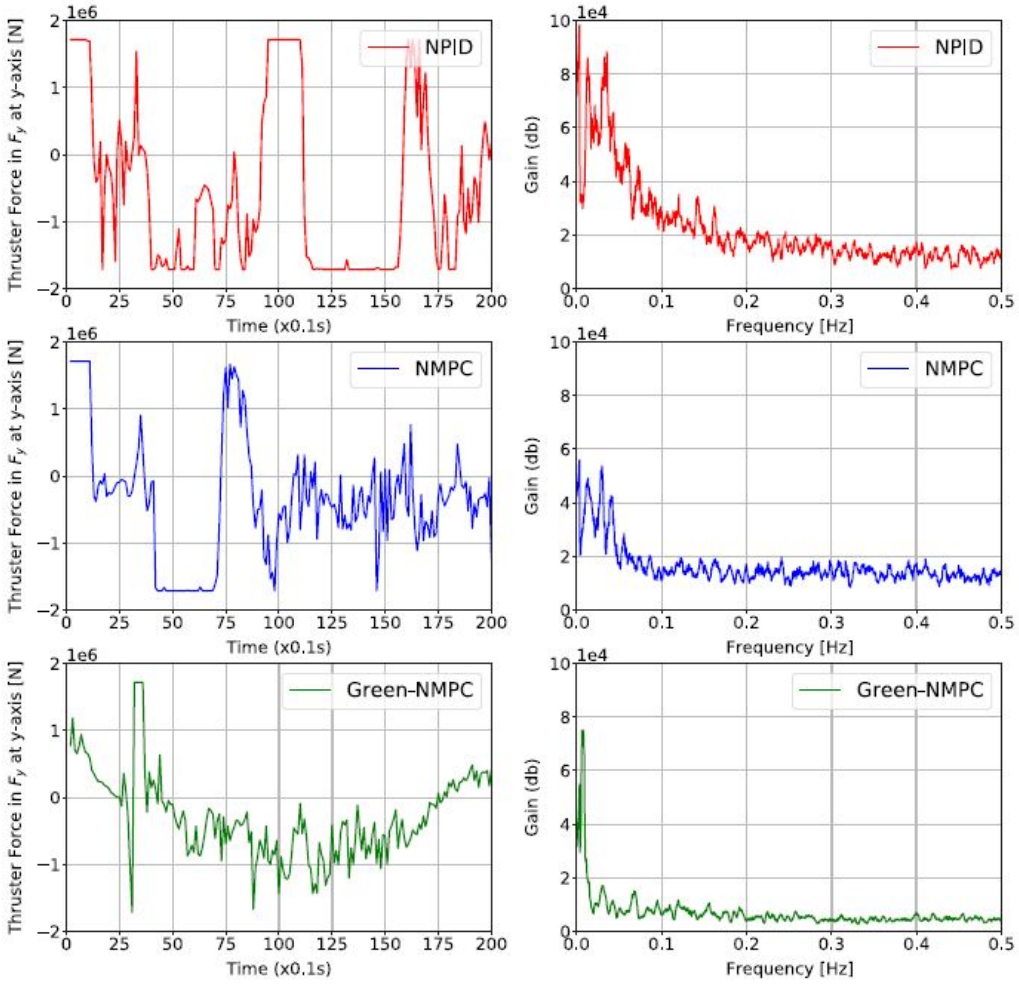

Figure 5.9: Thruster force and spectral density along y direction for different controllers for high sea state (wave parameters: $H_s = 6$ m, $\omega_p = 0.53\ rad/s$, $\beta_0 = 0$; current parameters: $V_{c0} = 1.5\ m/s$, $\beta_{c0} = 0$).

Cybership II model with detailed thruster dynamics.

Simulation Results: Low Frequency Cybership II Model

The starting position of the vessel is considered at (-4, -4, 0). The trajectory of the vessel on the XY plane is shown in Fig.5.7. As the starting position is close

to the safety limit, initially NPID, NMPC, and Green-NMPC act similarly. Hence the Figs. 5.8-5.10 show that thruster is almost saturated for all controllers initially. When the controller moves from the edge to the center of the safe operation zone, the Green-NMPC starts to put more weight on the thruster demand. Thus, the thruster demand are reduced significantly compared to the NMPC, and the vessel floats around within the safety limits. This claim is further verified by the spectral gain of control signals shown in Figs. 5.8-f, 5.9-f and 5.10-f. The spectral density of Green-NMPC shows a higher gain for low frequency region and lower gain for high frequency region compared to the other two benchmark controllers. A lower gain in high frequency region signifies that control actions of Green-NMPC has less high-frequency movements. Performance of the control action is quantified from the evaluated variance and power of the control signals. The variance of the control signals and relative power consumption of the thrusters are reported in Table 5.2 for the [-4, -4, 0] starting point. Clearly the weight function of the Green-NMPC is able to maintain a trade-off between keeping the position and minimizing thruster movements. Especially the controller was effective in minimizing high frequency movements of the thruster. The results suggest that Green-NMPC has significantly less thruster demand compared to NMPC, up to 50% less thruster demand in sway direction, and hence reduces the overall power consumption and wear and tear of the thruster.

5.5.4 Simulation Results: Cybership II with Detailed Thruster Dynamics

Finally, the optimized controller was implemented on the Cybership II model with detailed thruster dynamics. The performance of the Green-NMPC was compared qualitatively against the NMPC in Figs. 5.11 and 5.12. Clearly the thruster demand calculated by the controllers are noisy compared to the applied thruster force and torque.

The time plot shows fluctuations in thruster demands is much higher in NMPC

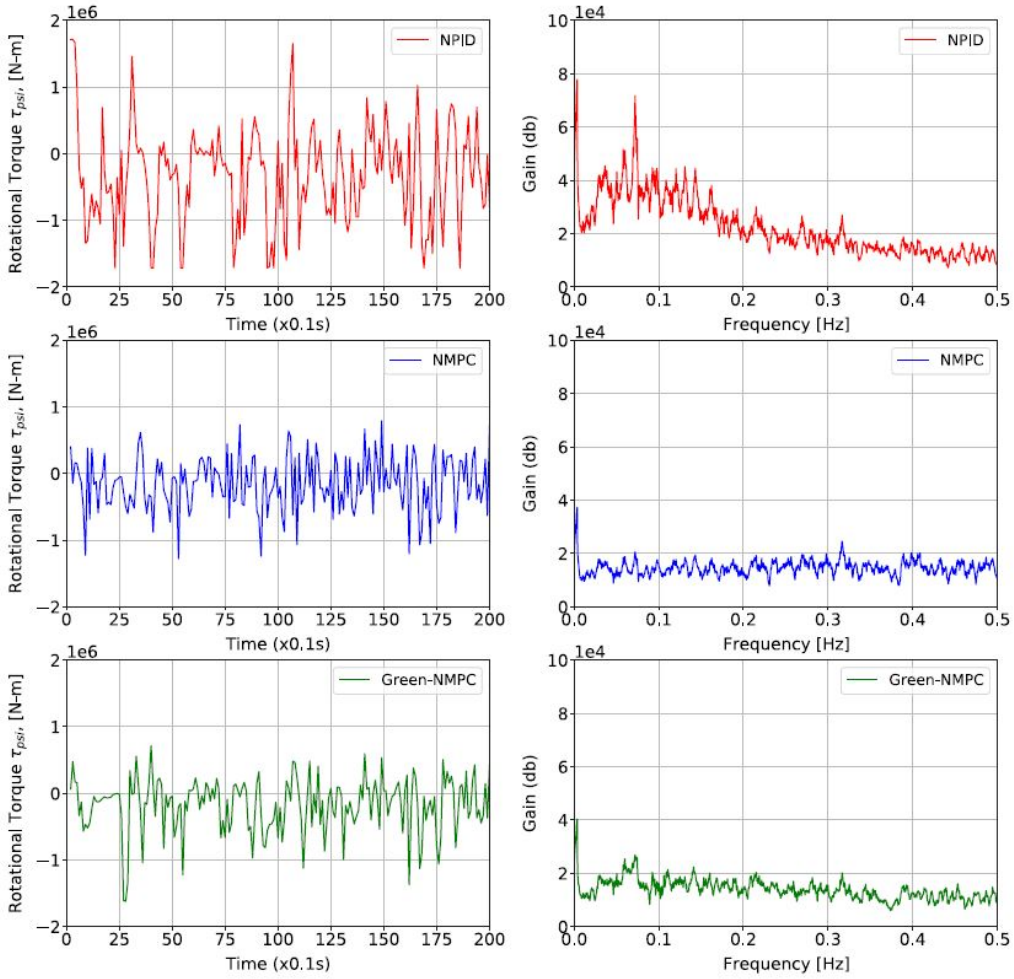

Figure 5.10: Thruster torque and spectral density along the rotational axis for different controllers for high sea state (wave parameters: $H_s = 6$ m, $\omega_p = 0.68\ rad/s$, $\beta_0 = 0$; current parameters: $V_{c0} = 1.5\ m/s$, β_{c0} 0).

compared to the Green-NMPC. Further the spectral plot shows that the gain in the low frequency region is lower for Green-NMPC compared to the NMPC. Due to the inertia of the thrusters, part of the high frequency noise was filtered from the signal. There is no marked difference between the spectral plots in the high frequency region.

The performance of the controllers are compared quantitatively in Table 5.3. In

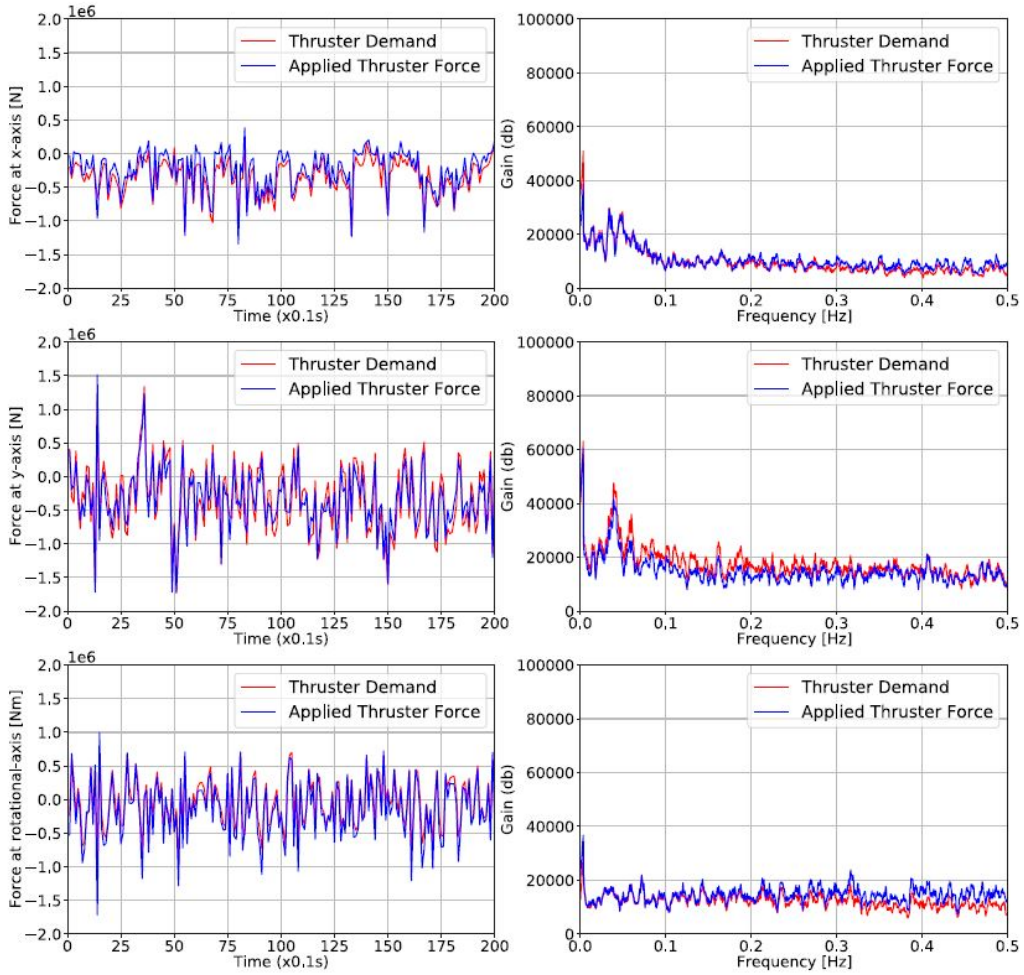

Figure 5.11: Cybership II with detailed thruster model controlled using NMPC under high sea condition (wave parameters: $H_s = 6$ m, $\omega_p = 0.68\ rad/s$, $\beta_0 = 0$; current parameters: $V_{c0} = 1.5\ m/s$, β_{c0} 0).

all three directions the variances of the thrusters are less for Green-NMPC compared to the NMPC. Power consumption is also less for Green-NMPC. These results further validate the advantages of Green-NMPC in conserving energy. The ship model used for the simulation cases is more realistic as it has detailed thruster model. This provides further assurance for the potential energy savings of Green-NMPC in real-life application.

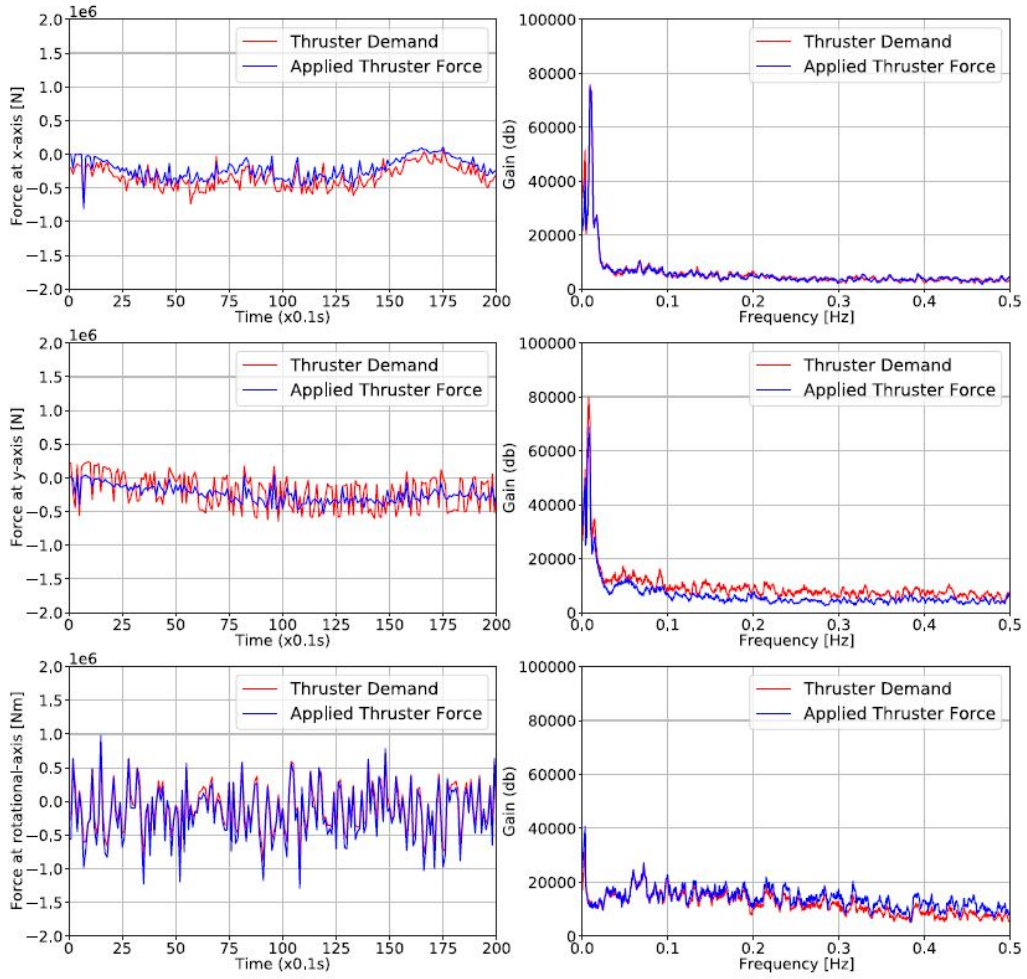

Figure 5.12: Cybership II with detailed thruster model controlled using Green-NMPC under high sea condition (wave parameters: $H_s = 6$ m, $\omega_p = 0.68\ rad/s$, $\beta_0 = 0$; current parameters: $V_{c0} = 1.5\ m/s$, β_{c0} 0).

5.6 Conclusions

In this study, an energy-efficient NMPC based controller is developed for the dynamic positioning of marine vessels, we call the controller Green-NMPC. The Green-NMPC is motivated by the control goal of minimizing thruster demand. It is based upon

the theoretical framework of the economic MPC (ENMPC). The controller uses dynamic weights in the cost function depending on the vessel position in contrast to the constant weights in conventional NMPC. Thus, if the vessel is well within the safety limit, the controller weighs more on the thruster movements and reduces the thruster movement. On the contrary, if the vessel approaches the unsafe region, the cost function weighs more on state deviation and thus works similar to the conventional NMPC. The proposed controller was implemented for 'moderate' and 'high' sea conditions. The controller performance, specifically energy efficiency of the ship, was compared against a conventional NMPC and a NPID controller. For all cases, including high sea conditions, the controller was found energy efficient while it maintained the vessel position inside the safety limits. The Green-NMPC showed less thruster demand in the time domain plots. It is further verified quantitatively from the variance and the spectral strength of the thruster demand. Relatively lower power demand was observed in the spectral plot for the Green-NMPC at the higher frequency range. The weight function for this study was developed empirically for the current safety targets. It needs further study to develop a methodology to select a weight function that is applicable for more general purpose.

Appendix A. SeaRose low frequency vessel model

The 3-DOF vessel model and the model parameters are given below (see Table 5.4):

$$M_{RB} = \begin{bmatrix} m & 0 & 0 \\ 0 & m & mx_G \\ 0 & mx_G & I_Z \end{bmatrix}$$

$$M_A = \begin{bmatrix} -X_{\dot{u}} & 0 & 0 \\ 0 & -Y_{\dot{v}} & -Y_{\dot{r}} \\ 0 & -N_{\dot{v}} & -N_{\dot{r}} \end{bmatrix}$$

$$C_{RB} = \begin{bmatrix} 0 & 0 & -m(x_G)r + v) \\ 0 & 0 & mu \\ m(x_G r + v) & -mu & 0 \end{bmatrix}$$

$$C_A = \begin{bmatrix} 0 & 0 & Y_{\dot{v}} v_r \\ 0 & 0 & -X_{\dot{u}} u_r \\ -Y_{\dot{v}} v_r & X_{\dot{u}} u_r & 0 \end{bmatrix}$$

$$D_L = \begin{bmatrix} -X_u & 0 & 0 \\ 0 & -Y_v & -Y_r \\ 0 & -N_v & -N_r \end{bmatrix}$$

$$D_{NL} = \begin{bmatrix} X_{|u|u}|u_r| & 0 & 0 \\ 0 & -Y_{|v|v}|v_r| - Y_{|r|v}|r| & -Y_{|v|r}|v_r| - Y_{|r|r}|r| \\ 0 & -N_{|v|v}|v_r| - N_{|r|v}|r| & -N_{|v|r}|v_r| - N_{|r|r}|r| \end{bmatrix}^T$$

Table 5.4: Ship parameters used in the study.

Parameter	Value
Mass, m	7.889×10^6 kg
Length of ship, L	85 m
Width, w_d	22m
Draught, d	7.2 m
x_G	3.22 m
I_Z	2.958×10^9 Kg.m^2
$X_{\dot{u}1}$	-6.86×10^5 Kg
$Y_{\dot{u}2}$	-2.0806×10^7 Kg
$N_{\dot{\omega}}$	-1.6807×10^9 Kg.m^2/s
X_{u1}	-6.5044×10^3 Kg/s
Y_{u2}	-8.2835×10^7 Kg/s
Y_{ω}	-2.0806×10^7 Kg.m/s
N_{u2}	8.9823×10^4 Kg.m/s
N_{ω}	-3.8168×10^8 Kg.m^2/s
$X_{\|u1\|u1}$	-2.9621×10^4 Kg/m
$Y_{\|u2\|u2}$	-3.6472×10^4 Kg/m
$Y_{\|\omega\|u2}$	-2.76115×10^5 Kg
$Y_{\|u2\|\omega}$	-2.76115×10^5 Kg
$Y_{\|\omega\|\omega}$	-1.7874×10^5 Kg.m
$N_{\|\omega\|\omega}$	-1.2605×10^9 Kg.m^2

References

[1] Amrit, R., Rawlings, J. B., and Angeli, D. Economic optimization using model predictive control with a terminal cost. *Annual Reviews in Control 35*, 2 (2011), 178–186.

[2] Balchen, J. G., Jenssen, N. A., and Sælid, S. Dynamic positioning using kalman filtering and optimal control theory. In *IFAC/IFIP symposium on automation in offshore oil field operation* (1976), vol. 183, Amsterdam, Holland, p. 186.

[3] Brodtkorb, A. H., Sørensen, A. J., and Teel, A. R. Increasing the operation window for dynamic positioned vessels using the concept of hybrid control. In *International Conference on Offshore Mechanics and Arctic Engineering* (2014), vol. 45370, American Society of Mechanical Engineers, p. V01AT01A046.

[4] Diehl, M., Amrit, R., and Rawlings, J. B. A lyapunov function for economic optimizing model predictive control. *IEEE Transactions on Automatic Control 56*, 3 (2010), 703–707.

[5] Fannemel, Å. V. Dynamic positioning by nonlinear model predictive control. Master's thesis, Institutt for teknisk kybernetikk, 2008.

[6] Fossen, T. I. *Handbook of marine craft hydrodynamics and motion control*. John Wiley & Sons, 2011.

[7] Fossen, T. I., and Perez, T. Kalman filtering for positioning and heading control of ships and offshore rigs. *IEEE control systems magazine 29*, 6 (2009), 32–46.

[8] Hassani, V., Pascoal, A. M., Aguiar, A. P., and Athans, M. A multiple model adaptive wave filter for dynamic ship positioning. *IFAC Proceedings Volumes 43*, 20 (2010), 120–125.

[9] Hvamb, O. G. A new concept for fuel tight dp control. In *Dynamic Positioning Conference* (2001).

[10] Jayasiri, A., Nandan, A., Imtiaz, S., Spencer, D., Islam, S., and Ahmed, S. Dynamic positioning of vessels using a ukf-based observer and an nmpc-based controller. *IEEE Transactions on Automation Science and Engineering 14*, 4 (2017), 1778–1785.

[11] Liu, Z. Sensor fusion and observer design for dynamic positioning. *Ph. D. dissertation* (2015).

[12] Mayne, D. Q., Rawlings, J. B., Rao, C. V., and Scokaert, P. O. Constrained model predictive control: Stability and optimality. *Automatica 36*, 6 (2000), 789–814.

[13] Miller, P. A., Farrell, J. A., Zhao, Y., and Djapic, V. Autonomous underwater vehicle navigation. *IEEE Journal of Oceanic Engineering 35*, 3 (2010), 663–678.

[14] Nguyen, T. D., Sørensen, A. J., and Quek, S. T. Design of hybrid controller for dynamic positioning from calm to extreme sea conditions. *Automatica 43*, 5 (2007), 768–785.

[15] Price, W. G. Probabilistic theory of ship dynamics. *University College London, Published by: Chapman & Hall Ltd, London, ISBN: 0 412 12430 0, Printed in the United Kingdom* (1974).

[16] Saelid, S., Jenssen, N., and Balchen, J. Design and analysis of a dynamic positioning system based on kalman filtering and optimal control. *IEEE Transactions on Automatic Control 28*, 3 (1983), 331–339.

[17] Sorensen, A., Strand, J. P., and Nyberg, H. Dynamic positioning of ships and floaters in extreme seas. In *OCEANS'02 MTS/IEEE* (2002), vol. 3, IEEE, pp. 1849–1854.

[18] Veksler, A., Johansen, T. A., Borrelli, F., and Realfsen, B. Dynamic positioning with model predictive control. *IEEE Transactions on Control Systems Technology 24*, 4 (2016), 1340–1353.

[19] Wang, Y., Sui, Y., Wu, J., and Jiao, J. Research on nonlinear model predictive control technology for ship dynamic positioning system. In *2012 IEEE International Conference on Automation and Logistics* (2012), IEEE, pp. 348–351.

[20] Xia, G., Liu, J., Chen, X., Wang, D., and Yang, R. Ekf based model identification for a relaxed dynamic positioning ship using nmpc method. In *2015 IEEE International Conference on Mechatronics and Automation (ICMA)* (2015), IEEE, pp. 1313–1318.

[21] Yu, M., and Biegler, L. T. A reduced regularization strategy for economic nmpc. *Journal of Process Control 73* (2019), 46–57.

[22] Yu, S., Li, X., Chen, H., and Allgöwer, F. Nonlinear model predictive control for path following problems. *International Journal of Robust and Nonlinear Control 25*, 8 (2015), 1168–1182.

[23] Zaman, H., Islam, M., Alagili, O., Khan, M., Imtiaz, S., and Ahmed, S. Efficient modelling of harsh environment disturbances for dp and autonomous ships simulations. In *International Conference on Offshore Mechanics and Arctic Engineering* (2021), vol. 85161, American Society of Mechanical Engineers, p. V006T06A067.

Chapter 6

Experimental Investigations of an Energy-Efficient Dynamic Positioning Controller for Different Sea Conditions

This chapter was published.

https://www.sciencedirect.com/science/article/pii/S0029801824006346

Abstract

The primary objective of a Dynamic Positioning (DP) controller is to maintain vessel position under varying environmental disturbances, while minimizing thruster usage. This work presents the development of an innovative energy-efficient DP controller, named Green NMPC (GNMPC), which minimizes thruster demand while upholding position constraints. Inspired from the structure of the economic nonlinear model predictive controller (ENMPC), GNMPC aligns with "green" objectives and performance metrics, notably thruster energy efficiency. Extensive DP tests were conducted across a spectrum of wave conditions, including head seas, oblique angles, and large position set-point changes, to validate the efficacy of the GNMPC approach and evaluate the dynamic positioning system's effectiveness in diverse challenging situations. The results demonstrated that the proposed controller is energy efficient compared to a benchmark NMPC and proportional-integral-derivative (PID) controller. It successfully reduced thruster demand in the sway direction compared to NMPC while preserving the vessel's positioning objectives.

6.1 Introduction

A dynamic positioning (DP) system keeps a ship at a designated position and desired heading using its thrusters [12]. DP technology is crucial in various applications, such as exploring deep-sea petroleum resources, off-shore supply operations, off-shore survey applications, etc. Accuracy, precision, and energy efficiency are key factors

when designing and developing a DP system. In earlier studies, the main focus was on the accuracy and precision of the controller [11, 27]. In recent years, there has been a significant discussion on developing solutions prioritizing high efficiency and low carbon emissions. Improving efficiency within the DP system reduces carbon emissions during operation and mitigates the overall stress of components, enhancing their longevity. This study aims to implement and test popular DP control strategies, including one newly proposed energy-efficient DP controller, to compare performance and evaluate the efficiency and frequency of thruster movements.

The first DP systems developed in the 1960s used the standard proportional, inertial, derivative (PID) controllers for horizontal motion (surge, sway, and yaw). Tuning the gains of the PID controller to perform under various sea states is challenging. Various approaches have been reported in the literature for tuning PID controllers for DP. In a recent study, authors in [37] proposed a fuzzy rule based PID controller for DP applications, where the controller gains were obtained through fuzzy inference.[4, 15, 26]. Following the PID based DP controllers, more complex controllers based on modern control theory were introduced to DP application. Authors in [15, 4] proposed an optimal control theory based DP controller with a Kalman filter based estimator to separate low frequency and high frequency motion of the vessel due to disturbances. Separating high and low frequency motions enabled the controllers to apply control actions only for low frequency motions due to forces such as wind, current and wave drift forces.

Another control strategy widely used in industry is model predictive control (MPC). A key feature of MPC is its ability to handle nonlinear and multi-input-multi-output system constraints. Early MPC-based DP systems utilized a linearized model of the vessel. The nonlinear dynamics of the vessel were linearized using the small angle theory [34]. The vessel might deviate significantly from the operating point in practical DP applications. Hence, the assumptions made during linearization are violated, and the MPC might not provide the optimal control. Recent studies have proposed nonlinear model predictive controllers (NMPC) that utilize the vessel's nonlinear dynamics without linearization [9, 19, 33].

The control objectives of DP applications in literature have primarily aimed at maintaining the desired position and heading of the vessel. Continuously trying to correct the offset has often resulted in control demand that is large, erratic, and shortens the thrusters' life span. Several techniques have been proposed to minimize the variations in control demands. One such technique is to isolate the low frequency (LF) and high frequency (HF) motion of the vessel due to effect of waves using Kalman filter techniques and apply control based on the LF motion [28]. In the similar line of work recently [36] proposed a control strategy called composite hierarchical anti-disturbance control (CHADC) integrating stochastic disturbance observer-based control (DOBC) theory, robust wave filter (RWF) method with H-infinity control. Other approaches minimize control demands artificially through imposing ramp rates, applying move accumulation, or using hysteresis switching to minimize back and forth switching of thrusters. An alternative approach is proposed by Kongsberg Inc. called "Green DP", which is an eco-conscious control system. Their system is designed to address excessive thruster activity, particularly in moderate environmental conditions, to decrease energy consumption, and provide an environmentally friendly solution. The Green DP controller has three main parts: the model predictive controller, the position predictor, and the environmental compensator. The system defines a working area inside the operational area, where the vessel can drift within. These areas are incorporated in the constraints and the cost function of the NMPC controller. The environmental compensator generates smooth attractive force towards the desired position, and the MPC generates more aggressive demands to prevent predicted overshoots. The authors claim that the combination of environmental compensator and MPC reduces dynamic thruster demands compared to a standard DP system. [18]

In line with the Green DP, we have successfully developed a controller whose structure is similar to an economic NMPC (ENMPC) [16]. The developed controller does not incorporate the operational area in the constraints or in the cost function directly. Instead, the weights of the economic NMPC are defined as a function of the deviation from the desired position. Our achievement in building the controller

has resulted in the reduction of DP's operational costs, particularly with regard to thruster demands, which in turn mitigates thruster wear and tear. We have transitioned costs related to an NMPC's setpoint tracking stage into economic costs within the optimization layer of our ENMPC. The controller was tested in a simulation environment and showed good promise [1].

Table 6.1 presents a compilation of key studies on DP that have implemented various control strategies. Many studies have proposed a single controller without comparative evaluation against alternative controller types. Another observation is that most of the studies have used simulations to validate and compare the performance of the controllers. Very few experimental implementations of DP systems have been reported in the literature, and most of the experiments have taken place in open waters, mostly under calm conditions, where disturbances cannot be controlled. In contrast, our work focuses on conducting experiments in a controlled environment, allowing us to compare the performance of different controllers under various wave conditions. We seek to understand better how these controllers operate under specific settings and assess their efficacy in real-world scenarios by carefully controlling the experimental conditions.

Table 6.1: A summary of selected DP controllers reported in the literature

		Scope of study		
Reference	Controller(s)	Simulation	Experiments	Comparing controllers
[31], [23]	PID	Yes	No	No
[5], [2]	PID	Yes	Yes	No
[25]	PID, SMC	Yes	Yes	Yes
[30]	MPC	Yes	No	No
[17]	Lag-MPC, Lag-NMPC	Yes	No	Yes
[33],[9], [35]	NMPC	Yes	No	No
[18]	NMPC	No	Yes	No
[19]	NMPC, PID	Yes	No	Yes
[1]	NMPC, GNMPC, PID	Yes	No	Yes

This current research presents the implementation and experimental validation

of the GNMPC proposed in [1]. Experimental implementation of the controller poses many challenges: (i) the accuracy of the mathematical model developed using the first principle and 3D design was insufficient for the NMPC implementation. So, to get the model's parameters, we used system identification to get a more accurate estimation of model parameters. (ii) implementation in real-time requires a fast optimizer to solve the nonlinear minimization problem. The optimizer needs to converge within the sampling interval, and (iii) data communication and implementation issues also need to be sorted for the experimental implementation.

The performance of the GNMPC is compared with a PID based DP controller and NMPC based DP controller. To the best of the authors' knowledge, this is the first study that has experimentally compared the performance of three different DP controllers under different sea conditions. We tested each controller under four different sea conditions: Sea with no waves (NW), regular waves (RW), irregular waves (IRW), and white noise waves (WNW). We conducted three types of tests to analyze the performance of the controllers properly: Station keeping in head seas, station keeping at oblique angles, and large position setpoint change.

The structure of this paper is as follows. The mathematical model of the vessel used in the NMPC is described in Section 2. The formulation of the GNMPC controller is discussed in Section 3. The experimental setup and the implementation details of the wave filter, communication, and controller are presented in Section 4. Section 5 presents the experimental results and comparison of the PID, NMPC, and GNMPC controllers. Finally, the findings and conclusion of the experiments are discussed in Section 6.

6.2 Mathematical Modeling of Vessel

A vessel floating freely in 3D space can move in six degrees of freedom (DOF). Figure 6.1 shows the 6 DOF of the vessel and coordinate frames used in this paper. In DP applications, the main focus is to control the three motions: surge, sway, and heading. Therefore, a simplified vessel model with three DOF is defined as in Eq. (6.1), and

Eq. (6.3) [19].

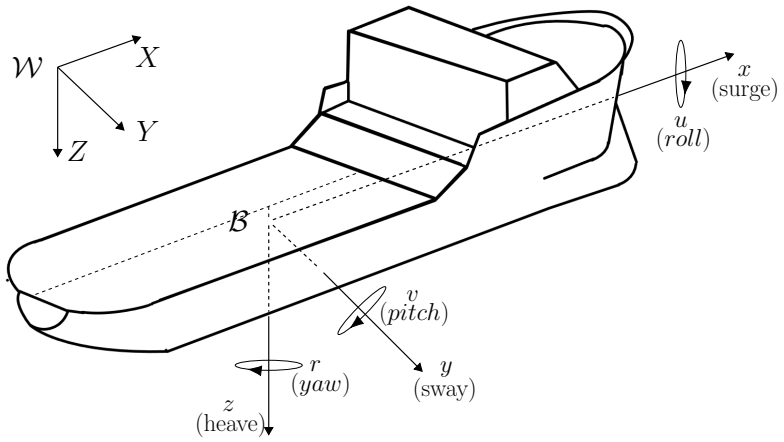

Figure 6.1: The coordinate system of generic dynamic positioning vessel.

$$\dot{\eta} = J(\psi)\nu. \tag{6.1}$$

The 3DOF kinematics are shown in Eq. (6.1), where $\eta = [x,\ y,\ \psi]^T$. $[x,\ y]$ is the horizontal position vector expressed in the inertial frame $\mathcal{W}$, and ψ is the heading of the vessel. The rotation matrix, $J(\psi) \in R^{3\times3}$, defines the rotation between the inertial and body frames and can be expressed as

$$J(\psi) = \begin{bmatrix} cos(\psi) & -sin(\psi) & 0 \\ sin(\psi) & cos(\psi) & 0 \\ 0 & 0 & 1 \end{bmatrix}. \tag{6.2}$$

The body-fixed surge velocity, sway velocity, and yaw rate are represented by $u, v, and\, r$, respectively, and the body-fixed velocity vector is defined as $\nu = [u,\ v,\ r]^T$. The dynamics of the vessel are defined as follows.

$$(M_{RB} + M_A)\dot{\nu} + (C_{RB}(\nu) + C_A(\nu) + D(\nu))\nu = \tau, \tag{6.3}$$

where $M_{RB} \in R^{3\times3}$ and $M_A \in R^{3\times3}$ are the inertia matrices representing rigid body

mass and the hydrodynamic added-mass.

$$M_{RB} = \begin{bmatrix} m & 0 & 0 \\ 0 & m & mx_G \\ 0 & mx_G & I_Z \end{bmatrix}, \tag{6.4}$$

$$M_A = \begin{bmatrix} -X_{\dot{u}} & 0 & 0 \\ 0 & -Y_{\dot{v}} & -Y_{\dot{r}} \\ 0 & -N_{\dot{v}} & -N_{\dot{r}} \end{bmatrix}, \tag{6.5}$$

where m is the mass of the ship, I_z is the moment of inertia about the z axis, and x_G is the distance to the center of gravity of the ship along the x axis of the body frame $\mathcal{B}$.

$C_{RB} \in R^{3\times3}$ and $C_A \in R^{3\times3}$ are the rigid body Coriolis and centrifugal components as well as added-mass derivatives corresponding to the velocity coupling and can be defined as

$$C_{RB}(\nu) = \begin{bmatrix} 0 & 0 & -m(x_G)r + v) \\ 0 & 0 & mu \\ m(x_G r + v) & -mu & 0 \end{bmatrix}, \tag{6.6}$$

$$C_A(\nu) = \begin{bmatrix} 0 & 0 & Y_{\dot{v}}v \\ 0 & 0 & -X_{\dot{u}}u \\ -Y_{\dot{v}}v & X_{\dot{u}}u & 0 \end{bmatrix}. \tag{6.7}$$

$D(\nu) \in R^{3\times3}$ represents the energy dissipative terms (drag) due to relative motion between the vessel and surrounding fluid. The drag effects are nonlinear and can be divided into linear and nonlinear components as $D(\nu) = D_L + D_{NL}(\nu)$, where

$$D_L = \begin{bmatrix} -X_u & 0 & 0 \\ 0 & -Y_v & -Y_r \\ 0 & -N_v & -N_r \end{bmatrix}, \tag{6.8}$$

$$D_{NL}(\nu) = \begin{bmatrix} X_{|u|u}|u| & 0 & 0 \\ 0 & -Y_{|v|v}|v| - Y_{|r|v}|r| & -Y_{|v|r}|v| - Y_{|r|r}|r| \\ 0 & -N_{|v|v}|v| - N_{|r|v}|r| & -N_{|v|r}|v| - N_{|r|r}|r| \end{bmatrix}^T . \tag{6.9}$$

The forces applied to the vessel can be expressed as $\tau = \tau_c + \tau_w$, where τ_c is the forces from the thrusters, and τ_ω is the force exerted on the vessel by the ocean waves. The constants, m, x_G, I_Z, $X_{\dot{u}}$, $Y_{\dot{v}}$, $Y_{\dot{r}}$, $N_{\dot{v}}$, $N_{\dot{r}}$, X_u, Y_v, Y_r, N_v, N_r, $X_{|u|u}$, $Y_{|v|v}$, $Y_{|r|v}$, $Y_{|v|r}$, $Y_{|r|r}$, $N_{|v|v}$, $N_{|r|v}$, $N_{|v|r}$, $N_{|r|r}$ are vessel-specific constants, and they are identified through system identification.

6.3 Green-NMPC Theory

In this study we compare our energy efficient Green NMPC with other traditional controllers. A detailed formulation of the Green NMPC and simulation results are presented in [1]. This section presents a concise overview of the Green NMPC to enhance the readability of the manuscript.

The continuous time dynamics of the vessel described in the previous section can be converted to a discrete time dynamic system as

$$\chi_{k+1} = f(\chi_k, \upsilon_k), \tag{6.10}$$

where f is the nonlinear system dynamics with states, $\chi = [\eta^T, \nu^T]^T$, and inputs $\upsilon = \tau_c$. In practical applications, the states and the inputs have constraints and the linear or nonlinear constraints can be defined as

$$g(\chi_k, \upsilon_k) \leq 0. \tag{6.11}$$

The objective on NMPC is to determine the control actions υ_k that minimize a cost function while satisfying the constraints given in (6.11). The cost function of the proposed GNMPC comprises the economic cost function and the quadratic regularization term. The economic cost function $\varphi^{ec}(\chi_k, \upsilon_k)$, is defined as follows:

$$\varphi^{ec}(\chi_k, \upsilon_k) = L_x \left(F_{x,k} - F_{x,k-1}\right)^2 + L_y \left(F_{y,k} - F_{y,k-1}\right)^2 + L_\psi \left(T_{\psi,k} - T_{\psi,k-1}\right)^2 \quad (6.12)$$

where, F_x, F_y, T_ψ are the thruster forces in surge and sway directions and the torque for yaw rotation, respectively, and $\tau_c = [F_x, F_y, T_\psi]^T$. L_x, L_y, L_ψ represent the weights associated with the control actions. When the cost function is not strongly convex, a quadratic regularization term is added to the cost function [22]. The regularization term has the following form:

$$\varphi^{rc}(\chi_k, \upsilon_k) = \left(x_k - x_r\right)^2 \pi_1 + \left(y_k - y_r\right)^2 \pi_2 + \left(\psi_k - \psi_r\right)^2 \pi_3, \quad (6.13)$$

where x_r, y_r, ψ_r are the reference position and heading, and π is the weight matrix. The total stage cost function can be expressed as

$$\begin{aligned} \varphi(\chi_k, \upsilon_k) =& \varphi^{ec}(\chi_k, \upsilon_k) + \varphi^{rc}(\chi_k, \upsilon_k) \\ =& L_x \left(F_{x,k} - F_{x,k-1}\right)^2\Big)^2 + L_y \left(F_{y,k} - F_{y,k-1}\right)^2 + L_\psi \left(T_{\psi,k} - T_{\psi,k-1}\right)^2 \\ &+ \left(x_k - x_r\right)^2 \pi_1 + \left(y_k - y_r\right)^2 \pi_2 + \left(\psi_k - \psi_r\right)^2 \pi_3. \end{aligned} \quad (6.14)$$

The formulation of the NMPC problem can be expressed as follows:

$$\begin{aligned} &\arg\min_{\chi_k, \upsilon_k} \sum_{j=k+1}^{k+N} \varphi(\chi_j, \upsilon_j) \\ &\text{subjected to} \\ &\chi_{j+1} = f(\chi_j, \upsilon_j), \\ &g(\chi_j, \upsilon_j) \leq 0, \quad \forall j \in [k, k+N]. \end{aligned} \quad (6.15)$$

Weights used in the objective function play a critical role in shaping the optimization objective. The weights $L = [L_x \;\; L_y \;\; L_\psi]$ governs the penalization of input variations, while $\pi = [\pi_1 \;\; \pi_2 \;\; \pi_3]$ determines the penalty for state errors. When a higher weight values are chosen for a specific component, it results in a greater

penalty for changes of the corresponding component during optimization. This effectively steers the optimizer towards minimizing the associated error or variations in the control inputs. A traditional NMPC uses constant weight values and the values are tuned for the best performance. However, the proposed Green NMPC introduces variable weights in the cost function, and the variable weights are specified to satisfy two key performance requirements.

1: When the vessel is well within the safety limits, the main focus of the controller is to reduce energy consumption.

2: When vessel approaches the safety limit the focus of the controller shifts to maintaining the vessel at the set position.

When the vessel is well within the safety limits, the weights corresponding to the surge and sway thruster forces are adjusted to a high value. The higher weights force the optimizer to penalize variations in the thruster forces. Therefore, when the vessel deviates from the set point, the controller does not perform sudden thruster variations. As a result, the overall thruster demands are greatly reduced, and this behavior allows the vessel to drift inside the safe operation zone instead of closely maintaining the set point.

When the vessel is approaching the safety limits, the weights corresponding to the surge and sway thruster forces are adjusted to a lower value, allowing drastic changes in the thruster values. This allows the controller to perform quick maneuvers and bring the vessel back to the desired set point.

The weight functions (L_x, L_y) were set as continuously varying nonlinear functions of the respective axis distance to satisfy these two requirements. For instance, L_x is defined as a function of x satisfying the aforementioned conditions and penalizes the thruster force F_x. Acceptable shape of the wave function is shown in Figure 6.2. The weights can be selected to be over compensated (blue line of Figure 6.2), where the controller focus more on maintaining the position, or be lenient (green line of Figure 6.2), where the vessel is allowed to drift a longer distance.After much trial and error,

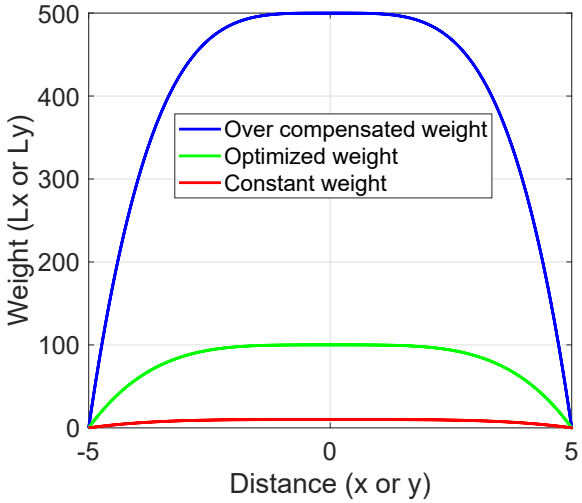

Figure 6.2: Acceptable shape of weighting function for GNMPC.

we finally settled on the nonlinear function specified in Eq.(6.16).

$$L_x = 100 - \frac{x^4(log(|T_{th}|) - |x|)}{|T_{th}|}, \tag{6.16}$$

where, T_{th} is the position threshold, and x is the current x-axis position of the vessel. L_y is also defined similarly.

The constraints of the GNMPC expressed in (6.11) comprise the upper and lower bounds of the states and inputs. The constraints can be expressed as

$$g(\chi_k, \upsilon_k) = \begin{bmatrix} \chi_k - \chi_{max} \\ -\chi_k + \chi_{min} \\ \upsilon_k - \upsilon_{max} \\ -\upsilon_k + \upsilon_{min} \end{bmatrix} \tag{6.17}$$

6.4 Methodology and Experimental Setup

This section provides a comprehensive overview of the experimental setup employed in our study. The overall configuration of the experimental setup is shown in Figure

6.3. Additionally, we present the system identification process, where we aim to accurately characterize the dynamics and behavior of the ship. Furthermore, we detail the implementation of the wave filter utilized in our experiments. The wave filter is a crucial component that mitigates the response to high-frequency wave action, that is outside the vessel response capability, or efficient bandwidth of control. Finally, we outline the test cases that were executed to evaluate and compare the three controllers. These test cases were carefully designed to evaluate the performance and robustness of the system under different conditions and scenarios.

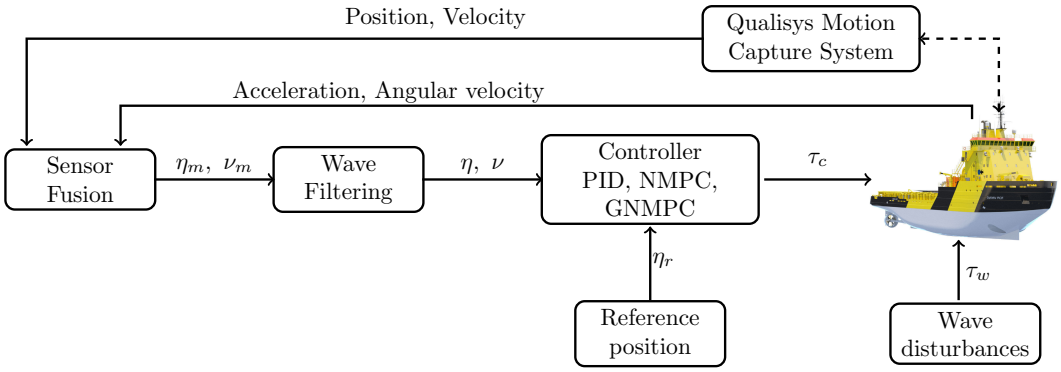

Figure 6.3: Flowchart of the experiments

6.4.1 Experimental Setup

The experiments were carried out in the Offshore Engineering Basin (OEB) at the National Research Council (NRC) Ocean, Coastal, and River Engineering Research Center in St. John's, Canada. The OEB facility is one of the world's most advanced indoor model ocean facilities. The basin, which measures 75 m by 32 m by 4 m, can simulate extreme model sea-state conditions that happen only once per 10,000 years (scale dependent). The OEB is equipped with 168 individually controlled and vertically adjustable wave-maker modules in a fixed "L" configuration. Each segment is 2m high and 0.5m wide and are grouped together in fours to form a module. The wave-maker system can generate unidirectional or multi-directional waves up to 1m

tall. Passive wave absorbers are fitted around the other two sides of the tank. The basin can also produce wind to replicate actual sea conditions. The basin is capable of testing models at a sizeably large scale and evaluates concepts in a controlled environment to get high-quality, realistic results.

Figure 6.4: The Magne Viking model vessel

The experiments of the DP controllers were carried out on a scaled model of a Magne Viking supply vessel (Figure 6.4). The model ship is a 1:19.5 scale model of the actual vessel and has the following dimensions: mass (m) = 1229 kg, length (L), 4.44 m, and width (B) = 1.16 m. The vessel is equipped with two main propellers, one bow thruster, and one stern thruster for propulsion. A computer onboard the model vessel controls the internal hardware including the propulsion system, collect sensor data from onboard sensors and communicate with the main control computer through the Data Acquisition System (DAS) network. The OEB is equipped with a Qualisys motion capture system that measures the Earth-fixed position orientation and speed of the vessel. Active markers are placed on the model to allow the motion tracking using the cameras mounted around the basin. The Qualisys motion capture system is capable of providing position feedback with 1 mm accuracy. However, in practice there can be dropouts due to the sheer size of the OEB tank. To minimize the effects of dropouts, an EKF is implemented to fuse inertial measurements from the vessel with the motion capture feedback.

The Magne Viking model is retrofitted with Crossbow VG700CB-200 inertial measurement unit (IMU). The IMU measures the accelerations and angular rates of the vessel, and these measurements are used in an EKF based attitude heading reference system [20]. The EKF predicts the position and orientation at 50 Hz using the measurements from the IMU, and then do the correction based on the absolute position and orientation measurements from the motion capture system. The AHRS allows the controller to have an accurate, uninterrupted feedback even during a dropout of motion capture feedback.

The NMPC and GNMPC controllers run on a separate computer, which is connected to the main control computer via the OPC server. The communication setup between the model, motion capture system, and the main and secondary control computers is shown in Figure 6.5.

6.4.2 System Parameter Identification

The performance of an MPC depends on the quality and accuracy of the vessel's model. Hence, an accurate mathematical representation of the vessel's dynamics is essential for successful MPC implementation. In the case of the experimental setup involving the scaled model of the Magne Viking supply vessel, the physical parameters, such as mass, length, etc. were identified through a set of comprehensive measurements. The initial hydrodynamic parameters were calculated using the 3D model of the model vessel. Over time, several modifications were made, and several sensors were added to the initial design to improve the capabilities of the model. During experiments it became apparent that the initial parameters no longer adequately reflected the true dynamics of the modified ship. Therefore the new model parameters had to be identified.

Multiple approaches exist for parameter identification in models. A common method involves separating transient and steady-state elements and using linear regression to estimate parameter values. In a study by [10], a non-first-principles model

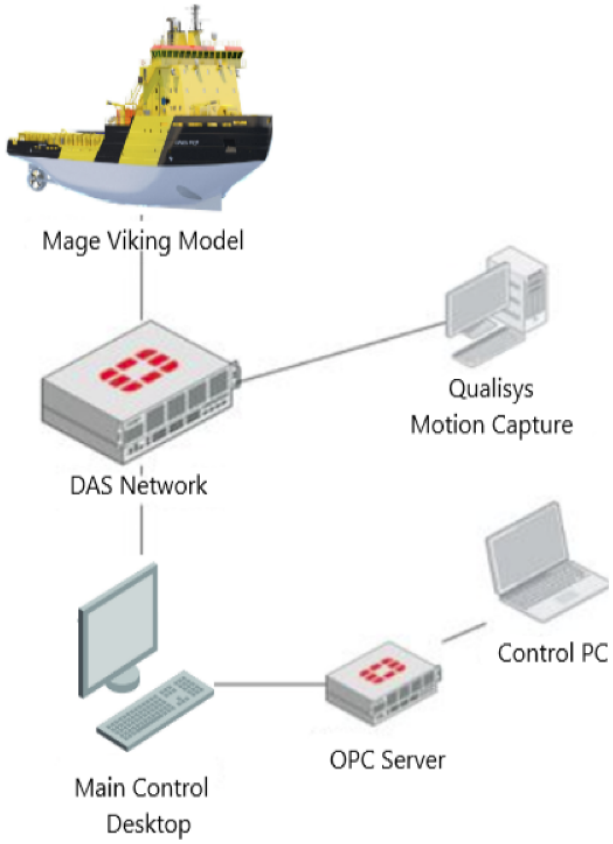

Figure 6.5: Communication network.

was identified for a high-speed autonomous surface vehicle's motion. The parameter values were determined through weighted linear least squares regression with a regularization term to discourage large parameter values. The model's accuracy was verified by comparing simulated vessel response with experimental data and was subsequently employed in a controller with feed-forward terms. In another study by [13], an offline parallel extended Kalman filter (EKF) algorithm was utilized to estimate parameters for a nonlinear dynamic positioned ship model. A decoupled identification scheme involved three different ship maneuvers, with parameters from one scheme serving as input for the next until all parameters were identified. The approach's effectiveness was verified by implementing and testing it on a supply vessel, with the results compared against experimental data. In our experiments, we

used the optimization-based system identification technique that was developed in [24].

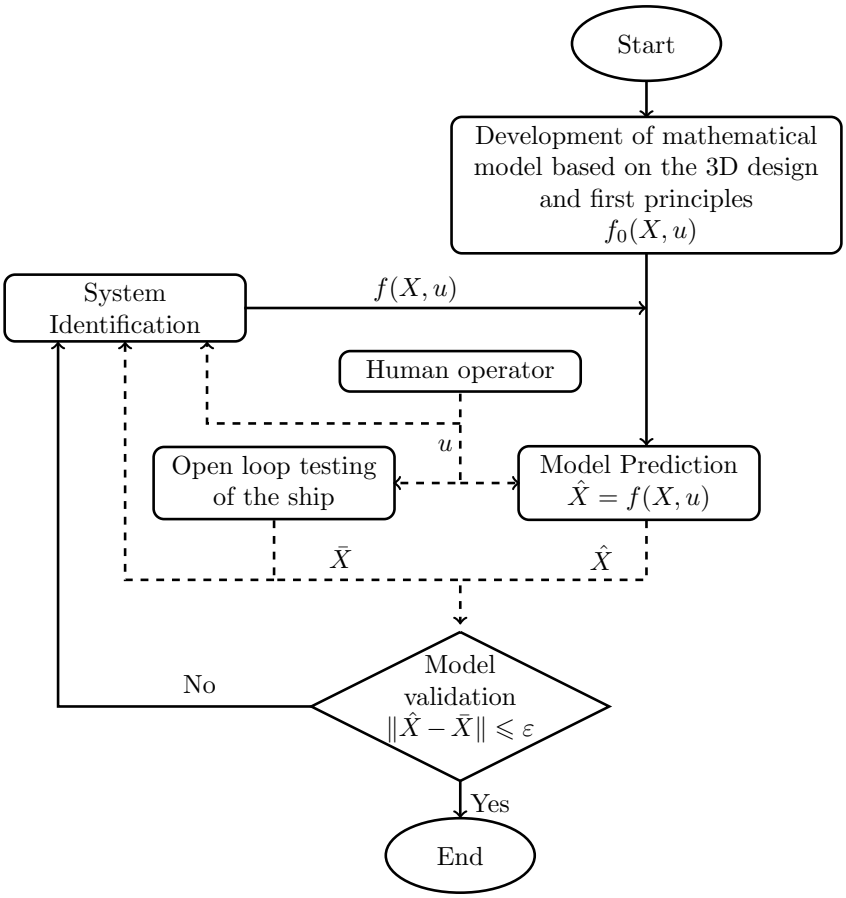

Figure 6.6: Workflow of system identification

We piloted the vessel at various speeds and in various trajectories to collect data. When sufficient motion data are available we conducted the identification and validation workflow shown in Figure 6.6. The optimization technique calculates the system parameters by minimizing a weighted sum of square errors. The objective

function is defined as

$$\begin{aligned} \boldsymbol{L}(\chi, \hat{\chi}) &= \sum_{k=t_0}^{t_0+T_s} (\chi_k - \hat{\chi}_k)^T \boldsymbol{W} (\chi_k - \hat{\chi}_k) \\ \hat{\chi}_k &= f(\chi_{k-1}, \upsilon_{k-1}, \Theta), \end{aligned} \tag{6.18}$$

where f is the ship dynamics given in (6.3), and Θ is the vector of physical and hydrodynamic parameters to be identified.

$$\Theta = \left[I_Z, X_{\dot{u}}, Y_{\dot{v}}, Y_{\dot{r}}, N_{\dot{v}}, N_{\dot{r}}, X_u, Y_v, Y_r, N_v, N_r, X_{|u|u}, Y_{|v|v}, N_{|r|r} \right] \tag{6.19}$$

χ is the measured state vector of the ship. $\hat{\chi}$ is the calculated states based on the system dynamics given in (6.1) and (6.3). The weight matrix W is defined $W = diag(W_1, W_2.W_3, W_4, W_5, W_6)$, where $W_i > 0$. Proper initialization is crucial when performing optimization, and the parameters identified using the measurement and the 3D model are used as the initial values for the optimization. Calculated parameters are shown in Table 6.2.

Table 6.2: Identified parameter values of Magne Viking model

Physical Parameter	Value	Identified Parameter	Value	Identified Parameter	Value
Length	4.44 (m)	I_Z	1577.65 (kgm^2)	$X_{\dot{u}}$	158.23
Beam	1.16 (m)	$Y_{\dot{v}}$	1087.3	$Y_{\dot{r}}$	$\sim$0
m	1358.5 (kg)	$N_{\dot{v}}$	$\sim$0	$N_{\dot{r}}$	1559.92
x_G	0.18 (m)	X_u	41.788	Y_v	336.06
		Y_r	$\sim$0	N_v	$\sim$0
		N_r	26	$X_{\|u\|u}$	194
		$Y_{\|v\|v}$	$\sim$0	$N_{\|r\|r}$	3913.5

6.4.3 Wave Filter Setup

The motion of a ship under the influence of waves is generally modeled as the superposition of low-frequency (LF) and wave-frequency (WF) motion components. The

LF motions, i.e., drift, result from second-order wave drift forces and control thrust forces. On the other hand, the WF motions are predominantly caused by first-order wave motions, leading to the vessel's oscillatory movements. Controlling the vessel based on the oscillatory position feedback can lead to excessive control actions and poor DP performance.

There has been extensive research on the WF for DP systems. In the study by Sørensen et. al., WF filtering was employed by utilizing Kalman filter theory and assuming linearization of the ship's kinematic equations around predefined constant yaw angles[29]. This approach was necessary for the application of linear Kalman filter theory and gain scheduling techniques. In [14], a nonlinear observer incorporating wave filtering capabilities and bias estimation was developed based on the principle of passivity.

Furthermore, [32] introduced gain scheduled wave filtering as an additional technique. In our experiments, we utilized the wave filtering approach proposed in reference [14] for effective filtering of wave disturbances. In [12], Fossen derives a linear state space model for the first-order wave response. The response model in surge, sway, and heading can be expressed as

$$\dot{\xi} = A_w \xi + E_w w_2 \tag{6.20}$$

$$\eta_w = C_w \xi, \tag{6.21}$$

where $\xi \in R^6$ is the state vector, and $w_2 \in R^3$ is a zero-mean Gaussian white noise. Matrices $A_w \in R^{6\times6}, E_w \in R^{6\times3}$, and $C_w \in R^{3\times6}$ are constant matrices defined as

$$A_w = \begin{bmatrix} 0_{3\times3} & I_{3\times3} \\ -\Omega_{3\times3} & -\Lambda_{3\times3} \end{bmatrix}, \quad E_w = \begin{bmatrix} 0_{3\times3} \\ I_{3\times3} \end{bmatrix}, \quad C_w = \begin{bmatrix} 0_{3\times3} & I_{3\times3} \end{bmatrix},$$

with

$$\Omega = diag(\omega_1,\ \omega_2,\ \omega_3) \quad \Lambda = diag(2\omega_1\zeta_1,\ 2\omega_2\zeta_2,\ 2\omega_3\zeta_3)$$

where $\omega = [\omega_1, \omega_2, \omega_3]$ is the dominant wave frequency, and $\zeta = [\zeta_1, \zeta_2.\zeta_3]$ is the relative damping coefficients.

η_w is the WF motion of the ship due to the first-order waves. Effects of the second-order mean and slowly varying wave loads are modeled as a random walk process (Wiener process) and can be expressed as

$$\dot{b} = w_3 \tag{6.22}$$

where $w_3 \in R^3$ is a vector of zero-mean Gaussian white noise.

The bias $b \in R^3$ is incorporated into the ship's dynamics in (6.1) as a bias force, and the modified dynamics can be expressed as

$$M_{RB}\dot{\nu} + M_A\dot{\nu} + C_{RB}(\nu)\nu + C_A(\nu)\nu + D(\nu)\nu = \tau_c + J(\psi)^T b + w_1 \tag{6.23}$$

where $w_1 \in R^3$ is a vector of zero-mean Gaussian white noise.

In this study, we implemented a UKF-based wave filter to filter out the WF motions due to waves. UKF performs the propagation of the uncertainties of the Gaussian Random Variable (GRV) through a deterministic sampling method (unscented transform). Using equations (6.3), (6.23), (6.20), and (6.22), the process model used for the UKF can be expressed as

$$\dot{\eta} = J(\psi)\nu \tag{6.24}$$

$$\dot{\nu} = (M_{RB} + M_A)^{-1}\left(-C_{RB}(\nu)\nu - C_A(\nu)\nu - D(\nu)\nu + \tau_c + J(\psi)^T b + w_1\right) \tag{6.25}$$

$$\dot{\xi} = A_w\xi + E_w w_2 \tag{6.26}$$

$$\dot{b} = w_3 \tag{6.27}$$

Feedback for the experiment was obtained through the Qualisys motion capture system, which provided the ship's position and heading. The measured position and heading can be modeled using the linear superposition of the WF motion component and the LF motion component. Hence the position and heading measurement can

be modeled as

$$y = \eta + \eta_w + w_4 \tag{6.28}$$

where $w_4 \in R^3$ is the measurement noise vector.

Mathematical formulation and implementation of UKF are well documented in the literature and the UKF pseudo code is shown in Algorithm 1. Detailed implementation of UKF can be found in [7, 19, 21].

Algorithm 1: UKF-Based Wave Filter

```
Initialize the states (Ξ) and their covariance (P_Ξ), Ξ = [η^T, ν^T, ξ^T, b^T]^T;
for k ∈ (1, ..., ∞) do
    Calculate sigma points for states (Ξ) and measurements (y);
    Propagate the sigma points through system model (6.24) - (6.27);
    Compute the predicted mean and covariance Ξ_{k⁻}, P_{Ξ,k⁻};
    Propagate the measurement sigma points through measurement model
     (6.28);
    Read pose and velocities of the vessel;
    Calculate the Kalman gain;
    Compute the updated sates and covariance Ξ_{k⁺}, P_{Ξ,k⁺};
end
```

The wave filter was tuned for each type of wave. This involves adjusting the tuning matrix A_w in (6.20) based on the dominant frequency of the wave and appropriate damping coefficients. The initial guess of the dominant frequency was determined by analyzing the wave spectrum, and then fine-tuned through a process of trial and error. The values used for ω and ζ are shown in Table 6.3

Table 6.3: Tuning parameters of wave filter

Wave Type*	Dominant Frequency	Damping Coefficient
White Noise Wave	[2.1, 2.1, 2.1]	[0.02, 0.02, 0.02]
Irregular Wave	[2.3, 2.3, 2.3]	[0.01, 0.01, 0.01]
Regular Wave	[2.7, 2.7, 2.7]	[0.02, 0.02, 0.02]

* See Table 6.4 for the definitions of waves

Figure 6.7 illustrates the measured position and heading of the ship influenced

by a regular wave and the LF motion of the ship after filtering the WF motion. Figure 6.7 demonstrates that the wave filter based on UKF successfully estimates the WF motion components from the feedback and produces LF motion feedback for the controller.

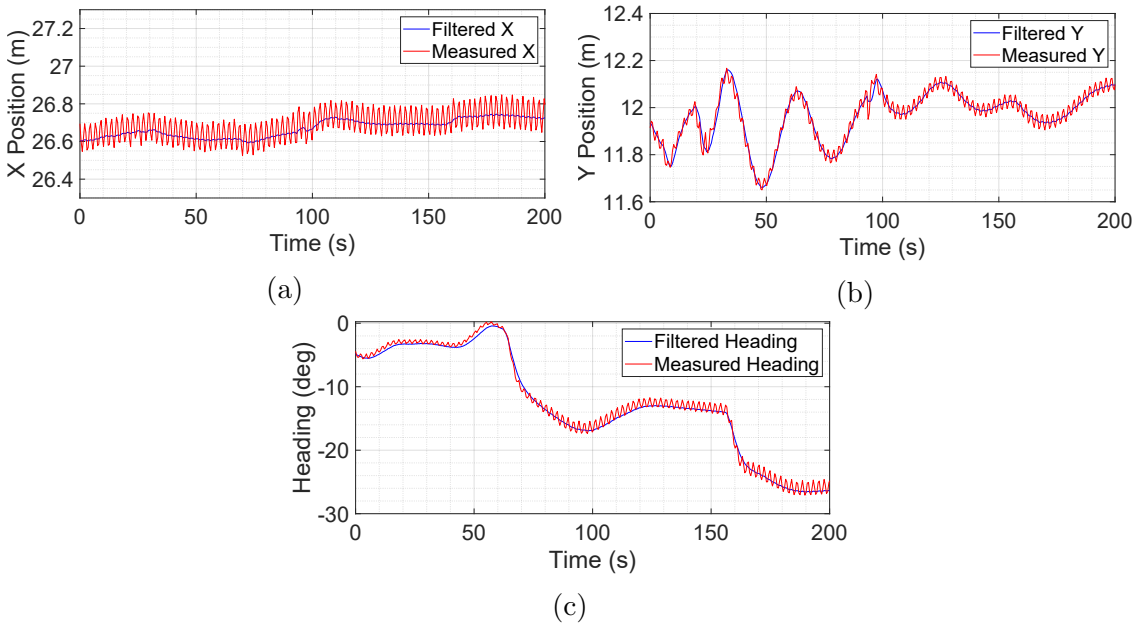

Figure 6.7: Position and heading of the ship under the influence of regular waves

6.4.4 Controller implementation

The proposed GNMPC is optimization based control algorithm, which calculates the optimum control actions by solving the optimization problem defined in (6.15) at each time step. Optimization based algorithms demand significant computational resources and may result in longer execution times posing challenges for real-time implementation. The optimal control problem was formulated using direct multiple shooting (DMS) approach. We opted for the DMS approach due it's robustness to model uncertainty and better convergence [8]. However, the DMS approach has more optimizing variables which lead to increased computational complexity.

In this study we used the CasAdi framework to implement the NMPC and Green NMPC controller [3]. CasADi is an open-source software framework that provides a powerful set of tools for modeling and solving optimization problems. CasAdi supports a variety of programming languages, including Python, MATLAB, and C++, making it versatile. As the solver for the optimization problem we selected built-in interior point optimizer (IPOPT). IPOPT algorithm is computationally efficient and can handle large-scale optimization problem generated using DMS approach.

The NMPC and GNMPC controllers are implemented using MATLAB in a laptop equipped with AMD Ryzen 5 5600H and 16GB of RAM. Number of samples in the prediction horizon is a key factor determining the execution time of the controller. Since the vessel has slow dynamics, a controller with shorter prediction horizon does not yield the best performance. Controller with a longer prediction horizon performs better but with a longer execution time. After much trial and error, we decided a prediction horizon of 16 seconds, 80 prediction horizon samples at 5Hz. The selected controller rate and number of samples provided a better compromise between the performance and computation time.

The controller communicates with the main control computer through the OPC server at 5Hz. In each iteration, the controller requests the pose and velocity feedback of the vessel, and then the control actions are forwarded to vessel. The state and input limits used in (6.17) are selected based on the experimental setup. The limits used in the experiment are as follows

$$
\begin{aligned}
\chi_{max} &= [0(\mathrm{m}),\ 0(\mathrm{m}),\ 2\pi(\mathrm{rad}),\ 0.3(\mathrm{ms}^{-1}),\ 0.3(\mathrm{ms}^{-1}),\ -0.3(\mathrm{rads}^{-1})] \\
\chi_{min} &= [-75(\mathrm{m}),\ -32(\mathrm{m}),\ -2\pi(\mathrm{rad}),\ -0.3(\mathrm{ms}^{-1}),\ -0.3(\mathrm{ms}^{-1}),\ -0.3(\mathrm{rads}^{-1})] \\
\upsilon_{max} &= [35\mathrm{N},\ 45\mathrm{N},\ 65\mathrm{N}] \\
\upsilon_{min} &= [-35\mathrm{N},\ -45\mathrm{N},\ -65\mathrm{N}]
\end{aligned}
\tag{6.29}
$$

6.5 Test Cases

A key contribution of this paper is conducting experiments under different wave conditions in an controlled environment. Wavemakers in OEB can generate various types of waves. Based on the height and period, the waves can be divided into sea states. In this study we chose three differnt wave conditions along with no wave condition (NW) to compare controller performances. Waves area characterized by the peak wave frequency and the significant wave height. The characteristics of the waves used in the experiments are listed in Table 6.4.

Table 6.4: Definition of waves

ID	Significant wave height, H_s[m]	Peak Wave Frequency ω_p[rad/s]	Wave Type
1	0.178	2.3	Regular
2	0.178	Range	White noise
3	0.1	1.26711	Irregular, Short crest

The regular waves (RW) are waves with a single frequency and periodic wave height, period, and wavelength. The irregular waves (IRW) are a superposition of several regular waves, which have a significant wave height, and a dominant frequency. The white noise waves (WNW) has a wide frequency range with a flat power spectrum [6]. The WNW used in this study has an incident angle of 20 degrees, where as the other two waves, have zero incident angle.

In this study we carried out three different tests, 1: DP at head seas (HS), 2: DP at oblique angles (OA), 3: DP with large setpoint changes (LSP). These tests were carried out under different wave conditions, and with each controller. During each experiment, the vessel was initially maneuvered to the initial set point in calm waters, and once the vessel was in position the waves were introduced. Through out this transition, each controller was actively controlling the vessel. The experimental data was collected once the waves reached a steady state condition. We conducted a total of 32 experiments and a summary of the experiments is shown in Table 6.5.

Table 6.5: Summary of experiments

Type of Wave	PID	NMPC	GNMPC
No Wave	HS, OA, LSP	HS, OA, LSP	HS, OA
White Noise Wave	HS, OA, LSP	HS, OA, LSP	HS, OA
Irregular Wave	HS, OA, LSP	HS, OA, LSP	HS, OA
Regular Wave	HS, OA, LSP	HS, OA, LSP	HS, OA

6.6 Experimental Results

This section presents the comprehensive results obtained from the DP tests conducted under different wave conditions. Three tests, HS, OA, and LSP, were carried out to assess and compare the performance of the three controllers. The experiments aimed to evaluate the effectiveness of the dynamic positioning system in different challenging situations. Due to space limitations, this paper will present the plots showing the position holding, and spectral density of the thrusters of the controllers only for the regular wave (RW) conditions. All other results are reported for no wave (NW), white noise wave (WNW), irregular wave (IRW) and regular wave (RW) conditions.

6.6.1 DP Head Seas

The main task of the DP head seas experiment is to maintain the vessel at a given position with zero heading amidst disturbances. In most of the practical DP applications, the heading of the ship will be adjusted to match the wave direction.

Figure 6.8 shows the position and heading accuracy of the three controllers under the four sea conditions. The bars in the plot represent the root mean square error (RMSE) values for each test, with the height of each bar corresponding to the magnitude of the mean error. The error bars on each bar indicate the 95% confidence interval of the root square errors. Under the NW conditions, all controllers' errors are extremely small. The maximum position error is around 3% of the total ship length. The coupling effect of the four propellers can cause motion in the ship. The

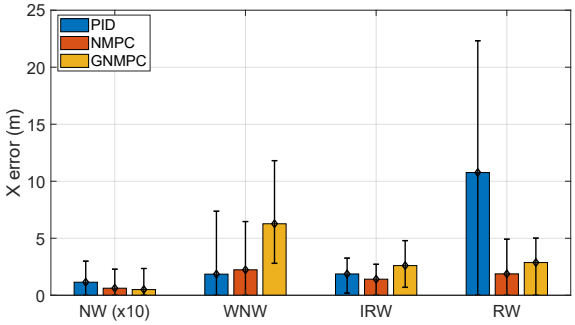

(a) RMSE of X position

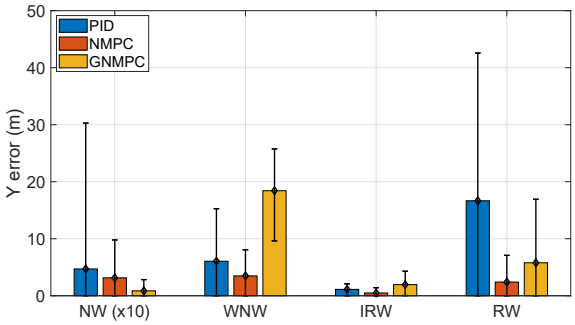

(b) RMSE of Y position

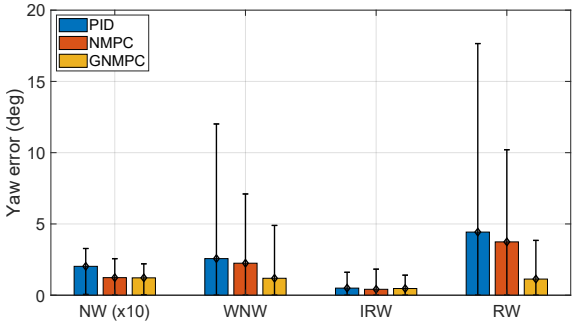

(c) RMSE of heading

Figure 6.8: Position and heading accuracy of HS tests under different wave conditions.

PID tries to minimize the error in the set point, and therefore, the PID has more actuator movements. NMPC considers the dynamics of the ship and calculates the optimum control action. Therefore, the corrections applied by the controller are less aggressive than the PID, and the errors are less. Since the vessel is within the safety

boundary, the GNMPC does not make any corrections. Therefore, disturbances due to the coupling effects are less and the accuracy is the highest. Under the WNW conditions, the NMPC provides the best performance in terms of accuracy. The x position RMSE of the PID controller is lower compared to the NMPC, but when closely observing, we can see the maximum error of the PID controller is higher than the maximum error of the NMPC. The error of the GNMPC is larger compared to both PID and the NMPC. However, we can see that the GNMPC errors did not exceed the safety limit. Since the white noise reached the ship at an oblique angle, the wave pushed the ship to one side of the set point. We can see the minimum RMSE has a positive value, which shows a drift of the ship to one side of the set point. Under the IRW conditions, the vessel movement is small. We can see a higher accuracy in the NMPC compared to the PID. GNMPC error is larger compared to both NMPC and PID. In order to maintain the ship within the safety limit and has reduced thruster usage, the GNMPC allows the vessel to drift slightly. The regular wave is the most challenging wave for the vessel. We can clearly see a significant improvement in the accuracy of NMPC compared to the PID controller. Following a similar trend, the GNMPC position accuracy is lower compared to NMPC. When comparing the heading accuracies, the GNMPC has the highest accuracy compared to the PID and NMPC. Since dynamic weights are not assigned for the heading control, the GNMPC performs similarly to a NMPC controller for the heading correction. Since the thruster movements from the GNMPC controller are less compared to the NMPC, the cross coupling effects on the ship are minimized in the GNMPC controller. This results in a higher accuracy in the heading angle.

Figure. 6.9. Shows the vessel's XY position for PID, MPC, and GNMPC controllers under regular wave case. Results indicate that the vessel locations were within the safe range in every case. Compared to the NMPC control, the PID has wider spread movements about the setpoint. Moreover, there is more vessel movement for Green-NMPC, as the point reference monitoring is relaxed to area tracking within the safety limitations. It is evident that the Green-NMPC's weight function is able to maintain a trade-off between maintaining position and limiting thruster

motions.

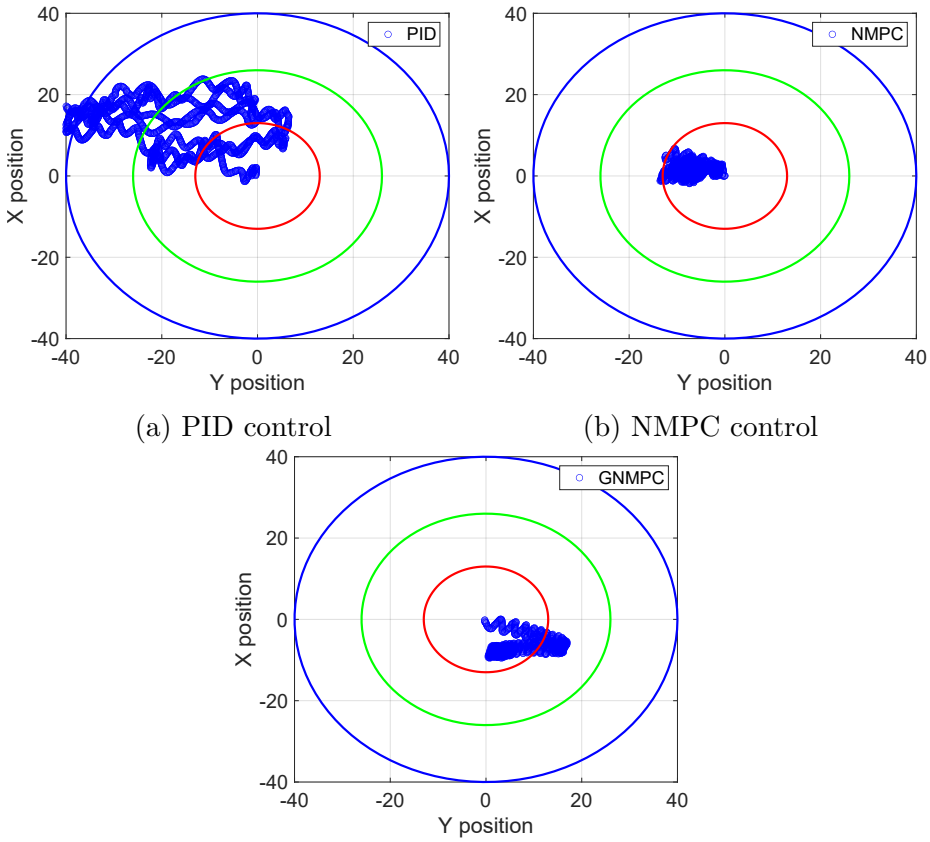

(a) PID control (b) NMPC control

(c) GNMPC control

Figure 6.9: Comparing the position holding performance of PID,NMPC, and GNMPC controller under regular wave

Figure. 6.10a. shows the energy consumption of the three controllers under each wave condition. We can observe that the GNMPC controller has the lowest power consumption compared to the PID and NMPC. The PID controller has the highest power consumption.

The primary reason for preferring less variation in ship thrusters is to ensure safe and stable ship operations. The thrusters control the ship's movement and maintain its position, especially in dynamic positioning operations. If the thrusters'

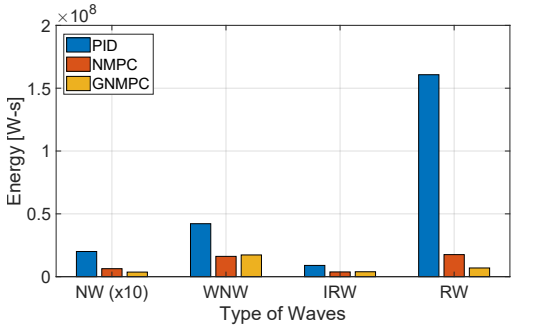

(a) Power consumptions of the thrusters

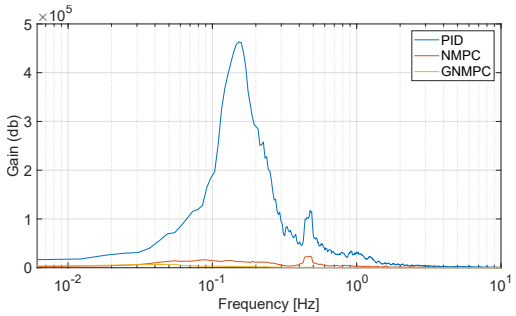

(b) Spectral density of Fx force.

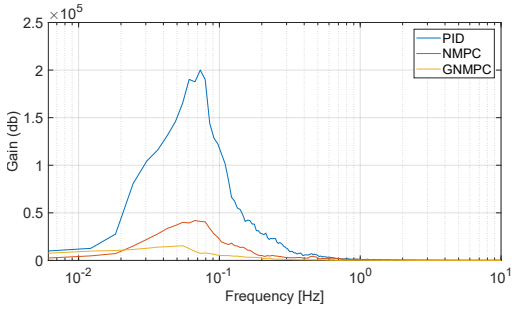

(c) Spectral density of Fy force.

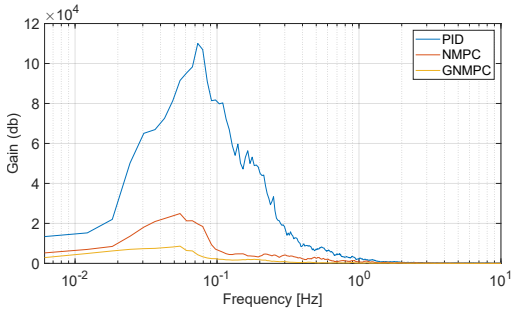

(d) Spectral density of F $_{\psi}$ torque.

Figure 6.10: Comparison of energy consumption of the HS test under different wave conditions and power spectrum of the thrusters under RW conditions.

output varies too much at quick succession, it can lead to unstable ship movement. Moreover, excessive variation in thruster output can also cause unnecessary wear and tear on the thrusters and other ship components, leading to increased maintenance costs and downtime. Figure 6.10b, Figure 6.10c, and Figure 6.10d show the spectrum of the forces on the x,y, and torque rotational axes under RW condition. It is clearly visible that the GNMPC has more low frequency movements compared to the rest of the controllers. This means that the GNMPC reduces high frequency variations in thrusters which can result in less wear and tear.

6.6.2 DP Oblique Angles

The DP oblique angles test is an additional dynamic positioning (DP) test used to confirm that a vessel can maintain its position at various angles. The vessel is then kept in the same X-Y orientation while rotating about its axis at 30, and 45 degrees. Figure. 6.11. shows the position and heading accuracy of the three controller under different sea conditions. The errors made in these tests are minimal in the no wave condition since there is no external disturbances. The ship may move as a result of the four propellers coupling effect. The PID makes an effort to reduce setpoint errors. PID has more actuations as a result, which reduced its precision. The actuator actions by the other controllers are smaller than those made by PID since NMPC considers the ship's dynamics. Given the small position error, the GNMPC applies the least correction, resulting in the highest accuracy in no wave conditions. The RMSE of the PID controller at the white noise wave case in the X , and Y error position is marginally higher than the RMSE of the NMPC. A closer look at the results also show that the maximum inaccuracy in the PID is higher. Also it is observed that the NMPC performs better than the PID controller in X, and Y and heading error minimization. NMPC, and PID almost always have smaller errors than the GNMPC. However, the GNMPC position errors were within the acceptable safety limit. The white noise wave pushed the ship to one side of the setpoint due to the oblique angle. We can observe that the minimal root square error is positive, indicating that the ship is drifting to one side. Ship movement under irregular waves is small. When compared to the PID, the NMPC has a higher accuracy. The GNMPC error is larger than NMPC and PID errors. Regular waves are the most difficult waves to manage, the precision of the NMPC controller is significantly better than the PID controller in this situation. The GNMPC position accuracy is lower than NMPC, continuing a similar pattern. The vessel's trajectory on the XY plane under regular wave case is shown in Figure. 6.12. However, there is more vessel movement with GNMPC as area tracking is allowed instead of point reference monitoring within the bounds of safety. The GNMPC's weight function is able to maintain a trade-off between maintaining position and limiting thruster

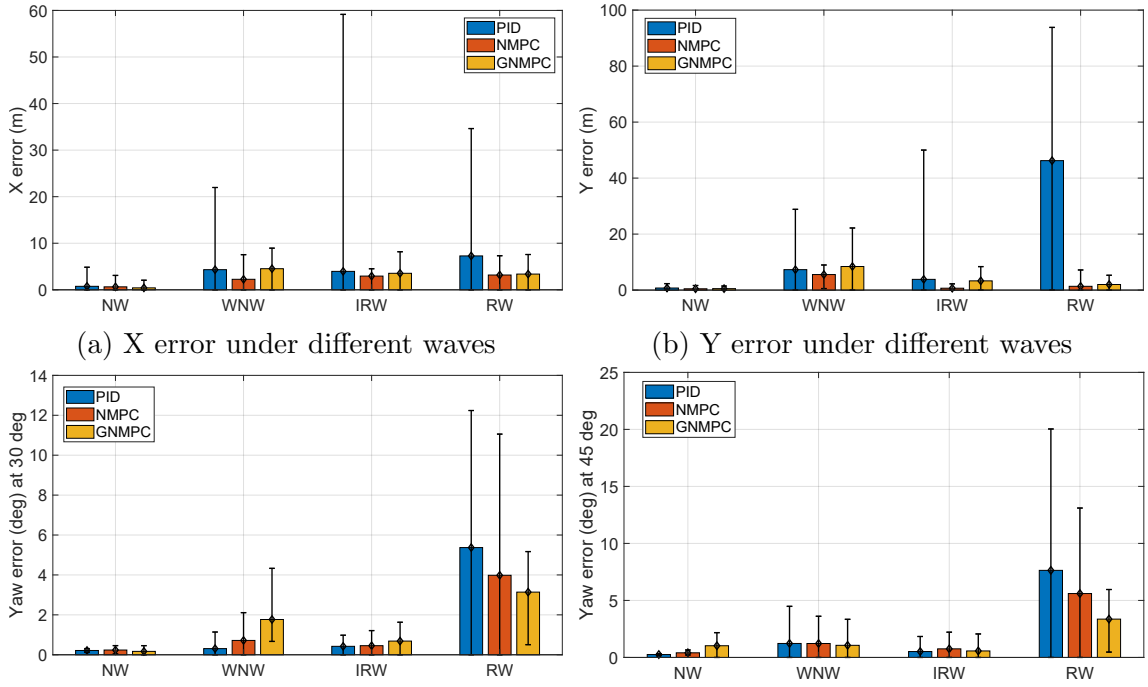

(a) X error under different waves

(b) Y error under different waves

(c) Yaw error at the 30 deg under different waves

(d) Yaw error at the 45 deg under different waves

Figure 6.11: Position and heading accuracy in DP angle setpoint change test under different wave conditions

motions. To evaluate the control action's efficacy, the control signals' variance and power are analyzed. According to the results, GNMPC has the lowest overall power consumption as shown in Figure. 6.13a. GNMPC control actions have lower gain in the mid and high frequency area, as seen in Figure. (6.13b,6.13c,6.13d). This indicates that there will be less high-frequency movement in the thrusters which will help to keep the wear and tear of the thrusters to minimal.

6.6.3 Large Position Setpoint Changes

Though the objective of DP is not to track trajectories, it is occasionally required to make small position changes during DP operation. This test is done to evaluate the

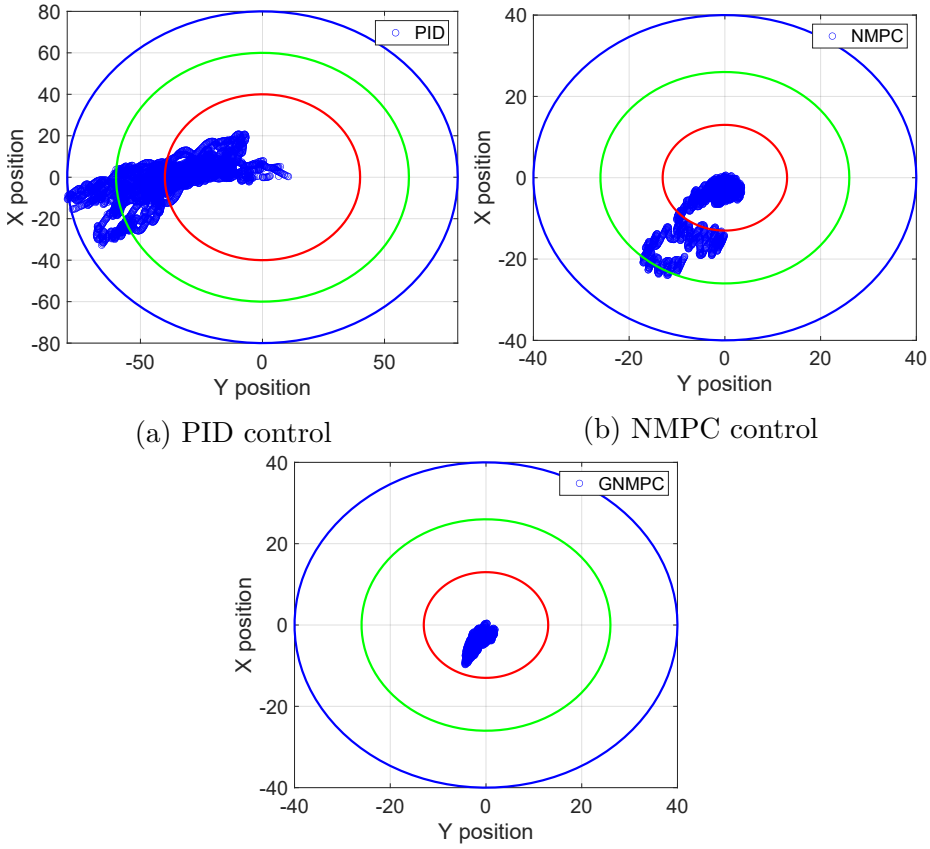

(a) PID control

(b) NMPC control

(c) GNMPC control

Figure 6.12: Comparing the position holding performance of PID,NMPC, and GNMPC controllers under regular wave

controllers' ability to make small adjustments in position and angles.

The controllers were tested for their ability to navigate to the four corners of a rectangular area under irregular wave conditions. Figure. 6.14 shows the trajectory tracked by the vessel under the PID and the NMPC. Note that GNMPC is not tested for trajectory tracking since its objective function is not suitable for position tracking. Depending on the state of the irregular waves, in the PID controller case, the ship departs from point (-33,15) and stops along the way at points (-28,15), (-28,10), (-33,10), and (-28,15) as illustrated in Figure 14. In the NMPC case, the ship moves from the point (-27,14) to stops (-23,14), (-23,10), (-27,10), and (-23,14).

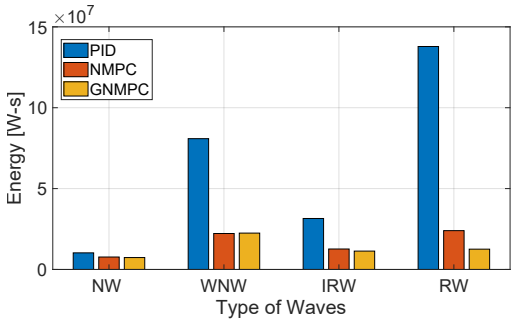

(a) Power consumptions of the thrusters

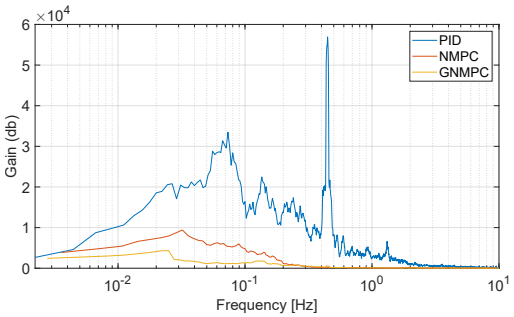

(b) Spectral density of Fx force.

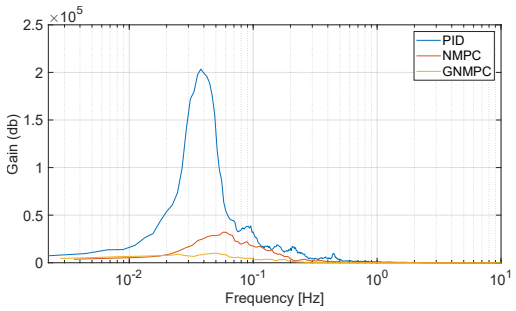

(c) Spectral density of Fy force.

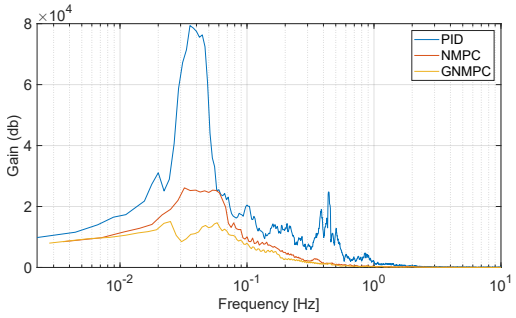

(d) Spectral density of F_psi torque.

Figure 6.13: (a) Power consumptions of the thrusters for the DP angle setpoint change test under different waves; and (b), (c), (d) power spectral of the thrusters in regular wave conditions

Furthermore, Figure. 6.14. shows the NMPC performance is more stable and closer to meeting the trajectory reference than PID.

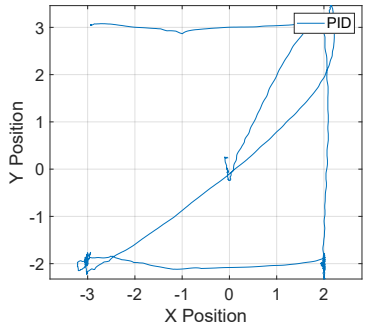

(a) XY plot in PID control

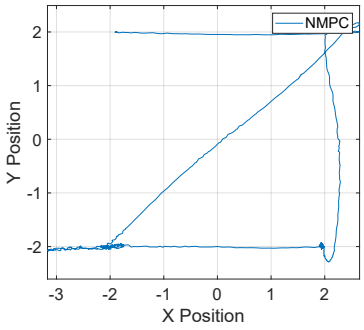

(b) XY plot in NMPC control

Figure 6.14: Setpoint tracking using PID, and NMPC controllers: ship X,Y

Figure. 6.15a shows the energy usage of the two controllers for different wave situation. For all wave conditions the NMPC uses less energy than the PID control. Figure. (6.15b,6.15c,6.15d). shows that NMPC control actions have reduced gain in the high-frequency region indicating less high-frequency thruster movement.

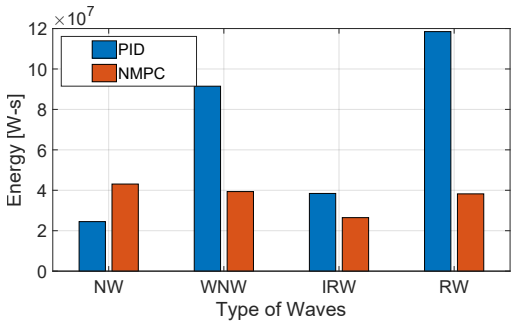

(a) Power consumptions of the thrusters

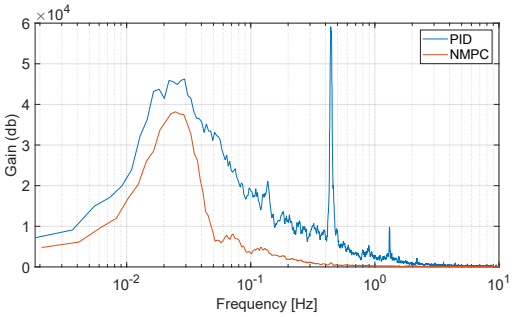

(b) Spectral density of Fx force.

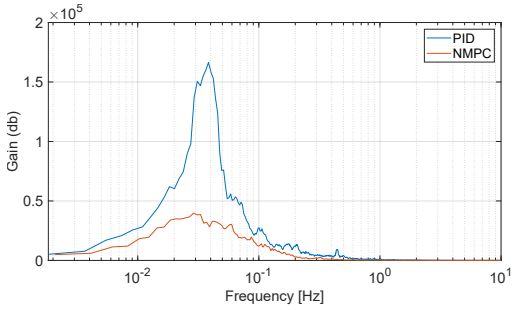

(c) Spectral density of Fy force.

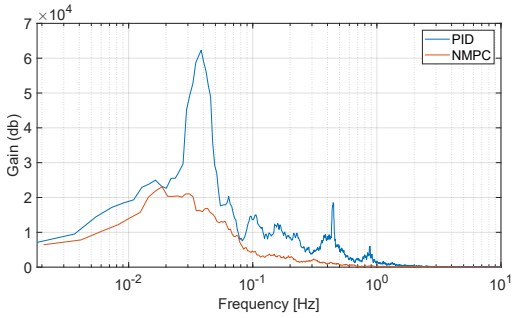

(d) Spectral density of F $_{\psi}$ torque.

Figure 6.15: Power consumptions of the thrusters for the large setpoint changes test under different waves and Power spectral of the thrusters in regular wave conditions

6.7 Conclusion

This study reports an experimental implementation of NMPC and an energy efficient GNMPC controller. This is one of the very few experiments where the NMPCs were tested in a controlled environment with varying wave conditions, and to the best of our knowledge, this is the first experimental implementation of the GNMPC.

The extensive tests provided many valuable insights which will be useful during the implementation of model based controllers on DP systems.

The experimental results on the station keeping tests showed that on average, the GNMPC is the most energy efficient controller for the application. The GNMPC minimizes the thruster movement by implementing a relaxed control policy, which results in low energy consumption and less wear and tear. The controller only reacted aggressively when it hit the boundaries of the safe operation zone. Hence the GNMPC can be implemented on applications where extreme levels of accuracy is not required. However, GNMPC is not suitable for large position setpoint changes. NMPC delivers the best performance in large setpoint changes with lower energy compared to the benchmark PID controller. In a situation where setpoint tracking is necessary, the GNMPC can be switched to a NMPC seamlessly by changing the weights in the objective function to constant values.

Another observation made during the experiment is the impact of the model accuracy on the performance of the NMPCs. The benchmark PID controller does not need any numerical model for the operation. However, the NMPCs highly depend on the accuracy of the numerical model. When the prediction horizon of the NMPCs is short, then the impact of an accurate model is minimal. However, when the prediction horizon is longer, the performance degrades significantly if the numerical model does not represent the actual vessel dynamics. Therefore, it is critical to validate the accuracy of the numerical model by conducting several test maneuvers.

The NMPC and GNMPC use optimization to calculate the optimal control action at each time step. The computation time required by the optimizer to calculate the optimal control sequence is a key consideration when implementing an NMPC controller. An NMPC with a longer prediction horizon generally performs better than an NMPC with a shorter prediction horizon. However, when the prediction horizon is longer, the optimizer requires more computational time to solve for the control action. Therefore, careful consideration has to be given when determining the optimizer, sampling time, and the length of the prediction horizon.

Wave filter was a critical part, especially in the NMPC implementations. When

the direct feedback of the vessel motion is given to the NMPC, the controller attempts to over-compensate for the oscillatory motion due to the first-order wave motions. In order to filter out the oscillatory motion from the feedback, a well-tuned wave filter is required. In this study, we used a UKF based wave filter to filter out the first-order wave effects, and the filter was reasonably easy to tune.

References

[1] Alagili, O., Khan, M. A. I., Ahmed, S., Imtiaz, S., Zaman, H., and Islam, M. An energy-efficient dynamic positioning controller for high sea conditions. *Applied Ocean Research 129* (2022), 103331.

[2] Alfheim, H. L., Muggerud, K., Breivik, M., Brekke, E. F., Eide, E., and Engelhardtsen, Ø. Development of a dynamic positioning system for the revolt model ship. *IFAC-PapersOnLine 51*, 29 (2018), 116–121.

[3] Andersson, J. A. E., Gillis, J., Horn, G., Rawlings, J. B., and Diehl, M. CasADi – A software framework for nonlinear optimization and optimal control. *Mathematical Programming Computation 11*, 1 (2019), 1–36.

[4] Balchen, J. G., Jenssen, N. A., Mathisen, E., and Saelid, S. Dynamic positioning of floating vessles based on kalman filtering and optimal control. In *1980 19th IEEE Conference on Decision and Control including the Symposium on Adaptive Processes* (1980), IEEE, pp. 852–864.

[5] Brodtkorb, A. H., Værnø, S. A., Teel, A. R., Sørensen, A. J., and Skjetne, R. Hybrid controller concept for dynamic positioning of marine vessels with experimental results. *Automatica 93* (2018), 489–497.

[6] Cavaleri, L., Alves, J.-H., Ardhuin, F., Babanin, A., Banner, M., Belibassakis, K., Benoit, M., Donelan, M., Groeneweg, J., Herbers, T., et al. Wave modelling–the state of the art. *Progress in oceanography 75*, 4 (2007), 603–674.

[7] Deng, F., Yang, H.-L., and Wang, L.-J. Adaptive unscented kalman filter based estimation and filtering for dynamic positioning with model uncertainties. *International Journal of Control, Automation and Systems 17* (2019), 667–678.

[8] Diehl, M., Bock, H., Diedam, H., and Wieber, P.-B. *Fast Direct Multiple Shooting Algorithms for Optimal Robot Control*. Springer Berlin Heidelberg, Berlin, Heidelberg, 2006, pp. 65–93.

[9] Du, J., Hu, X., Krstić, M., and Sun, Y. Robust dynamic positioning of ships with disturbances under input saturation. *Automatica 73* (2016), 207–214.

[10] Eriksen, B.-O. H., and Breivik, M. Modeling, identification and control of high-speed asvs: Theory and experiments. In *Sensing and control for autonomous vehicles: Applications to land, water and air vehicles*. Springer, 2017, pp. 407–431.

[11] Fannemel, Å. V. Dynamic positioning by nonlinear model predictive control. Master's thesis, Institutt for teknisk kybernetikk, 2008.

[12] Fossen, T. I. Marine control systems–guidance. navigation, and control of ships, rigs and underwater vehicles. *Marine Cybernetics, Trondheim, Norway, Org. Number NO 985 195 005 MVA, www. marinecybernetics. com, ISBN: 82 92356 00 2* (2002).

[13] Fossen, T. I., Sagatun, S. I., and Sørensen, A. J. Identification of dynamically positioned ships. *Control Engineering Practice 4*, 3 (1996), 369–376.

[14] Fossen, T. I., and Strand, J. P. Passive nonlinear observer design for ships using lyapunov methods: full-scale experiments with a supply vessel. *Automatica 35*, 1 (1999), 3–16.

[15] Grimble, M. J., Patton, R. J., and Wise, D. The design of dynamic ship positioning control systems using stochastic optimal control theory. *Optimal Control Applications and Methods 1*, 2 (1980), 167–202.

[16] Grüne, L., Pannek, J., Grüne, L., and Pannek, J. *Nonlinear model predictive control*. Springer, 2017.

[17] Hou, X., Deng, F., Yang, H., Yu, D., Zhang, H., and Li, B. Robust nonlinear model predictive control for ship dynamic positioning using laguerre function. *IEEE Access 10* (2022), 127563–127574.

[18] Hvamb, O. G. A new concept for fuel tight dp control. In *Dynamic Positioning Conference* (2001).

[19] Jayasiri, A., Nandan, A., Imtiaz, S., Spencer, D., Islam, S., and Ahmed, S. Dynamic positioning of vessels using a ukf-based observer and an nmpc-based controller. *IEEE Transactions on Automation Science and Engineering 14*, 4 (2017), 1778–1785.

[20] Johansen, T. A., and Brekke, E. Globally exponentially stable kalman filtering for slam with ahrs. In *2016 19th International Conference on Information Fusion (FUSION)* (2016), IEEE, pp. 909–916.

[21] Julier, S. J., and Uhlmann, J. K. New extension of the kalman filter to nonlinear systems. In *Signal processing, sensor fusion, and target recognition VI* (1997), vol. 3068, Spie, pp. 182–193.

[22] Miller, P. A., Farrell, J. A., Zhao, Y., and Djapic, V. Autonomous underwater vehicle navigation. *IEEE Journal of Oceanic Engineering 35*, 3 (2010), 663–678.

[23] Nguyen, T. D., Sørensen, A. J., and Quek, S. T. Design of hybrid controller for dynamic positioning from calm to extreme sea conditions. *Automatica 43*, 5 (2007), 768–785.

[24] Pedersen, A. A. Optimization based system identification for the milliampere ferry. Master's thesis, NTNU, 2019.

[25] Rabanal, O. M., Brodtkorb, A. H., and Breivik, M. Comparing controllers for dynamic positioning of ships in extreme seas. *IFAC-PapersOnLine 49*, 23 (2016), 258–264.

[26] Saelid, S., Jenssen, N., and Balchen, J. Design and analysis of a dynamic positioning system based on kalman filtering and optimal control. *IEEE Transactions on Automatic Control 28*, 3 (1983), 331–339.

[27] Sorensen, A., Strand, J. P., and Nyberg, H. Dynamic positioning of ships and floaters in extreme seas. In *OCEANS'02 MTS/IEEE* (2002), vol. 3, IEEE, pp. 1849–1854.

[28] Sørensen, A. J. A survey of dynamic positioning control systems. *Annual reviews in control 35*, 1 (2011), 123–136.

[29] Sørensen, A. J., Sagatun, S. I., and Fossen, T. I. Design of a dynamic positioning system using model-based control. *Control Engineering Practice 4*, 3 (1996), 359–368.

[30] Sotnikova, M. V., and Veremey, E. I. Dynamic positioning based on nonlinear mpc. *IFAC Proceedings Volumes 46*, 33 (2013), 37–42.

[31] Tannuri, E. A., and Morishita, H. M. Experimental and numerical evaluation of a typical dynamic positioning system. *Applied Ocean Research 28*, 2 (2006), 133–146.

[32] Torsetnes, G., Jouffroy, J., and Fossen, T. I. Nonlinear dynamic positioning of ships with gain-scheduled wave filtering. In *2004 43rd IEEE Conference on Decision and Control (CDC)(IEEE Cat. No. 04CH37601)* (2004), vol. 5, IEEE, pp. 5340–5347.

[33] Veksler, A., Johansen, T. A., Borrelli, F., and Realfsen, B. Dynamic positioning with model predictive control. *IEEE Transactions on Control Systems Technology 24*, 4 (2016), 1340–1353.

[34] Wang, Y. Application of model predictive control to dynamic positioning system. *Master thesis* (2006).

[35] Wang, Y., Sui, Y., Wu, J., and Jiao, J. Research on nonlinear model predictive control technology for ship dynamic positioning system. In *2012 IEEE International Conference on Automation and Logistics* (2012), IEEE, pp. 348–351.

[36] Wei, X., Zhang, H., and Wei, Y. Composite hierarchical anti-disturbance control for dynamic positioning system of ships based on robust wave filter. *Ocean Engineering 262* (2022), 112173.

[37] Xu, S., Wang, X., Yang, J., and Wang, L. A fuzzy rule-based pid controller for dynamic positioning of vessels in variable environmental disturbances. *Journal of Marine Science and Technology 25* (2020), 914–924.

Chapter 7

Conclusions and Recommendations for Future Research

7.1 Conclusions

The goal of the thesis is to develop energy efficient DP systems that are capable of operating under harsh environmental conditions. The thesis scope encompassed modelling and characterization of environmental disturbances; evaluation of the benchmark controllers including nonlinear PID, SMC, MRPID as well as more advanced controller such as MPC and NMPC under various extreme weather conditions; and development of an energy efficient controller based on the principles of Economic NMPC. Throughout the thesis we employed theoretical development, simulation studies, and experimental implementation to achieve the goal. Below we summarize the major accomplishments of the thesis.

1. Disturbance modelling

   (a) Detailed numerical modelling and simulation of waves, currents, wind, and ice were carried out that comply with the real-time simulation requirements and adequately capture the dynamic characteristics of the most

relevant physical processes.

(b) A 3D dispersive numerical model was deployed to predict the wave parameters to compute the wave loads on a ship with known Response Amplitude Operators (RAO). A uniform current load was incorporated in a superposition manner by using a combined wave-current field dispersion relation capable of expressing the wavenumber of an interactive wave-current field.

(c) A multiple regression-based ice model was used to predict the loads caused by an ice field characterized by varied ice thickness, concentration, floe size, drift speed and directions. The interaction between the ice field and waves is assumed negligible.

(d) The external disturbance models developed or recommended in this research are expected to help in the development and evaluation of the most effective control scheme for different extreme sea conditions. Another application may be developing a realistic simulation environment to train conventional, DP and autonomous ship operators.

2. Comparative evaluation of DP controllers

(a) Performances of a set of control schemes for DP system were studied in this work. The linear and nonlinear model predictive control (MPC), the nonlinear proportional integral and derivative (PID) control, the sliding mode control (SMC) as well as the multi-resolution PID (MRPID) control schemes are evaluated for moderate and extreme sea states.

(b) Based on the simulation study it was concluded that all of the above control algorithm for DP can effectively control the vessel under moderate sea conditions. However, under extreme conditions, the performance may deteriorate to the extent that the controller may fail to stabilize the system. For the extreme sea conditions considered for this study, only the NMPC and the MRPID controllers were able to stabilize the vessel.

(c) The control actions and thruster movements of the existing controllers are

often very high. The results supports further development of control system for dynamic positioning and autonomous shipping systems, especially for improving the energy efficiency.

3. Development of an energy efficient DP

   (a) An energy-efficient NMPC based controller, called Green-NMPC is developed for the dynamic positioning of marine vessels. The Green-NMPC is motivated by the control goal of minimizing thruster demand. It is based upon the theoretical framework of the economic NMPC (ENMPC). Green-NMPC uses dynamic weights in the cost function depending on the vessel position in contrast to the constant weights in conventional NMPC.

   (b) Green NMPC was implemented for 'moderate' and 'high' sea conditions in a simulation environment. The controller performance, specifically energy efficiency of the ship, was compared against a conventional NMPC and a NPID controller. For all cases, including high sea conditions, the controller was found energy efficient while it maintained the vessel position inside the safety limits. The Green-NMPC showed less thruster demand in the time domain plots. It is further verified quantitatively from the variance and the spectral strength of the thruster demand. Relatively lower power demand was observed in the spectral plot for the Green-NMPC at the higher frequency range.

4. Experimental implementation of energy efficient DP

   (a) Experimental implementation of NMPC and an energy efficient Green NMPC controller were done at the National Research Council's wave basin. This is one of the very few experiments where the NMPCs were tested in a controlled environment with varying wave conditions, and the first experimental implementation of the Green NMPC.

   (b) The experimental results on the station keeping tests validated that on average, the Green NMPC is the most energy efficient controller for the

application. The Green NMPC minimizes the thruster movement by implementing a relaxed control policy. The power spectrum of the thrusters further confirmed that Green NMPC has less high-frequency movements compared to the rest of the controllers. This implies that Green NMPC will cause less wear and tear on the thruster system.

(c) Green NMPC is not suitable for large position setpoint changes. NMPC delivers the best performance in large setpoint changes with lower energy compared to the benchmark PID controller. In a situation where setpoint tracking is necessary, the Green NMPC can be switched to a NMPC seamlessly by changing the weights in the objective function to constant values.

(d) It was observed that the impact of model accuracy on the performance of the model based controllers including NMPC and Green NMPC is significant. For short prediction horizon the NMPCs impact on an inaccurate model is minimal. However, when the prediction horizon is longer, the performance degrades significantly if the numerical model does not represent the actual vessel dynamics. Therefore, it is critical to validate the accuracy of the numerical model by conducting several test maneuvers.

(e) NMPC with a longer prediction horizon generally performed better than an NMPC with a shorter prediction horizon. However, when the prediction horizon is longer, the optimizer required more computational time to solve for the control action. Therefore, careful consideration has to be given when determining the optimizer, sampling time, and the length of the prediction horizon.

(f) Wave filter was found to be critical in the NMPC implementations. When the direct feedback of the vessel motion is given to the NMPC, the controller attempts to over-compensate for the oscillatory motion due to the first-order wave forces. In order to filter out the oscillatory motion from the feedback, a well-tuned wave filter is required. In this study, we used a UKF based wave filter to filter out the first-order wave effects, and the

filter was reasonably easy to tune.

7.2 Recommendations

We have the following recommendations for future research:

1. The wave and ice interaction models are still in the development phase, and besides some rudimentary empirical techniques, the complex interactions are not well understood. The ice force models need further theoretical development and validated using an extensive dataset of DP vessel's interactions with managed ice-field.

2. In tuning the NMPC and Green NMPC we used a trial and error method. There is scope for developing more systematic methods for tuning of the controllers. Future researchers may explore use of reinforcement learning for tuning of the controllers.

3. The performance of an NMPC and Green NMPC depends on the quality and accuracy of the vessel's model. However, through zig-zag test it is always not possible to identify the vessel parameters especially the nonlinear terms. In the experimental implementation, significant effort was required to fine tune the vessel model. In many studies researchers have used reinforcement learning to calibrate model in real-time. Similar approach may be taken to fine tune vessel model for NMPC applications.

Chapter 8

Appendix A

8.1 DP Head Seas Test

Station keeping, or the system's capacity to maintain the vessel in a constant location despite of external forces like wind, waves, and currents, is a crucial component of DP. A station-keeping test is often performed to ensure the DP system is capable of doing this duty.

8.1.1 Spectral Density of Thrusters in No wave Conditions

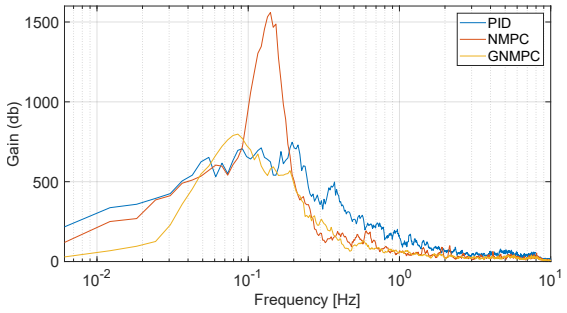

(a) Spectral density of Fx force.

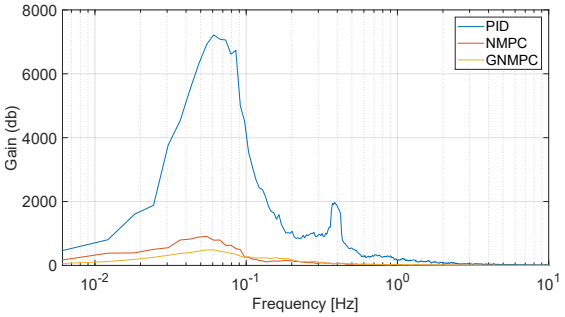

(b) Spectral density of Fy force.

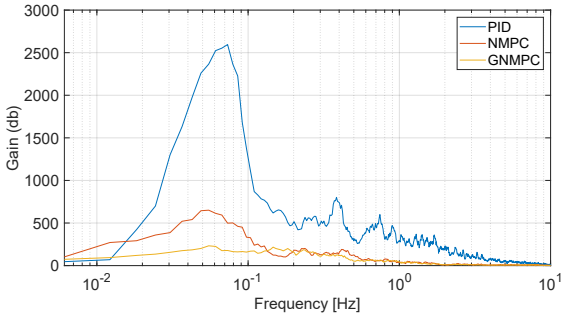

(c) Spectral density of Fpsi torque.

Figure 8.1: Spectral density of thrusters in No wave conditions

8.1.2 Spectral Density of Thrusters in White noise wave Conditions

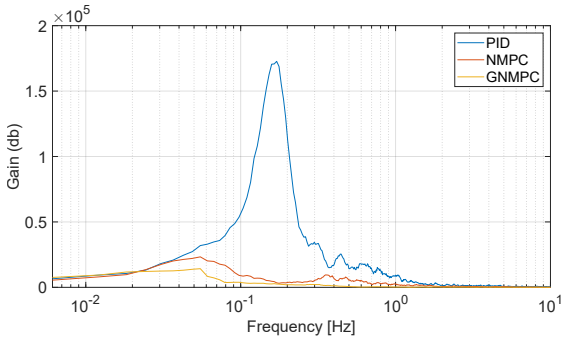

(a) Spectral density of Fx force.

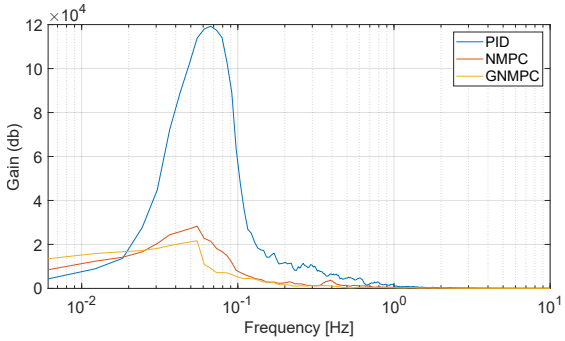

(b) Spectral density of Fy force.

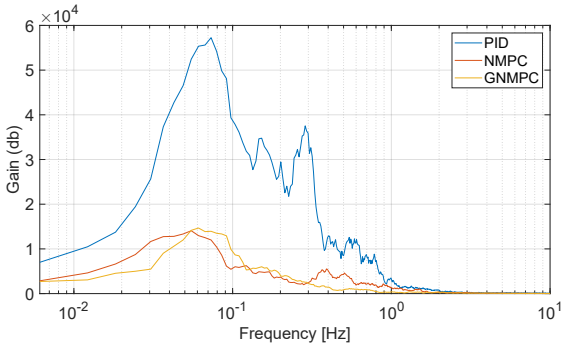

(c) Spectral density of Fpsi torque.

Figure 8.2: Spectral density of thrusters in White noise wave conditions

8.1.3 Spectral Density of Thrusters in Irregular wave Conditions

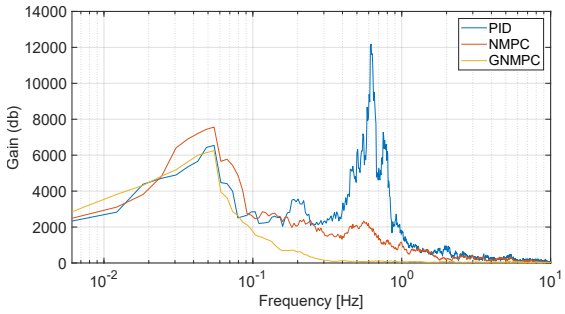

(a) Spectral density of Fx force.

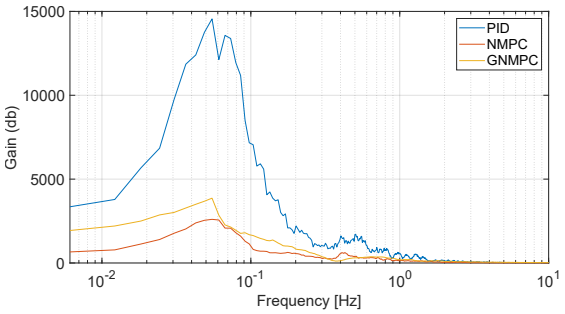

(b) Spectral density of Fy force.

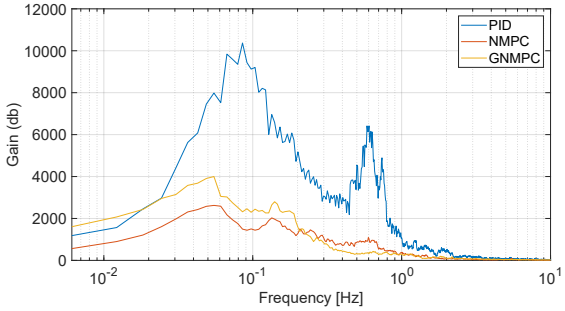

(c) Spectral density of Fpsi torque.

Figure 8.3: Spectral density of thrusters in Irregular wave conditions

8.1.4 XY plots in PID,NMPC, and GNMPC under Different Waves Conditions

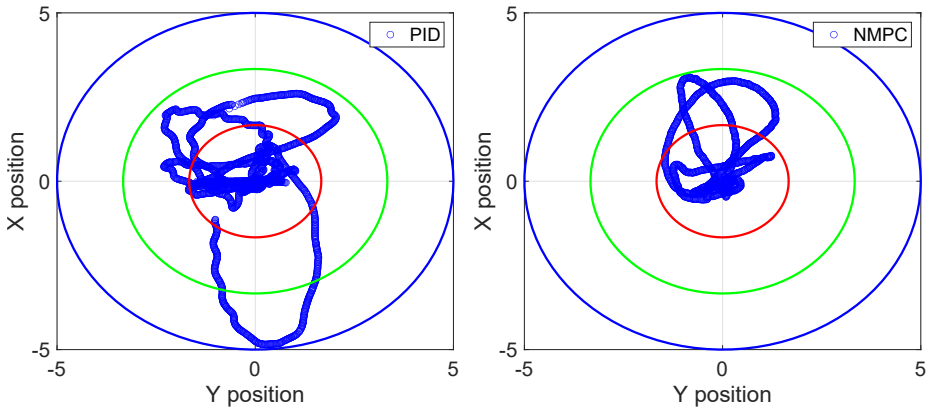

(a) XY plot in PID control

(b) XY plot in NMPC control

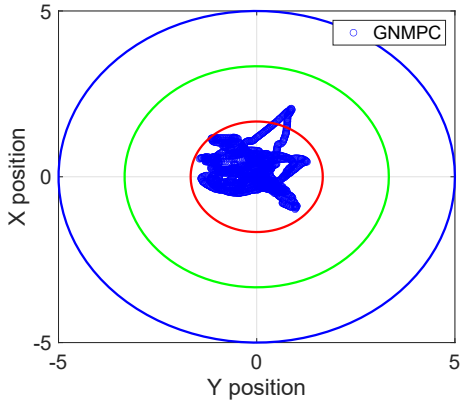

(c) XY plot in GNMPC control

Figure 8.4: Convergence comparison of PID,NMPC and GNMPC controllers: ship X,Y position at No waves

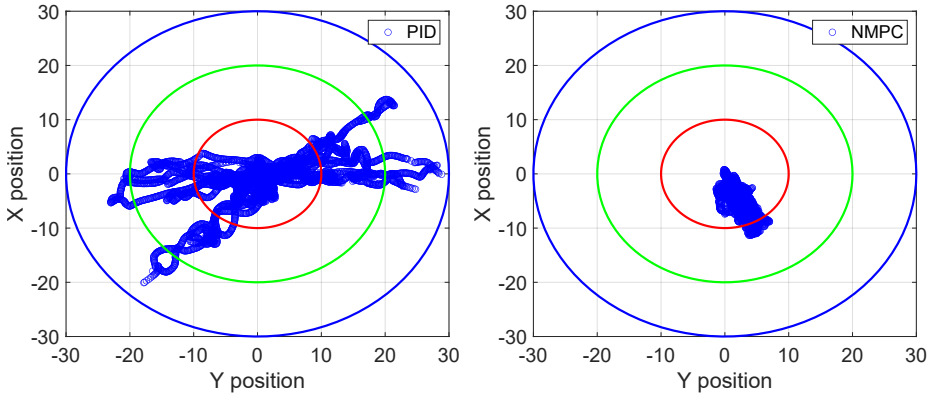

(a) XY plot in PID control

(b) XY plot in NMPC control

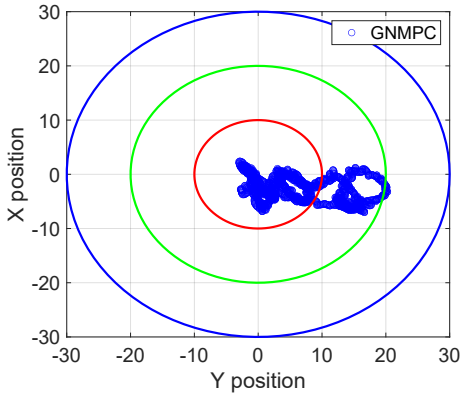

(c) XY plot in GNMPC control

Figure 8.5: Convergence comparison of PID,NMPC and GNMPC controllers: ship X,Y position at White noise waves

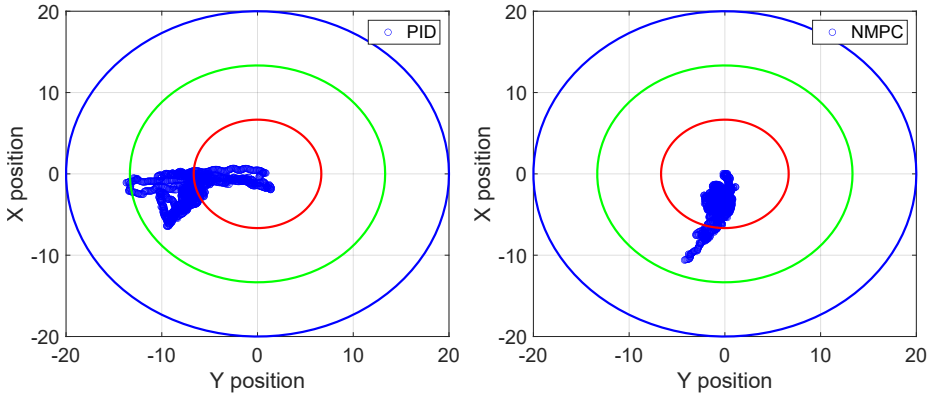

(a) XY plot in PID control

(b) XY plot in NMPC control

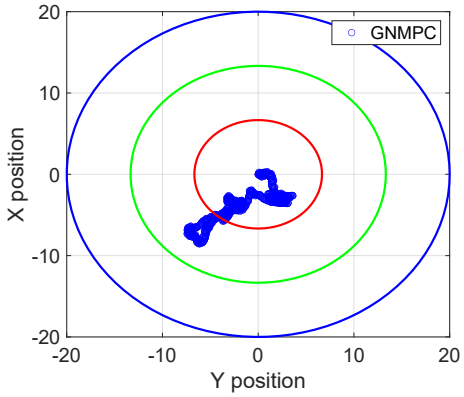

(c) XY plot in GNMPC control

Figure 8.6: Convergence comparison of PID,NMPC and GNMPC controllers: ship X,Y position at Irregular waves

8.1.5 Thrusters Forces and Spectral Densities under No waves Condition

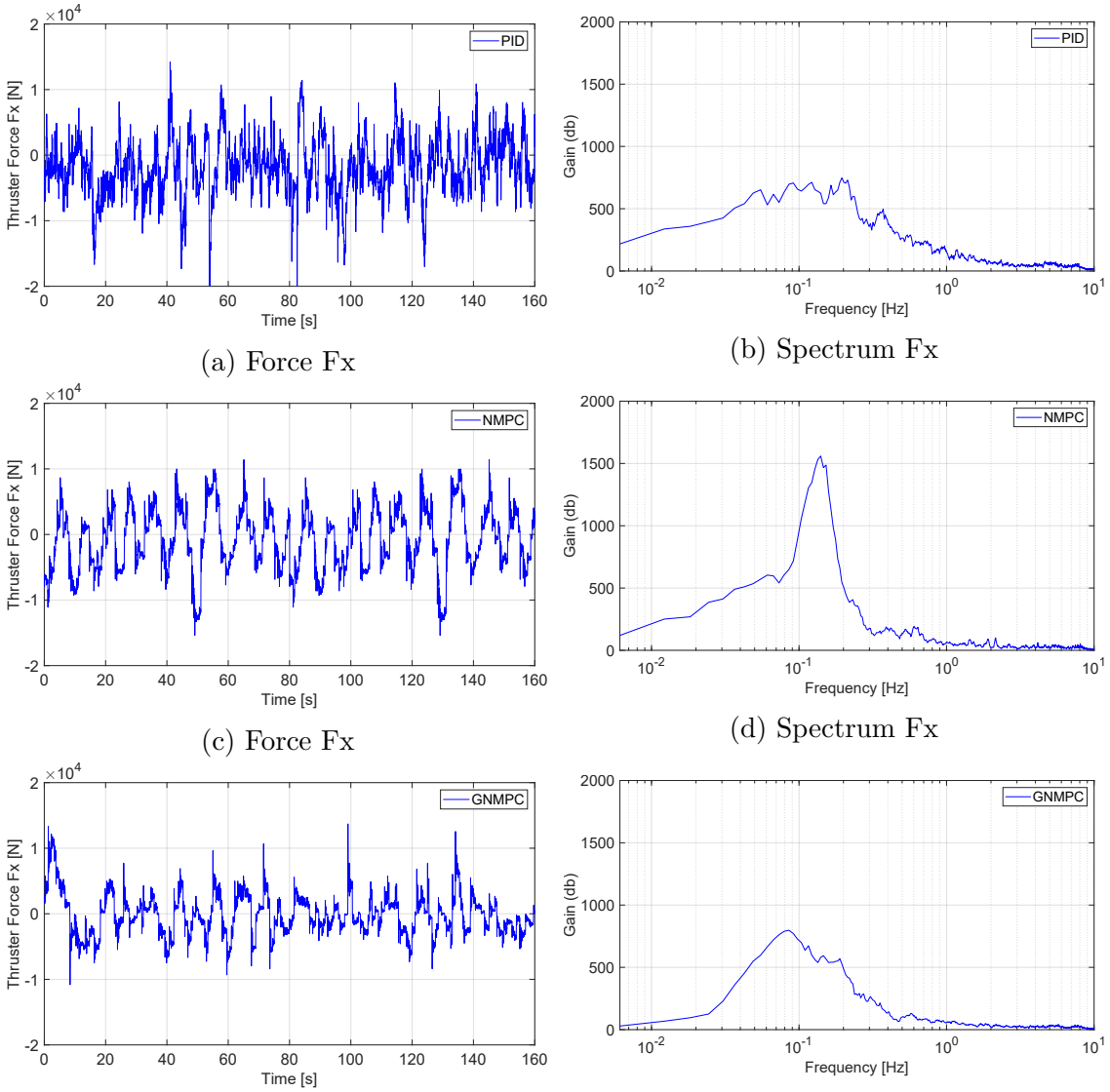

(a) Force Fx

(b) Spectrum Fx

(c) Force Fx

(d) Spectrum Fx

(e) Force Fx

(f) Spectrum Fx

Figure 8.7: Fx Thruster force and spectral density along x direction for different controllers.

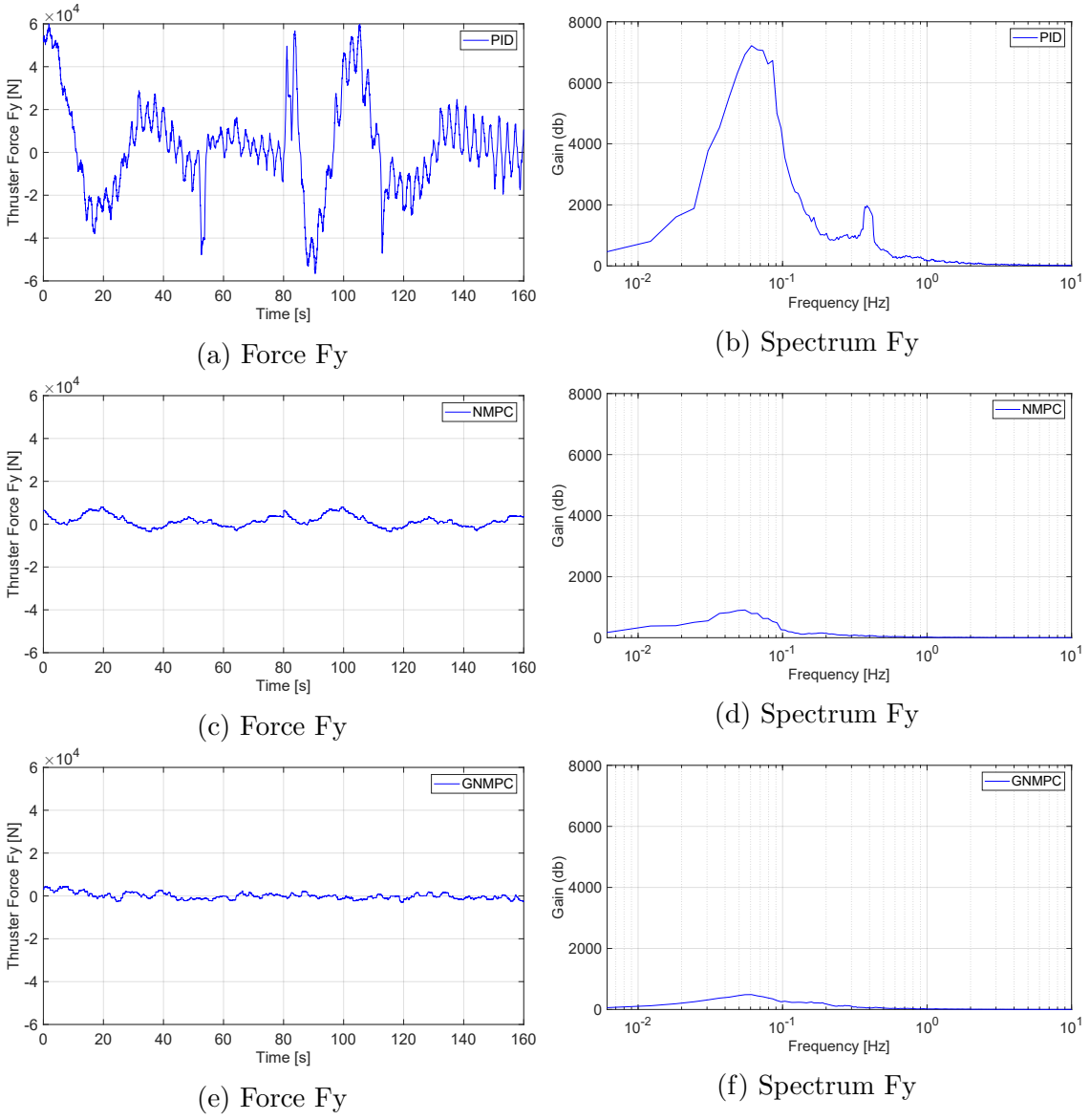

(a) Force Fy

(b) Spectrum Fy

(c) Force Fy

(d) Spectrum Fy

(e) Force Fy

(f) Spectrum Fy

Figure 8.8: Fy Thruster force and spectral density along y direction for different controllers.

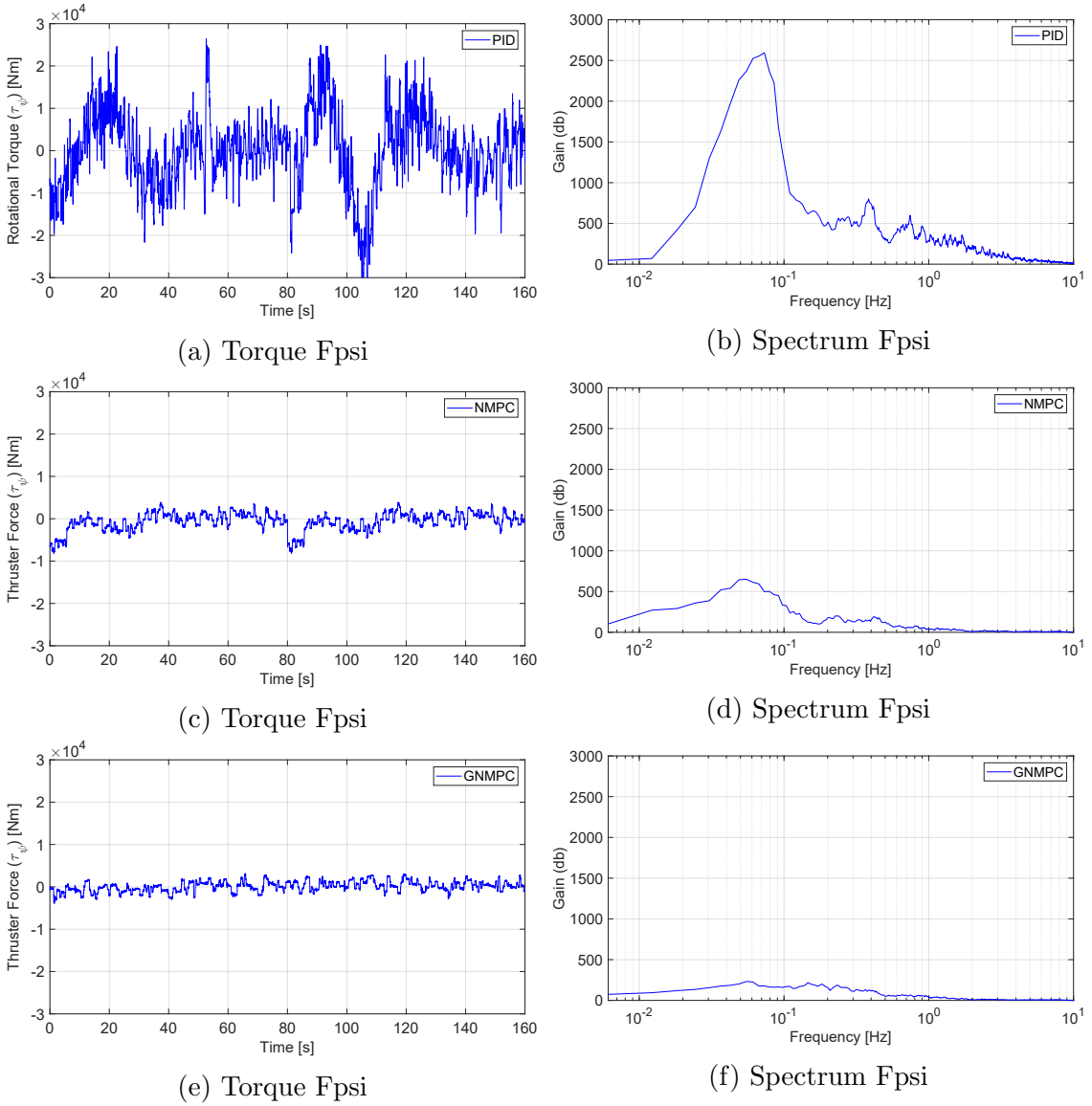

(a) Torque Fpsi

(b) Spectrum Fpsi

(c) Torque Fpsi

(d) Spectrum Fpsi

(e) Torque Fpsi

(f) Spectrum Fpsi

Figure 8.9: Fpsi Thruster torque and spectral density along rotational axis for different controllers.

8.1.6 Thrusters Forces and Spectral Densities under Regular Waves

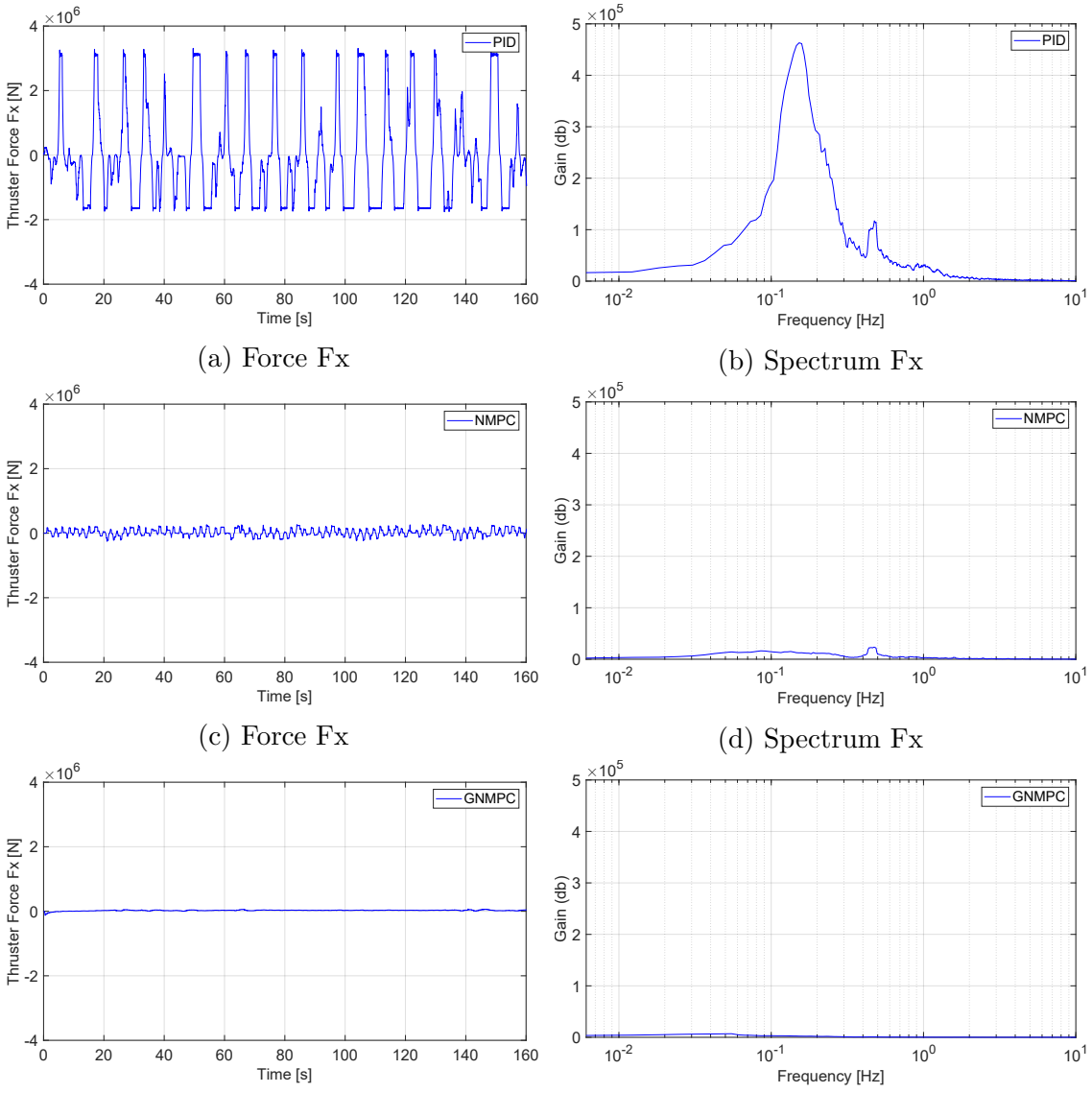

(a) Force Fx

(b) Spectrum Fx

(c) Force Fx

(d) Spectrum Fx

(e) Force Fx

(f) Spectrum Fx

Figure 8.10: Fx Thruster force and spectral density along x direction for different controllers.

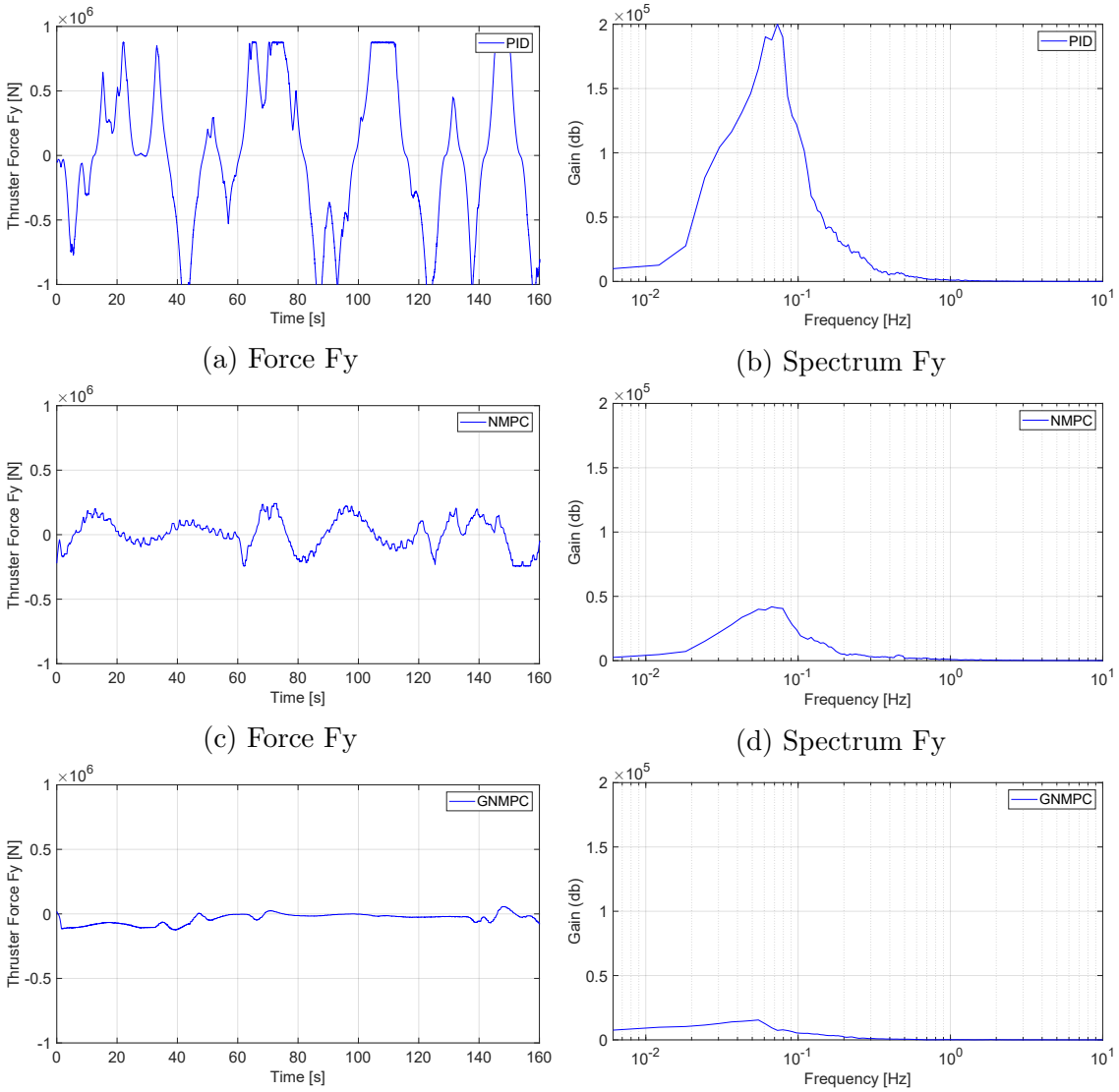

(a) Force Fy

(b) Spectrum Fy

(c) Force Fy

(d) Spectrum Fy

(e) Force Fy

(f) Spectrum Fy

Figure 8.11: Fy Thruster force and spectral density along y direction for different controllers.

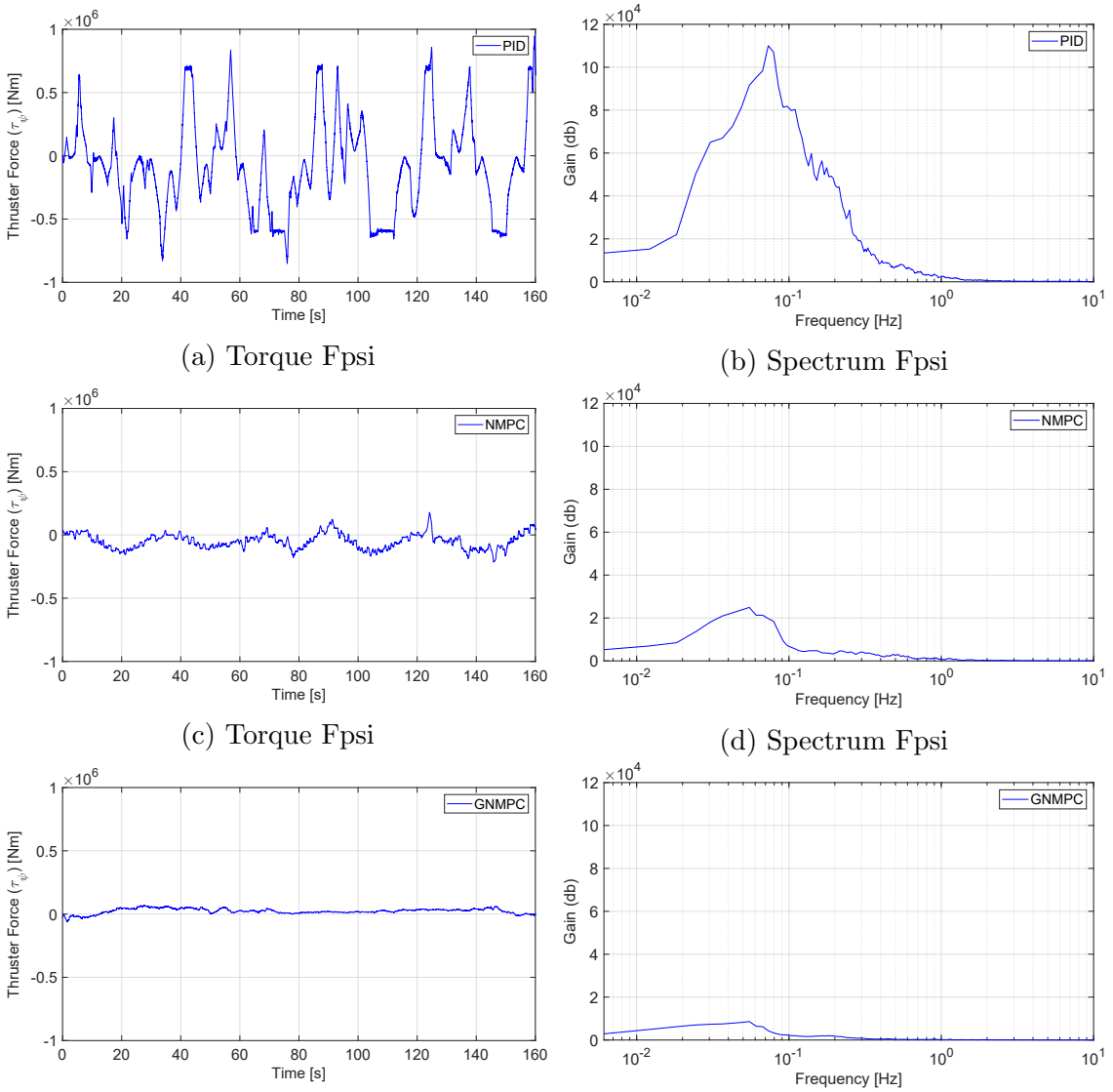

(a) Torque Fpsi

(b) Spectrum Fpsi

(c) Torque Fpsi

(d) Spectrum Fpsi

(e) Torque Fpsi

(f) Spectrum Fpsi

Figure 8.12: Fpsi Thruster torque and spectral density along rotational axis for different controllers.

8.1.7 Thrusters Forces and Spectral Densities under White noise Waves

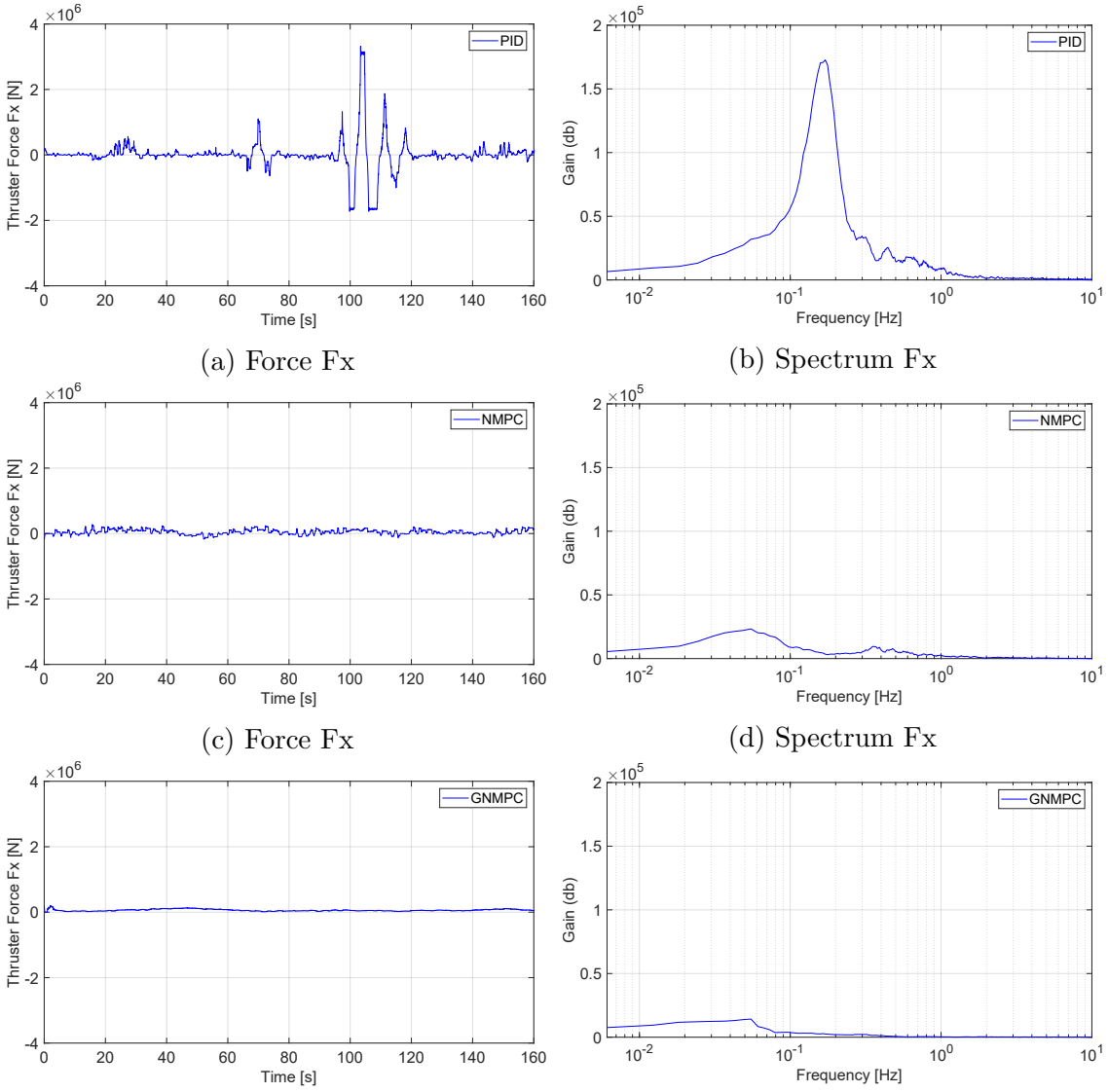

(a) Force Fx (b) Spectrum Fx

(c) Force Fx (d) Spectrum Fx

(e) Force Fx (f) Spectrum Fx

Figure 8.13: Fx Thruster force and spectral density along x direction for different controllers.

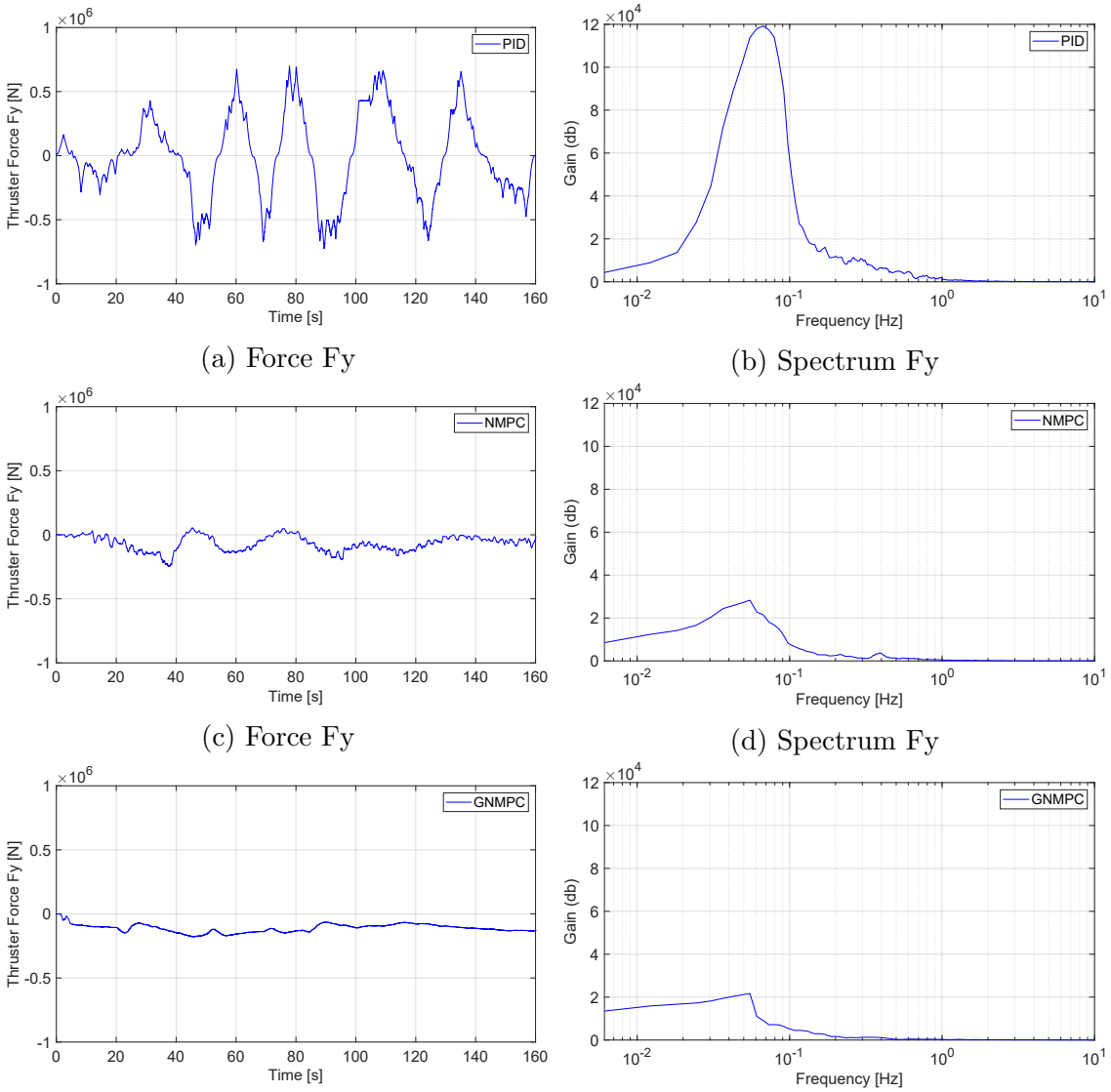

(a) Force Fy

(b) Spectrum Fy

(c) Force Fy

(d) Spectrum Fy

(e) Force Fy

(f) Spectrum Fy

Figure 8.14: Fy Thruster force and spectral density along y direction for different controllers.

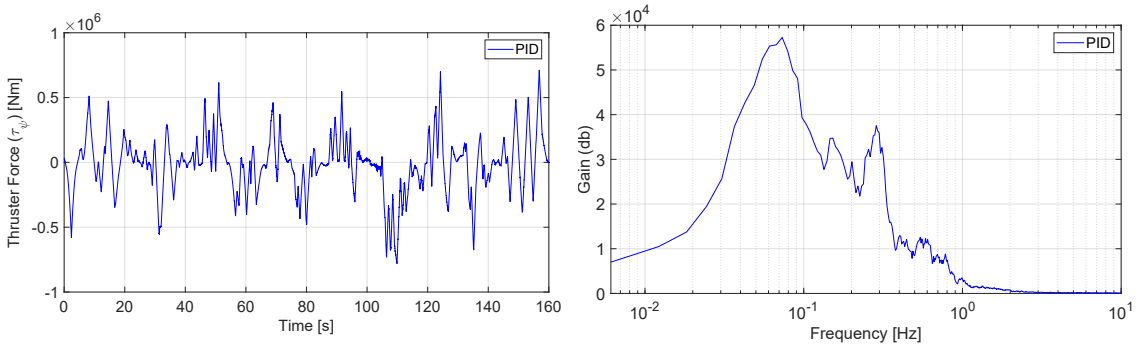

(a) Torque Fpsi

(b) Spectrum Fpsi

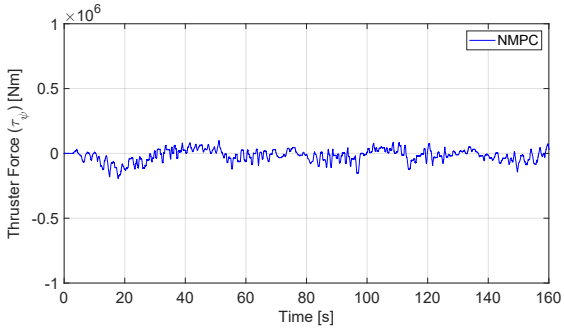

(c) Torque Fpsi

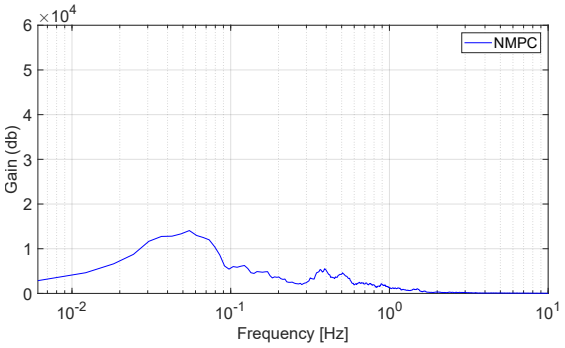

(d) Spectrum Fpsi

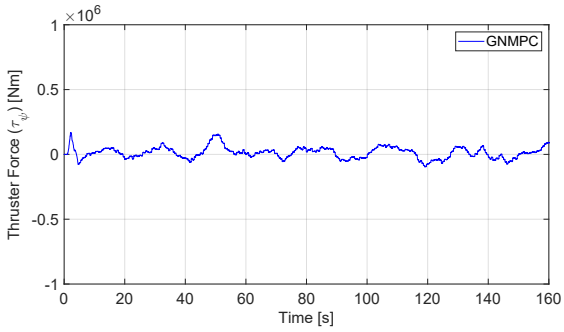

(e) Torque Fpsi

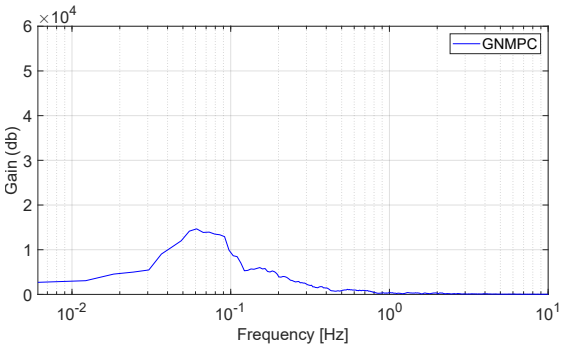

(f) Spectrum Fpsi

Figure 8.15: Fpsi Thruster torque and spectral density along rotational axis for different controllers.

8.1.8 Thrusters Forces and Spectral Densities under Irregular Waves

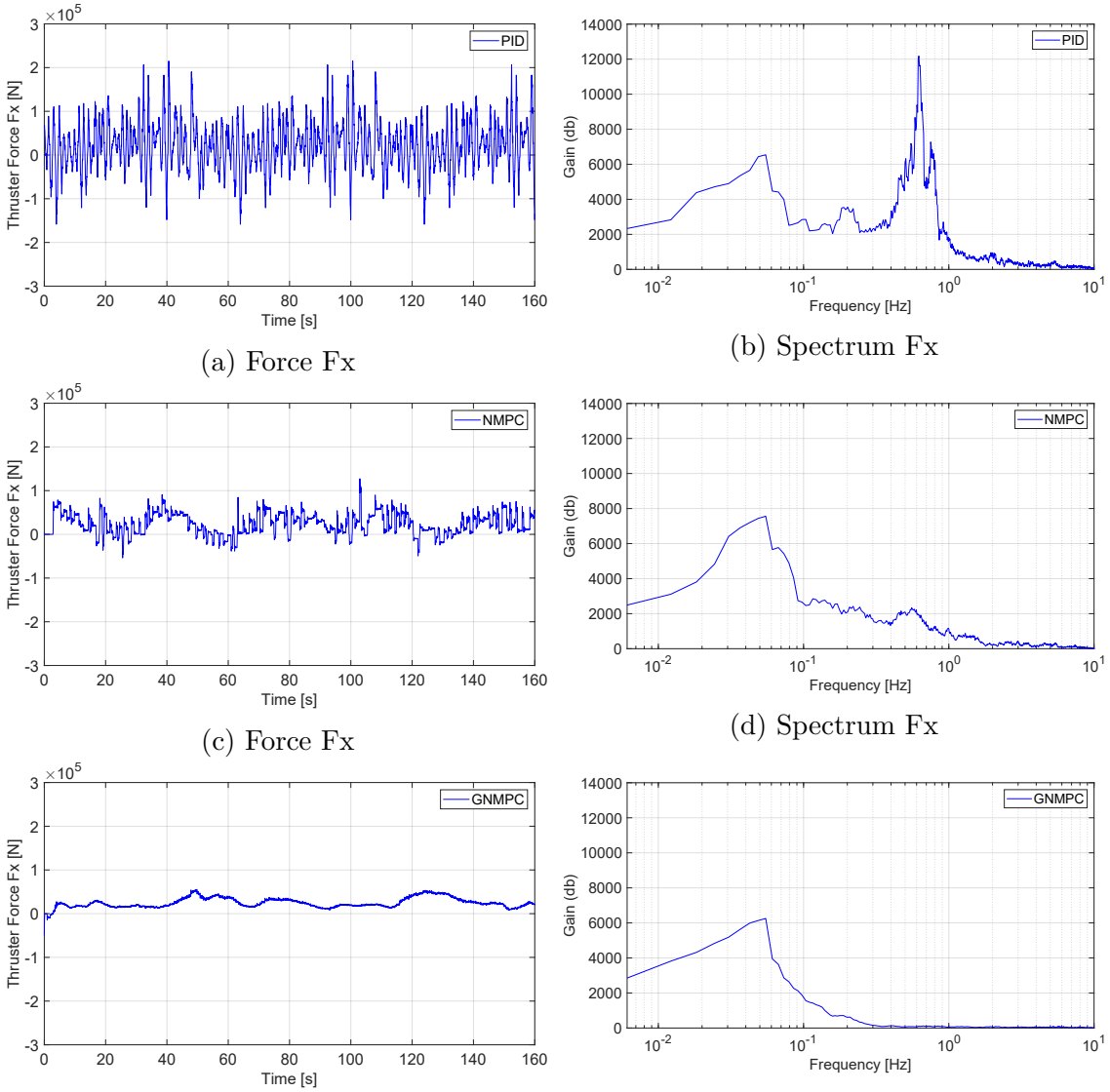

(a) Force Fx

(b) Spectrum Fx

(c) Force Fx

(d) Spectrum Fx

(e) Force Fx

(f) Spectrum Fx

Figure 8.16: Fx Thruster force and spectral density along x direction for different controllers.

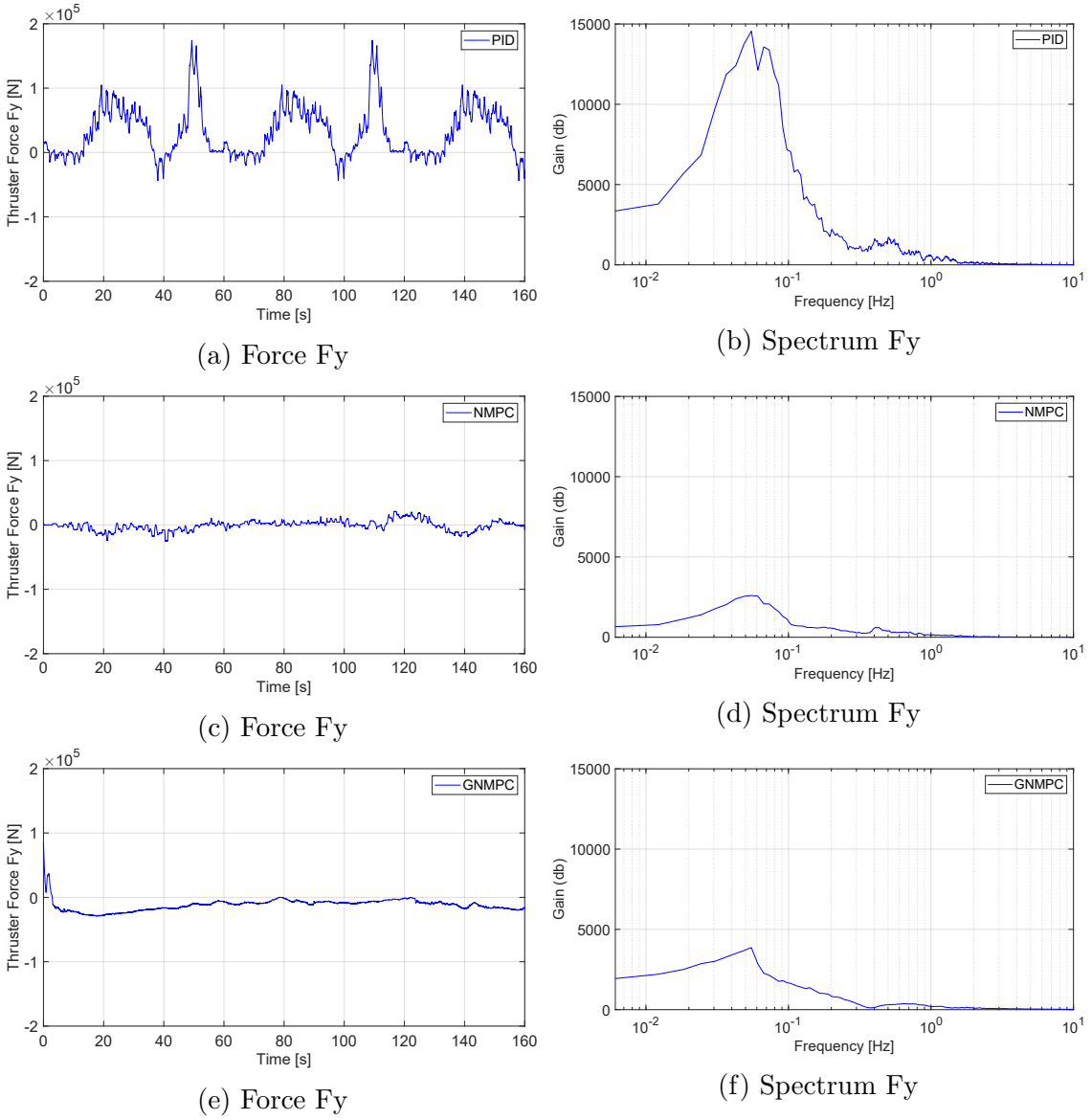

(a) Force Fy

(b) Spectrum Fy

(c) Force Fy

(d) Spectrum Fy

(e) Force Fy

(f) Spectrum Fy

Figure 8.17: Fy Thruster force and spectral density along y direction for different controllers.

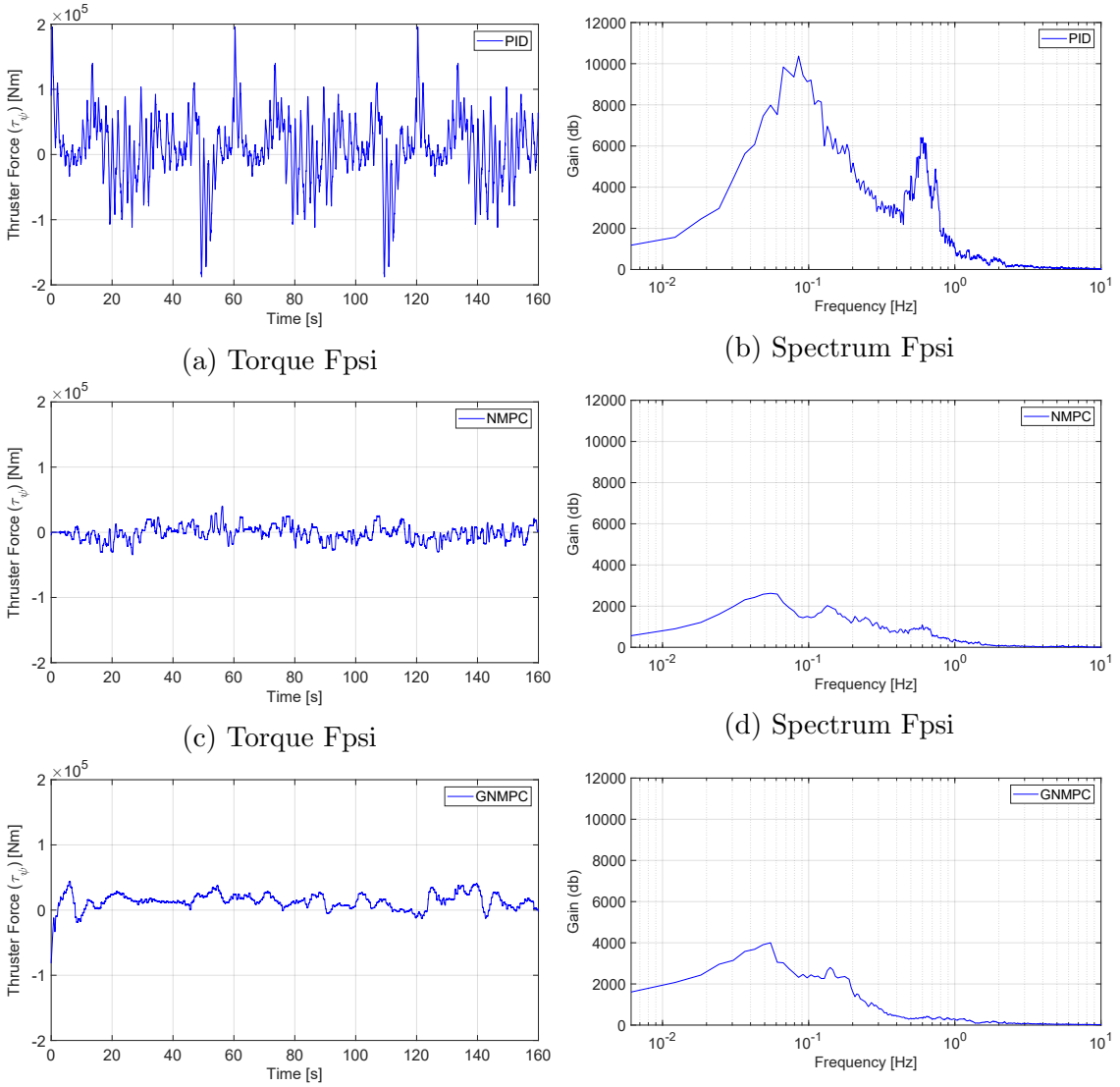

(a) Torque Fpsi

(b) Spectrum Fpsi

(c) Torque Fpsi

(d) Spectrum Fpsi

(e) Torque Fpsi

(f) Spectrum Fpsi

Figure 8.18: Fpsi Thruster torque and spectral density along rotational axis for different controllers.

8.2 DP Oblique Angles Test

The DP oblique angles test is an additional dynamic positioning (DP) test used to confirm that a vessel can maintain its position at various angles. The vessel is then kept in the same X-Y orientation while rotating about its axis at 15, 30, and 45 degrees.

8.2.1 Spectral Density of Thrusters in No wave Conditions

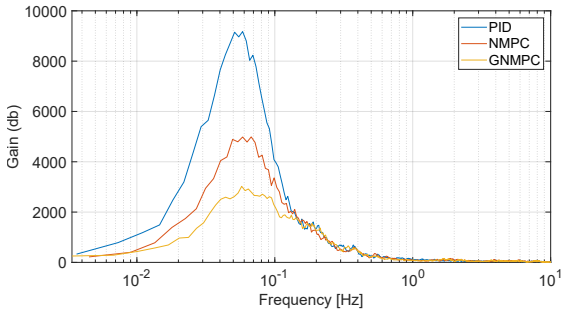

(a) Spectral density of Fx force.

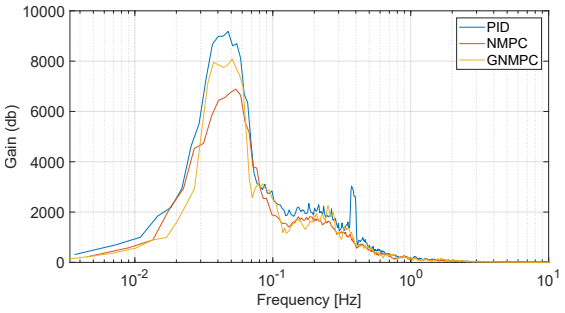

(b) Spectral density of Fy force.

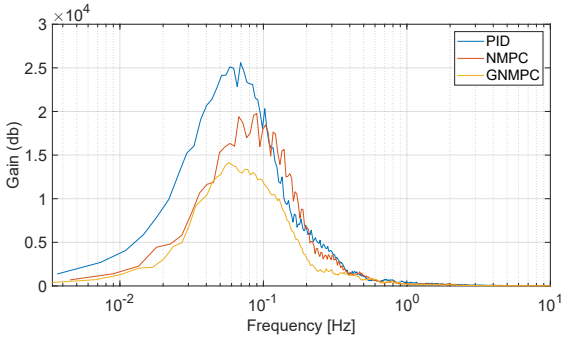

(c) Spectral density of Fpsi torque.

Figure 8.19: Spectral density of thrusters in No wave conditions

8.2.2 Spectral Density of Thrusters in White noise wave Conditions

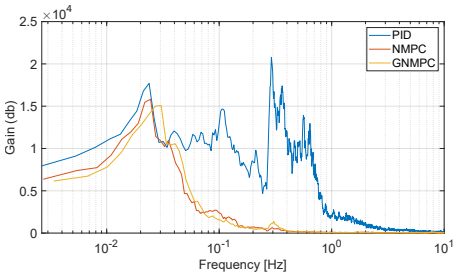

(a) Spectral density of Fx force.

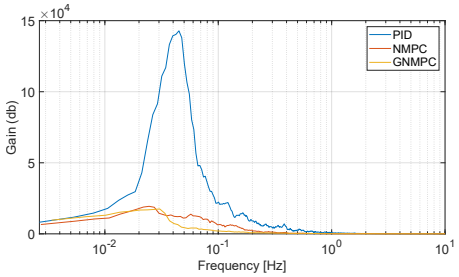

(b) Spectral density of Fy force.

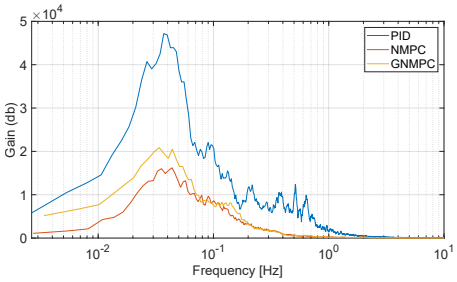

(c) Spectral density of Fpsi torque.

Figure 8.20: Spectral density of thrusters in White noise wave conditions

8.2.3 Spectral Density of Thrusters in Irregular wave Conditions

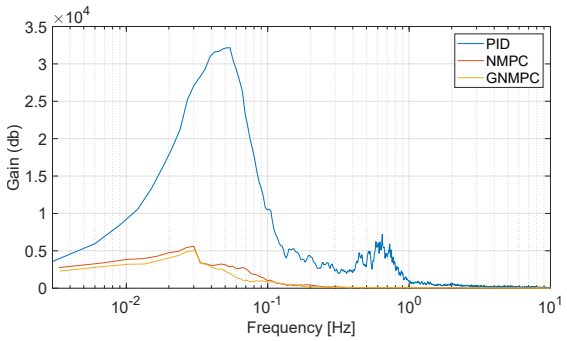

(a) Spectral density of Fx force.

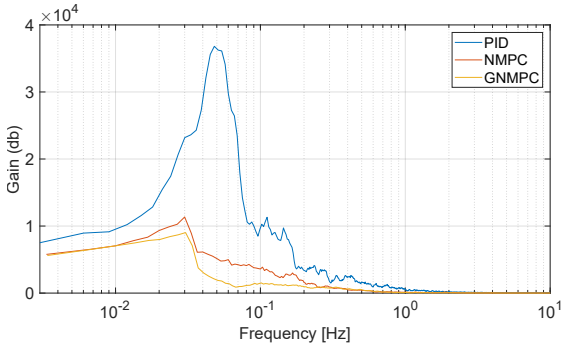

(b) Spectral density of Fy force.

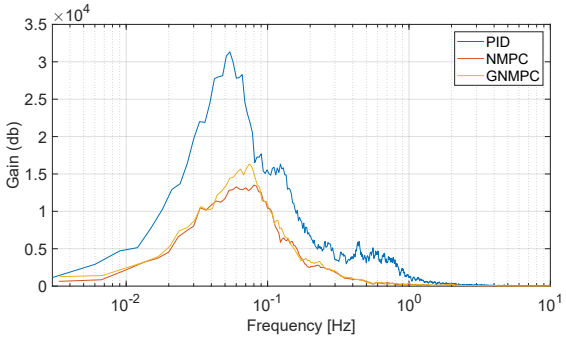

(c) Spectral density of Fpsi torque.

Figure 8.21: Spectral density of thrusters in Irregular wave conditions

8.2.4 XY plots in PID,NMPC, and GNMPC under Different Waves Conditions

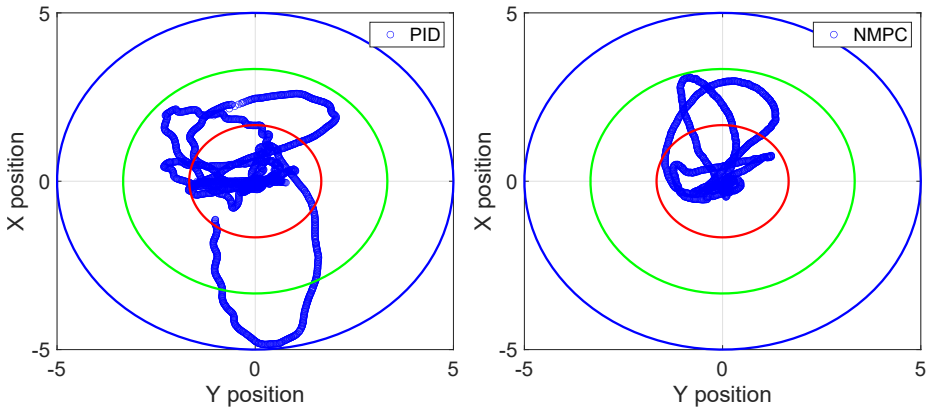

(a) XY plot in PID control

(b) XY plot in NMPC control

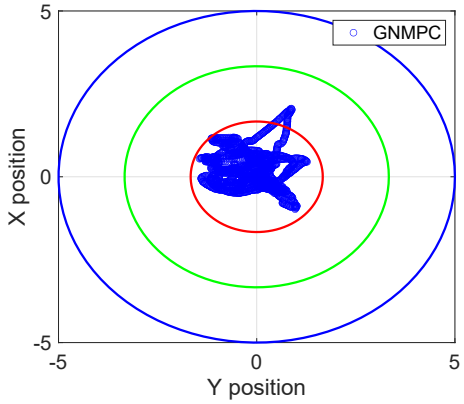

(c) XY plot in GNMPC control

Figure 8.22: Convergence comparison of PID,NMPC and GNMPC controllers: ship X,Y position at No waves

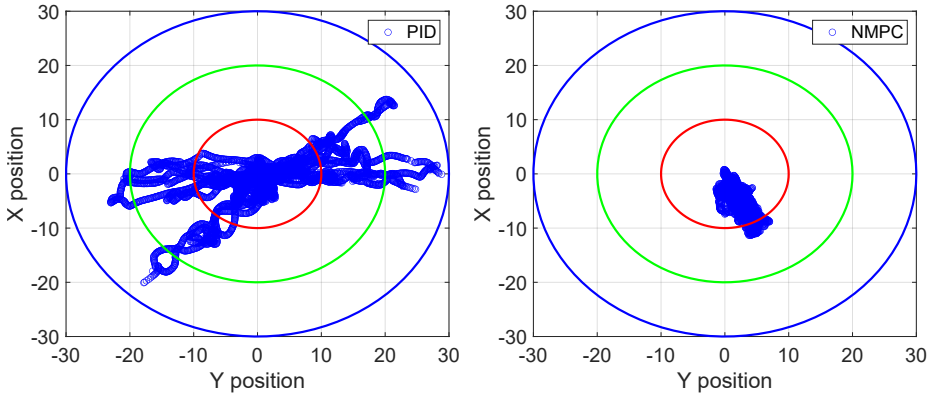

(a) XY plot in PID control

(b) XY plot in NMPC control

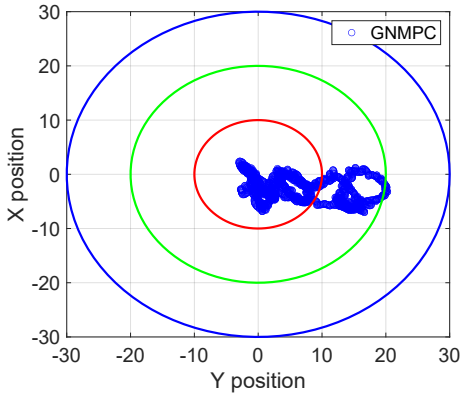

(c) XY plot in GNMPC control

Figure 8.23: Convergence comparison of PID,NMPC and GNMPC controllers: ship X,Y position at White noise waves

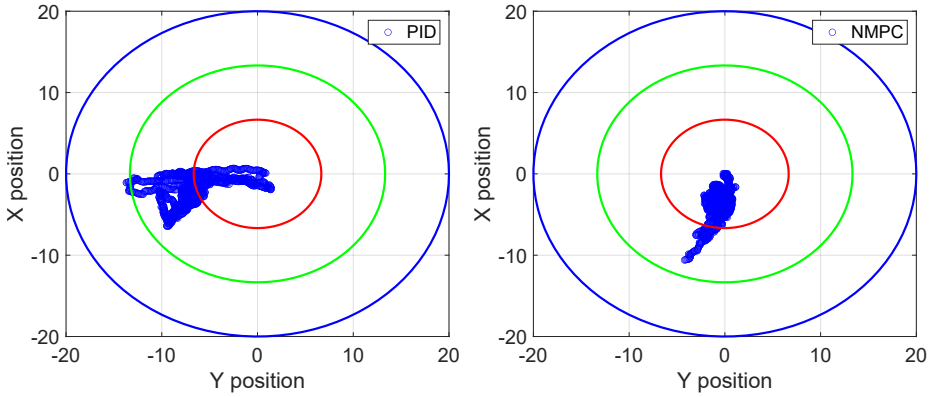

(a) XY plot in PID control

(b) XY plot in NMPC control

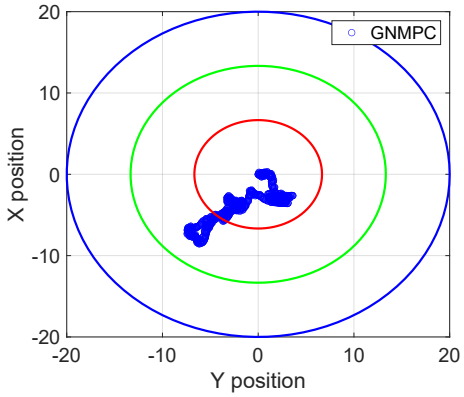

(c) XY plot in GNMPC control

Figure 8.24: Convergence comparison of PID,NMPC and GNMPC controllers: ship X,Y position at Irregular waves

8.2.5 Thrusters Forces and Spectral Densities under No Waves

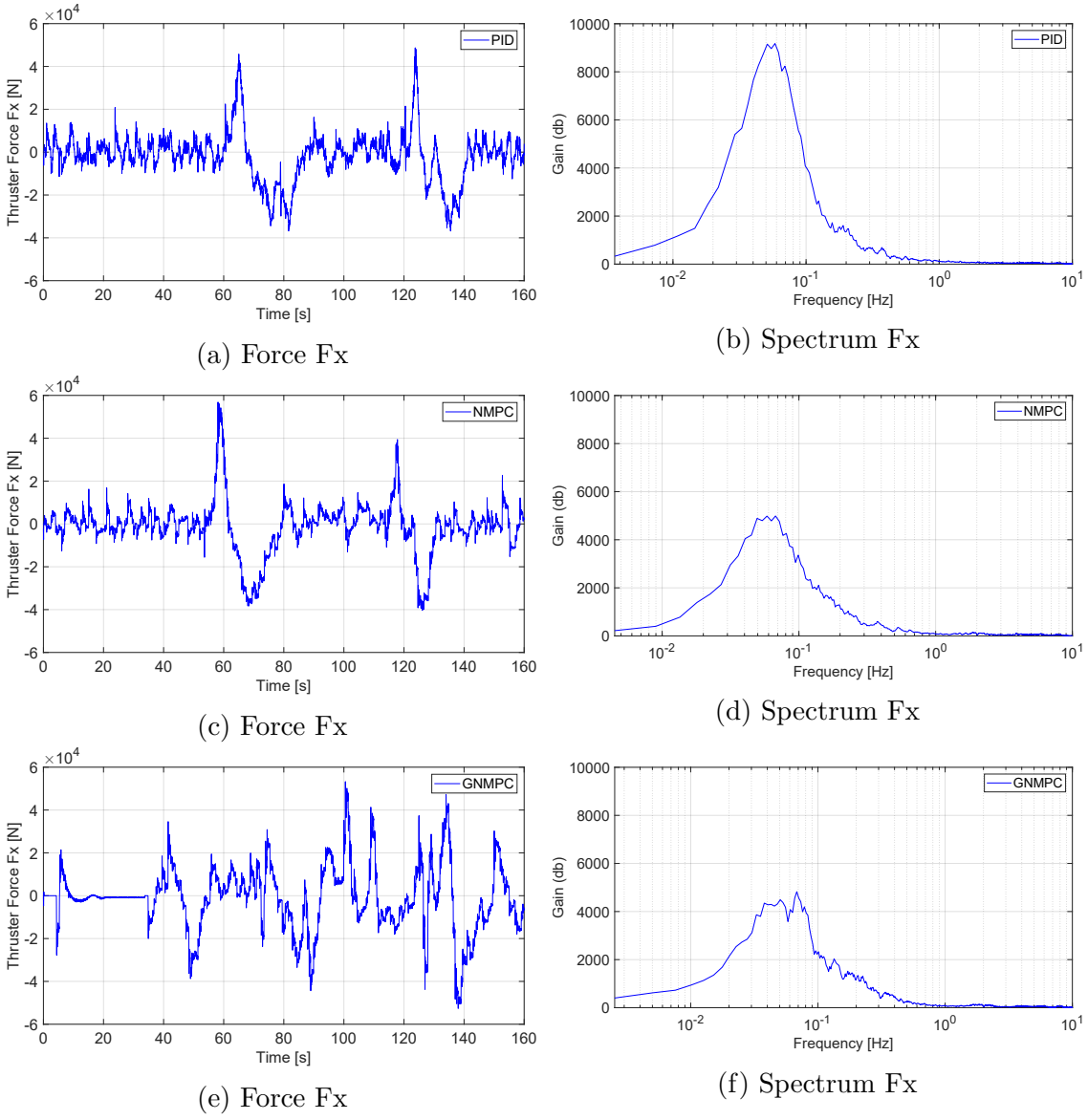

(a) Force Fx

(b) Spectrum Fx

(c) Force Fx

(d) Spectrum Fx

(e) Force Fx

(f) Spectrum Fx

Figure 8.25: Fx Thruster force and spectral density along x direction for different controllers.

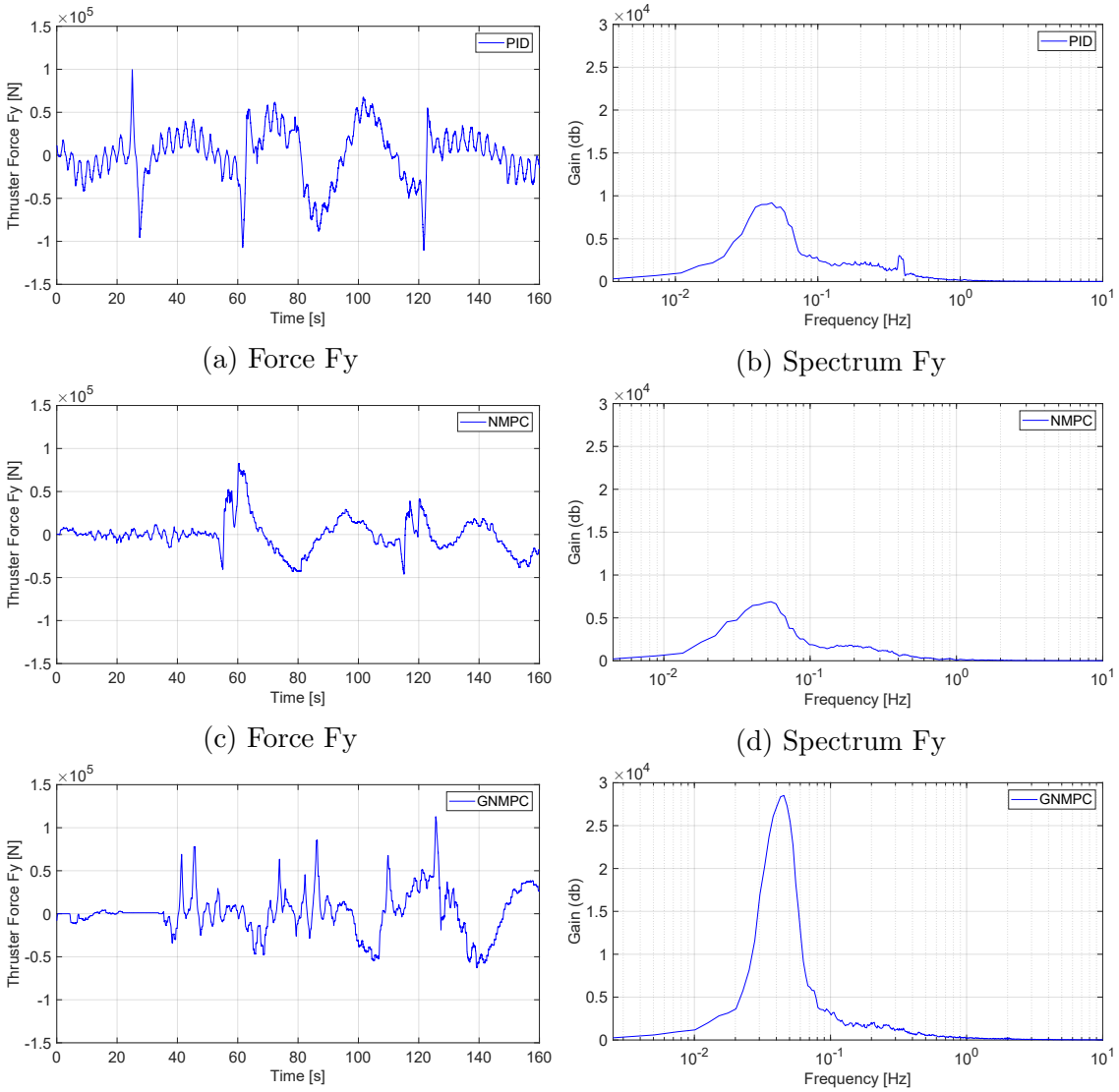

(a) Force Fy (b) Spectrum Fy

(c) Force Fy (d) Spectrum Fy

(e) Force Fy (f) Spectrum Fy

Figure 8.26: Fy Thruster force and spectral density along y direction for different controllers.

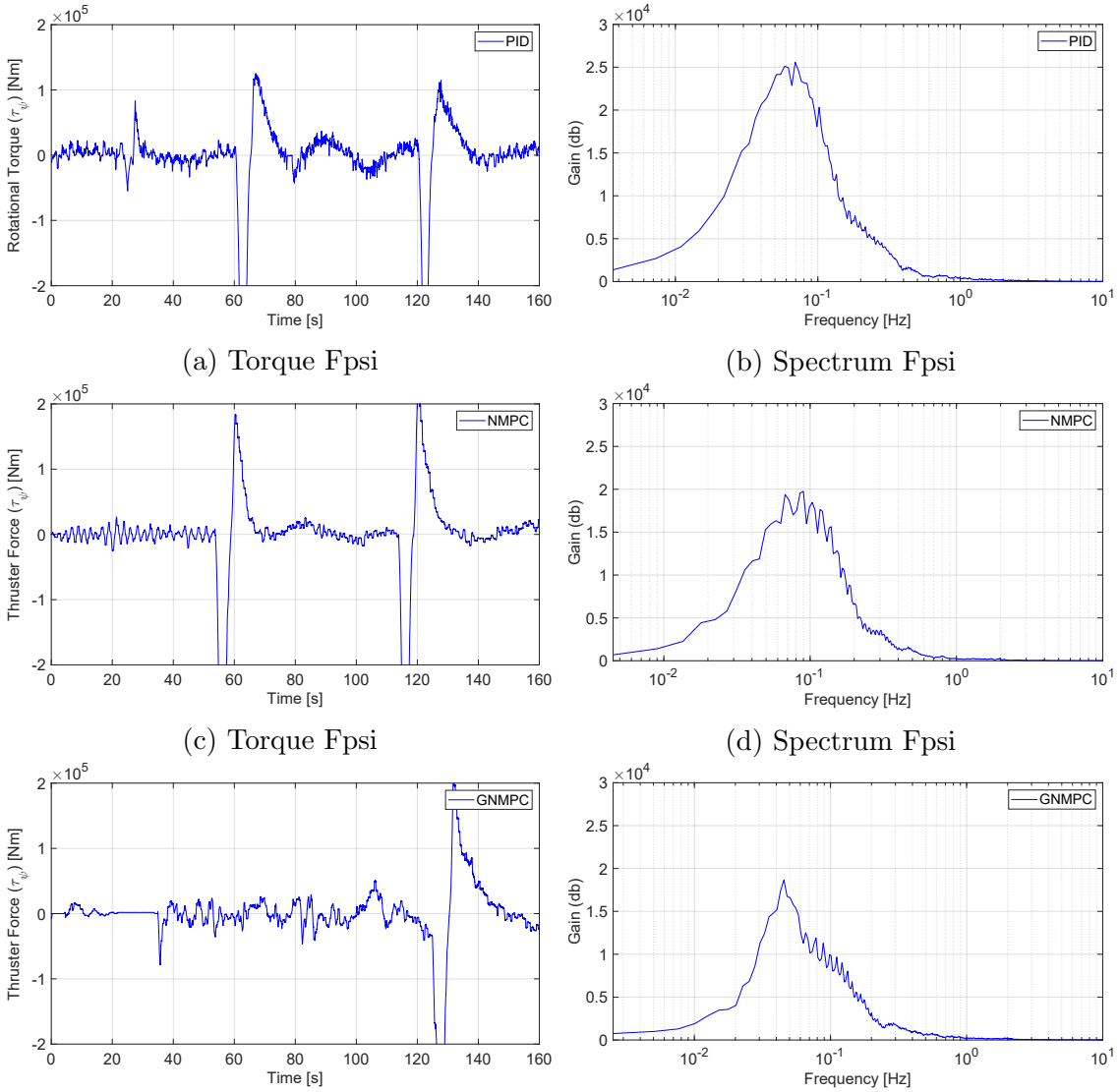

(a) Torque Fpsi

(b) Spectrum Fpsi

(c) Torque Fpsi

(d) Spectrum Fpsi

(e) Torque Fpsi

(f) Spectrum Fpsi

Figure 8.27: Fpsi Thruster torque and spectral density along rotational axis for different controllers.

8.2.6 Thrusters Forces and Spectral Densities under Regular Waves

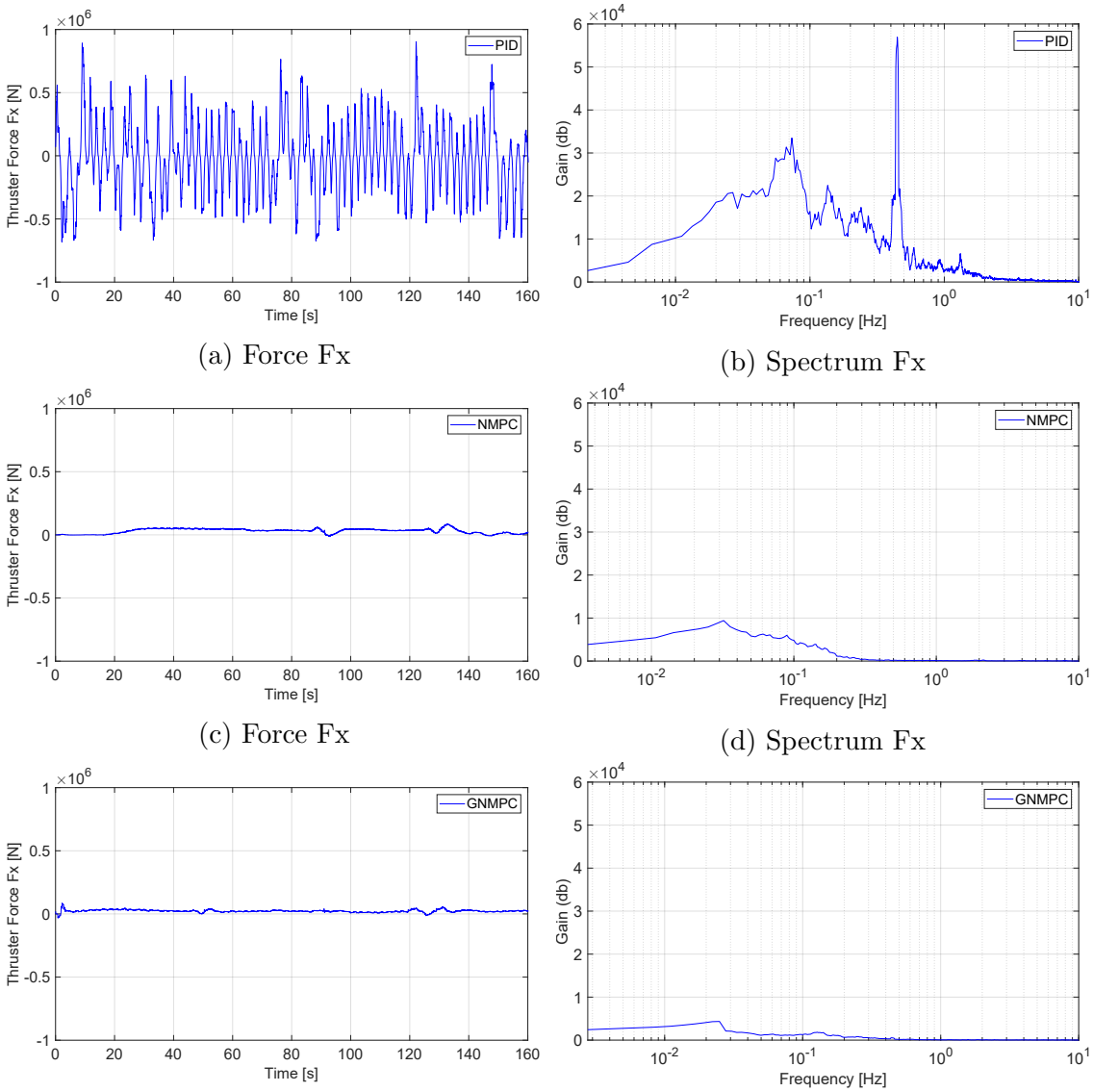

Figure 8.28: Fx Thruster force and spectral density along x direction for different controllers.

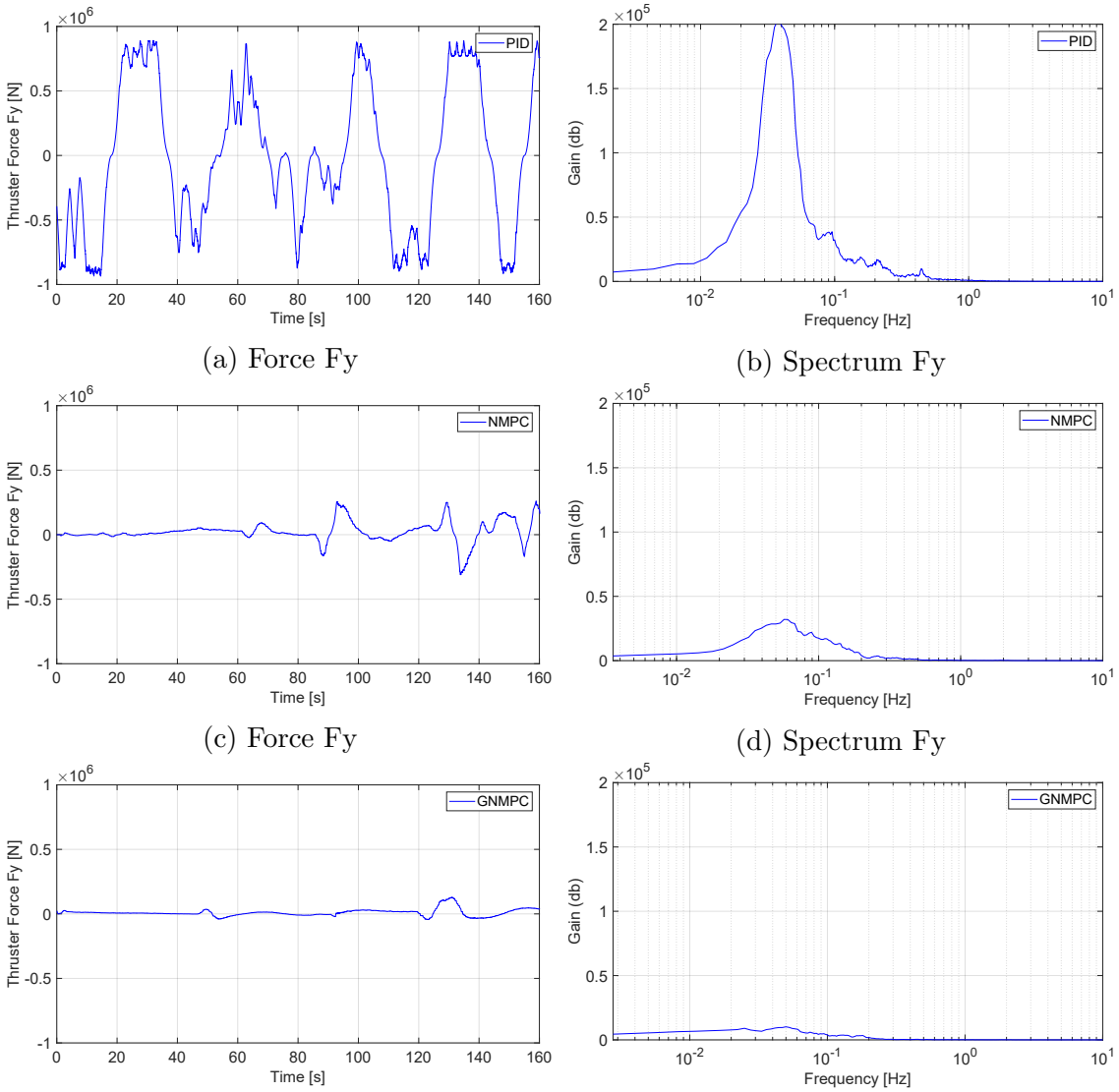

(a) Force Fy

(b) Spectrum Fy

(c) Force Fy

(d) Spectrum Fy

(e) Force Fy

(f) Spectrum Fy

Figure 8.29: Fy Thruster force and spectral density along y direction for different controllers.

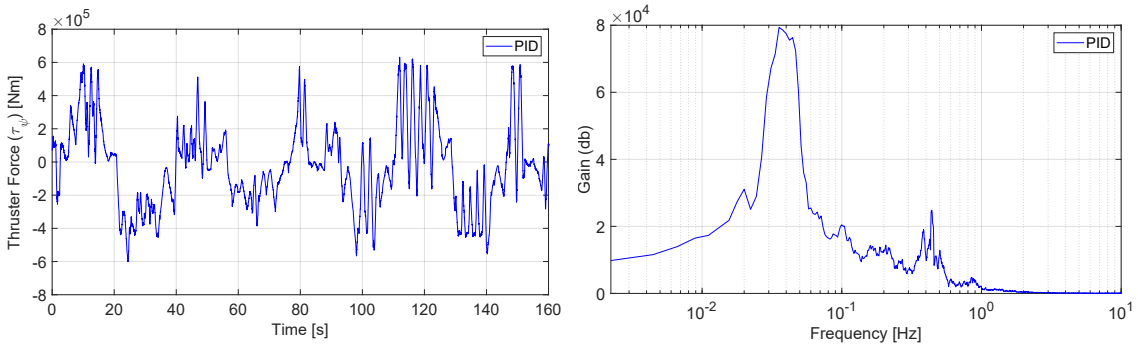

(a) Torque Fpsi

(b) Spectrum Fpsi

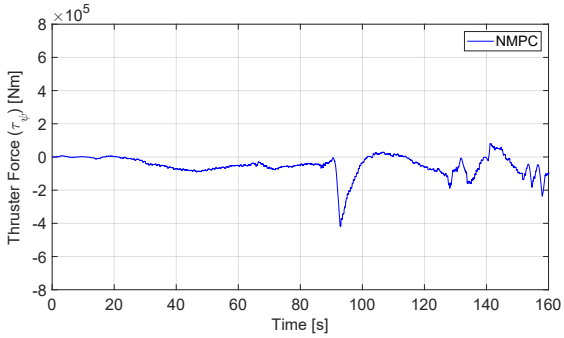

(c) Torque Fpsi

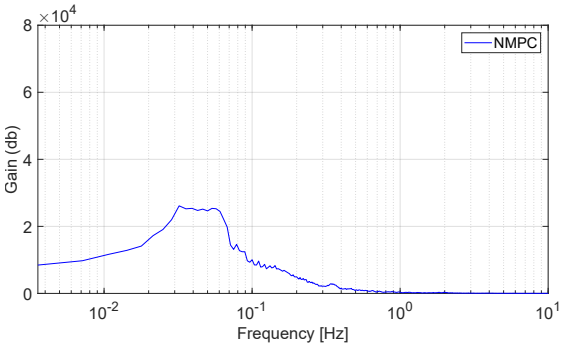

(d) Spectrum Fpsi

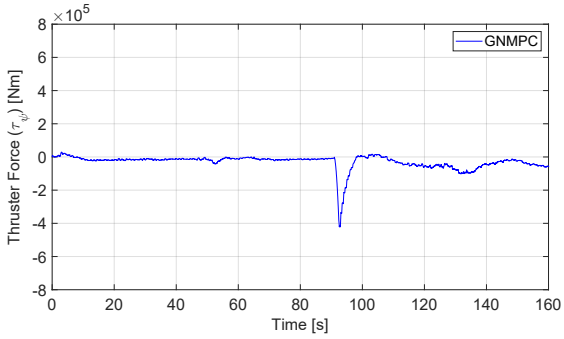

(e) Torque Fpsi

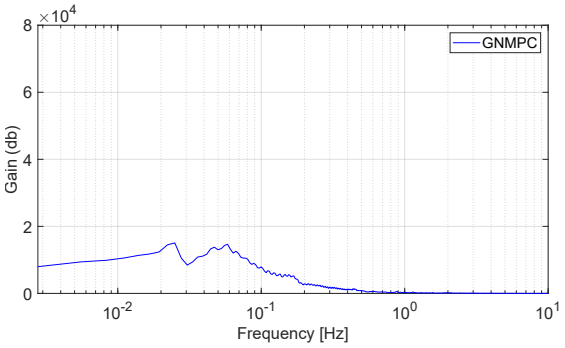

(f) Spectrum Fpsi

Figure 8.30: Fpsi Thruster torque and spectral density along rotational axis for different controllers.

8.2.7 Thrusters Forces and Spectral Densities under White noise Waves

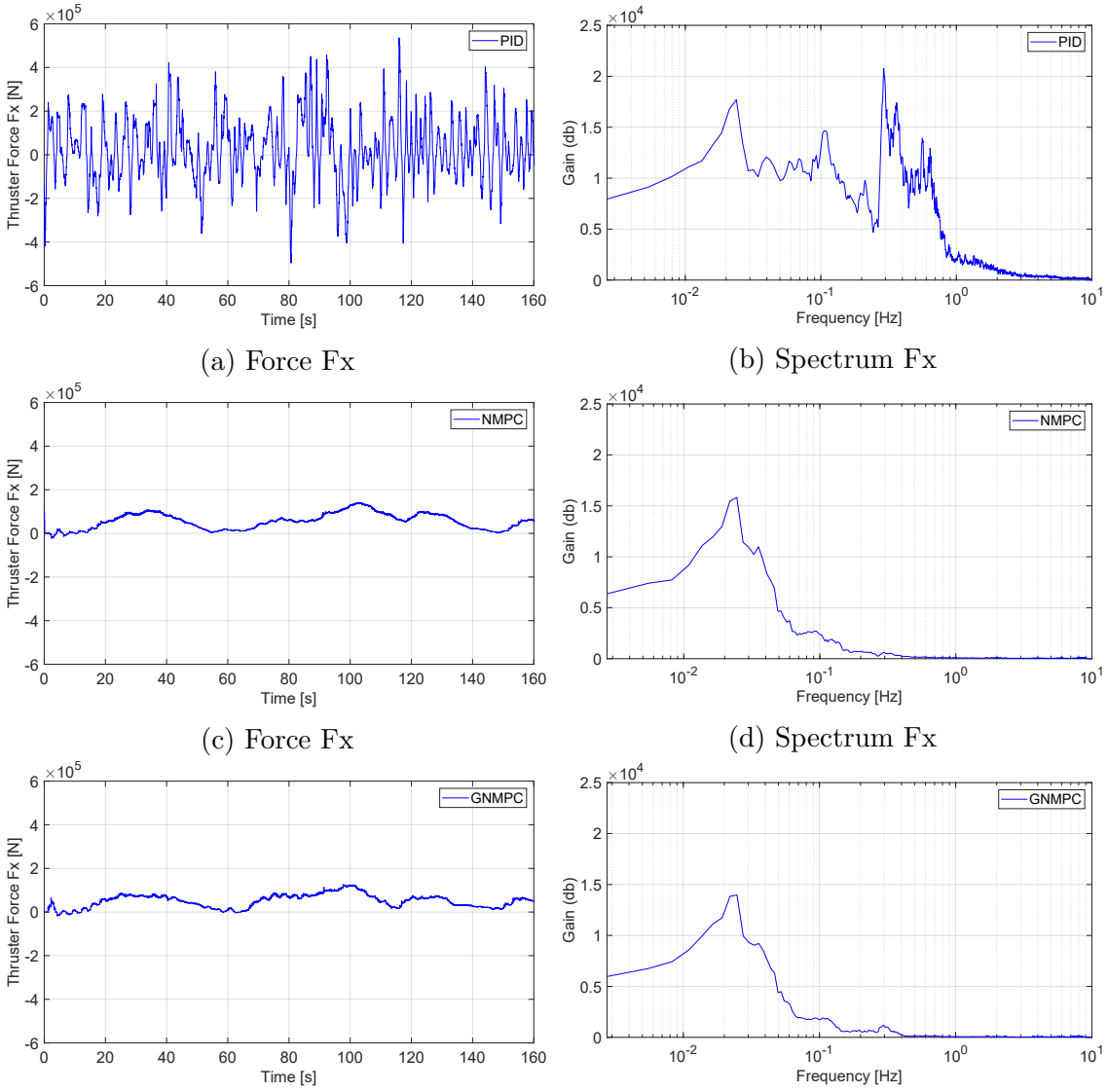

(a) Force Fx (b) Spectrum Fx

(c) Force Fx (d) Spectrum Fx

(e) Force Fx (f) Spectrum Fx

Figure 8.31: Fx Thruster force and spectral density along x direction for different controllers.

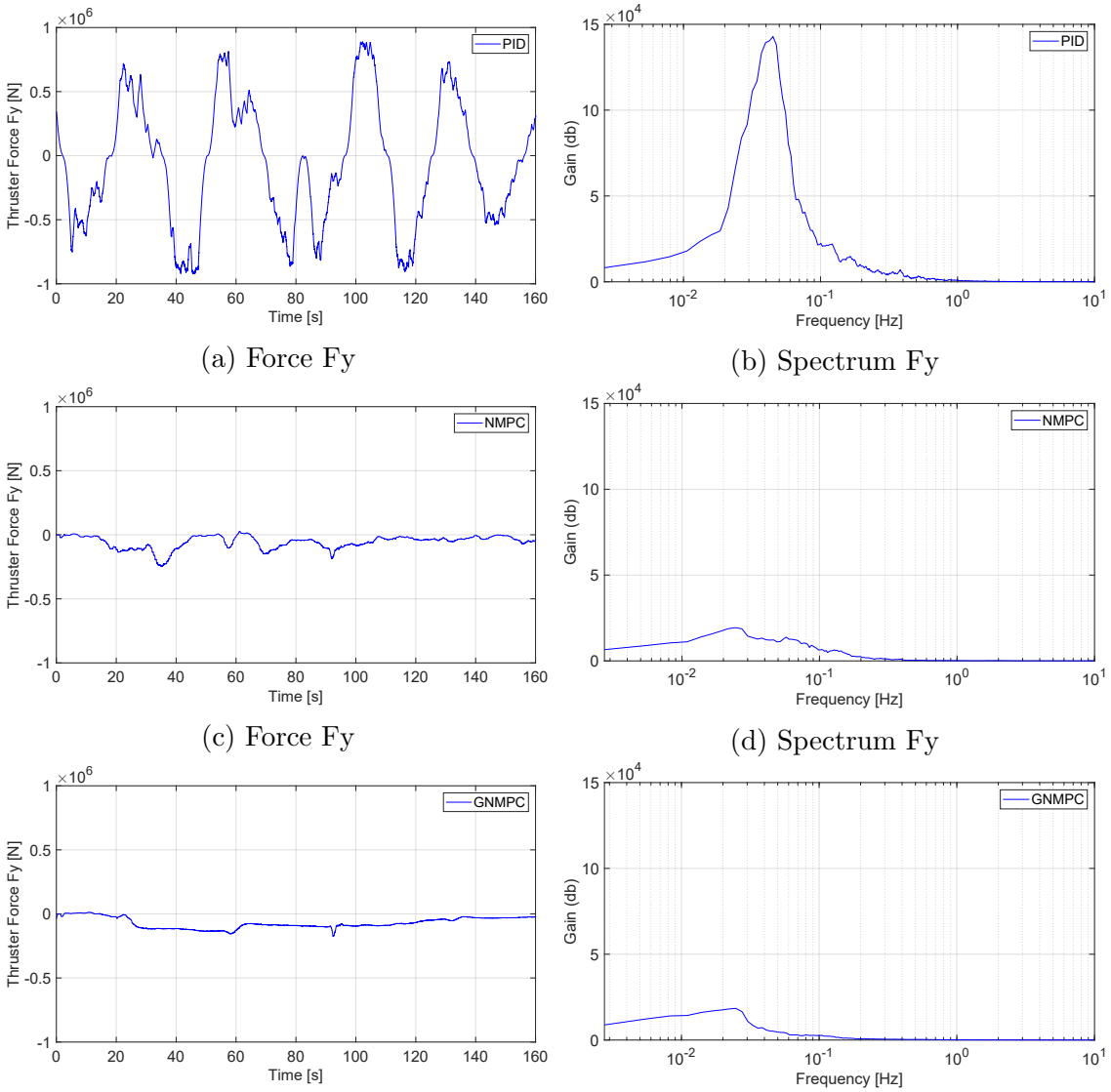

(a) Force Fy

(b) Spectrum Fy

(c) Force Fy

(d) Spectrum Fy

(e) Force Fy

(f) Spectrum Fy

Figure 8.32: Fy Thruster force and spectral density along y direction for different controllers.

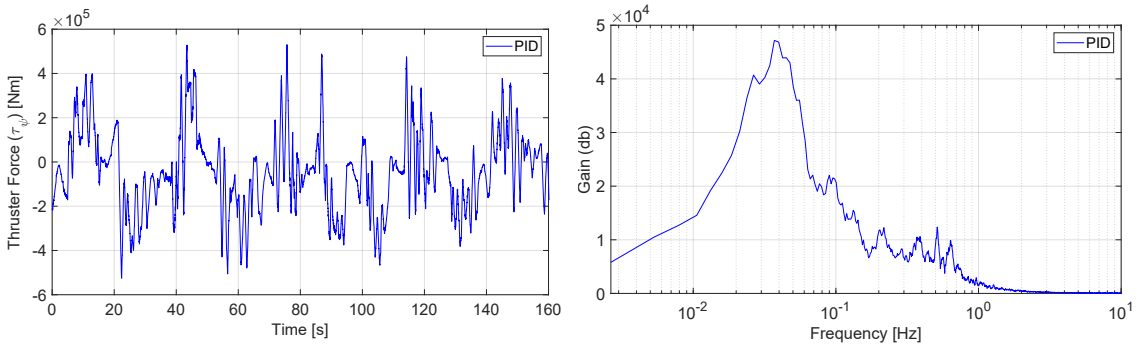

(a) Torque Fpsi

(b) Spectrum Fpsi

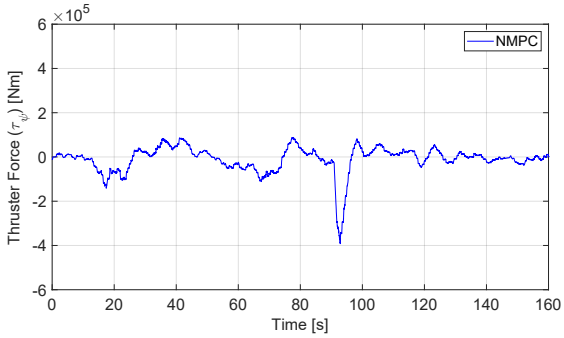

(c) Torque Fpsi

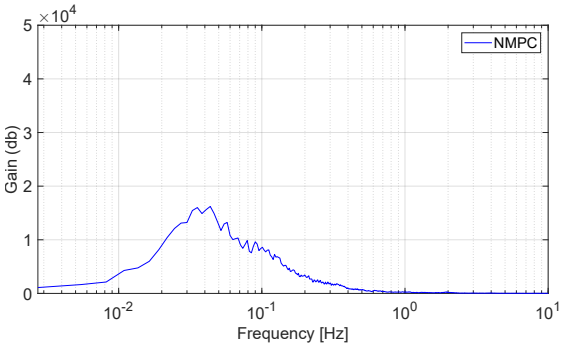

(d) Spectrum Fpsi

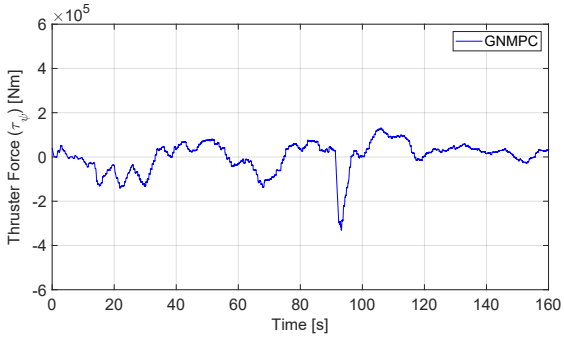

(e) Torque Fpsi

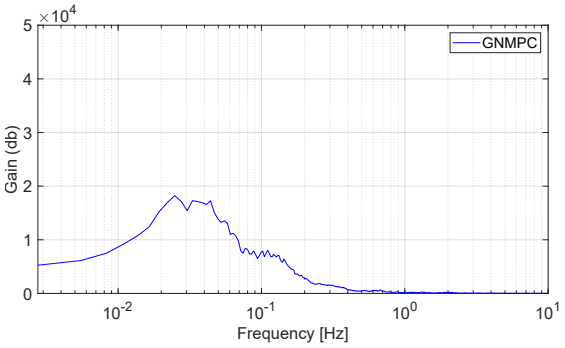

(f) Spectrum Fpsi

Figure 8.33: Fpsi Thruster torque and spectral density along rotational axis for different controllers.

8.2.8 Thrusters Forces and Spectral Densities under Irregular Waves

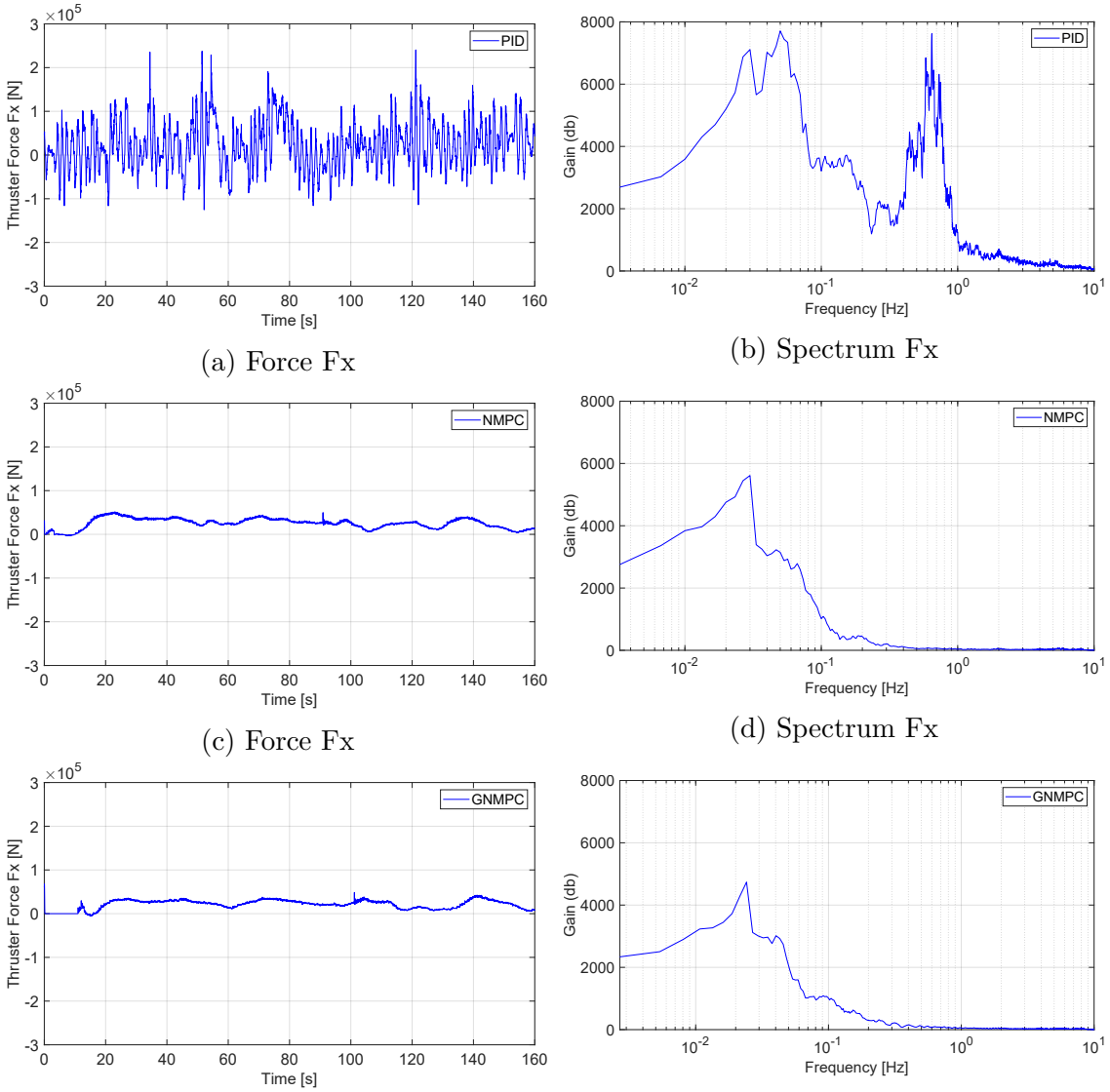

(a) Force Fx

(b) Spectrum Fx

(c) Force Fx

(d) Spectrum Fx

(e) Force Fx

(f) Spectrum Fx

Figure 8.34: Fx Thruster force and spectral density along x direction for different controllers.

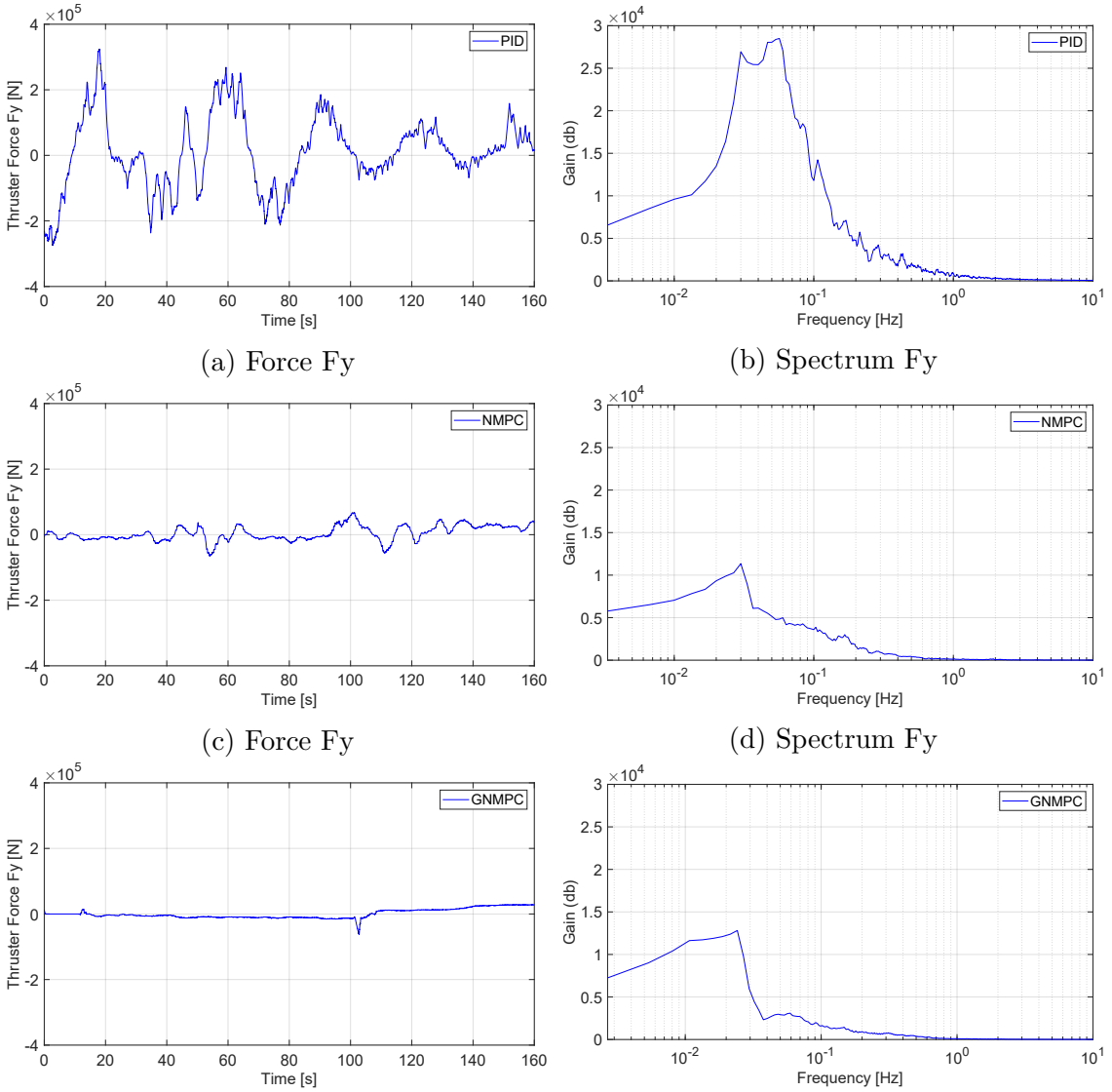

(a) Force Fy (b) Spectrum Fy

(c) Force Fy (d) Spectrum Fy

(e) Force Fy (f) Spectrum Fy

Figure 8.35: Fy Thruster force and spectral density along y direction for different controllers.

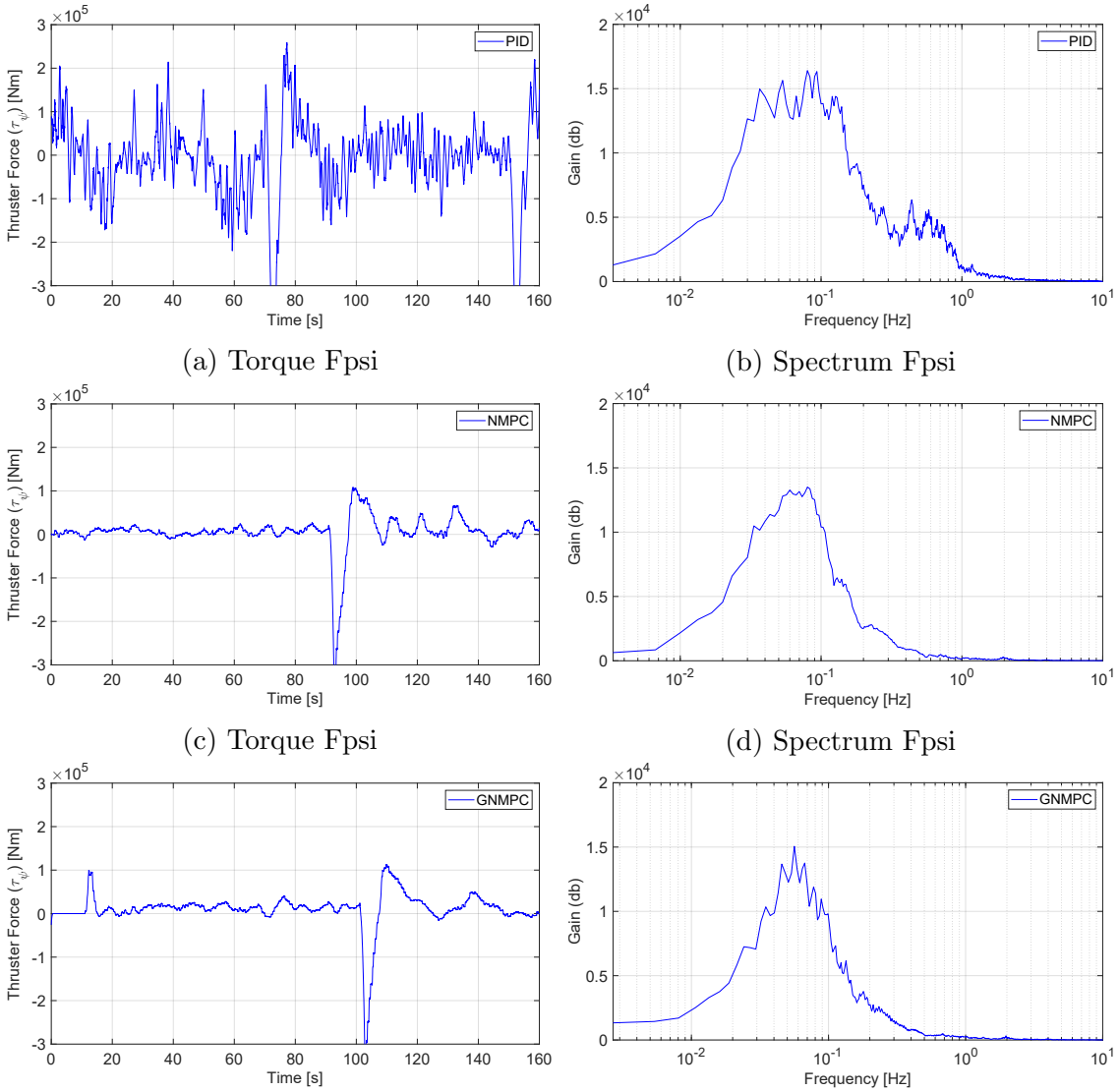

(a) Torque Fpsi

(b) Spectrum Fpsi

(c) Torque Fpsi

(d) Spectrum Fpsi

(e) Torque Fpsi

(f) Spectrum Fpsi

Figure 8.36: Fpsi Thruster torque and spectral density along rotational axis for different controllers.

8.3 Large Position Setpoint Changes Test

This test is used in dynamic positioning (DP) to ensure a vessel can maintain its position under multiple locations and set angles.

8.3.1 Spectral Density of Thrusters in No wave Conditions

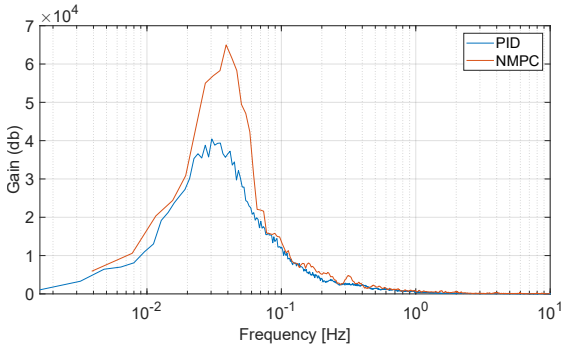

(a) Spectral density of Fx force.

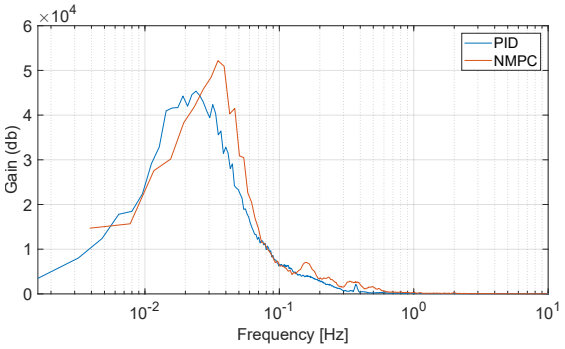

(b) Spectral density of Fy force.

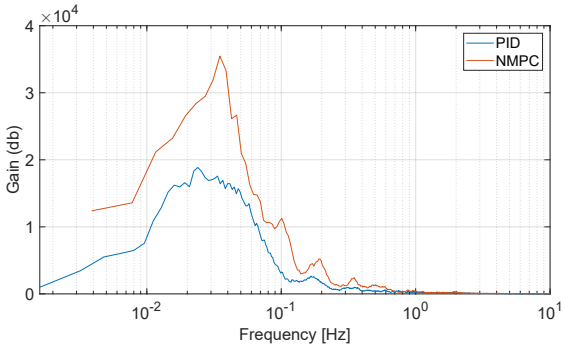

(c) Spectral density of Fpsi torque.

Figure 8.37: Spectral density of thrusters in No wave conditions

8.3.2 Spectral Density of Thrusters in White noise wave Conditions

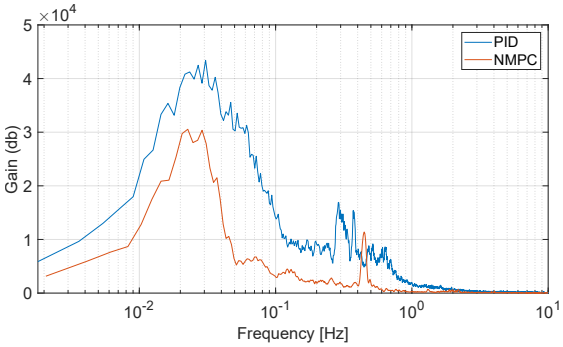

(a) Spectral density of Fx force.

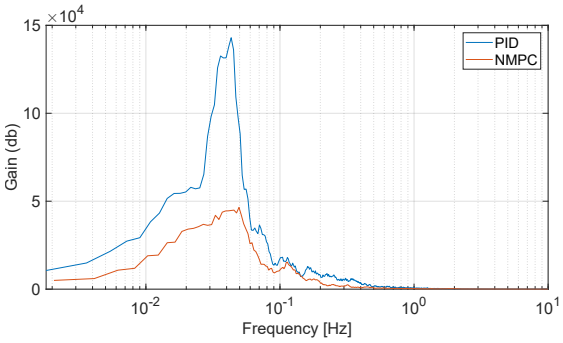

(b) Spectral density of Fy force.

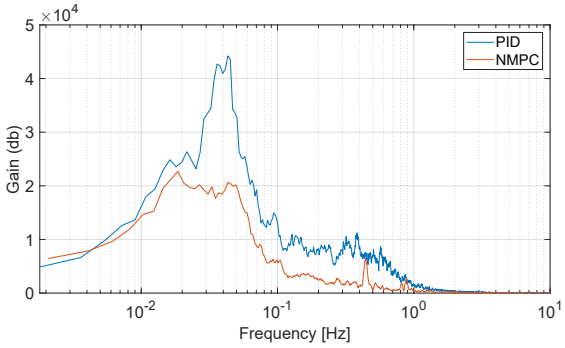

(c) Spectral density of Fpsi torque.

Figure 8.38: Spectral density of thrusters in White noise wave conditions

8.3.3 Spectral Density of Thrusters in Irregular wave Conditions

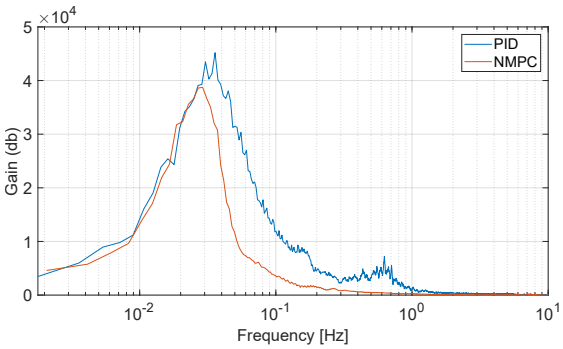

(a) Spectral density of Fx force.

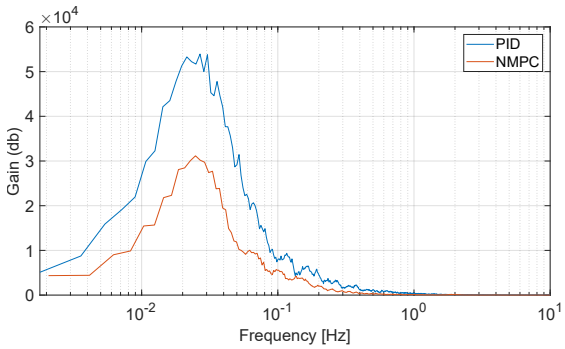

(b) Spectral density of Fy force.

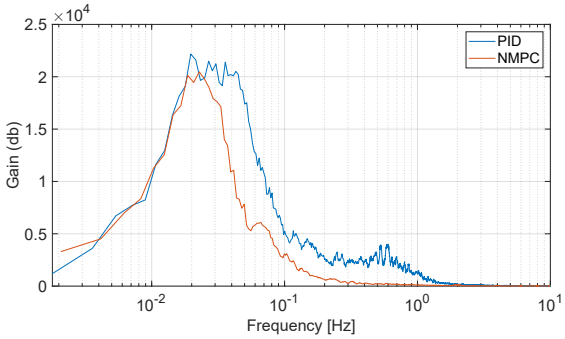

(c) Spectral density of Fpsi torque.

Figure 8.39: Spectral density of thrusters in Irregular wave conditions

8.3.4 XY plots in PID,and NMPC under Different Waves Conditions

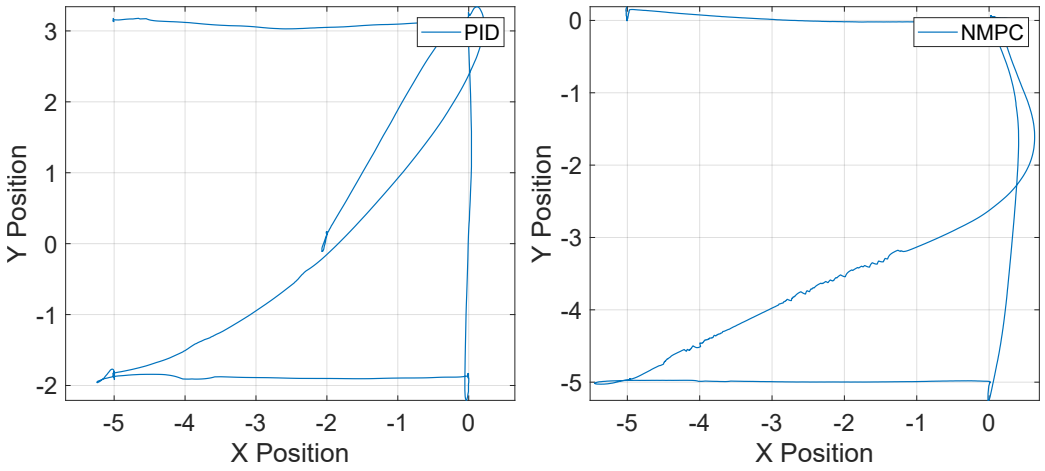

(a) XY plot in PID control (b) XY plot in NMPC control

Figure 8.40: Convergence comparison of PID,and NMPC controllers: ship X,Y position at No waves

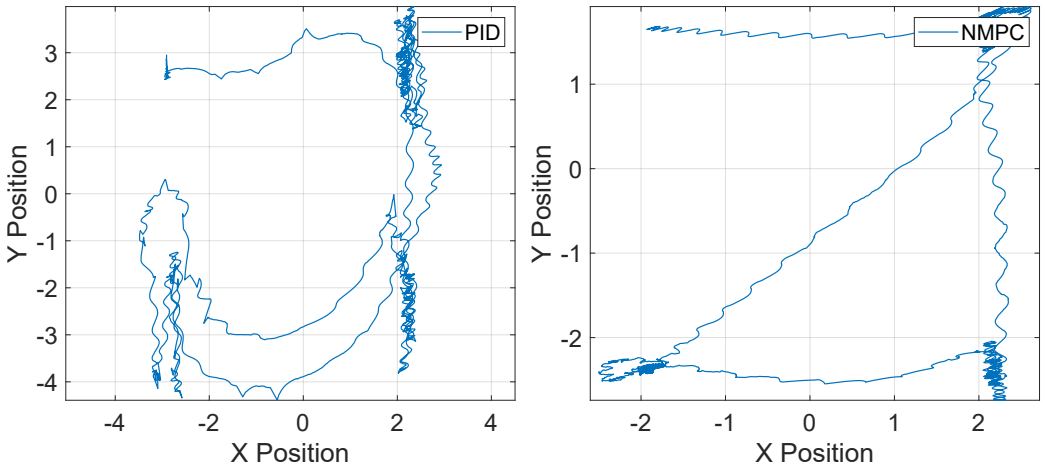

(a) XY plot in PID control (b) XY plot in NMPC control

Figure 8.41: Convergence comparison of PID,and NMPC controllers: ship X,Y position at Regular waves

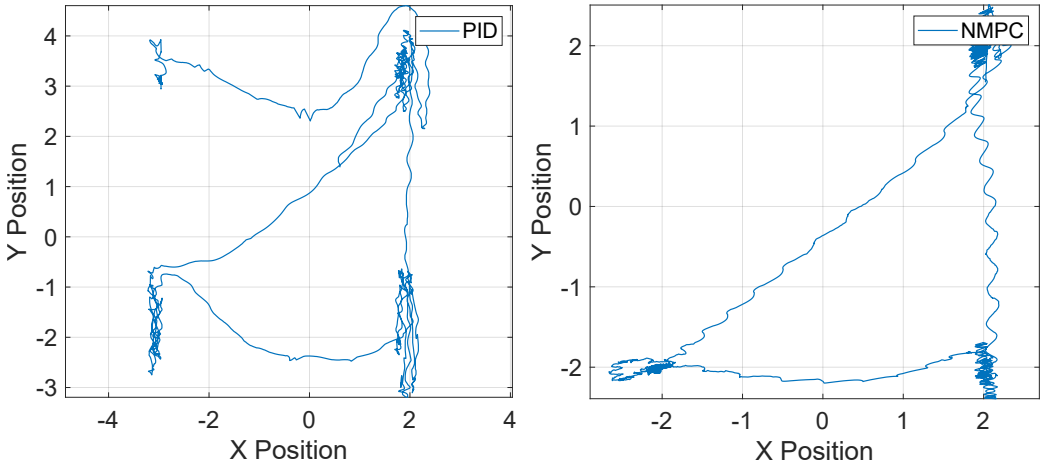

(a) XY plot in PID control (b) XY plot in NMPC control

Figure 8.42: Convergence comparison of PID,and NMPC controllers: ship X,Y position at White noise waves

8.3.5 Thrusters Forces and Spectral Densities under No Waves

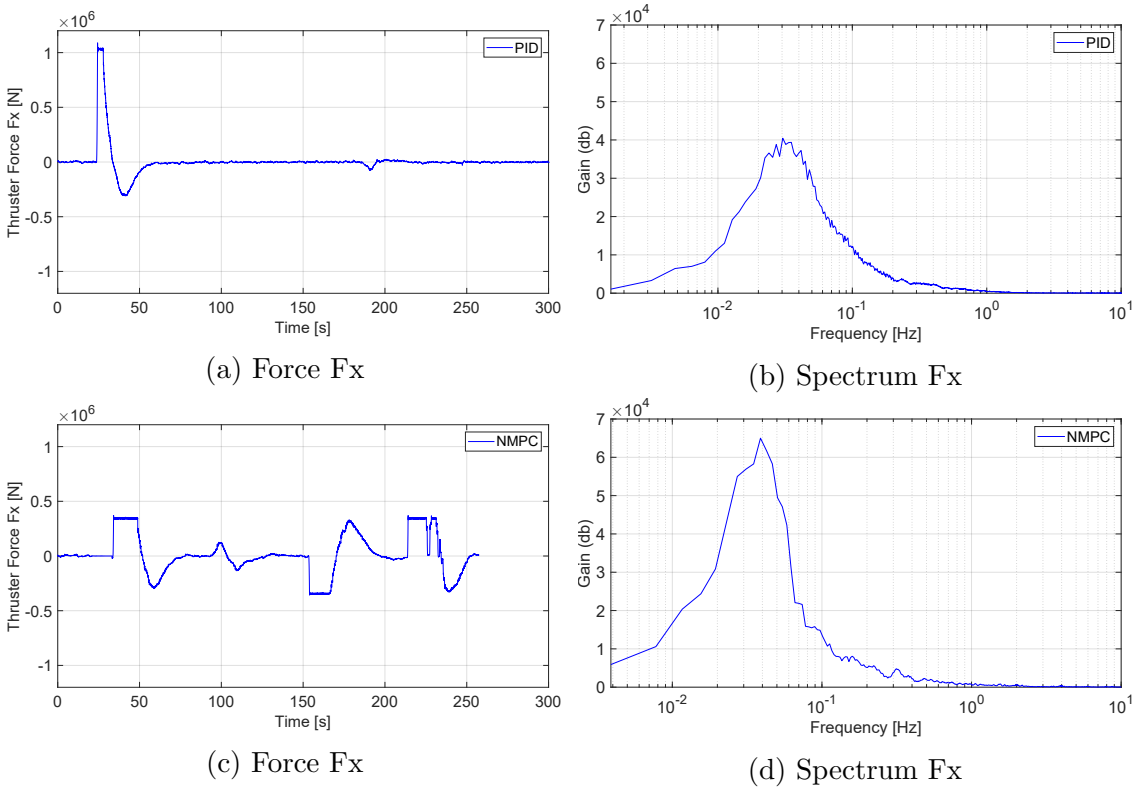

(a) Force Fx

(b) Spectrum Fx

(c) Force Fx

(d) Spectrum Fx

Figure 8.43: Fx Thruster force and spectral density along x direction for different controllers.

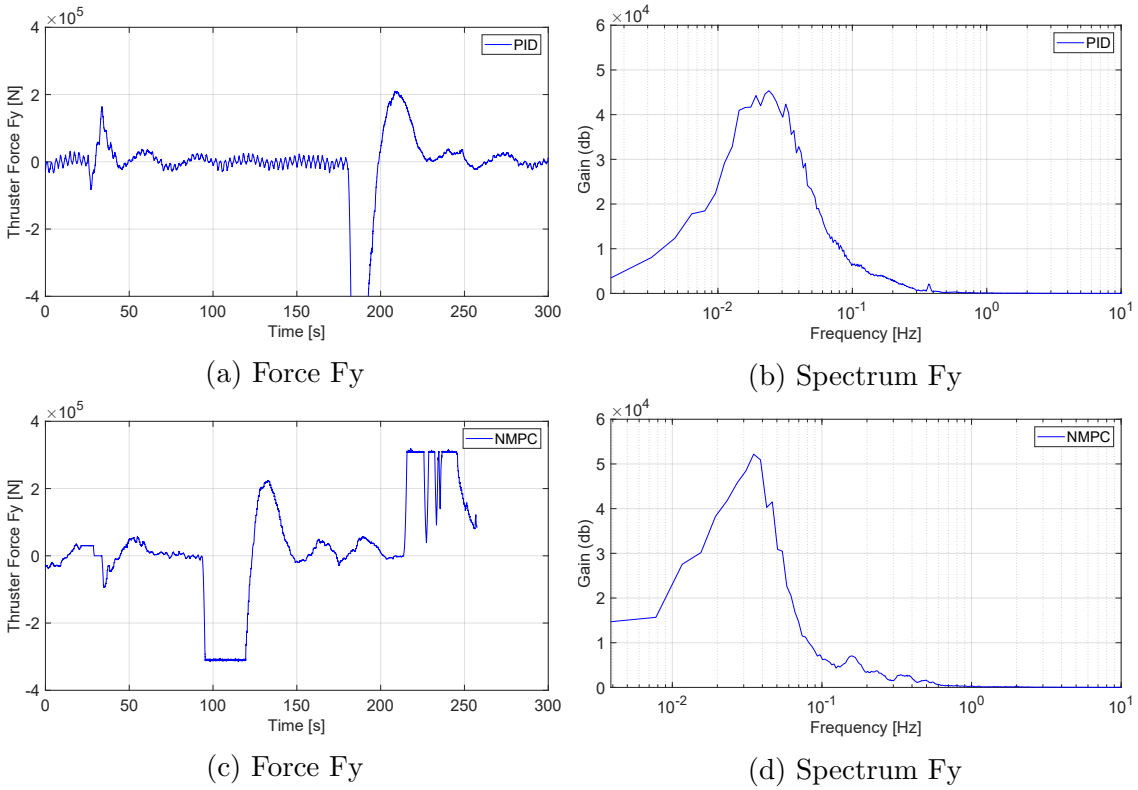

(a) Force Fy

(b) Spectrum Fy

(c) Force Fy

(d) Spectrum Fy

Figure 8.44: Fy Thruster force and spectral density along y direction for different controllers.

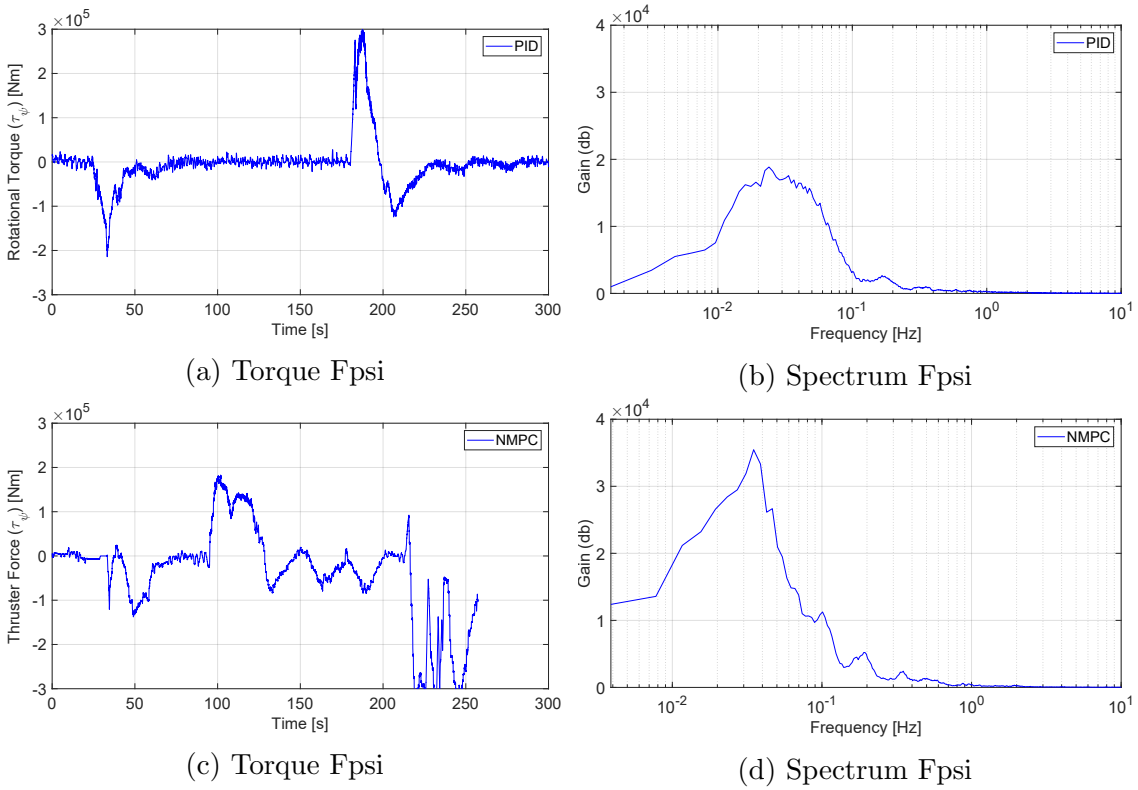

(a) Torque Fpsi

(b) Spectrum Fpsi

(c) Torque Fpsi

(d) Spectrum Fpsi

Figure 8.45: Fpsi Thruster torque and spectral density along rotational axis for different controllers.

8.3.6 Thrusters Forces and Spectral Densities under Regular Waves

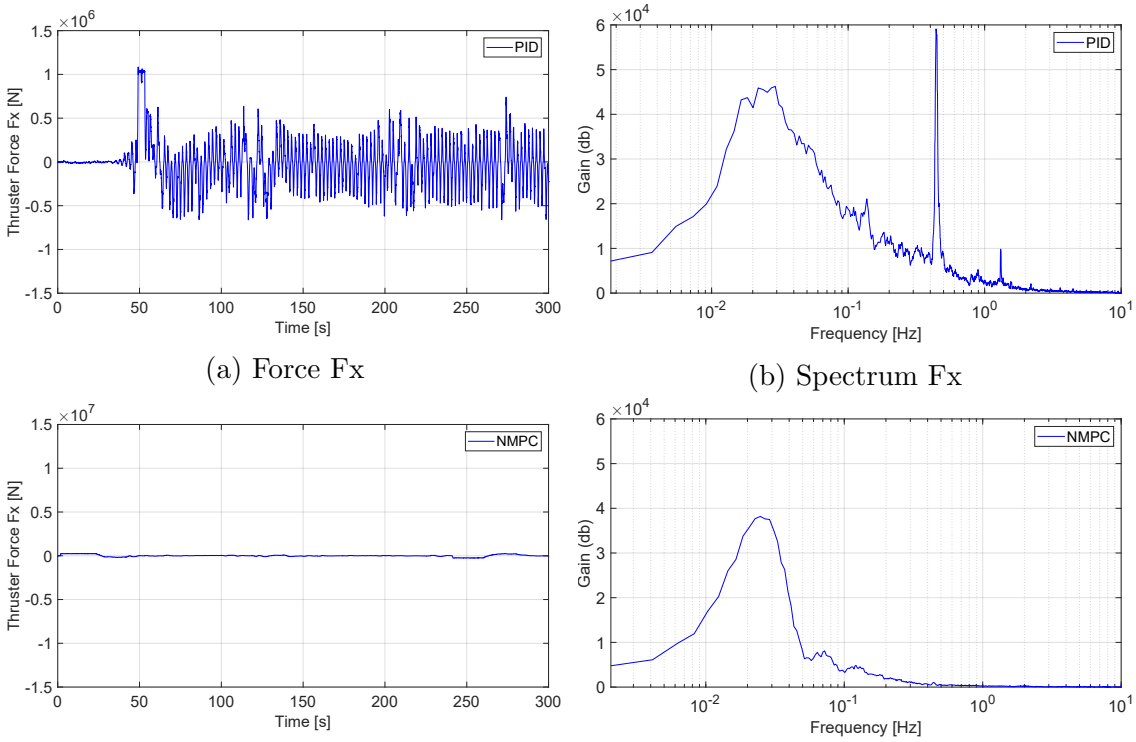

(a) Force Fx

(b) Spectrum Fx

(c) Force Fx

(d) Spectrum Fx

Figure 8.46: Fx Thruster force and spectral density along x direction for different controllers.

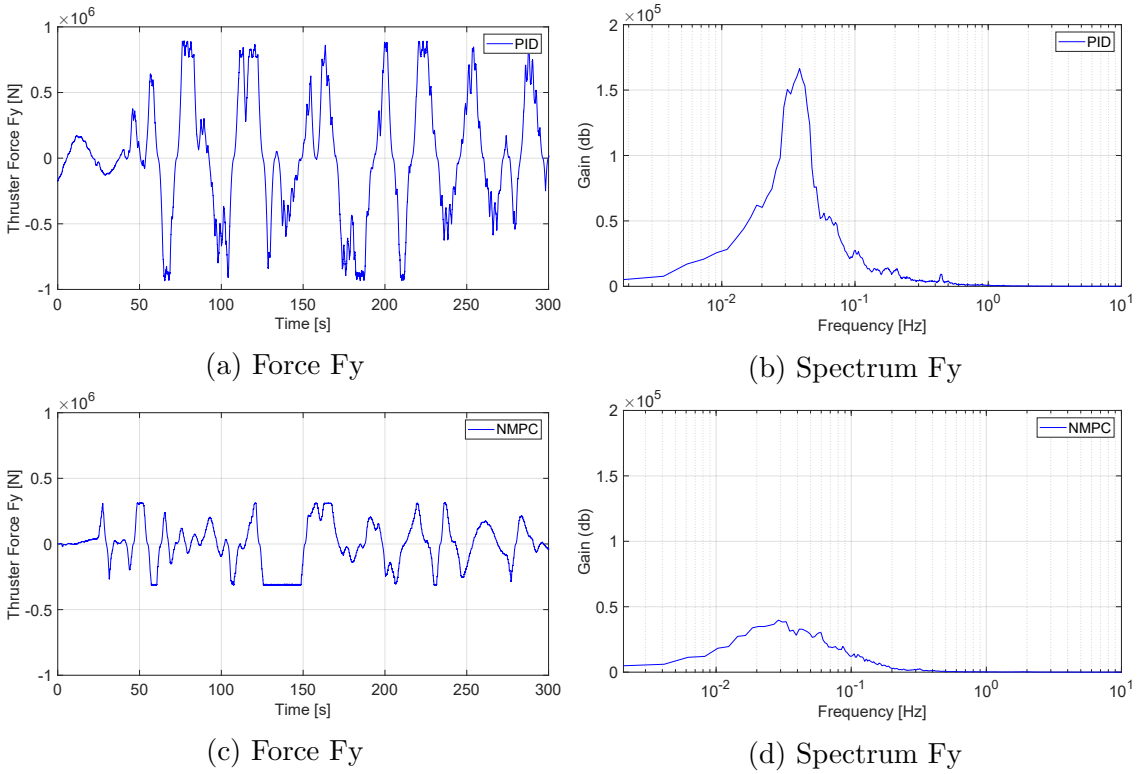

(a) Force Fy

(b) Spectrum Fy

(c) Force Fy

(d) Spectrum Fy

Figure 8.47: Fy Thruster force and spectral density along y direction for different controllers.

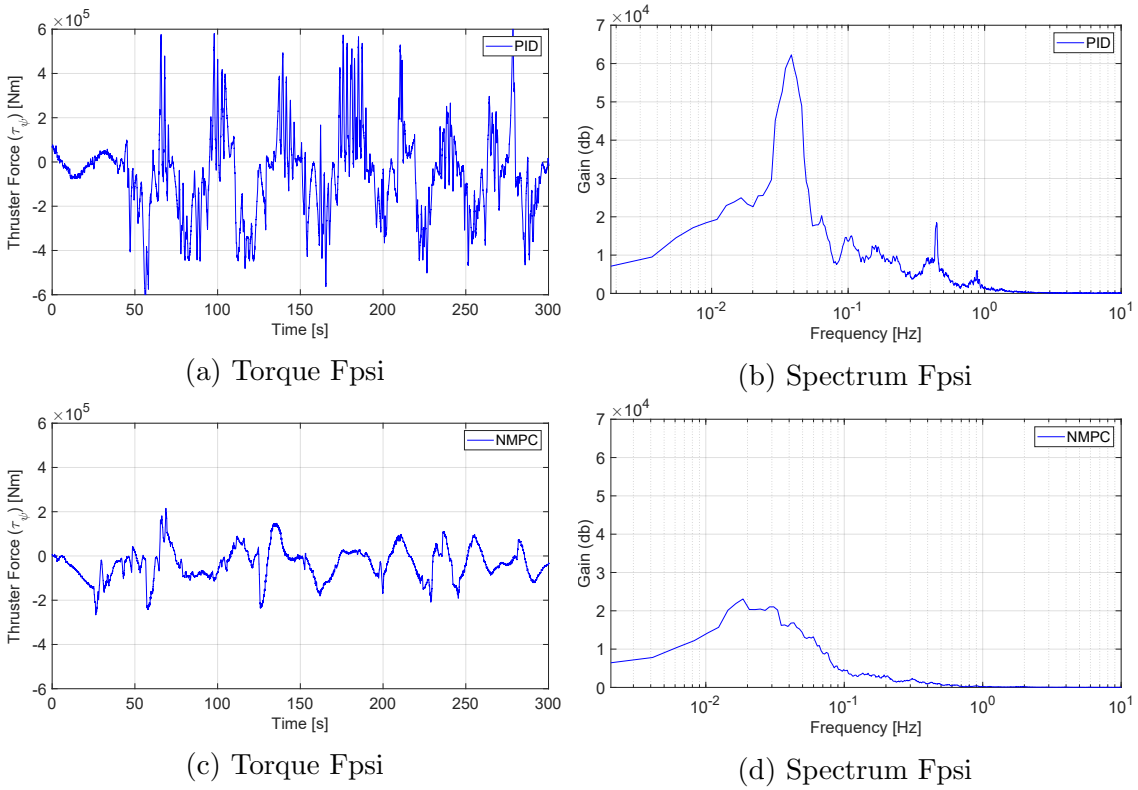

(a) Torque Fpsi

(b) Spectrum Fpsi

(c) Torque Fpsi

(d) Spectrum Fpsi

Figure 8.48: Fpsi Thruster torque and spectral density along rotational axis for different controllers.

8.3.7 Thrusters Forces and Spectral Densities under White noise Waves

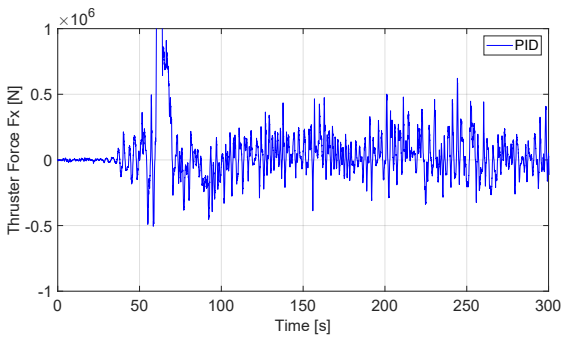

(a) Force Fx

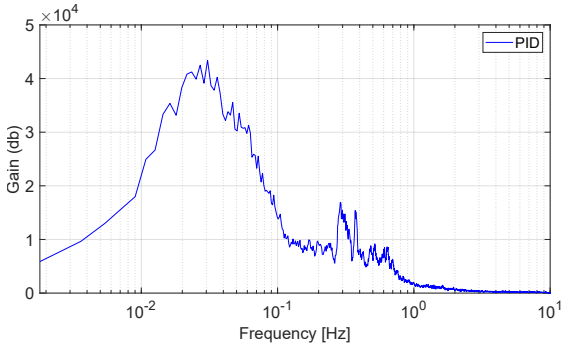

(b) Spectrum Fx

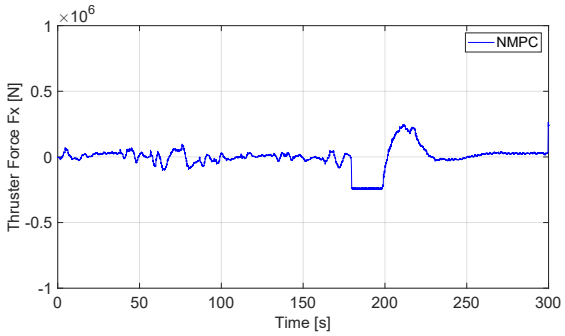

(c) Force Fx

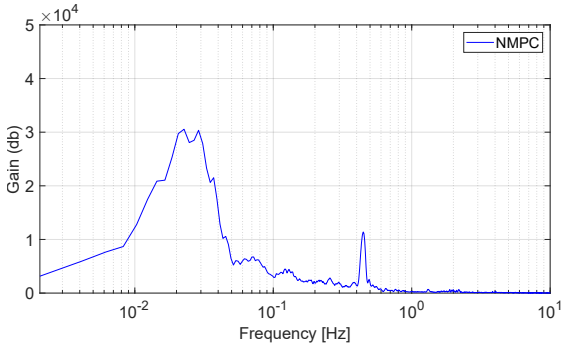

(d) Spectrum Fx

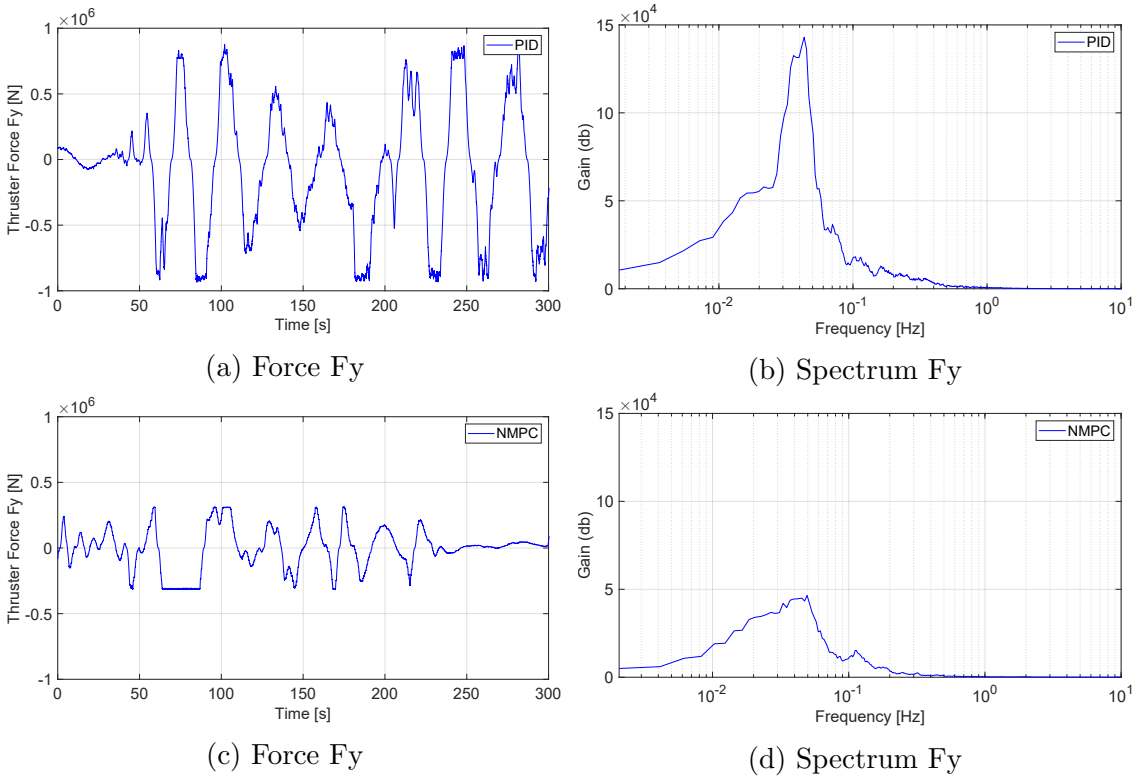

(a) Force Fy

(b) Spectrum Fy

(c) Force Fy

(d) Spectrum Fy

Figure 8.50: Fy Thruster force and spectral density along y direction for different controllers.

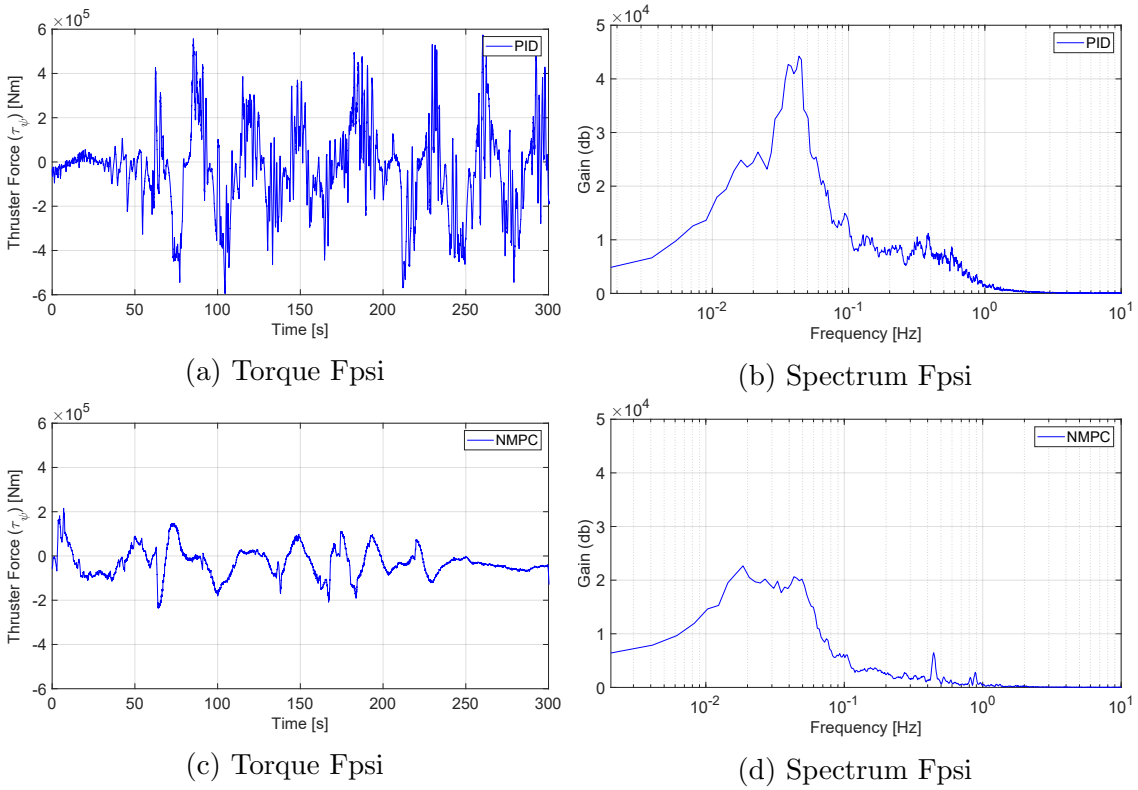

Figure 8.51: Fpsi Thruster torque and spectral density along rotational axis for different controllers.

8.3.8 Thrusters Forces and Spectral Densities under Irregular Waves

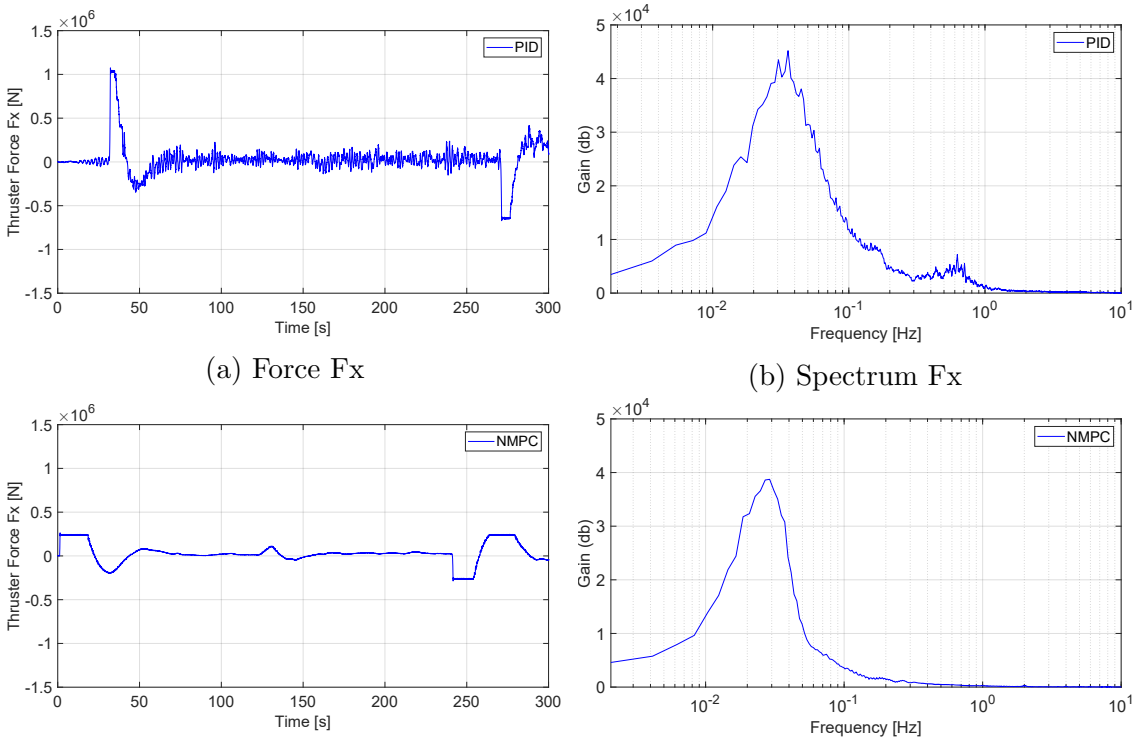

(a) Force Fx

(b) Spectrum Fx

(c) Force Fx

(d) Spectrum Fx

Figure 8.52: Fx Thruster force and spectral density along x direction for different controllers.

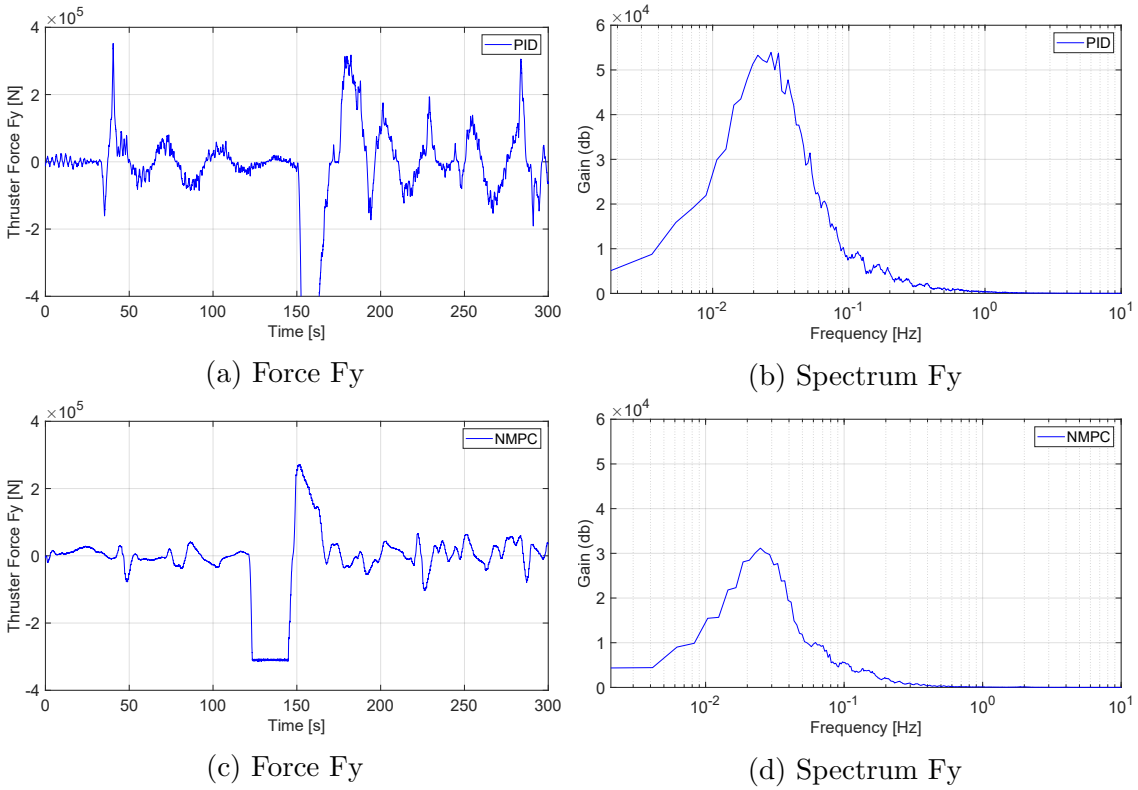

(a) Force Fy

(b) Spectrum Fy

(c) Force Fy

(d) Spectrum Fy

Figure 8.53: Fy Thruster force and spectral density along y direction for different controllers.

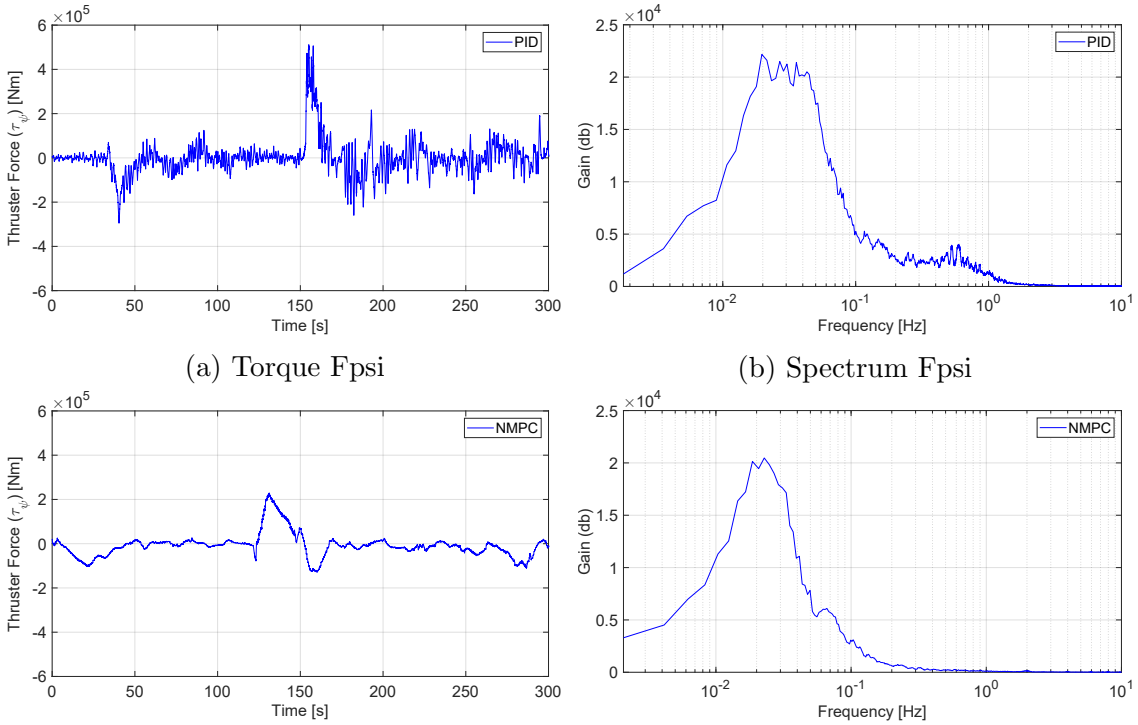

(a) Torque Fpsi

(b) Spectrum Fpsi

(c) Torque Fpsi

(d) Spectrum Fpsi

Figure 8.54: Fpsi Thruster torque and spectral density along rotational axis for different controllers.